CARGEN™: A NOVEL TECHNOLOGY TO ADVANCE METHANE REFORMING USING CO_2

A Dissertation

by

MOHAMEDSUFIYAN AZIZURREHMAN CHALLIWALA

Submitted to the Office of Graduate and Professional Studies of
Texas A&M University
in partial fulfillment of the requirements for the degree of

DOCTOR OF PHILOSOPHY

Chair of Committee,	Nimir O. Elbashir
Co-Chair of Committee,	Mahmoud M. El-Halwagi
Committee Members,	Stratos Pistikopoulos
	Ibrahim Galal Hassan
Head of Department,	Arul Jayaraman

May 2021

Major Subject: Chemical Engineering

ABSTRACT

Recent decades have witnessed groundbreaking advancements in the field of carbon dioxide (CO_2) utilization and conversion, primarily due to the commitment put forth by the top global economies to address climate change. Dry reforming of methane (DRM) is one of the many pathways that enable CO_2 utilization to produce precursors for chemical and fuel production; however, due to several process limitations, DRM technology has yet to be commercialized. The major advantage of this technology is that it catalytically converts two greenhouse gases (CO_2 and methane [CH_4]) into a mixture of carbon monoxide and hydrogen, which is known as *synthesis gas* or *syngas*. Syngas is an essential precursor in the production of value-added chemicals, hydrocarbons, and alternative fuels. In the present work, an innovative advancement in the DRM field—carbon generation technology (CARGEN™)—is developed. The CARGEN™ technology addresses some of the major challenges facing the commercialization of DRM technology while bringing compelling economic advantages over benchmark methane reforming processes (i.e., steam reforming, partial oxidation, and autothermal reforming). CARGEN™ technology is built on a system of two integrated reactors in series, which are meant to segregate two opposing reactions occurring in the DRM: (a) carbon formation at low temperatures (at 400-600°C, via Boudouard and methane decomposition reactions) and (b) syngas formation at high temperatures (at ≥ 750°C). This unique feature of CARGEN™ entails exceptional flexibility that overcomes all the DRM challenges. A detailed energy assessment via thermodynamic analysis has demonstrated that CARGEN™ enables at least 65% CO_2 conversion while consuming 50% of the typical energy required in an

equivalent-capacity DRM process. Additionally, in contrast to DRM, CARGEN™ presents the flexibility to produce syngas that meets downstream process requirements. Another study involving a lifecycle assessment of the process indicates that CARGEN™ enables at least a 40% reduction in both CO_2 emissions and operational costs, compared to benchmark commercial technologies such as autothermal reforming and partial oxidation. The unique, transformational benefit of the CARGEN™ process, which was discovered during the experimental proofing stage, is its ability to produce a high-quality form of carbon material: specifically, multiwalled carbon nanotubes. Moreover, dedicated reproducibility tests utilizing state-of-the-art reactor systems at microgram, milligram, and multigram scales have revealed reproducibility and consistency in the quality of the multiwalled carbon nanotubes, which were tested and validated employing scanning electron microscopy, transmission electron microscopy, thermogravimetric analysis, and the Raman analysis.

DEDICATION

To my daughter, my wife, my parents, and my brothers.

ACKNOWLEDGEMENTS

In the name of God, Most Gracious, and Most Merciful.

I am profoundly grateful to my committee chair, Professor Nimir Elbashir, for his support throughout my Master's and Ph.D. degrees at TAMU. Prof. Elbashir encouraged and provided me with countless opportunities to work on several different projects in the Gas and Fuels research field. I consider myself very fortunate and honored to this lifetime opportunity to work under Prof. Elbashir's supervision and can't thank enough for his tireless and unconditional mentorship, guidance, and never-ending support. Because of his guidance, intellectual support, and supervision during the course of my Ph.D. work, I was able to develop a novel and cutting-edge CO_2 conversion technology- CARGEN™, and I am extremely grateful for this, and several other opportunities that Prof. Elbashir provided me.

My special thanks and gratitude goes to my committee co-chair, Professor Mahmoud El-Halwagi, who had provided invaluable guidance, support, and motivation throughout my Ph.D. course. Prof. El-Halwagi's guidance played an important and critical role in directing the activities of my thesis, and in development of the novel CARGEN™ technology. Prof. El-Halwagi also hosted me in college-station in his research team, which provided an excellent ecosystem for new Ph.D. students like me to learn and become a part of the system very quickly, and I am very grateful to him for all the support.

I would like to thank my committee members, Professor Stratos Pistikopoulos and Professor Ibrahim Galal Hassan, for their most valuable feedback and support during my Ph.D. study, which strengthened my work and made it more robust and comprehensive.

I would also like to thank Professor Benjamin Wilhite for his excellent mentorship and guidance on the Fischer Tropsch computational fluid dynamics (CFD) project. Working with him greatly helped me learn advanced CFD skills and allowed us to write three high impact factor peer-reviewed journal publications on Fischer Tropsch reaction, which is considered one of the most challenging heterogeneous chemical reaction.

I want to thank all the research members in Prof. Elbashir's group, especially Dr. Hanif A. Choudhury- who was instrumental in guiding and mentoring me on several experimental activities during my Ph.D. course. Dr. Choudhury's exceptional chemical engineering and chemistry background helped me in learning remarkable experimental and analytical skills. I am proud to mention that I had the opportunity of developing several novel concepts, proposals, patents, and papers with Dr. Choudhury. Our combined team efforts led to the development of five patents, three journal articles, and one book chapter. My special thanks goes to my colleagues and friends- Dr. Minhaj Ghouri, Mr. Anuj Prakash, Dr. Shaik Afzal, Dr. Anjaneyulu Chatla, Dr. Ziyan Sheriff, Mr. Raid Hassiba, Dr. Khaled Elsaid, Dr. Wubuliqasimo Yiming, Dr. Zafar Khan Ghouri, Mr. Gasim Ibrahim, Mr. Nasr Mohammed, Ms. Aya Abusrafa, Ms. Zeinab Ataya, Mr. Murtaza Khan, Mr. Marwan Elwahsh, and the entire TAMU family for always being there for me, and making it a memorable experience throughout my time at TAMU.

A very special thanks to my College Station friends in Prof. El-Halwagi's research group; Dr. Debalina Sengupta, Dr. Rajib Mukherjee, Dr. Marc Panu, Dr. Kevin Topolski, Dr. Hassan Baakeel, Mr. Abdulrahman Al Suhaibani, Ms. Jinyoung Choi, Ms. Erfika Maria, and others.

Finally, I thank my wife-Aasiya, my daughter-Iqra, my mother-Shirin, my father-Aziz, brothers- Abdulkarim and Saad, for their constant love and support motivation, and enthusiasm throughout my life.

CONTRIBUTORS AND FUNDING SOURCES

Contributors

This work was supervised by a dissertation committee consisting of Professor Nimir Elbashir [Chair], Professor Mahmoud El-Halwagi [Co-Chair], Professor Stratos Pistikopoulos [Member], and Professor Ibrahim Galal Hassan [Member].

I would like to thank Dr. Dingdi Wang and Professor Eric Weitz at Northwestern University for providing us with Raman Microscopy results from their experiments. I would like to thank Dr. Wubuliqasimo Yiming at the central materials laboratory for training me on Scanning Electron Microscopy (SEM), X-ray Diffraction (XRD), and X-ray Photoelectron Spectroscopy (XPS) equipment, and for providing the characterization of several materials developed in this work. I would also like to acknowledge Dr. Said Mansour of Qatar Environment and Energy Research Institute (QEERI) for providing us the transmission electron microscopy [TEM] results of various materials presented in this work.

All other work conducted for the dissertation was completed by the student independently.

Funding Sources

This work was supported by the Qatar National Research Fund (QNRF), a member of the Qatar Foundation. This work was also made possible in part by [NPRP-EP] under Grant Number [NPRP X - 100- 2 - 024]. Its contents are solely the responsibility of the author and do not necessarily represent the official views of the Qatar National Research Fund. The statements made herein are solely the responsibility of the author.

NOMENCLATURE

DRM	Dry reforming of methane
POX	Partial oxidation of methane
SRM	Steam reforming of methane
ATR	Autothermal reforming of methane
TRM	Tri-reforming of methane
CARGEN™	Carbon Generator technology
FT	Fischer Tropsch
TPR	Temperature Programmed Reduction
TPO	Temperature Programmed Oxidation
RGA	Residual Gas Analyzer
TGA	Thermogravimetric Analyzer
FTIR	Fourier Transform Infrared Spectroscopy
SEM	Scanning Electron Microscopy
TEM	Transmission Electron Microscopy
BET	Brunauer–Emmett–Teller
BJH	Barrett, Joyner, and Halenda
XRD	X-ray Diffractometer
XPS	X-ray Photoelectron Spectroscopy
MWCNT	Multi-Walled Carbon Nanotubes

TABLE OF CONTENTS

Page

LIST OF FIGURES

Page

LIST OF TABLES

Page

1. INTRODUCTION[1,2,3,4,5]

The global energy utilization trend has led to a significant rise in greenhouse gas emissions. Fossil fuels, such as crude oil, coal, and natural gas, form almost 80% of the current global energy supply. Although energy production from renewable sources, including solar, wind, and geothermal, is increasing, the overall dependence on fossil fuels has not changed significantly due to economic and technological challenges. However, a significant shift is forecasted in the dependence on cleaner fuels, such as natural gas and biomass fuel from crude oil and coal. Figure 1.1 elaborates this expected transition in the next three decades, in which the dependency on coal and oil is projected to decrease by 14%.

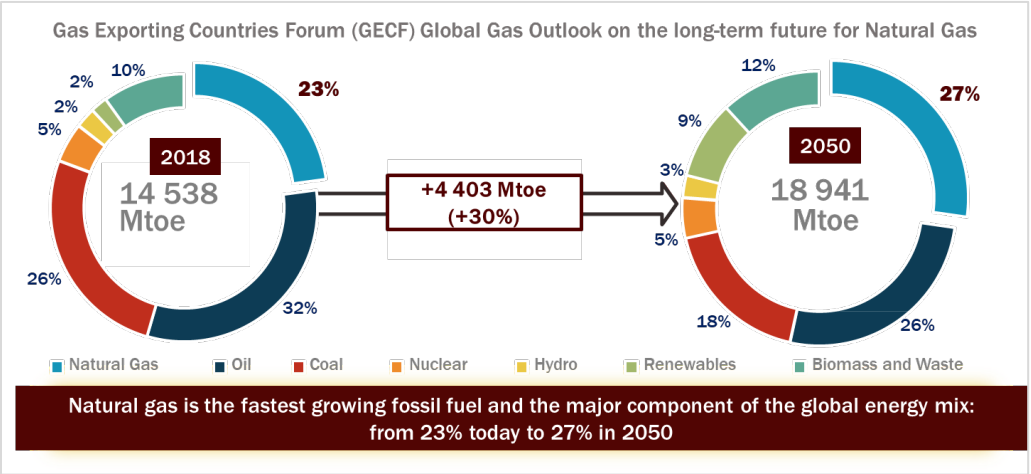

Figure 1.1 The Gas Exporting Countries Forum's gas outlook on natural gas utilization

A portion of this section has been published/submitted in:
[1]Advances in Carbon Management Technologies: Carbon Removal, Renewable and Nuclear Energy, Volume (2020): 253 Copyright 2020Taylor & Francis [114],
[2]Challiwala, M. S., et al. "Production of high-quality carbon nanotubes from natural gas and carbon dioxide using a novel CARGEN™ process", Chemical Engineering Progress, AIChE, Wiley, October 2020
[3]Challiwala, M.S., et al. "A novel CO2 utilization technology for the synergistic co-production of multi-walled carbon nanotubes and syngas", Scientific Reports, Nature, Accepted December 2020
[4]Challiwala, M. S., et al. "Method and Apparatus for producing Carbon black and Syngas from Carbon dioxide" – Provisional patent. US Patent WO2018187213A1, October 2018.
[5]Challiwala, M. S., et al. "Catalysts for CARGEN™, methods of preparing, and uses of same", Provisional Application Number (62/949,133), Disclosure submitted on: 6 November 2019

The discovery of extensive amounts of recoverable natural gas in several non-associated wells in the Middle East and shale deposits in the United States has led to a steep rise in global natural gas production. More importantly, the commitment set forth by global economies to limit the temperature rise to 2^{o} C above the pre-industrial era in the Paris agreement has further bolstered the shift toward natural gas as a cleaner fossil fuel alternative. Natural gas is considered to be relatively cleaner since it emits the lowest amount of carbon dioxide (CO_2; compared to other fossil fuels) to produce the same amount of energy. Currently, Russia possesses the most considerable fraction of the world's proven natural gas reserves, with approximately 1,688 trillion cubic feet (tcf), followed by Iran (1,187 tcf), Qatar (~890 tcf), the United States (~388 tcf), and others.[1] Qatar is the sixth-largest producer of natural gas and has demonstrated a success story in monetizing its natural gas wealth in terms of liquefied natural gas (LNG), synthetic fuels, and petrochemical products.

Natural gas reforming is the first step in a typical gas-to-liquid (GTL) process that produces synthetic fuels and chemicals. In this reaction, natural gas is oxidized utilizing steam, oxygen, or their combination to produce synthesis gas (syngas), which is a mixture of carbon monoxide and hydrogen. Furthermore, syngas is an important precursor needed for the production of ultra-clean fuels and value-added chemicals. Natural gas reforming is known to consume up to 50-70% of the overall energy needs of GTL plants. Therefore, immense scientific efforts are underway to improve its energy efficiency and CO_2 emissions.

The specific focus of this dissertation is on the dry reforming of methane process (DRM), which is an alternative reforming model that utilizes CO_2 and methane (CH_4) to produce syngas. DRM has gained considerable scientific attention due to its inherent ability to convert two greenhouse gases (CO_2 and CH_4). Therefore, via DRM, it is possible to re-insert the greenhouse gases into the energy cycle for reuse. However, DRM processes faces several challenges that must be addressed before its commercial implementation. This thesis work is dedicated to the development of a novel, technological solution that addresses the inherent process limitations of DRM to make its commercial implementation a possibility.

A clear outline of the various topics that are discussed in this introduction is presented below.

(Section 1.1) *The global energy perspective* describes the trend in global energy utilization, the major players in the energy market, the importance and significance of natural gas as a highly efficient and clean energy fuel, the CO_2 emission challenge, and the various technological advancements that are available for efficient CO_2 conversion.

(Section 1.2) *Natural gas reforming: background and history* describes the various natural gas reforming processes, their importance, and the various stages in which the advancements occurred in this field.

(Section 1.3) *CO_2 as a part of natural gas reforming* describes the various methods by which CO_2 could be utilized in the natural gas reforming processes as well as its critical role therein. The specific focus is on DRM, its significance, and challenges that limit its commercial applicability.

(Section 1.4) *Addressing carbon formation challenges in DRM via novel process design* describes the plausible reaction pathways that lead to carbon formation and the literature advancements, specifically in the field of catalysis, that enable elimination of carbon during the reforming process.

1.1 The global energy perspective

Energy derived from fossil fuels forms almost 80% of global energy distribution, which is in the following order: crude oil (31%), coal (25%), and natural gas (25%). The ever-increasing rate of energy utilization has led to an un-compensatory rise in CO_2 emissions. Natural gas is the cleanest and arguably the most abundant form of fossil fuel available today. In addition to being an attractive research topic, natural gas' simplistic nature provides a plethora of conversion possibilities already known to humankind.[2] According to a 2019 statistic, the United States ranks first globally in natural gas production (21.4 %), followed by Russia (17.8%), Iran (5.1%), and Qatar (2-3%). Figure 1.2 provides a graphical mapping of the production of top ten natural gas producing countries in billion cubic meters (bcm) as per 2019 Enerdata statistic[3].

Middle eastern countries like Qatar and Iran enjoy the benefit of owning the world's largest single-point, non-associated natural gas offshore field, which makes production inexpensive—due both to the capacity available and to the access to the latest technology from global energy corporations. Iran is not able to benefit from such an advantage due to decades-long economic sanctions. However, Qatar has fairly benefitted from its natural gas wealth and has recently announced a 64% increase in its LNG production capacity

that it expects to be essential to meet the increasing global natural gas demands. [4] Qatar Petroleum, the state-run energy company, has successfully formed joint-venture oil and gas businesses with companies including Shell, Sasol, Total, Exxon Mobil, and Chevron that make it an influential energy producer. The recent discovery of shale gas in the United States has led to a significant boom in exploration, production, and investment opportunities, which has decreased the price of energy considerably. The transition in the United States was so drastic that the gas importing ports are now being converted into exporting ports, demonstrating the exponential increase in the production capacity. However, the stranded nature of shale gas makes its production far more expensive than natural gas.[5] Nevertheless, the availability of several monetization opportunities, access to the latest fracking technologies, and high local demand has allowed shale gas to remain a lucrative option. The ready conversion of natural or shale gas into hydrocarbon fuels via the Fischer-Tropsch (FT) process indicates that natural gas has significant demand in the downstream chemical industry in general. Among several applications of natural gas, the critical examples are (i) precursors for the downstream chemical industry and premium products, (ii) LNG production, (i) power generation, (ii) hydrogen production, and (iii) production of natural gas liquids. [6]

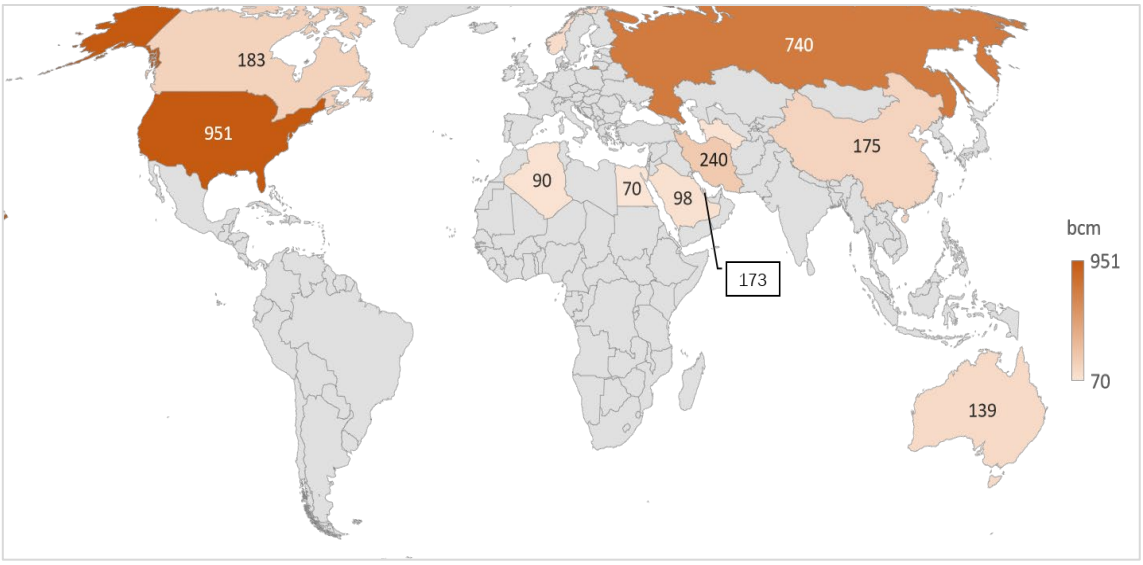

Figure 1.2 Graphical mapping of the top 10production countries in the world as per 2019 statistic[3]

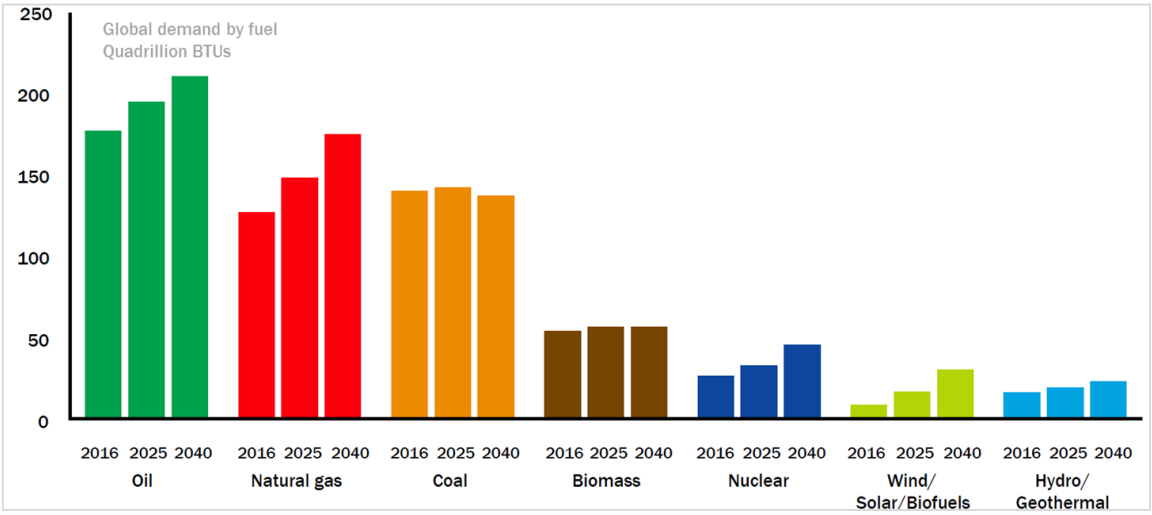

Figure 1.3 A snapshot of Exxon Mobil's 2018 world energy outlook[1]

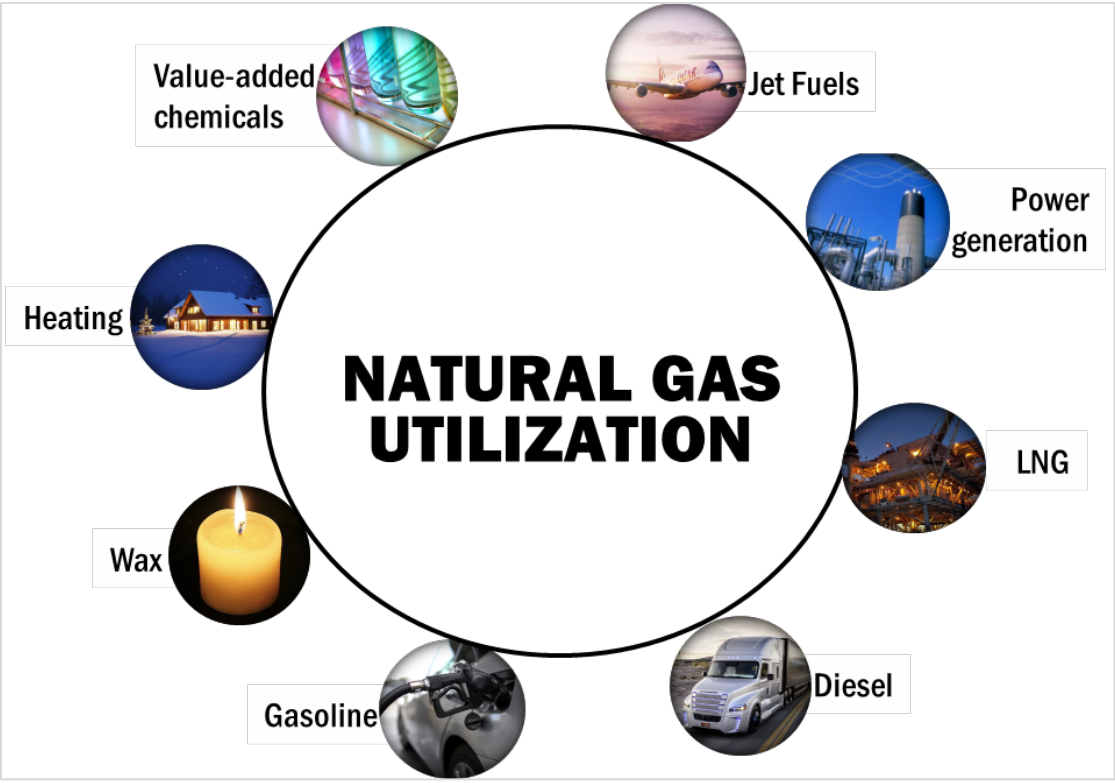

Figure 1.4 Natural gas utilization to produce several products

CO_2 is the prime gaseous emission from all the chemical industries and is the main reason for global warming. The CO_2 Information Analysis Center (CDIAC) report of 2014 showed that more than 400 billion tons of CO_2 emissions occurred due to fossil fuel consumption and the production of cement since 1751[7]. About half of this value was emitted since the 1980 s only which shows a rapid increase in dependency on fossil fuels. Figure 1.5 shows that liquid and solid fossil combustion causes ca. three fourths of overall CO_2 emissions, which is about 9.9 billion tons in 2014. The report also shows that the emissions caused cement production is at least 5.8 percent of the overall in 2014[7]. Another study showed that the energy sector produces approximately two-thirds of total

anthropogenic greenhouse gases, of which CO_2 comprises approximately 80%[8]. Approximately 8-18% of the natural gas produced from oil and gas fields is CO_2, which is directly flared.[8] The flue gas from any chemical plant in general forms approximately 10% CO_2.[9] There are countless other sources of CO_2 emissions that cannot be ultimately captured, including those from transport vehicles, airplanes, biomass processing, and landfills. However, the primary sources mentioned above provide an excellent opportunity for CO_2 capture and utilization.

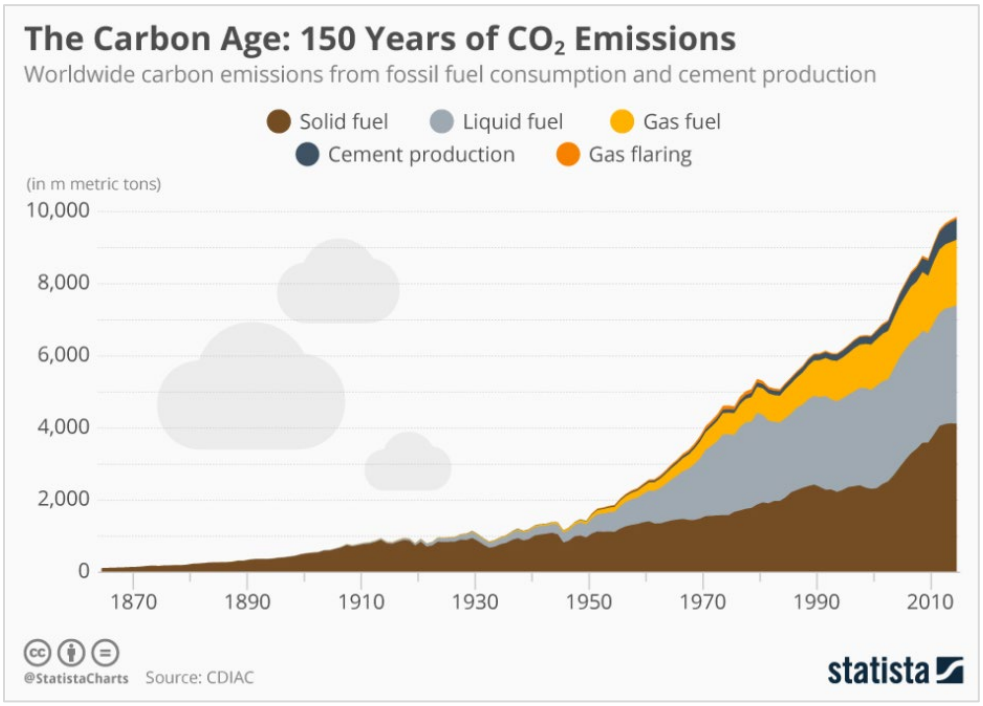

Figure 1.5 Report on the historical carbon dioxide emissions from various sectors[7]

For a country such as Qatar, where all the sources are localized in an industrial city, the capture of CO_2 becomes easier due to the close proximity and density of CO_2 in each of the point sources. In particular, a simple calculation on the total capacity of Qatargas' current 14 midstream gas processing trains reveals that at least approximately 7,000 tons

of CO_2/day is available in almost pure form (as shown in Figure 1.6), which provides an excellent opportunity for quick capture and conversion.

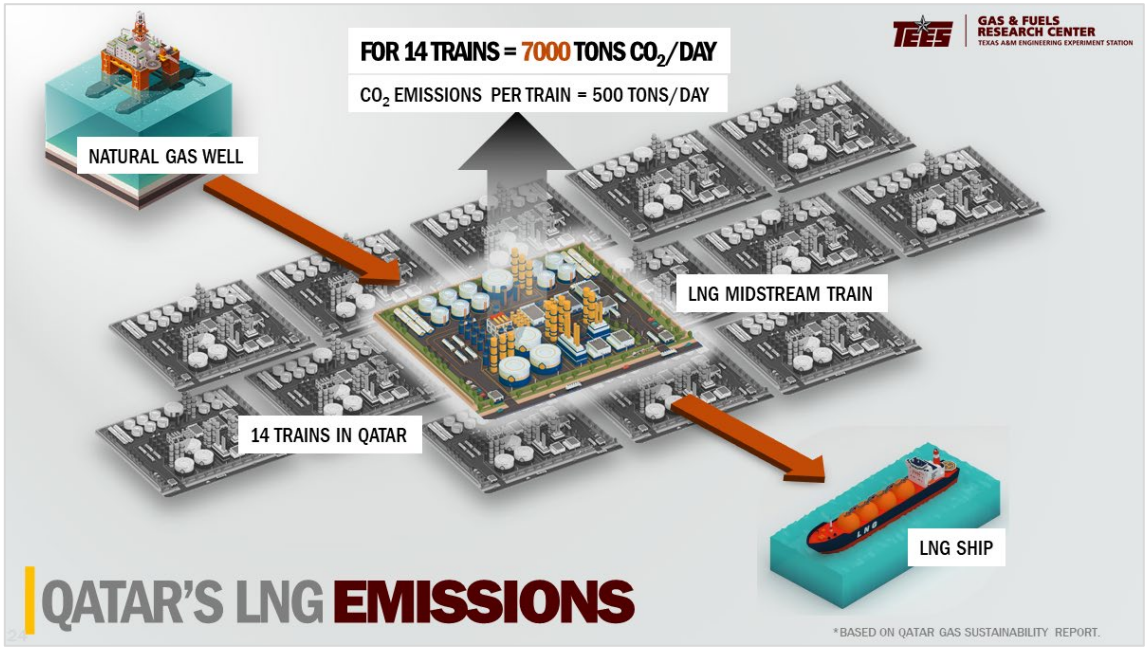

Figure 1.6 An estimation of total point CO_2 emissions from Qatar's LNG process trains; adopted from Qatargas' sustainability report[10]

New opportunities to utilize CO_2 in the development of products and services have captured the attention of governments, industries, and the investment community. Addressing climate change has become the primary driver for this heightened interest; however, other factors, such as technology leadership and circular economies, have become profoundly consequential.[11] Some of the recent topics of research in the area of CO_2 utilization are (i) methanol synthesis, (ii) oxidative coupling with methane, (iii) oxychlorination, (iv) production of chemicals and oxygenates via co-reaction with hydrocarbons, and (v) DRM to produce syngas, among others. [9,11] However, since the majority of these conversion processes require a considerable amount of energy, which is

primarily derived from fossil fuels, all the processes become net CO_2 producers. Therefore, the concept of CO_2 fixation is essential; it is typically evaluated utilizing lifecycle assessment (LCA) calculations that account for the CO_2 footprint at each step of the process.

1.2 Natural gas reforming: background and history

Reforming methane is a crucial step to produce a valuable chemical precursor syngas, which is a mixture of carbon monoxide and hydrogen that is an essential intermediate to produce a broad range of value-added chemicals (i.e., methanol, acetic acid, dimethyl ether, etc.) in addition to ultra-clean fuels via FT technology.[12–16] Commercially, reforming methane is performed via three well-known technologies: steam reforming of methane (SRM), partial oxidation of methane (POX), and autothermal reforming (ATR). All the reforming technologies utilize oxidants to convert methane to syngas chemically. Figures 1.6 and 1.7 illustrate the key difference between the aforementioned reforming processes. For instance, SRM utilizes steam at high pressure, while POX utilizes oxygen to produce syngas. ATR utilizes a combination of both steam and oxygen in a specific ratio that yields a syngas ratio that is compatible with downstream FT reactions while allowing the reaction to occur under autothermal temperature conditions. The autothermal condition signifies a temperature point wherein no external heat is required to drive the reaction. In other words, the reaction produces enough energy in-situ to drive itself spontaneously. The chemical equations below summarize the stoichiometric reactions and

associated energy requirements for SRM (Eq. 1.1), POX (Eq. 1.2), and ATR (Eq. 1.3-1.5) reactions:

SRM:

$$CH_4 + H_2O \rightarrow 2H_2 + CO \qquad \Delta H_{298K} = 206\ kJ/mol \qquad (1.1)$$

POX:

$$CH_4 + \frac{1}{2}O_2 \rightarrow 2H_2 + CO \qquad \Delta H_{298K} = -36\ kJ/mol \qquad (1.2)$$

ATR:

$$CH_4 + 1\frac{1}{2}O_2 \rightarrow CO + 2H_2O \qquad \Delta H_{298K} = -520 kJ/mol \qquad (1.3)$$

$$CH_4 + H_2O \rightarrow CO + 3H_2 \qquad \Delta H_{298K} = 206\ kJ/mol \qquad (1.4)$$

$$CO + H_2O \rightarrow CO_2 + H_2 \qquad \Delta H_{298K} = -41\ kJ/mol \qquad (1.5)$$

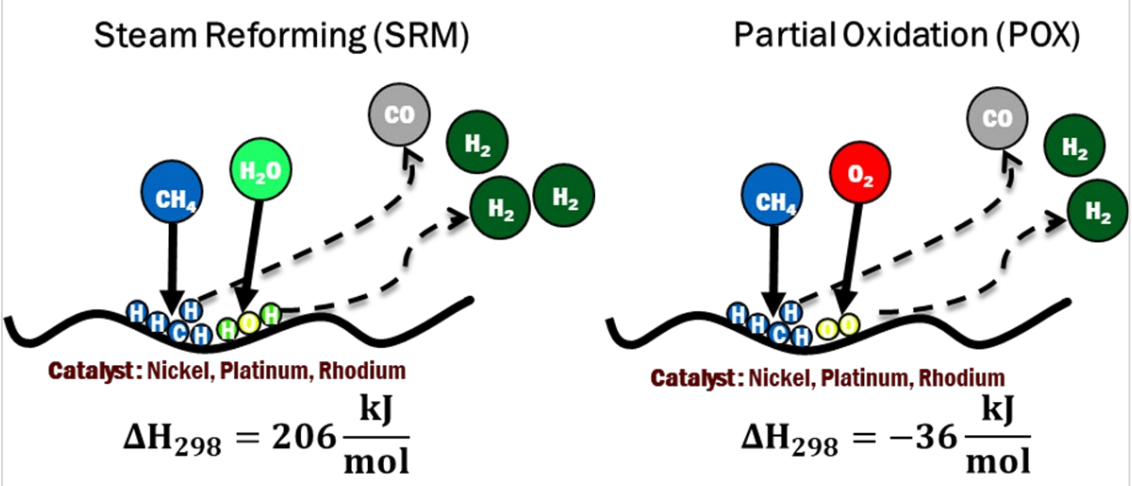

Figure 1.7 An illustration of SRM and POX chemistry

First introduced in the 1930 s, [17] SRM technology was implemented on a small scale and was limited to few locations in the United States, where accessibility to natural gas was simple. The significant development of this technology occurred in the 1960 s when ICI

opened two reforming plants utilizing tubular reactors at high-pressure conditions with naphtha as the primary feedstock.[18] However, almost a decade before ICI established their facility, Haldor Topsoe had designed the first reforming and hydrogen plant based on the SRM technology at 40bar pressure.[18] The primary utilization of syngas from SRM was for hydrogen production for ammonia, which is a starting material for urea fertilizer. The implementation of Haldor Topsoe's technology had significantly reduced the energy demands of the ammonia plants and had resulted in significant cost savings.[19] Further energy reductions were realized when MW Kelloggs built integrated reforming plants, combining SRM with steam turbines. As naphtha was the primary feedstock in Europe, the steam reforming of naphtha became a crucial technology in building the town gas industry of the United Kingdom, which consequently replaced erstwhile low-pressure gasification processes. Apart from the technologies of ICI and Topsoe,[18] SRM at low temperatures under adiabatic conditions, which was pioneered by British Gas, served as an attractive option to produce methane-rich gas for heating and other utility purposes.[20] Later, the focus of SRM shifted to methanol, acetic acid synthesis, and other oxo-alcohols in addition to ammonia production.[21] The low-temperature reforming process developed by British Gas was an essential pathway for the conversion of naphtha to methane during the energy crisis of the 1970 s. The application of SRM was not limited to the production of hydrogen, methanol, and other petrochemicals but was also utilized in the iron and steel industry for direct reduction of iron ore.[20,22] The trend in the 1990 s was primarily toward the hydrocracking of heavy hydrocarbons to produce gasoline in refineries.[23] The later part of 1990 s and early 2000 s saw considerable demand on hydrogen production from

SRM for two main reasons: (a) the availability of cheap natural or shale gas and (b) the boom in fuel cell technology and refineries around the globe. Although renewable technologies, such as wind, solar, biofuels, and other alternative technologies, have drawn significant attention in the 2000 s, the dependency on SRM for hydrogen production has not declined.[23]

The predominant challenge associated with SRM since its inception has been its inherent ability to produce solid carbon at low steam-to-carbon ratios. This challenge was addressed by operations at high temperatures (> 1000° C) and under the presence of large quantities of steam. The presence of such a quantity of steam, however, led to lower conversions and resulted in a significant increase in energy costs. Nevertheless, the utilization of SRM has not lost popularity throughout its existence. Another less commonly adopted method of carbon reduction was to passivate it with sulfur;[24] this, however, resulted in the contamination of products, leading to issues in downstream FT and other synthesis processes. Noble metals such as Pt and Rh additionally provided an alternative catalytic system to Ni, but were economically less viable options for reducing the coking tendency of the SRM reaction.[25]

1.3 Dry Reforming of Methane

In the later 1970 s, CO_2 utilization as a part of SRM provided an attractive pathway for stabilizing the syngas ratio of the SRM product.[26,27] However, similar to SRM, the possibility of carbon formation in the combined reaction was significantly high, which had long been a crucial factor limiting the application of this reaction on a standalone basis.

However, the presence of CO_2 in SRM continued to be necessary to adjust the quality of syngas for downstream applications, such as FT and methanol synthesis reactions that require an H_2:CO ratio of 2:1. The introduction of ATR technology further provided an attractive yet expensive pathway to alleviate the coking tendency in SRM since its inception in the early 1980 s.[26,27] In addition to the SRM process, POX is a well-known and established technology that has been utilized since the 1940 s; [28] it is a relatively simple reaction compared to SRM and DRM, as it typically represents the partial combustion of methane. The challenge with this reaction is the cost associated with the production of pure oxygen. However, the benefit is that the reaction could be conducted under homogenous conditions at high temperatures without the need for a catalyst. Low-temperature operations require a catalyst and result in lower energy requirements compared to high-temperature homogeneous reactions. Additionally, such a reaction could be beneficial in generating high-pressure steam, as the combustion process is highly exothermic. In 2007, Shell built the world's largest GTL plant—the Pearl GTL Plant in Ras Laffan, Qatar. The plant utilizes POX reforming technology to produce syngas and has the world's largest air separation unit for oxygen generation. Due to the benefit of the economy of scale, the syngas production by POX at a large scale (the syncrude plant has a 140,000bbl/day capacity) is reportedly cheaper compared to smaller-scale plants.[29] A combination of POX and SRM in the form of ATR has also gained significant traction recently. A joint venture between Sasol and Qatar Petroleum built a state-of-the-art GTL facility, the ORYX GTL plant, also in Ras Laffan, Qatar, utilizing ATR technology. The capacity of this plant is approximately 35,000bbl/day of syncrude products, which

primarily comprise diesel and naphtha. Against this backdrop, the DRM process becomes vital to consider since it can produce syngas by utilizing CO_2 as the oxidant, as illustrated in Eq. 1.6. Since CO_2 is abundantly available in the flue gas streams (albeit at lower concentrations), it is anticipated that employing it will reduce the operating costs and carbon footprint of syngas production.

DRM mainly utilizes CO_2 as a soft oxidant to reform methane, as portrayed in Eq. 1.6:

$$CH_4 + CO_2 \rightarrow 2H_2 + 2CO \qquad \Delta H_{298K} = 247\ \text{kJ/mol} \qquad (1.6)$$

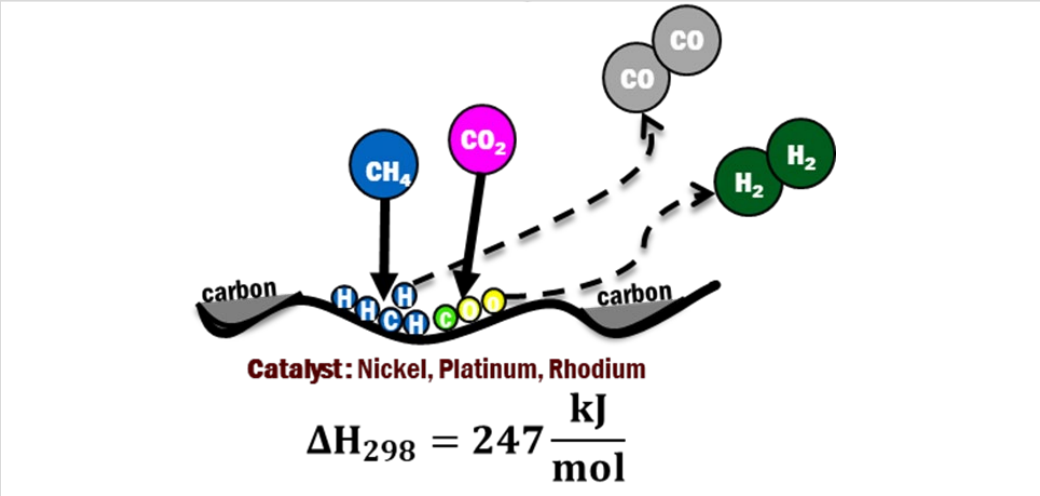

Figure 1.8 An illustration of DRM chemistry

As stated previously, the major challenges associated with DRM are its significant coking tendency that affects the catalyst performance, its increased endothermic properties over SRM, and its production of low-quality syngas (H_2:CO ratio of 1:1). The syngas ratio is particularly important, as only a specific quality is desirable for downstream applications. For instance, for FT reaction and methanol synthesis, a syngas ratio of 2:1 is acceptable.

Due to the reverse water-gas shift reaction (RWGSR) activity at high temperatures, the H_2:CO ratio becomes even lower than 1:1.

Additionally, the energy demand to drive the reaction is high; it requires approximately 1.2 times more energy than the endothermic SRM process. The CO_2 that evolves from combusting methane or other fossil fuels to drive this reaction can significantly increase the carbon footprint of the DRM process. Nevertheless, if the reaction-required heat can be generated by other renewable sources of energy, such as solar energy or from excess heat from other parts of the plant, then the CO_2 fixation can be achieved.

Carbon formation in the DRM process generally occurs via the following pathways:

Methane Decomposition:

$$CH_4 \rightarrow 2H_2 + C \tag{1.7}$$

Boudouard Reaction:

$$2CO \rightarrow C + CO_2 \tag{1.8}$$

The reactions above (methane decomposition and Boudouard reaction) are highly active at low-temperature conditions (400° C to 650° C), while at high temperatures (≥ 750° C), the rate of primary reforming reactions is considerably higher, resulting in significantly low carbon formation. The other problem with carbon formation in this scenario is that it physically damages the catalyst bed and the reactor tube, which either require serious maintenance or complete replacement of the tube. Due to these three limitations, DRM is still considered to be a gray area that requires further investigation.

The literature suggests that the issues related to the practical implementations of DRM should be addressed by synergistically combining DRM, SRM, and POX reforming into

a tri-reforming of methane (TRM) process. [30–32] Noureldin et al.[32] report the comparison between the three reforming techniques in terms of their syngas quality, energy requirements, and operating conditions. They suggest the combined operation of these reforming techniques with their potential benefits in view of CO_2 fixation. The same authors in a later study[33] also present a realistic quantification of the CO_2 fixation utilizing the DRM process via integration of the conventional reforming technologies. They further highlight the critical tradeoffs between the CO_2 chemical fixation and its effect on the syngas yield ratio. Similarly, Jonas et al. [34] present a comparative study of five alternative TRM routes that compete with the DRM process on an annual total cost basis, and they demonstrate that the DRM-SRM process requires minimum total annual cost. Luyben et al. [34] report a practical dynamic modeling study highlighting the major tradeoff that could be expected during standalone operations of the DRM process. Özkara-Aydınoğlu et al.[30] analyzed different operating scenarios of the combined DRM-SRM process by tuning the reforming feed mole ratio and report that the activity of the methane and the H_2:CO yield ratio increases considerably upon the addition of steam to DRM. Zhang et al. [35] studied the effect of varying the feed mole ratio on the product distribution and propose an optimum feed ratio (CH_4:CO_2:H_2O:O_2 = 1:0.291:0.576:0.088) to maximize H_2 yield and CO_2 conversion while maintaining a desirable H_2:CO yield ratio for the downstream methanol synthesis. Chein et al. [36] performed a thermodynamic study of the effect of the addition of inert gas on the product distribution of the DRM process and report that the reactant conversion drops significantly due to the presence of inert gases. They additionally studied the combined performance of DRM-POX and DRM-SRM bi-

reforming processes targeted to suppress carbon formation in a single DRM process. Amin et al. [37] report an optimum feed mole ratio (CO_2:CH_4:O_2 = 1:1:0.1) that reduces the reforming temperature while maximizing H_2 yield and CO_2 conversions. A thermodynamic analysis was also performed by Nematollahi et al., [31] and they report that pressure has an inverse effect on methane conversion in combined DRM-POX reforming of methane. Nikoo et al. [38] conducted a similar analysis of carbon formation in a DRM process, and they observe that high-pressure operations suppress the effect of high temperatures on reactant conversions, resulting in increased carbon formation. They also compared the experimental and thermodynamically calculated results to study the differences between the real and thermodynamic equilibrium profiles in a DRM process.

As seen from these previous studies, the parameters that control the operation of the TRM process are not only temperature and pressure conditions, but also the feed mole ratios.[39–42] In this study, we have taken a base case scenario of CH_4:H_2O:O_2:CO_2 with a feed ratio of 1:0.6:0.1:0.6. This ratio can be approximated to the flue gas composition, which can potentially act as a possible feed to the TRM reactor.[43]

The challenge related to carbon formation is hypothesized to be addressed in one of the two following ways: (a) by introducing either steam, oxygen, or both in the feed (i.e., replacing DRM with a TRM process) or (b) by developing novel catalysts that can either work effectively in a carbon environment or resist the formation of carbon layers on its surface. Choudhury et al.[44] report a rare-earth element catalyst—comprising a Neodymium (Nd)/Cobalt (Co) base—that could prevent itself from carbon deposition. Later, the same authors demonstrate the utility of this catalyst for TRM at different process

conditions.[44] The effect of the addition of oxygen to reduce carbon formation is reported by Song et al., [43] who were among the first to perform an experimental study on the TRM process. They utilized flue gas samples as a feed to the TRM process and observed that carbon formation occurs in relatively lower quantities compared to the DRM process. A similar study was conducted by Lee et al., [45] the objective of which was to produce syngas for DME synthesis. They observe that carbon deposition could be suppressed by utilizing carbon-resistant catalysts and by introducing oxidants such as steam and oxygen in the DRM process. More recently, syngas production for FT utilizing the TRM process has gained attention, owing to the many advantages this process offers compared to the conventional reforming processes.

Much of the research work previously considered the reaction mixture at the reforming operating conditions to be ideal.[31,32,36,46] However, non-ideality could be expected due to the high-pressure and high-temperature conditions. In this work, the effect of non-ideality in the reaction mixture has been accounted for by incorporating the fugacity coefficients, which were calculated utilizing the Redlich-Kwong, Soave-Redlich-Kwong, and Peng-Robinson equations of state.

One of the predominant shortcomings of DRM is related to the significant energy requirements associated with this process, the costs of which directly influence the overall GTL product cost. Minimizing this cost could present an opportunity to lower the costs of GTL technology. A precise analysis regarding the energy requirement assessment is inevitable to overcome this limitation. While there are numerous studies, both experimental and modeling, reported in the literature that address carbon deposition and

the low syngas quality of DRM products, only Noureldin et al. [32] address the energy requirements for this technology. An extensive energy analysis is integral to this work, and the amount of energy required to sustain various process conditions is utilized as a significant criterion to comment on the merit of said conditions. All the results of this analysis are discussed in detail in Section 3.

1.4 Addressing the carbon formation challenge in DRM via novel process design

As presented in the previous discussion (Section 1.2), carbon formation is one of the foremost challenges in the DRM process. There are two plausible pathways for this, as illustrated below:

Route 1: mechanism for carbon formation from methane:

$$CH_4(s) \rightarrow CH_x(s) + (4 - x)H(s) \quad (1.9)$$

$$CH_x(s) \rightarrow C(s) + xH(s) \quad (1.10)$$

$$H(s) + H(s) \rightarrow H_2(g) \quad (1.11)$$

Route 2: carbon formation from carbon dioxide

$$CO_2(g) \leftrightarrow CO(s) + O(s) \quad (1.12)$$

$$CO(s) \leftrightarrow C(s) + O(s) \quad (1.13)$$

$$O(s) + O(s) \leftrightarrow O_2(g) \quad (1.14)$$

$$O(s) + H(s) + H(s) \leftrightarrow H_2O(g) \quad (1.15)$$

As can be seen from these pathways, carbon formation occurs with both methane and carbon dioxide. Several previous studies suggest that the activation energy for methane

decomposition (Route 1) is considerably lower than that of carbon dioxide decomposition (Route 2). Therefore, it should be expected that the extent of conversion via Route 1 will be more than that of Route 2. Nevertheless, it is also known that the feasibility of WGSR is relatively significant at reforming temperature conditions. Therefore, the reaction of hydrogen produced by methane decomposition with carbon dioxide to form water and carbon monoxide is also feasible. The conversion of carbon monoxide, formed via WGSR and a DRM reaction, will lead to the initiation of a secondary dominant reaction of CO disproportionation, also called a Boudouard reaction. Along with Eqs. 1.7 and 1.8, the following reaction set provides a systematic understanding:

$$2H_2 + 2CO_2 \leftrightarrow 2CO + 2H_2O \quad (1.16)$$

The overall reaction therefore becomes the following (including reactions 1.7 and 1.8):

$$CH_4 + CO_2 \rightarrow 2C + 2H_2O \quad (1.17)$$

The reaction mentioned (Eq. 1.17) is therefore hypothesized to be the dominant reaction to the DRM reaction (Eq. 1.6). The selectivity toward a particular product is directly related to the operational conditions as well as the choice of the catalyst. Therefore, the design of the reaction system that handles carbon formation, selection of operational conditions, and choice of catalyst will be the key parameters that influence the formation of carbon.

Designing novel carbon-resistant catalyst material has been a prominent approach in mitigating the carbon formation challenges. Some of the noble metal catalysts, such as platinum, rhodium, and ruthenium, have indicated more significant activity toward DRM reactions with suitable resistance to carbon formation than the conventionally utilized

transition metals[47–51] but are prohibitively expensive. Promoting cheaper reforming catalysts, such as nickel, with the aforementioned noble metals has also been demonstrated to be a promising approach to reduce the carbon formation tendencies of DRM,[52–55] making its implementation economically feasible. Some of the bi-metallic systems, such as Ni-Pt supported on zirconia,[56] have also demonstrated potential. In other examples, the presence of rhodium in the nickel system has been proven to help nickel retain its metallic form by reducing hydrogen spill-over, which eventually aids in prolonged activity and reduces carbon formation. [54] In a similar work, the role of palladium in reducing nickel reoxidation is presented,[52] wherein the authors compared the activity of the Ni-Pd system with a monometallic nickel system. Several other catalysis works are dedicated to studying the role of support on the catalyst activity [56–58] with a goal of reducing carbon formation. Yet another approach is to study the role of catalyst synthesis procedures on DRM activity and carbon formation. One such work by Stagg et al. [59] indicates that the activity of a strontium-promoted Pt-ZrO_2 and Pt-SiO_2 catalyst is higher when it is synthesized via reductive deposition compared to co-impregnation. The authors[59] attribute this effect to the Sn-Pt alloy formation. Another study reveals that the co-impregnation technique of catalyst synthesis leads to a closer interaction of Pt and Ce in the Ce-Pt-ZrO_2 system, which increases the oxygen storage property of the catalyst, increasing its resistance to carbon formation as opposed to a sequential impregnation technique. All of these approaches revolve around the core topic of catalysis and its impact on DRM carbon formation.

Although significant advancements have occurred in catalysis of the DRM process, relatively less work has been observed in the field of process systems engineering (PSE) and process design.[60–67] The recommendation from the majority of the cited literature is to conduct the DRM reaction at high temperatures to avoid a carbon-forming regime. However, insights from industrial observations suggest that carbon formation happens, regardless of efforts to eliminate it, at the entrance and exit of the reactor tube due to the presence of lower temperatures at these points. This is a significant challenge in existing industrial reforming since the goal is to produce syngas or hydrogen rather than solid carbon. However, if the target to produce syngas is changed to co-produce solid carbon, then the design of the reactor must be significantly modified to overcome the process challenges that arise with such an adjustment. Although solid carbon production is not new to the process industry, its co-production from the reforming process is a novelty. From an LCA viewpoint, such a process would enable a significant reduction in the CO_2 footprint, as it leads to the capture of carbon dioxide as a solid and stable product.

This dissertation's central objective is to identify a technological solution that simultaneously addresses the following three process challenges of the DRM:

- Catalyst deactivation by carbon formation
- Significant energy requirements that lead to more CO_2 than fixated by DRM
- Syngas quality that does not directly meet downstream process requirements

A combined PSE, catalysis, and reaction engineering approach is adopted to address these challenges. The culmination of the results in this work has enabled the development of a novel and modified DRM process, known as CARGEN™ technology. As depicted in

Figure 1, this technology is an integrated process of two distinct reactors—a CARbon GENerator reactor (CARGEN™ reactor) and a tri-reforming reactor—operating in series to convert CO_2 simultaneously to (a) carbon material (Reactor 1) and (b) syngas (Reactor 2 [Reforming]). A detailed thermodynamic assessment has demonstrated that CARGEN™ technology operates at 50% lower energy and provides at least 65% CO_2 conversion per pass compared to the stand-alone DRM. An LCA of the CARGEN™ technology demonstrates a reduction of the net operating costs and the CO_2 emissions by 40% compared to the benchmark technologies.

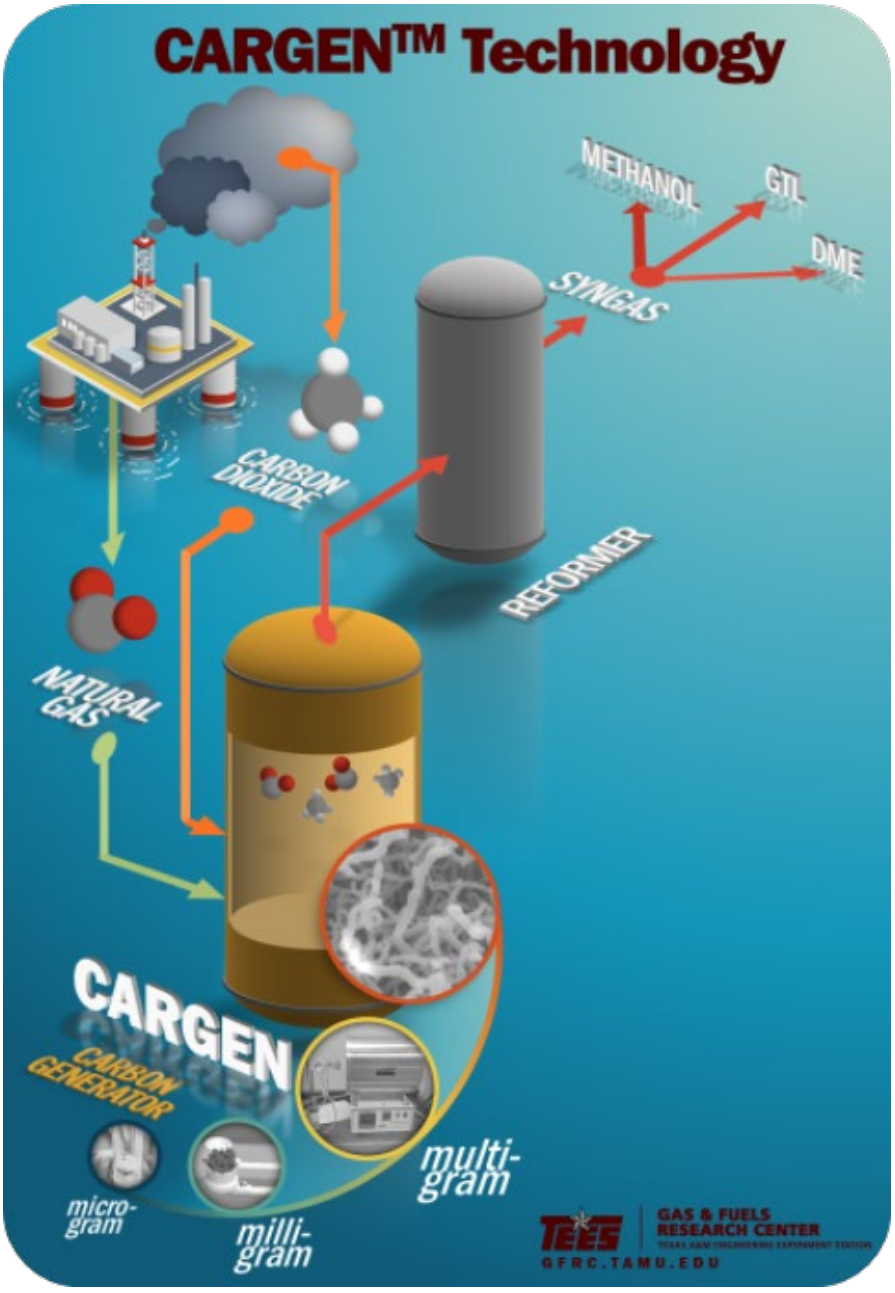

Figure 1.9 A schematic overview of the novel CARGEN™ technology developed in this work

Moreover, the experimental work has proven the concept of CARGEN™ technology and showcases that this technology produces one of the highest qualities of carbon material:

multiwalled carbon nanotubes. Furthermore, this dissertation provides a scalability study from micrograms to milligrams to multigram of carbon nanotube production. These results are confirmed via various state-of-the-art characterization studies, including scanning electron microscopy, transmission electron microscopy, x-ray photoelectron spectroscopy, x-ray diffraction, Raman analysis, and thermogravimetric analysis.

Finally, a preliminary techno-economic assessment indicates that, for a country such as Qatar, where the CO_2 is available in vast quantities, there is potential to produce 1,800 tons/day of multiwalled carbon nanotubes and approximately 26,000bbl/day of gasoline-equivalent syngas. Accounting for capital and operating calculations reveals the potential to reduce the carbon nanotube material's net cost by at least 50 times compared to the current market price of 500 to $10,000/kg.

These combined results from PSE, catalysis, reaction engineering, and techno-economics prove that CARGEN™ is a promising and commercially applicable future CO_2 conversion technology.

2. PROBLEM STATEMENT AND OUTLINE

Conversion of greenhouse gases (CO_2 and CH_4) to syngas via the DRM process is a topic receiving significant scientific interest. However, its successful commercial implementation requires overcoming several inherent process limitations, as highlighted previously. The first challenge relates to the syngas quality that does not meet most of the downstream process requirements. For instance, the downstream plants like FT or methanol synthesis require an H_2/CO ratio of 2:1, which cannot be fulfilled by the 1:1 ratio produced by DRM. Among several previous works, a study by Olah et al. 2013[68] reported a bi-reforming concept over NiO/MgO catalysts that produces a 2:1 syngas ratio. However, such a combination is energetically unsustainable and results in significant indirect CO_2 emissions. In this regard, LCA studies present a promising technique in evaluating the net CO_2 fixation[69]. The second challenge of carbon formation is also addressed via the invention of superior catalytic systems that showcase remarkable resistance towards carbon formation and sintering [70–78]. However, the third challenge of high energy requirement remains, and is suggested to be addressed via energy from renewable sources[79–82]. Thermodynamically, it has been proven that all the process challenges of DRM cannot be addressed simultaneously, as they have optimal points at different conditions. In other words, e.g., carbon formation is significantly reduced at high-temperature conditions, at which energy requirements are high. This is also true for syngas ratio and conversion, in which case, low temperature favors high syngas ratio, but at these conditions, conversions are low.

Another, and a consequent challenge relates to the scalability of the process, which is imminent for building a commercial-scale plant. Since DRM technology is still at a technology readiness level of 4-6[83], scalability testing at a larger capacity would be a goal for future studies once the said DRM process challenges have been satisfactorily addressed.

More details on each of the DRM process challenge are presented below:

1. Carbon formation challenge that leads to rapid catalyst deactivation

The main side reaction in a DRM process is the formation of solid carbon that deactivates the DRM catalyst and leads to frequent shut-downs and significant variation in the product syngas quality over time. Due to the formation of solid carbon, the selectivity of the catalyst is also affected, which leads to the change in the resulting syngas ratio (H_2: CO). Since the downstream process facilities are pegged at a fixed syngas ratio, variation in the syngas quality would lead to undesirable effects.

2. High energy requirements

Since the purpose of the DRM process is to utilize CO_2, the equivalent CO_2 emission due to the endothermic energy of the DRM process should be either less than or equal to the total CO_2 converted from DRM. On a standalone basis, to eliminate carbon formation, high-temperature operations are desirable, however, such conditions lead to a significant increase in the CO_2 emissions if the source of energy is from fossil fuel. Therefore, it is required to find a technological solution that will reduce the operating temperature of DRM, so that less energy is required to drive the DRM process.

3. Syngas ratio

In general, the application of syngas in the industry is to produce liquid hydrocarbons via the FT process, or to produce methanol and other value-added chemicals. For most of these synthesis reactions, a syngas ratio (H_2:CO) of 2:1 or higher is desirable. DRM process produces only about 1:1 ratio, and therefore syngas adjustment is required to meet the downstream criteria of 2:1 or higher. The adjustment processes could either involve water gas shift reaction (Eq. 1.16) or addition of hydrogen, or both. Either of the processes are energy-intensive and would lead to additional CO_2 emissions. Therefore, for practical implementation of the DRM process, a significant process modification is required that will enable the production of syngas at a desirable downstream compatible syngas ratio.

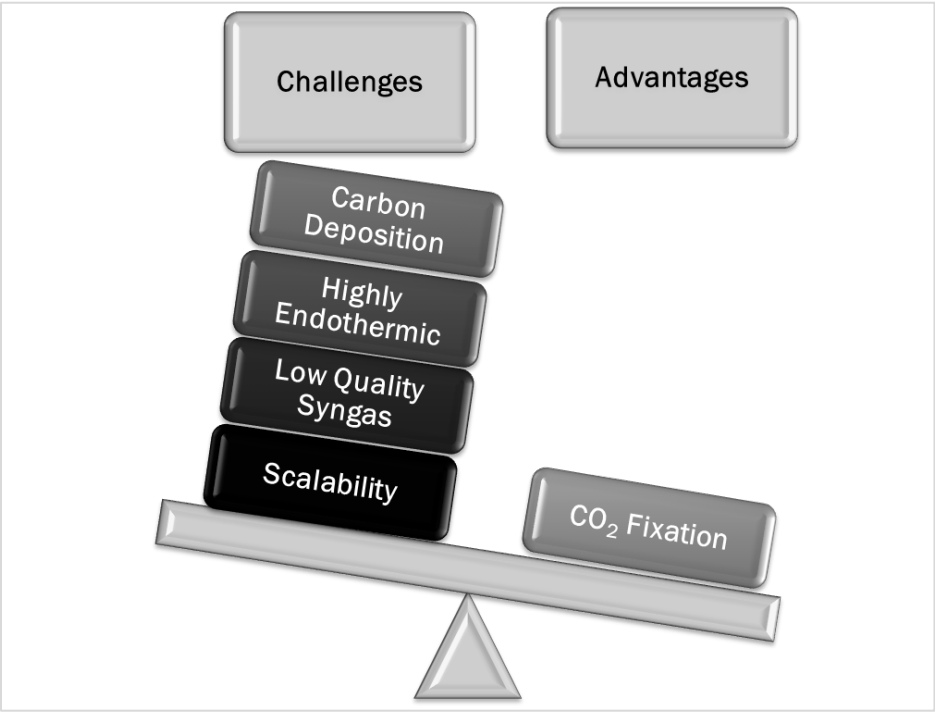

Figure 2.1 Presenting DRM challenges and advantages

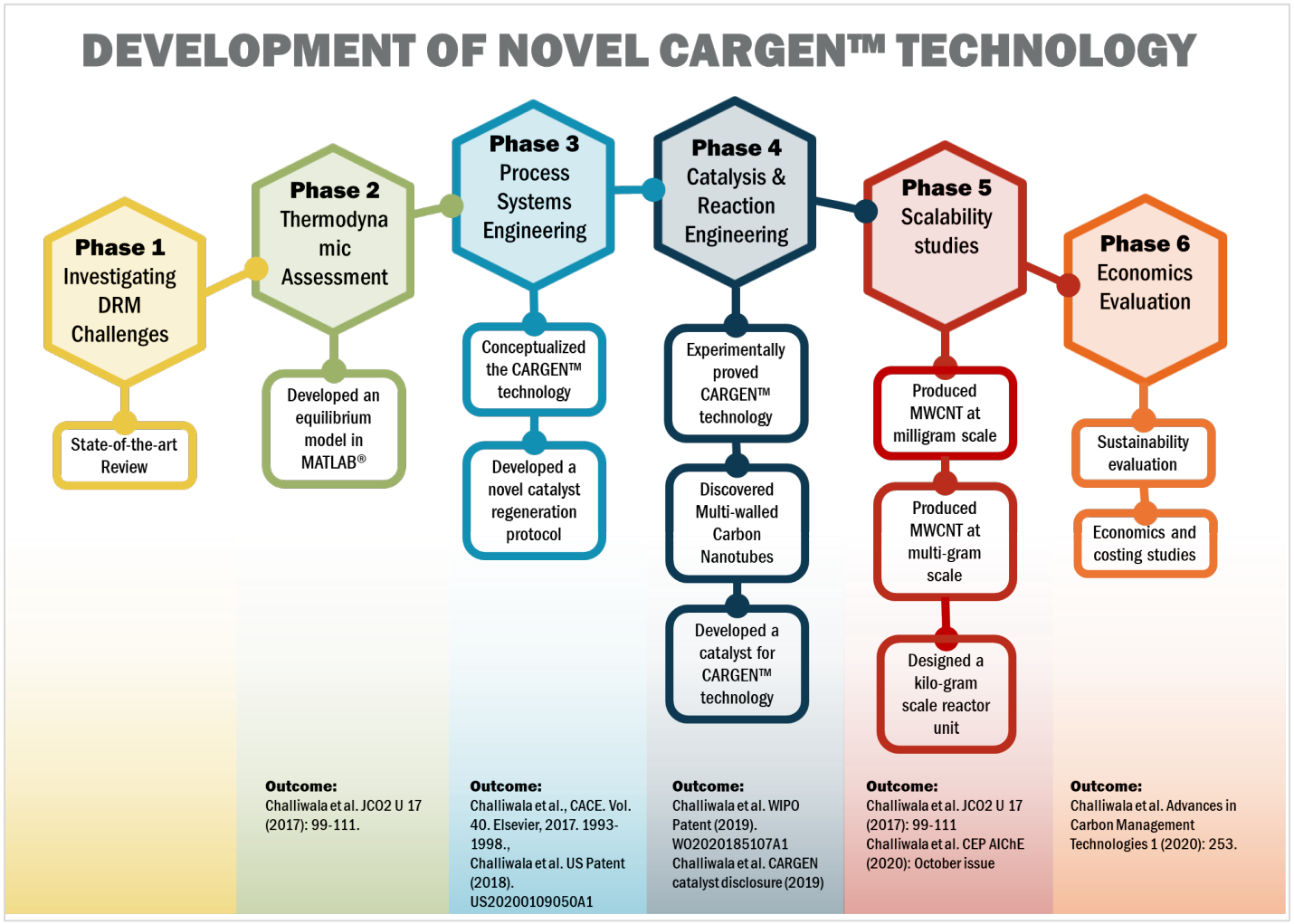

Figure 2.2 An overview of the approach undertaken to address DRM challenges that led to the development of novel CARGEN™ technology

Figure 2.2 presents an overview of the various studies conducted in this work to address DRM challenges. Also provided below are detailed discussion on each of the aforementioned studies.

Thermodynamics Assessment:

Thermodynamic assessment of methane reforming at various operational conditions to better understand the impact of operational conditions (Viz: temperature, pressure, feed composition) on the reforming products, such as syngas and solid carbon.

Development of novel reactor configuration:

From the results of the thermodynamic assessment, the impact of sensitive parameters and operational conditions on the formation of solid carbon and syngas is determined. The principles of process systems engineering and reaction engineering, such as contacting pattern, reaction segregation, heat integration, and mass integration, are employed to intensify the desired results such as feed conversion, energy reduction, production of solid carbon, and syngas.

The implementation of the aforementioned basic principles of thermodynamics, reaction engineering, and process systems engineering enabled the design of a novel reactor configuration, called CARGEN™ technology, which will be discussed in great detail in the next few sections.

Experimental proof of concept using State-of-the-art reaction systems

The initial goal of the experimental work was to conduct a *proof of concept* study of the novel CARGEN™ technology. For this, the state-of-the-art reaction systems, such as Thermogravimetric Analyzer (TA® TGA), Chemisorption equipment (Micromeritics®

Autochem II) and the Micro-Activity Effie (MA-Effi) reactor and the in-house developed Chemical Vapor Deposition (CVD) apparatus are used. The first set of experiments were done using a commercial catalyst material ($20\%\ Ni/\gamma Al_2O_3$) to establish proof that the theoretically suggested conditions for the carbon formation work. Next, a dedicated catalyst synthesis campaign was initiated with a core focus on designing a catalyst material that provides activity and stability close to the theoretical estimates deduced in step2. Following this, intensive experimental work was dedicated to the development of novel catalyst material for the CARGEN™ process. The outcome of catalysis work led to the development of tailor-made catalysts for the CARGEN™ process that was synthesized via a greener, scalable, and sustainable procedure.

Scalability testing of the novel CARGEN™ process:

The ultimate goal of any technology is the advancement in terms of technology readiness level (TRL). The proof of concept demonstrated in step 3 enabled the achievement of TRL 2, which essentially means that the technology is experimentally compliant with theoretical results. The next step is to scale-up the technology to higher TRL, which is TRL 3. In this work, a successful scale-up is accomplished from micro-gram to milli-gram to multi-gram scale using three independent reaction systems with different flow regimes. In particular, the MA-effi reactor system was used to test the process at a micro-gram scale, TGA reactor was used to test on a milli-gram scale, and finally, an in-house prepared Chemical Vapor Deposition (CVD) apparatus was used to demonstrate up to multi-gram scalability. Section 4.5 presents the results of the scalability testing.

Activation/Reactivation of reforming catalyst

As highlighted in section 1.4, one of the primary challenges in reforming processes, in general, is the formation of solid carbon that leads to catalyst deactivation. This results in frequent plant shutdowns and extensive maintenance activities that lead to a significant loss in revenue and time. One of the widely established industrial techniques of catalyst regeneration and removal of carbon is to oxidize the carbon on the catalyst surface using oxygen or air. However, the major disadvantage of this technique is the production of carbon dioxide (upon the reaction of oxygen with surface carbon). From a sustainability standpoint, this is highly discouraging and especially for the DRM process wherein the major aim is to convert CO_2.

In this work, an alternative catalyst regeneration technique is developed and patented. The technique involves the use of CO_2 as a regeneration media rather than oxygen or air. Section 5 presents the approach and the protocol developed, and its comparison with the conventional technique. Also presented in the same section are the results of various cycles of operation.

Economics and Sustainability studies

Economics evaluation is a critical step to assess commercial feasibility of any technology. In this work, economics evaluation of the CARGEN™ is done in terms of OPEX and CAPEX studies. Specifically two case scenarios are considered: (a) A multi-gram scale reactor unit which was built and used for the scalability testing studies. (b) A case study of commercial scale CARGEN™ process that includes its operational and capital cost to ultimately evaluate the cost of 1-kg MWCNT production and the resulting GTL products

in a case of converting 7000 tons/day CO_2 produced from Qatar's midstream processing facility.

The outcome of this work is the establishment of a techno-economic feasibility of the novel CARGEN™ technology via a comprehensive set of studies that combines elements from catalysis, reaction engineering, and process systems engineering. The various sections in this work presents an in-depth literature, approach, and the results obtained during the various stages of the CARGEN™ technology development.

3. TRI-REFORMING OF METHANE- AN APPROACH TO ADDRESS DRM CHALLENGES[1]

The central discussion in this section is on the thermodynamic assessment of benchmark reforming processes (i.e., SRM and POX) and their comparison with DRM. The specific objective is to identify the synergistic benefit of combining the said processes into a combined process that addresses the DRM challenges, as highlighted in section 2. A detailed study is conducted on the influence of independent parameters that has a profound impact on reforming, i.e.; temperature, pressure, and feed composition. Also, a detailed assessment is conducted on the influence of these parameters on the energy requirements, syngas ratio, and the carbon formation tendency, which are the most important metric that governs the selection of a reforming process. Ultimately, the feasibility of combining the benchmark processes in an optimal ratio is conducted to deduce a suitable operational range that satisfactorily addresses the DRM challenge.

3.1 Model Validation

TRM is a relatively new process compared to the conventional SRM, DRM, and POX processes. Extensive literature focusing on the various aspects (including thermodynamics, kinetics, reactors) of these processes is available and is discussed in detail in section 1.3 and 1.4. In contrast to earlier studies, which have employed well-established commercial software packages like Aspen plus® [36,38] a Matlab® model is developed in this work. A built-in minimization tool *'fmincon,' is* incorporated in the code*,*

[1]A major portion of this section has been published in Journal of CO_2 utilization 2017; 17:99-111 Copyright 2020Elsevier

which directly minimizes the GFE of the system without any introduction of Lagrange undetermined multiplier, unlike a few of the previous studies[32,84,85]. Therefore, before proceeding further and to verify the accuracy of the model results, we have made sufficient attempts to validate our model against the previously published experiments as well as theoretical models.

Due to the unavailability of published experimental reports on the TRM process (for the conditions under current analysis), we have used the currently accessible DRM experimental results to validate our model. A comparison of our model results with the previously published experimental DRM results by Khalesi et al.[85] and Liu et al.[86] in terms of the CH_4 percentage conversion is shown in Figure 3.1(a). Their results were found to be in good agreement with our model, specifically in the high-temperature regimes, typically in the temperature range of 700 ^oC and above. As DRM is a highly endothermic process, it requires high temperatures to bring the process to a feasible regime wherein positive CH_4 and CO_2 conversions could be achieved. This is also evident from the experimental results as shown in Figure 3.1 (a). The reaction temperature is observed to be a controlling factor leading to kinetic limitations, as can be seen, at lower temperatures, the conversion approach to equilibrium is much less compared to higher temperatures, which indicate that the process is kinetically limited, which is also claimed by Cui e al's proposition [87]. Reactant conversions are seen to be increasing with an increase in temperature. In particular, temperatures above 700 ^oC is seen to be a favorable regime for CH_4 to CO conversions. The CH_4 % conversion profile for strontium based catalyst is seen to incline more towards equilibrium conversion profile owing to the high activity of the

catalyst, however in general, kinetic limitations are always seen to effect at lower temperatures typically below ~500 ºC. For validation of the proposed model, results reported by Khalesi et al.[85] were seen to agree over a wider range of temperatures (500 ºC to 850 ºC).

Carbon deposition trends reported in our previous study by Noureldin et al. .[32], as shown in Figure 3.1 (b), were also found to be in an excellent agreement with our model results. Subsequent to this validation study, it is quite clear that the equilibrium analysis carried out using our technique holds credibility so as to provide a better understanding of a reformer system.

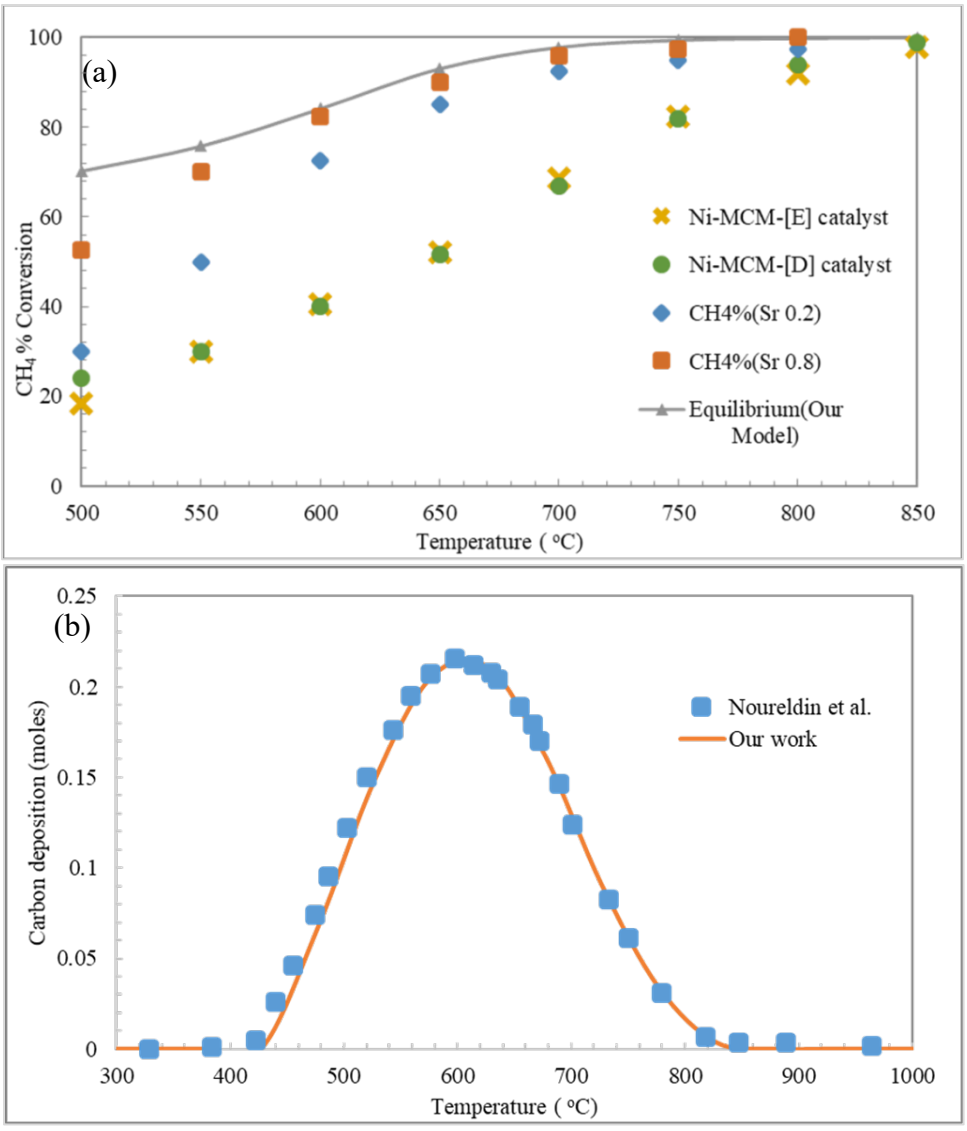

Figure 3.1 Validation of our model results with. (a)CH_4 % conversion experimental (Sr Catalyst) results from Khalesi et al. [85] and Liu et al.[86] (Ni-MCM Catalysts) (b) Carbon deposition equilibrium simulation results from Noureldin et al. [32]

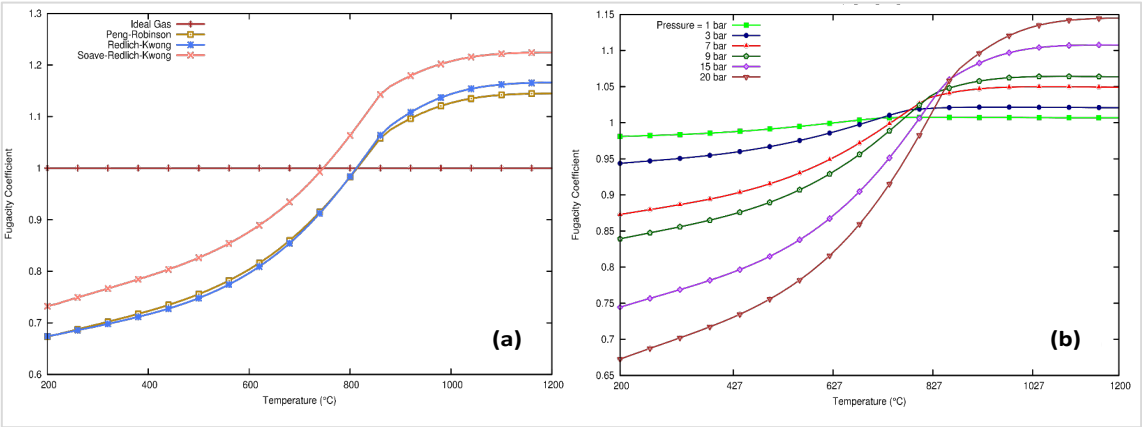

Figure 3.2 (a) Fugacity Coefficient trends using RK, SRK and PR EOS (b)Fugacity Coefficient of the inlet mixture as a function of temperature at various pressures calculated using the Peng-Robinson EOS. The feed composition is represented as follows: CH_4: H_2O: O_2: CO_2 = 1/0.6/0.1/0.6 moles.

3.2 Non-ideality of the reaction mixtures

Except for the low pressure and high-temperature conditions, the reaction mixture of a reformer is expected to behave non-ideally at all other conditions[88]. This non-ideality is mostly attributed to the differences between the physicochemical properties of the individual reacting species at respective process conditions. Essentially, most of the gaseous mixtures behave non-ideally at pressure and temperature ranges in which the reformers typically operate (900 °C and 20 bar) [89].

Figure 3.2 (a) shows a comparison between the calculated fugacity coefficients using the RK, SRK, and PR EOS. From this Figure, it can be seen that, while there is a significant deviation from ideality of the mixture at higher and lower temperatures as predicted by the three EOS; however, the SRK EOS is found to deviate consistently from the results of PR/RK EOS throughout the temperature range of 200 °C to 1200 °C as shown in Figure

3.2. The reason for this is attributed to the fact that SRK EOS is good at representing only hydrocarbons; however the reaction mixture considered in this system includes nonpermanent gases as well (CO_2, H_2O, CO, and H_2)[90]. Although the performance trend exhibited by PR EOS is very similar to the one displayed by SRK EOS, the latter is generally superior in calculating both the liquid and gaseous densities for a mixture of hydrocarbon, water, air, and combustion gasses, which represents a typical reformer reaction mixture[91]. On the other hand, even though the results generated from the RK EOS closely agree with those from PR EOS, RK EOS displays poor performance in representing vapor-liquid mixture behaviors above a ratio of $0.5T/T_c$. Thus at lower temperatures, RK EOS may not be able to provide accurate results comparitively[92]. For these reasons, to be more flexible, PR EOS has been used in all the subsequent calculations reported in this study.

Figure 3.2 (b) shows the calculated fugacity coefficient of the reformer inlet gas mixture using the PR EOS over a wide range of temperatures and pressures. We observe that the fugacity coefficient of the gaseous mixture approaches unity when the temperature reaches ~800 ºC for all studied pressure conditions. Deviation from ideality (which is the state of fugacity coefficient being unity) for this feed mixture can clearly be seen when the temperature goes above ~800 ºC (increased fugacity coefficient) as well as when the temperature is below ~800 ºC (decreased fugacity coefficient). This is a general observation in the case of all studied pressure conditions, except for 1 bar condition. For typical industrial operating conditions (of 900 ºC and 20bar), the reaction mixture is expected to deviate by approximately +10% from ideality. This indicates that the

consideration for the non-ideality of the reaction mixture becomes indispensable at any condition other than a temperature of ~800 ^{o}C and a pressure >1 bar.

The analysis mentioned above demonstrates that non-ideality is one of the critical factors to affect the equilibrium state of the reforming mixture. In particular, high pressure operation of the reformer is more impacted by the non-ideal behavior of the system. Therefore, it becomes sufficiently evident that any reliable thermodynamic analysis of the reforming process at near industrial conditions needs to incorporate non-ideality in the simulations properly.

3.3 Equilibrium temperature effect

In this section, the effect of temperature at which the reforming reaction takes place has been studied. At each temperature point, we calculated the equilibrium product distribution and evaluated it in terms of the CH_4 as well as CO_2 percentage conversions, H_2: CO yield ratio, amount of solid carbon deposited, and also the amount of energy required to sustain this reaction.

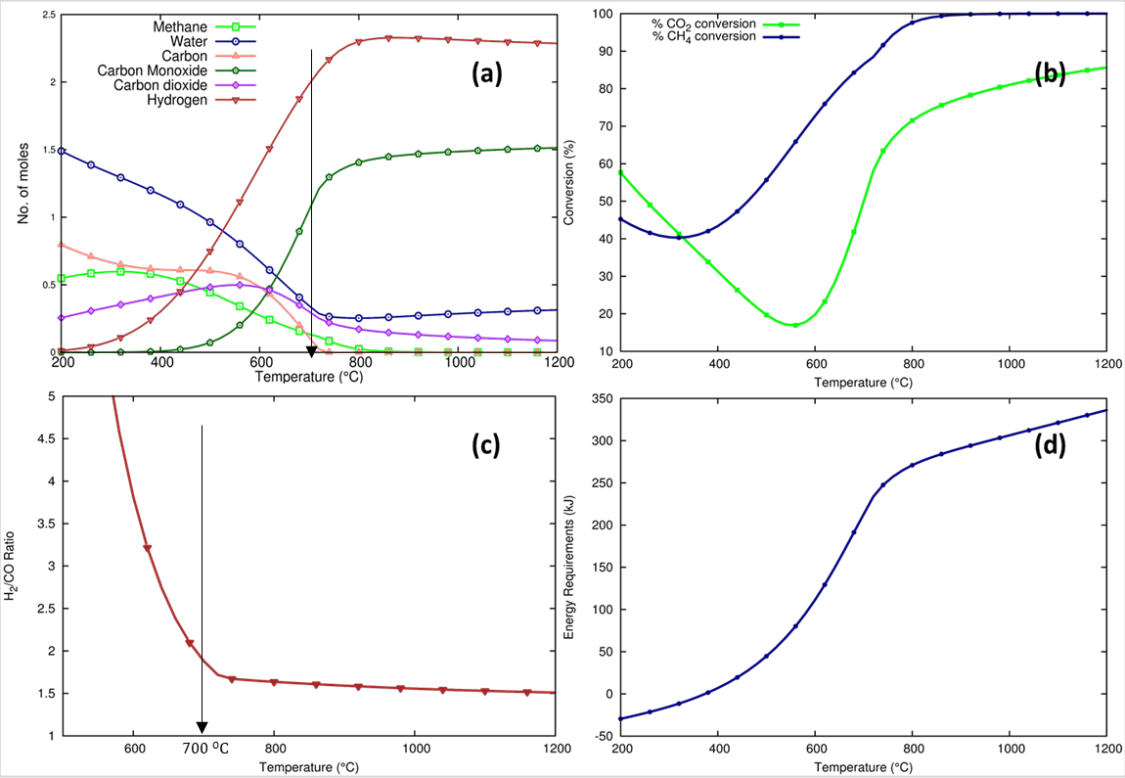

Figure 3.3 (a) Equilibrium product distribution (b) % CO_2 and CH_4 conversions (c) H_2: CO yield ratio (d) Energy requirements of the combined reforming process over a range of temperatures from 200°C to 1200°C at a pressure of 1 bar. Feed mole ratios are CH_4: H_2O: O_2: CO_2 = 1:0.6:0.1:0.6.

Reforming reactions are highly temperature sensitive. The chemical potential of a compound and, in turn, its GFE of formation is a function of temperature. For a typical

TRM process at a feed mole ratio of CH_4:H_2O:O_2:CO_2=1:0.6:0.1:0.6, Figure 3.3 illustrates the various performance evaluation trends as a function of temperature at 1 bar pressure. For this feed ratio, it was observed that the reaction behaves auto thermally at ~ 400°C temperature and 1 bar pressure. A closer analysis of Figure 3.3 leads to the verdict that at a temperature of ~700°C, the syngas (H_2: CO) yield ratio is ~2. Depending on the application of syngas, the H_2: CO ratio might be of prominence. For instance, a syngas ratio of 2 is imperative if it is to be used in a cobalt-based FT process[93]. At this condition, ~50% CO_2 and ~85 % CH_4 conversions are observed. An amount of ~200kJ is required to sustain this process, and ~0.25 moles of solid carbon is deposited. On a slight increase in the temperature by 20-30°C, carbon deposition reduces to a negligible amount. But, this presents a trade-off as energy demand increases by 20kJ along with an offset of H_2: CO ratio of ~1.5 with a significant increase in feed conversion.

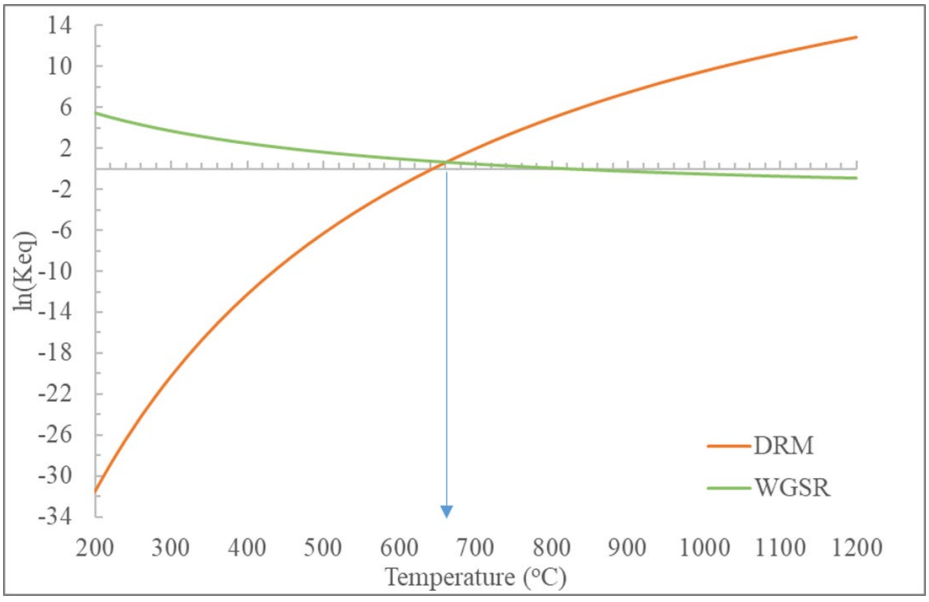

Figure 3.4 Equilibrium constant plots of DRM and WGSR

This analysis helps in finding an optimized condition at which we could operate a typical TRM process to maintain a syngas (H_2: CO) ratio near 2.

The CH_4 % conversion under the TRM process follows similar trends to the SRM and DRM reported by Noureldin et al. .[32]. This is presented in Figure 3.3 (b). The carbon deposition trend in Figure 3.3 (a) indicates significant carbon formation below ~700°C, which agrees with the SRM and DRM results reported by Noureldin et al. .[32]. The presence of three oxidants (CO_2, H_2O, and O_2) in the TRM process reduces carbon deposition significantly as compared to individual SRM, DRM, and POX process, as reported by Noureldin et al.[32]. CO_2, however, suffers from a reduced conversion compared to the DRM process, which can again be attributed to the presence of three oxidants. In this view, Noureldin et al. .[32] highlight the vital trade off that need to be considered in deciding an operating condition for a TRM process using an optimization software LINGO$^{(R)}$. As seen from Figure 3.3 (b), the CO_2% conversion increases quite steadily after 600°C, which indicates that reverse water gas shift reaction (RWGSR) (water gas shift reaction is shown in eqn: 20) accompanies the DRM reaction (as a part of TRM) at any temperature above ~ 600°C.

$$H_2O + CO \rightleftarrows CO_2 + H_2 \qquad \Delta H_{298} = -40.6 \text{ kJ/mol} \qquad (20)$$

As can be seen in Figure 3.4, the WGSR reaction rates are lower than that of the DRM reaction above ~600°C. This suggests that the TRM process should be carried out at temperatures above 600°C to increase CO_2% conversion.

The aforementioned results indicate that temperature is an extremely critical parameter for the optimization of the TRM, which affects not only the energy requirements but also

other important product distribution. In particular, we can observe that a temperature of ~700°C is reasonable for the operation of a TRM process, which would serve a syngas yield ratio of ~2:1 while keeping carbon deposition negligible. This temperature also provides a reasonable CO_2% conversion of ~50% while keeping energy requirements below 200kJ.

3.4 Equilibrium pressure effect

As a part of the equilibrium thermodynamic analysis of the TRM process, in the previous section, we looked very closely into independent effects of temperature on the equilibrium product distribution. In this section, we have evaluated the effect of pressure along with temperature on a TRM process by observing various performance evaluation trends, including the percentage CH_4 & CO_2 conversions, carbon deposition, the syngas yield ratio, and the corresponding energy requirements.

The GFE is a logarithmic function of pressure. Thermodynamically, a change in pressure changes the GFE of the system and pushes it in the reaction coordinates in which the effect is minimized. The effects due to the variation of pressure are shown in Figure 3.5. As pressure increases, we observe a steady decrease in methane conversion over the complete temperature range. As can be seen in Figure 3.5, methane conversion decreases initially up to ~400 ^oC and increases thereafter with an increase in temperature; however with the increase in pressure, it decreases through the entire range (1-20bar). Also, with regards to CO_2, a maximum conversion of 85% is realized at high temperatures (> 600 ^oC) for the chosen combination of input feed molar ratios. Unlike CH_4, a reversal of trend is observed

in CO_2% conversion as a function of pressure. A minor increase in CO_2% conversion up to 600°C followed by a significant decrease as a function of pressure, is observed. A similar reversal of trends is also seen in carbon deposition. At low temperature, it decreases as pressure increases, and at temperatures higher than 600°C, a significant increase with pressure is observed in carbon deposition. The syngas yield ratio increases with pressure up to 800°C and then slightly decreases to reach a steady value of 1.5.

Energy requirements are noted to decrease throughout the range of pressure examined in this study. However, the reaction remains slightly exothermic at lower temperatures up to ~400°C, and thereafter endothermicity increases steadily with an increase in temperature. This analysis leads to the inference that temperatures higher than ~850°C at low pressures result in no considerable incentive in terms of either syngas quality or conversions, but at the same time requires higher energy cost.

Thus, a temperature of ~800°C and 1 bar pressure seems to be one of the conditions that minimize carbon formation and energy requirements for a feed ratio of CH_4:H_2O:O_2: CO_2 = 1:0.6:0.1:0.6 operating at an energy requirement of 275 kJ yielding a syngas ratio of 1.5.

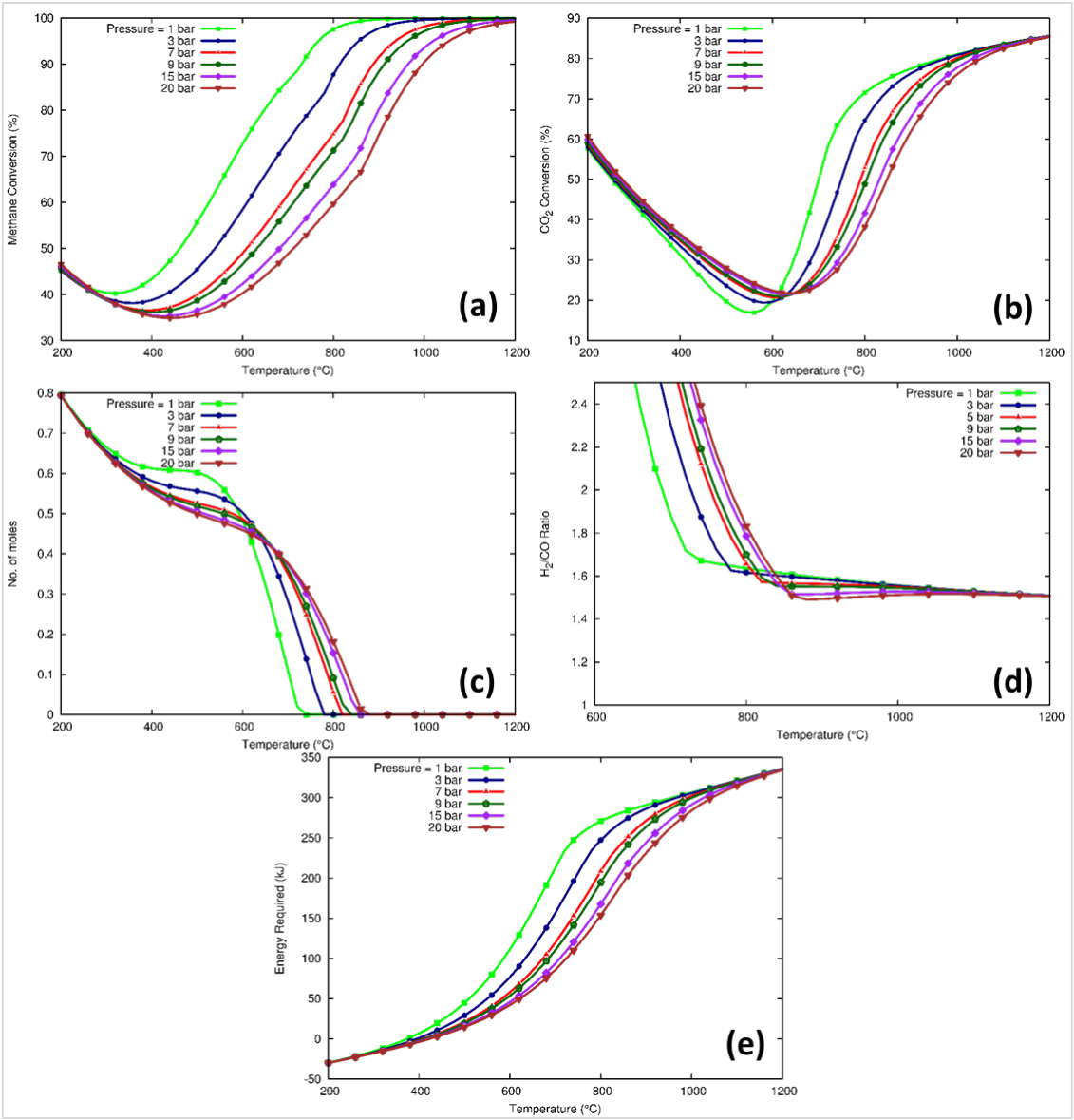

Figure 3.5 (a) Methane Conversion % (b) CO_2 conversion % (c) Number of moles of Carbon deposited (d) H_2: CO ratio (e) Energy requirements in the temperature range of 200°C to 1200°C as a function of reaction pressure. Feed mole ratios are CH_4:H_2O:O_2:CO_2 = 1:0.6:0.1:0.6.

3.5 Effect of adding Steam to Dry Reforming

DRM reactions typically produce syngas (H_2: CO) yield ratio of 1:1. To increase the syngas ratio, the DRM process can be carried out in the presence of steam. The addition of steam increases the hydrogen content of syngas to raise its H_2: CO ratio to 2:1. Figure 3.6 shows the various reformer performance trends that influenced by the addition of steam to the DRM process. As is evident from Figure 3.6 (a), methane conversion decreases with an increasing amount of steam in the system at lower temperatures.

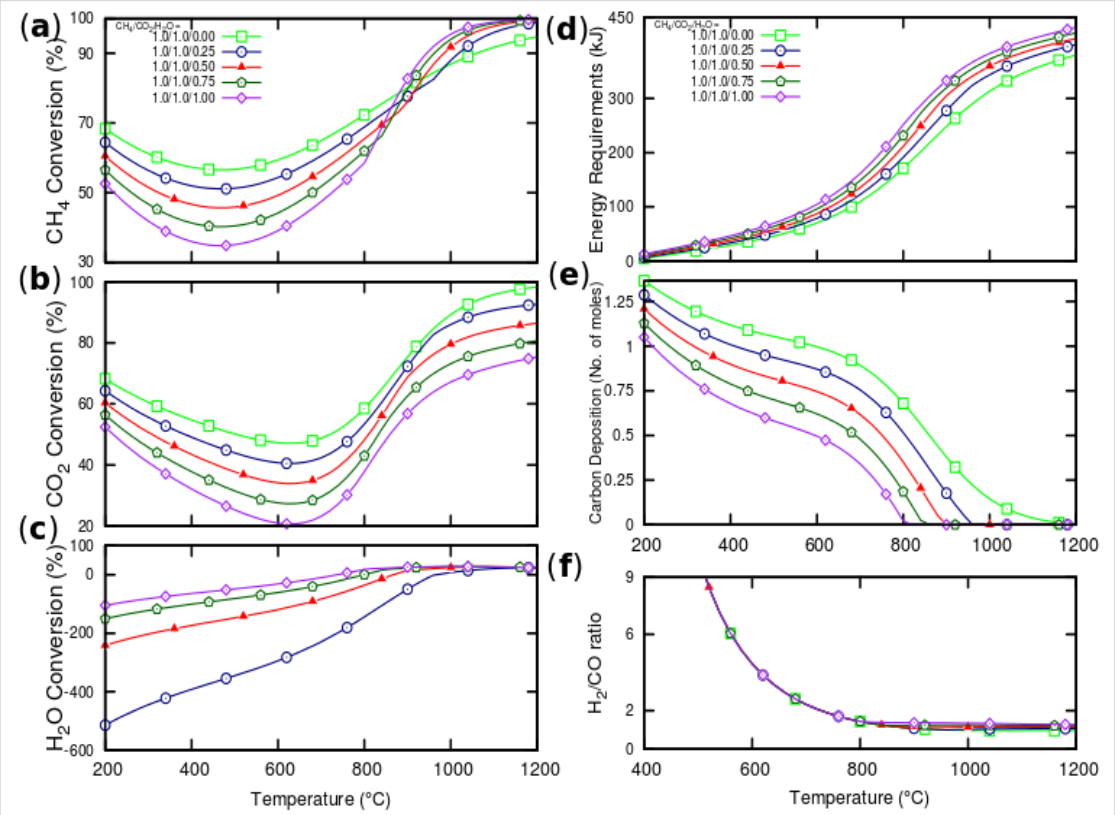

Figure 3.6 Effect of adding steam to the DR reaction. (a) CH_4 conversion %, (b) CO_2 conversion %, (c) H_2O conversion %, (d) Energy requirements, (e) Carbon Deposition and (f) H_2/CO ratio as a function of temperature for varying amounts of steam in the system.CH_4/CO_2 ratio is maintained constant at 1.

At higher temperatures of around 900 ºC, this trend reverses, and slightly higher CH_4% conversion is observed for increasing amounts of H_2O in the feed. Figure 3.6 (b) shows that the CO_2% conversion also decreases with the increasing proportion of steam in the input feed. One might speculate that as the proportion of steam increases in the feed, the probability that both the SRM and DRM reactions (eqn: 1& 2) increases and eventually lead to increased methane conversion. The contrary is, in fact, observed. The reason for this non-expectant behavior becomes more obvious when methane conversion is looked at in conjunction with the CO_2% conversion and solid carbon deposition in Figure 3.6 (e). At lower temperatures, both CH_4 and CO_2% conversions follow similar decreasing trends with increasing steam. We postulate that this may be due to the competition between DRM and SRM in lower temperature ranges caused due to the strong endothermicity of both the reactions. A similar analysis of steam addition to DRM reaction had previously been done by Özkara et al. .[91], but their analysis presented the equilibrium results without considering solid carbon formation. In view of the fact that a considerably higher amount of carbon deposition is observed over the entire temperature range of 200°C to 1200°C, even at a low pressure of 1 bar, exclusion of carbon deposition from similar analysis leads to considerable inaccuracies in the obtained results.

3.6 Effect of adding Oxygen to Dry Reforming

DRM process is highly endothermic in nature. In addition to this, carbon deposition during the DRM process deactivates the catalyst. To balance these limitations, the addition of oxygen to the DRM feed is observed to have notable benefits. Figure 3.7 illustrates the

different performance trends of a typical DRM process when oxygen is added to the process. As can be seen from Figure 3.7 (a) and Figure 3.7 (b), addition of oxygen has a similar effect on both the CH_4 and CO_2 % conversions, which are observed to decrease up to 600°C. This is because WGSR dominates the DRM reaction below 600°C. With the increase in the oxygen content of the feed, CO_2% and CH_4% conversions are seen to be decreasing owing to the reason of increased conversion of CH_4 to CO_2 rather than CO. From Figure 3.7 (c), it can be inferred that the energy requirements decrease continuously with an increase in oxygen content, attributing to the presence of POX reaction due to oxygen. A decrease of almost 25 % in carbon formation is observed (Figure 3.7 (d)) to happen when the oxygen content in the feed is 0.5 mole versus typical DRM condition in the absence of oxygen. A similar but less pronounced trend is seen (Figure 3.7 (e)) in syngas (H_2: CO) yield ratio, which eventually damp to almost one at all the feed mole ratios.

As a result of this analysis, it can be implied that the presence of oxygen in the feed greatly benefits the energy outlook as well as the carbon formation tendency of the DRM process. In particular, an optimized condition at a temperature of 800°C at 1 bar pressure with an oxygen content of 0.5 is expected to operate auto-thermally with almost negligible carbon deposition at a syngas ratio near to 1.5.

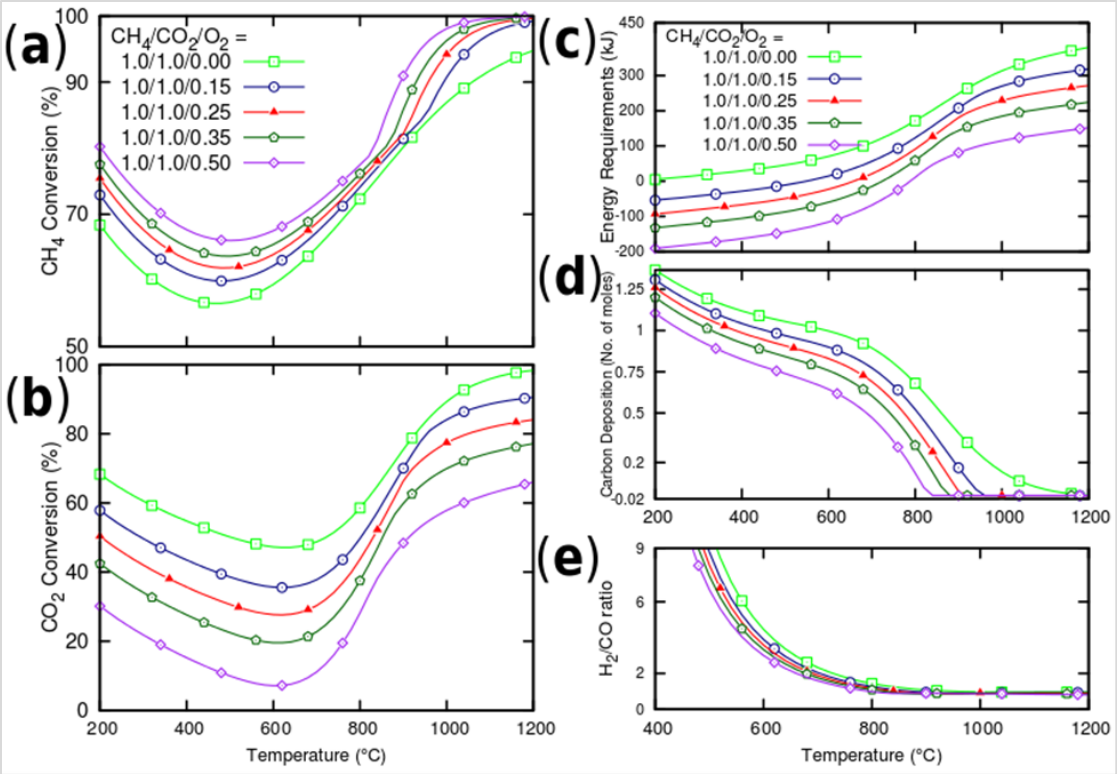

Figure 3.7 Effect of adding Oxygen to the DR reaction. (a) CH_4 conversion %, (b) CO_2 conversion %, (c) Energy requirements, (d) Carbon Deposition and (e) H_2/CO ratio as a function of temperature for varying amounts of steam in the system. CH_4/CO_2 ratio is maintained constant at 1

3.7 Effect of simultaneously adding Steam and Oxygen to Dry reforming:

The addition of steam and oxygen in a TRM process combines all the benefits of the addition of steam and oxygen (as mentioned in section 3.5 and 3.6), which, in particular, are the increased conversion of methane, reduced carbon deposition, and reduced energy requirements on a relative basis (to the conventional technologies). Figure 3.8 illustrates the different three-dimensional trends for variation of both the oxidants. Variation of steam and oxygen simultaneously clarifies the cumulative effect of both the components and also in finding optimum feed mole ratio. From Figure 3.8 (c), it can be seen that the

addition of steam and oxygen has an inverse effect on the energy requirement. Low steam and high oxygen content evaluates the minimum energy requirement of ~82 kJ, on the other hand, it decreases the CO_2 % conversion to a low value of ~48%. Carbon formation is seen (Figure 3.8 d) to decrease with an increase in both oxygen and steam concentration. This increase offsets the CO_2 % conversion to the lowest value of ~24%, and on the other hand, CH_4% conversion increases to the highest value of ~95%. Thus, CO_2 % and CH_4% conversion are seen to have an almost inverse effect by a simultaneous increase or decrease of steam and oxygen. From this analysis, an optimum feed mole ratio of CH_4:H_2O:O_2: CO_2 of 1:0.4:0.3:1 is deduced, which gives CO_2% conversion of ~52%, corresponding to an energy requirement of 180kJ with zero-carbon deposition.

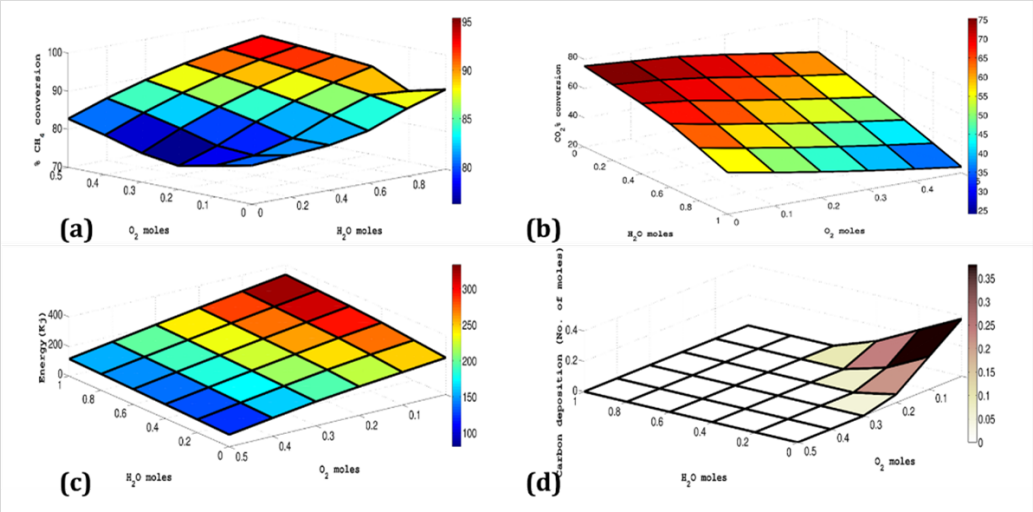

Figure 3.8 Effect of adding Oxygen and Steam simultaneously to the DR reaction. (a) CH_4 conversion %, (b) CO_2 conversion %, (c) Energy requirements, (d) Carbon Deposition for varying amounts of steam and oxygen in the system. CH_4/CO_2 ratio is maintained constant at 1. The process conditions are maintained at 900°C and 20bar pressure.

3.7.1 Kinetic Modeling

Owing to the fact that the reforming reactions are mostly heterogeneous reactions, kinetic limitations are always seen to affect the performance of the system. The condition of the system in the bulk phase is always different from the conditions inside the pore of the catalyst due to the presence of transport limitations, which in turn affects the product distribution. There have been numerous studies in the literature with an objective to understand such behaviors and to predict the product distribution in the reformer operating conditions accurately. However, these studies have been limited to either kinetics or thermodynamics individually. In the present work, we have performed a combined thermodynamic and kinetic study of the various reforming processes and their synergistic blends in the hope of being able to address the shortcomings of any individual reforming technology. This combined thermo-kinetic approach has provided us an opportunity to observe the role of the reaction parameters on the reformer behavior, meanwhile comparing the thermodynamic analysis and kinetic analysis. Such comparison provides as well an assessment of the validity of the different kinetic models to identify the most appropriate one to be employed in our reformer reactor model.

Xu et al .[94] is a well-known study on determining appropriate kinetics model for SRM reaction accompanied by WGSR on Nickel-based catalyst ($Ni/MgAl_2O_4$) using intrinsic rate expressions. In their work, they derived three rate equations by using rigorous model discrimination and parameter estimation technique for about two hundred twenty runs of the experiment. These rate expressions (eqn: 17-19) were derived based on the fact that

external diffusion and heat transfer limitations are negligible, which they proved to be true as per their experimental findings.

A similar rate expression (eqn: 1.16) for the DRM reaction was developed by Verykios et al.[95] for Nickel-based catalyst (Ni/La_2O_3). In their kinetic study, integral and differential reactions were conducted on an experimental setup similar to Xu et al., Verykios et al.'s model is based on the assumption that methane activation takes place at the catalyst surface, and it has also been considered as the rate-determining step, all the other intermediate steps are however considered faster than the methane bond cleavage step.

In the open literature, there are many other models on thermodynamic investigations of a combined DRM/SRM reforming reaction; however, only a few studies were done on the kinetic investigations [96] specifically for the TRM system. In the present work, we have performed an initial analysis to check the feasibility of a combined DRM/SRM kinetic model based on the existing individual kinetic models presently available in the literature [94,95] . Though there are many challenges related to such a task, any success in this presents huge benefits in the overall thermodynamic/kinetic analysis. One important point of consideration for this is the assumption used in the derivation of each model and their validity in the resulting process, which needs to be consistent. Another point is the temperature and pressure conditions over which individual models are derived and are expected to be valid. Upon integration of the two models, the calculated product distribution can be used as pre experimental results and for a simulation study of combined DRM/SRM reformer in the process simulators. This model will also allow us to accurately

understand the regimes of kinetic limitations and its deviation from thermodynamic predictions for a combined DRM/SRM reaction process.

The parameters that were used in the above-mentioned kinetic models are shown in Table 3.1. These kinetic parameters, however, can be fitted based on the experimental data for other catalysts, but they were kept as original values in order to preliminarily validate the combined kinetic model against the equilibrium predicted results. The MATLAB® code that was developed to calculate the kinetic profiles presented here were evaluated by simultaneous solution of the coupled ordinary differential equations as shown in Table 3.2 . In this code, the independent variable was chosen as the weight of the catalyst in order to limit the validation process to the kinetic study of the catalyst only. However, a reactor bed model can be developed by deriving the performance equation for a particular geometry of the reactor considered.[97,98]

Table 3.1 Kinetic Parameters of the SRM and DRM Langmuir Hinshelwood Hougen Watson mechanism

Rate Expressions	Kinetic Parameters
SRM Model by Xu et al.[94] $\boldsymbol{r_{I,SRM}} =$ $\frac{k_5(P_{CH_4}P_{H_2O} - \frac{P_{H_2}^3 P_{CO}}{K_4})}{P_{H_2}^{2.5}(1+K_{CO}P_{CO}+K_{H_2}P_{H_2}+K_{CH_4}P_{CH_4}+\frac{K_{H_2O}P_{H_2O}}{P_{H_2}})^2}$ $\boldsymbol{r_{II,SRM}} =$ $\frac{k_6(P_{CO}P_{H_2O} - \frac{P_{H_2}P_{CO_2}}{K_5})}{P_{H_2}(1+K_{CO}P_{CO}+K_{H_2}P_{H_2}+K_{CH_4}P_{CH_4}+\frac{K_{H_2O}P_{H_2O}}{P_{H_2}})^2}$ $\boldsymbol{r_{III,SRM}} =$ $\frac{k_7(P_{CH_4}P_{H_2O}^2 - \frac{P_{H_2}^4 P_{CO_2}}{K_6})}{P_{H_2}^{3.5}(1+K_{CO}P_{CO}+K_{H_2}P_{H_2}+K_{CH_4}P_{CH_4}+\frac{K_{H_2O}P_{H_2O}}{P_{H_2}})^2}$	$k_1 = 2.636 \times 10^{13} \times e^{-\frac{28879}{T}} \frac{kmol.kPa^{0.5}}{kg.s}$ $k_2 = 1.219 \times 10^{11} \times e^{-\frac{8074.3}{T}} \frac{kmol}{kPa.kg.s}$ $k_3 = 6.361 \times 10^{12} \times e^{-\frac{29336}{T}} \frac{kmol.kPa^{0.5}}{kg.s}$ $K_{CH_4} = 6.65 \times 10^{-6} \times e^{\frac{4604.28}{T}} \frac{1}{kPa}$ $K_{H_2O} = 1.77 \times 10^{3} \times e^{-\frac{10666.35}{T}} \frac{1}{kPa}$ $K_{H_2} = 6.12 \times 10^{-11} \times e^{\frac{9971.13}{T}} \frac{1}{kPa}$ $K_{CO} = 8.23 \times 10^{-7} \times e^{\frac{8497.71}{T}} \frac{1}{kPa}$ $K_1 = 10266.76 \times e^{\frac{-2630}{T}+30.11} kPa^2$ $K_2 = e^{\frac{4400}{T}-4.063}$ $K_3 = K_1 \times K_2\ kPa^2$
DRM Model by Verykios et al.[95] $\boldsymbol{R_{CH_4,DRM}} =$ $\frac{K_1k_2k_3k_4P_{CH_4}P_{CO_2}}{K_1k_2K_3P_{CH_4}P_{CO_2}+K_1k_2P_{CH_4}+K_3k_4P_{CO_2}}$	$K_1k_2 = 2.61 \times 10^{-3} \times e^{\frac{-4300}{T}} \frac{kmol}{kg.s.kPa}$ $K_3 = 5.17 \times 10^{-5} \times e^{\frac{8700}{T}} \frac{1}{kPa}$ $k_4 = 5.35 \times 10^{-1} \times e^{-\frac{7500}{T}} \frac{kmol}{kg.s}$

Table 3.2 Coupled Ordinary differential equations coded in MATLAB®

$\frac{dF_{CO}}{dW} = r_{I,SRM} - r_{II,SRM} + 2R_{CH_4,DRM}$
$\frac{dF_{H_2O}}{dW} = -(r_{I,SRM} + r_{II,SRM} + 2 \times r_{III,SRM})$
$\frac{dF_{CO_2}}{dW} = r_{II,SRM} + r_{III,SRM} - R_{CH_4,DRM}$
$\frac{dF_{H_2}}{dW} = 3r_{I,SRM} + r_{II,SRM} + 4r_{III,SRM} + 2R_{CH_4,DRM}$
$\frac{dF_{He}}{dW} = 0$
$\frac{dF_{CH_4}}{dW} = -(r_{I,SRM} + r_{III,SRM} + R_{CH_4,DRM})$

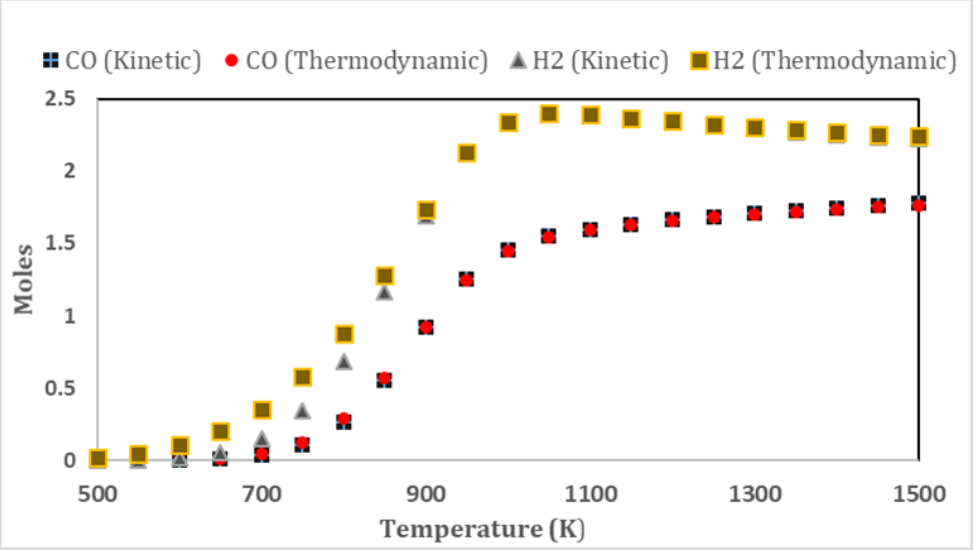

Figure 3.9 Kinetic Vs. Thermodynamic trends of CO & H_2 for DRM/SRM at 1 bar and CH_4:H_2O:CO_2=1:1

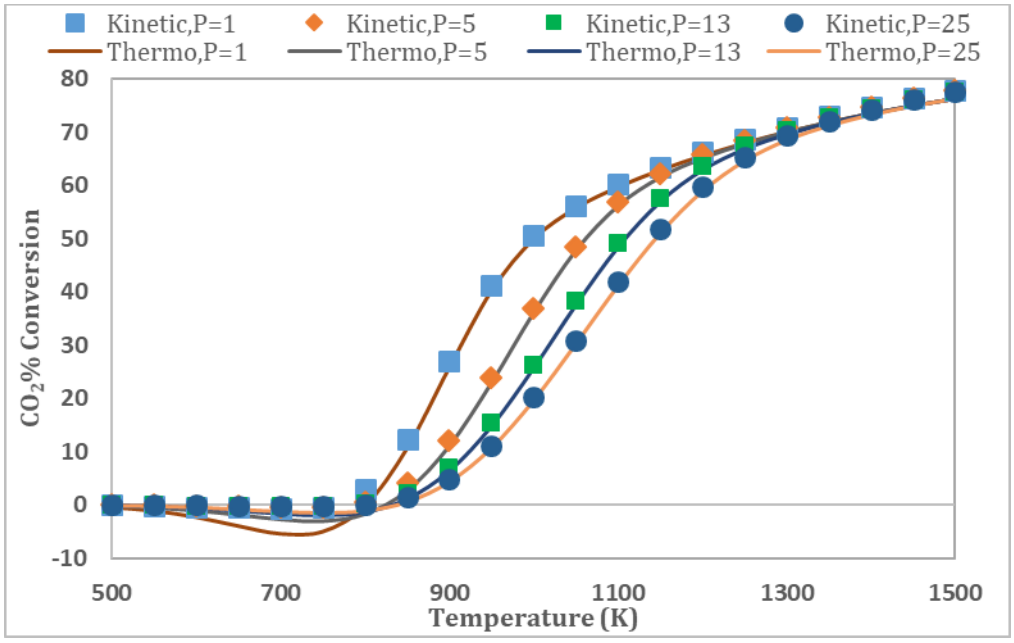

Figure 3.10 Kinetic Vs Thermodynamic trends of CO_2% conversion for DRM/SRM at 1 bar and CH_4:H_2O:CO_2=1:1:1

As an initial finding of this study, we were able to integrate and validate a combined DRM/SRM kinetic model with thermodynamic equilibrium predictions. Figure 3.10 shows the calculated CO and H_2 moles using both thermodynamic and kinetic analysis. The results are seen to be in good agreement with each other over a considerable range of temperatures (900K to 1500K), which is also supported by a completely different study by Elham et al. .[99]. However, at a lower temperature range of 500K to 900K, the hydrogen trend deviates by a small extent from the equilibrium values; this is expected to be addressed by tuning the kinetic parameters, which in this study were adopted from the original studies. This model was also tested over a range of pressure (Figure 3.11), and again, a very good agreement was found between the kinetically and thermodynamically calculated results. From Figure 3.10 and Figure 3.11, it can be noted that the

thermodynamic and kinetic trend agree considerably well throughout the temperature and pressure range, which shows that the proposed combined model holds credibility in predicting the product distribution of the combined DRM/SRM process. Another factor that contributes to better overlapping between the two predicted trends is due to the fact that we have not considered the heat, mass, and momentum transfer limitations that arise inside the bulk and pore of the catalyst bed in an experimental reformer reactor. These limitations can be accounted for by using the necessary transport equations, but these were not incorporated in the present work. However, this analysis is very critical for accurate predictions of the reforming reaction performance as it includes both thermodynamic and kinetic analysis of the combined DRM/SRM process. A complete analysis should, however, account for all the transport limitations pertaining to the type of catalyst used. Our efforts continue in the development of a pseudo homogeneous fixed bed reactor model, which would serve as a base for carrying out further experiments for catalyst scale-up studies for a TRM process.

3.7.2 Conclusions

In this study, a complete thermodynamic analysis of the TRM process was carried out by the GFE minimization method. Various relations between the operating conditions (temperature, pressure, and feed mole ratios) are analyzed to investigate an optimized condition with an objective to minimize the carbon deposition and maximize CO_2 conversion keeping energy requirements as low as possible. In a more realistic industrial case scenario, non-ideality associated with the reaction mixture was also accounted for

using PR, RK, and SRK EOS. The results indicate that the conditions of high temperatures and low pressures are beneficial for low carbon formation and high CO_2 conversions. It was also noted that the high energy demands of the DRM process could be balanced by the addition of oxygen, and at the same time, low syngas (H_2: CO) ratio can be raised by the addition of steam. The effects of the addition of large quantities of oxygen and steam were observed to be compromising with the low CO_2% conversion values and high energy demands. Thus, an optimized operating condition of a temperature of ~750 ^oC at 1 bar pressure at a feed mole ratio of CH_4: H_2O: O_2: CO_2 of 1:0.4:0.3:1 was identified to be a reasonable condition in order to meet the objective of minimizing energy requirements while eliminating carbon deposition at CO_2% conversion of 52%, CH_4% conversion of 100% and energy requirement of 182 kJ. As a further extension to better understand the TRM process, initial findings of the kinetic analysis revealed excellent compatibility of thermodynamic and kinetic results of combined DRM/SRM process using existing kinetic models available in the literature.

4. CARGEN™ TECHNOLOGY- AN ENHANCED CO2 FIXATION AND SYNGAS PRODUCTION PROCESS USING A TWO-REACTOR SETUP[1,2,3,4,5]

The approach adopted in the previous section was to utilize a synergistic benefit of combining the existing reforming processes into a single reactor system to address the DRM challenges. In particular, the focus was on the production of syngas, while eliminating the byproduct carbon. In this section, a detailed assessment is conducted to identify the possibility of producing both the products of reforming, i.e, solid carbon, as well as syngas. It is demonstrated herein that a significant benefit is achievable in terms of energy requirement, syngas ratio, and CO_2 conversion compared to the standalone DRM process when the *option of splitting a single reactor into two reactors is considered*. Due to the uniqueness of the developed process and its significance in the field of CO_2 reforming, an invention disclosure was filed on this work. This process, which is well established now, has been named as CARGEN™ technology, short for CARbon GENeration technology. This section of the dissertation document has been dedicated towards a detailed understanding of the CARGEN™ process, and therefore, it has been divided into the following sub-sections in order of the various stages in which it was developed:

A portion of this section has been published/submitted in:

[1]Advances in Carbon Management Technologies: Carbon Removal, Renewable and Nuclear Energy, Volume (2020): 253 Copyright 2020Taylor & Francis [114],

[2]Challiwala, M. S., et al. “Production of high-quality carbon nanotubes from natural gas and carbon dioxide using a novel CARGEN™ process”, Chemical Engineering Progress, AIChE, Wiley, October 2020

[3]Challiwala, M.S., et al. “A novel CO2 utilization technology for the synergistic co-production of multi-walled carbon nanotubes and syngas”, Scientific Reports, Nature, Accepted December 2020

[4]Challiwala, M. S., et al. "Method and Apparatus for producing Carbon black and Syngas from Carbon dioxide" – Provisional patent. US Patent WO2018187213A1, October 2018.

[5]Challiwala, M. S., et al. "Catalysts for CARGEN™, methods of preparing, and uses of same", Provisional Application Number (62/949,133), Disclosure submitted on: 6 November 2019

a. Section 4.1: Background Literature and Advancement on the State-of-the-Art
b. Section 4.2: Concept development via Thermodynamic Assessment
c. Section 4.3: Experimental proof of CARGEN™ technology
d. Section 4.4: Tailor-made catalyst for CARGEN™ technology
e. Section 4.5: CARGEN™ scale-up testing

4.1 Background Literature and Advancement on the State-of-the-Art

The discussion presented in section 1.3 highlighted several challenges pertaining to the DRM process that prohibits its commercialization. Also, it is evident from the background literature that the DRM process cannot be operated on a standalone mode or in the way, conventional SRM, POX, and ATR processes are operated. Therefore, the primary discussion in this sub-section is directed towards a possibility of addressing DRM challenges by using a novel reactor configuration that resulted from the work conducted in section 3 on tri-reforming of methane. A meaningful implementation of the DRM process requires that the overall CO_2 emission from the process be reduced to a value at which the commercially implemented reforming solutions are operated. Also, in addition to the sustainability requirements of the process, its economic requirement also needs to be fulfilled. Some of the recent literature advancement that accounts for both, economic as well as sustainability benefits of the DRM process are given below:

A recently developed C2CNT process by the Licht research group at George Washington University[100,101,110–112,102–109] have focused on the conversion of CO_2 to CNTs and oxygen via the molten electrolytic route. Their approach required the use of molten

lithium oxide as a catalyst while bubbling CO_2 through the catalyst. Although the said process demonstrated a reasonable possibility to convert CO_2 to CNTs and oxygen, the process is extremely energy-intensive, which may result in significant indirect CO_2 emissions of their own. Also, the operational challenges associated with the conversion of a solid catalyst into a molten state are also commendable.

Another work by Pint et al.[113] at the university of Tennesse have demonstrated an interesting possibility of producing small diameter carbon nanotubes using a reasonably similar approach as that of Licht et al. Their approach involved the use of molten salts in the electrochemical synthesis process to convert CO_2 present in ambient air to CNTs. The contrasting feature with the latter group (Licht et al. [100,101,110–112,102–109]) is the fact that in this study, authors utilized Iron catalyst layers deposited at different thicknesses onto stainless steel as a cathode and atomic layer deposited Al_2O_3 on Ni as a corrosion-resistant anode. An energy consumption analysis reported in their publication showed a high conversion of CO_2 into higher value and smaller diameter CNTs at relatively low energy input. The novelty in their approach, along with significantly reasonable economic assessment, enabled them to develop a startup company by the name Skynano[113,114].

As indicated earlier, The CARGEN™ technology utilizes two reactors to convert DRM feed gases to solid carbon as well as syngas. The approach requires the use of two reactors in such a way that the first reactor (CARGEN™) dedicatedly produces solid carbon, while its the effluent gases are processed in a second reactor (Tri-reforming) to produce syngas as shown in Figure 4.1.

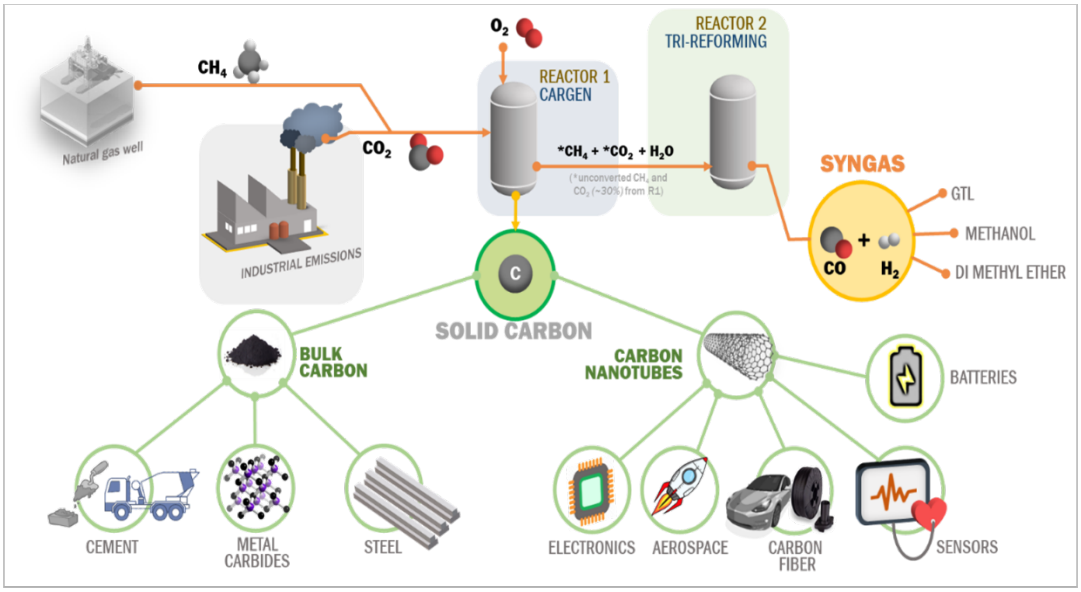

Figure 4.1 A systematic overview of the novel two-reactor CARGEN™ technology.

From a thermodynamic assessment study, it was observed that by operating the two reactors in a segregated approach, a significant reduction in the energy requirement was achieved. In particular, it was observed that the two-reactors could be combined operated at as low as 50% energy compared to the standalone DRM process of the same capacity. In addition, the overall CO_2 conversion was found to be at least 65%. These results are provided with great details in sub-section 4.2, along with several case studies. Following a theoretical investigation and concept development, an experimental proof of concept is essential. Section 4.3 provides all the details on the experimental proof of the CARGEN™ process. Not only was it proven that CARGEN™ technology is practically possible, but it is also demonstrated using advanced microscopy imaging that the CARGEN™ process produces an ultra-high quality of solid carbon, i.e. carbon nanotubes (CNTs), and in particular Multi-Walled CNTs (MWCNTs).

On a commercial scale, CNT production is generally carried out either by electric discharge, flame synthesis, chemical vapor deposition (CVD), or laser ablation[115]. The laser ablation method requires a high amount of energy and temperatures over 3000 ºC that induce reorganization of the carbon atoms to form CNTs without utilizing a catalyst material. However, this method has significantly high CO_2 footprints because of the requirements of a large amount of electricity for its operation. Unless the electricity comes from a renewable energy source, this process will not be sustainable from a CO_2 emission point of view. One of the most promising relatively low-temperature CNT production processes is the CVD method, which not only ensures proper control of the morphology and structure of CNTs but also allows for mass production at relatively low operational temperatures. Various scalable technologies have been reported that utilize the CVD approach for CNT production such as "Multiwall Carbon Nanotubes (FIBRIL™)" of Hyperion Company [116], the CoMoCAT process patented by University of Oklahoma [117,118], the HiPCO process by Rice University [119–121] and the "Nano Agglomerate Fluidized bed reactor" process developed by Tsinghua University [122,123]. Most of these processes implement fluidized bed technology to conduct CVD in a continuous mode of operation. Although the fluidized bed technology is the most attractive option for converting a CVD process from semi-batch to continuous mode of operation for large-scale production, it suffers from several challenges. These challenges pertain to the fluidization of the catalyst nanoparticles of the catalyst and their separation from CNTs [124–127].

One of the practical challenges that most of the aforementioned CNT production processes struggle with is the sustenance of the catalyst for prolonged activity. In other

words, since CNTs form at the surface of the catalyst, the catalyst activities are observed to decrease with time rapidly. Therefore, to keep the catalyst activity for a prolonged period, it was imminent to conduct catalysis studies to synthesize a tailor-made CARGEN™ catalyst that not only provides a high CNT production rate but also at a sustained activity. Sub-section 4.4 discusses the catalysis approach adopted to synthesize the CARGEN™ catalyst, along with some of its results compared to other catalyst systems.

Finally, for the TRL escalation of any process, its scale-up is essential. In this work, an attempt was made to demonstrate the scalability of the CARGEN™ process from the micro-gram scale of production to milli-gram scale and finally to multi-gram scale. The results of this part of the experimental work are covered in sub-section 4.5. A successful demonstration of the CARGEN™ process up to the gram-scale proved that TRL-3 is achieved. A mega proposal is being written in collaboration with a major energy company, as well as world-leading scientists, to further scale-up the CARGEN™ process to a higher TRL level for future industrial applications.

4.2 Concept development via Thermodynamic Assessment

In this section, firstly, a comparison is made between SRM, POX, and the DRM processes in terms of syngas ratio, energy requirements, and carbon formation tendency. The comparison is made at a pressure of 1 bar, and temperature is varied between 200 and 1200°C. The feed conditions for all these processes are kept based on stoichiometry as per Eq. 1-6 (SRM: $H_2O/CH_4=1$, POX: $O_2/CH_4=0.5$, DRM: $CO_2/CH_4=1$). Following this comparison, the proposed process of CARGEN™ is described in detail and compared with

the aforementioned commercial processes. Finally, an economic comparison between various combinations of the aforementioned processes in terms of their operational cost and carbon footprint is presented.

4.2.1 Comparison of Syngas ratio

In this analysis, the effect of reforming technology on the H_2/CO ratio of syngas is studied at different temperatures. The relative atomistic ratio of the feed components in terms of O:C:H in each reforming technology is key to determining the H_2/CO ratio of the syngas produced. In SRM, the O:C:H ratio in the feed is 1:1:6; for POX, it's 1:1:4, while for DRM, it is 1:1:2. This shows that the hydrogen content in SRM is the highest, followed by POX, and the lowest is in DRM. This low quantity of hydrogen in DRM results in significantly low H_2: CO of 1:1, which is not suitable for downstream operations that require at least 2:1. A comparison of H_2: CO of the three reforming technologies as a function of temperature is provided in Table 4.1 below.

The ratio of hydrogen to carbon monoxide at different temperature conditions provided in Table 4.1 above is seen to be highest for SRM, followed by POX, and the lowest is for DRM. Notably, this is in the same order as that of the O:C:H ratio stated earlier. If a hydrogen-rich gas, for instance, steam is added, it will change the relative ratio of hydrogen to carbon monoxide and consequently, other products from the reaction system.

Table 4.1 Syngas ratio of the three reforming technologies as a function of temperature

Temperature, °C	H_2/CO ratio		
	SRM	POX	DRM
200	33062.3	2649.5	940.3
300	1164.8	271.9	116.6
400	106.3	55.8	26.2
500	23.9	16.0	8.0
600	8.3	5.7	3.0
700	4.1	2.8	1.5
800	3.2	2.1	1.1
900	3.0	2.0	1.0
1000	3.0	2.0	1.0
1100	3.0	2.0	1.0
1200	3.0	2.0	1.0

4.2.2 Comparison of Energy requirements

The energy requirement to drive the reforming reactions forms the major portion of the energy requirements of reforming processes. Here, the energy requirements of the three reforming processes (SRM, POx, DRM) are shown as a function of temperature at a reaction pressure of 1 bar and depicted in Figure 4.2. The feed composition is kept at the stoichiometric conditions as indicated earlier. It can be observed that POX technology produces energy as its energy requirements are in negative. However, with an increase in

temperature, the energy requirements tend to increase, and at ~750 ºC, they tend to cross the zero-energy line indicating that it becomes net positive after this temperature. On the other hand, both SRM and DRM processes are observed to require energy for the reaction to happen under all temperature conditions. Another point to note is that the energy requirements of the DRM process are more than that of SRM beyond 650 ºC temperature, while below 650 ºC, the energy requirements from the SRM are slightly higher than that of DRM.

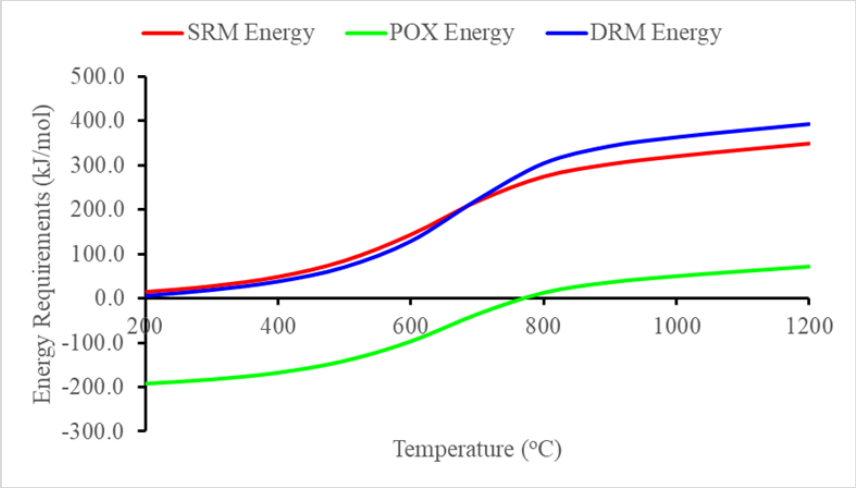

Figure 4.2 Energy Requirements of the SRM, POX and DRM processes Vs temperature at stoichiometric feed composition at 1 bar pressure.

Figure 4.2 shows the energy requirements for SRM, POX, and DRM. However, this cannot be used to make comparisons since each of these processes produces syngas of a different H_2/CO ratio, and their carbon footprint of oxidant production varies as the process. Section 3.6 includes comparison results that compare the overcall carbon footprint. Nevertheless, Figure 4.2 helps in understanding the energy requirements at different temperatures of the reformer reactor for different processes.

4.2.3 Comparison of Carbon Formation Tendency

This section compares the carbon formation tendency of each reforming technology as a function of temperature. The operational conditions of feed composition, reaction pressure, and temperature are identical to previous sections.

From several experimental and thermodynamic modeling studies, it is proven that the extent of methane decomposition (Eq. 1.7) reaction at low reforming temperature of 500 ºC is very high compared to Boudard reaction (Eq. 1.8). Many industrial reports also claim that methane decomposition reactions are extremely prone at the reactor entrance, wherein the concentration of methane is very high compared to any other reaction products. Near the reactor inlets, heating is generally done to increase the temperature of the reaction gases to reach desirable reforming temperatures of 900 ºC and beyond. During this transition, since the gases pass through coking temperatures, a huge quantity of carbon is deposited near the inlet. On the other hand, on the exits of the reactor, since the carbon monoxide concentrations are high, the carbon disproportionation tendency is much higher when temperatures are quenched to the target outlet temperatures of 400 ºC. Formation of solid carbon at the entrance and the exit of the reactor bed is not the only concern that the industry faces. The other and the most severe challenge is related to catalyst deactivation. Since reforming reactions take place in the presence of a catalyst, the formation of carbon deactivates the catalyst by clogging its active sites. In addition to this, sintering is another problem that is widely reported in the scientific literature. Due to these challenges, carbon formation in the reformer is undesirable. Much of the scientific attention at present in the

global community is dedicated to the reduction or elimination of solid carbon from the reforming process. Extensive literature studies are available that report novel methods of reduction of carbon formation tendency of the reforming reaction. Some of these studies are either process-related while others are purely catalytic. Figure 4.3 illustrates the carbon formation tendency of the three reforming reactions at the stoichiometric feed condition of each reforming process and 1 bar pressure.

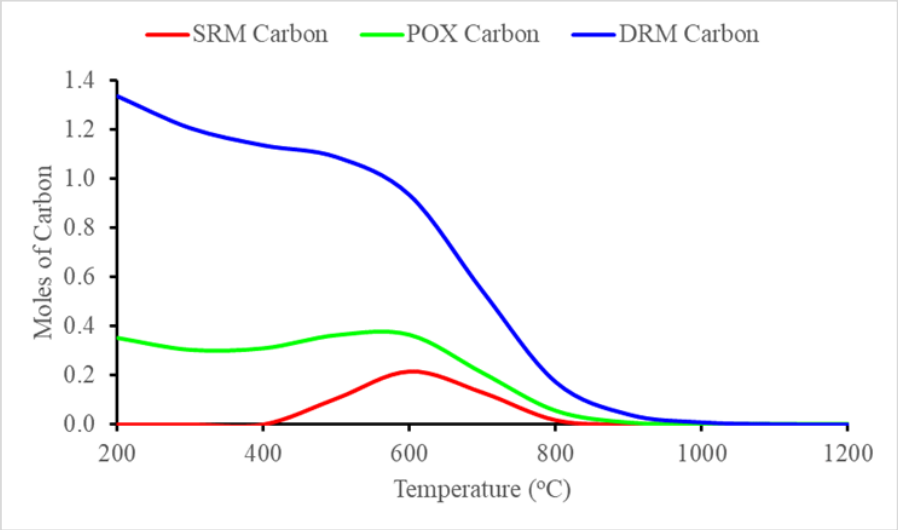

Figure 4.3 Carbon formation comparison between SRM, POX, and DRM process at stoichiometric feed conditions and pressure of 1 bar.

From Figure 4.3, it can be clearly observed that the carbon formation tendency from the DRM reaction is higher than the other two reforming techniques (DRM>POX>SRM). The lowest carbon formation is observed to be in SRM, as it contains the highest amount of hydrogen compared to the other reforming techniques. In conjunction with the discussion provided in the previous section of the syngas ratio, it could be observed that the ratio of O:C:H also carries a huge implication on carbon formation tendency. Since the DRM

process has the highest ratio of C/H compared to the other reforming technologies, the carbon formation tendency of this reaction is the highest. Therefore, in order to reduce carbon formation tendency, it would be advisable to either remove excessive carbon and or increase hydrogen concentration to reduce the C/H ratio. In addition to this, it can also be observed that low temperatures favor more carbon formation than higher temperatures for DRM and POX, while for SRM, a peculiar trend is observed, in which carbon formation is only in 400 to 800 ^{o}C temperature range.

4.2.4 CARGEN™ – Co-production of syngas and carbon black

As discussed in the previous sections, the process challenges of carbon formation and low syngas ratio are the most critical hurdles in the implementation of DRM technology on a commercial scale. One approach to overcome the challenge of high carbon formation in DRM is to segregate the carbon formation reaction and the syngas formation reaction. In this way, it is possible to systematically improve the C/H ratio that favors desirable operational conditions for industrial operation. From thermodynamic assessments, a novel approach to segregate the two reactions (carbon formation and syngas formation) is proposed that addresses the DRM challenges. In particular, the proposed reactor system utilizes the benefit of lower operating temperatures and high C/H ratio to selectively produce high-quality carbon from CO_2 and CH_4, while utilizing the benefit of high temperature and low C/H ratio to produce syngas as a desirable product. These reactions are made to essentially happen in two separate reactors that produce only a single product separately. Figure 4.4 illustrates the process concept. As the focus of the

first reactor is to produce solid carbon, it has been termed as "CARGEN™" or CARbon GENerator reactor, and the second reactor is the normal reforming process to produce syngas. In short, this process perceives carbon as a desirable marketable product instead of a problem that should be avoided. By doing so, two separate products can be obtained from 2 sequential reactors, thereby utilizing the DRM reaction.

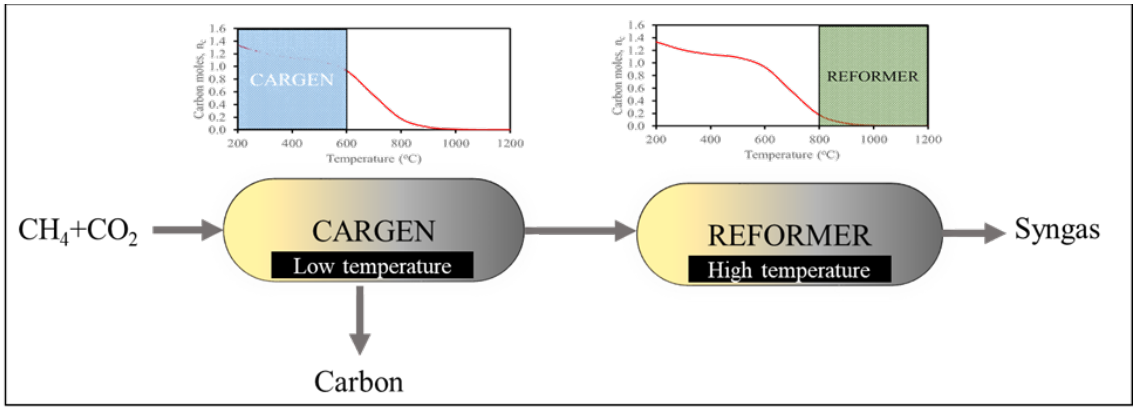

Figure 4.4 Illustration of a novel approach to implementing the DRM process. CARGEN™ (Or Carbon Generator) indicates the first reactor that produces solid carbon as a desirable product, while REFORMER indicates the second reactor that produces syngas as a desirable product

In Figure 4.4, two plots of carbon formation as a function of temperature are shown above both reactor blocks. The blue zone in the first plot referring to CARGEN™ is to indicate the operational window of the first reactor in terms of temperature. This operational window defines the most favorable operational zone for the CARGEN™ reaction. The second plot showing the green zone refers to the conditions in which carbon formation is minimal and pertains to the second reactor. Inherently in the first system, since carbon is the main product, the resultant syngas ratio is relatively high, however, its yield is low as the selectivity towards syngas under low temperatures is relatively low.

Additionally, a big portion of the feed is expected to remain unconverted in the first reactor, as thermodynamics under these conditions do not favor 100% conversions under these conditions. Nevertheless, the portion of feed that gets converted will only form solid carbon. In conjunction with the previous section, this method could also be seen as a way to reduce C/H ratio load on the reactants of the second reactor (Reformer unit), as all the products from the first reactor are essentially fed to the second reactor. The operational window of the second reactor pertains to high-temperature conditions beyond 800 ºC temperature and is expected to lead towards higher conversions of close of 100%. However, under these conditions, syngas is selectively produced. In this way, the reactor segregation based on the type of product produced helps to make a symbiotic relationship between the two reactors.

Now, will the carbon formation in the first reactor affect the catalyst and the design of the process? Wouldn't it lead to frequent shutdowns? The answer to these two important questions is that the know-how for handling "coking" reactions is already established and has been practiced extensively in the chemical industry. Chemical refineries generally employ an important unit called as "coker" unit that converts the residues of the Vacuum Distillation Unit (VDU) into pet-coke and light gases using a catalyst and thermal cracking. This unit is known to produce around 400-500 tons per day(TPD) of solid carbon in big refineries and utilize a well-known fluidized bed concept for their operation. The first reactor will be operated under these conditions, and therefore, not many design challenges may be expected. However, while segregating the carbon formation and syngas formation reactions, an important problem of the DRM reaction is solved by alleviating

its C/H ratio load on the “actual” reformer unit, which operates on the product gases of the first reactor.

There are numerous opportunities for further improving the two-reactor setup discussed above. The main opportunity lies in the symbiotic relationship between the two reactors in terms of both energy and mass exchange. Mass exchange is already discussed previously, and it is simply the transfer of products from the first reactor to the second reactor for upgradation. As for heat exchange, the opportunity lies in the fact that the two reactors are operated at different operational temperatures. Since the product gases from the first reactor are low temperatures relative to product gases of the second reactor, there is a possibility of preheating the product gases of the first reactor by the relatively hot gases exiting from the second. As carbon formation tendency increases with an increase in pressure, if the first reactor is operated at high-pressure condition and the second reactor at low pressure (syngas formation favors low-pressure condition), then there is also scope to generate external work. In this, the high-pressure gases from the first reactor will be passed through a gas turbine to derive external work, while low-pressure gases will be sent to the second reactor for reforming reaction. An illustration of this scheme is provided in Figure 4.5 below.

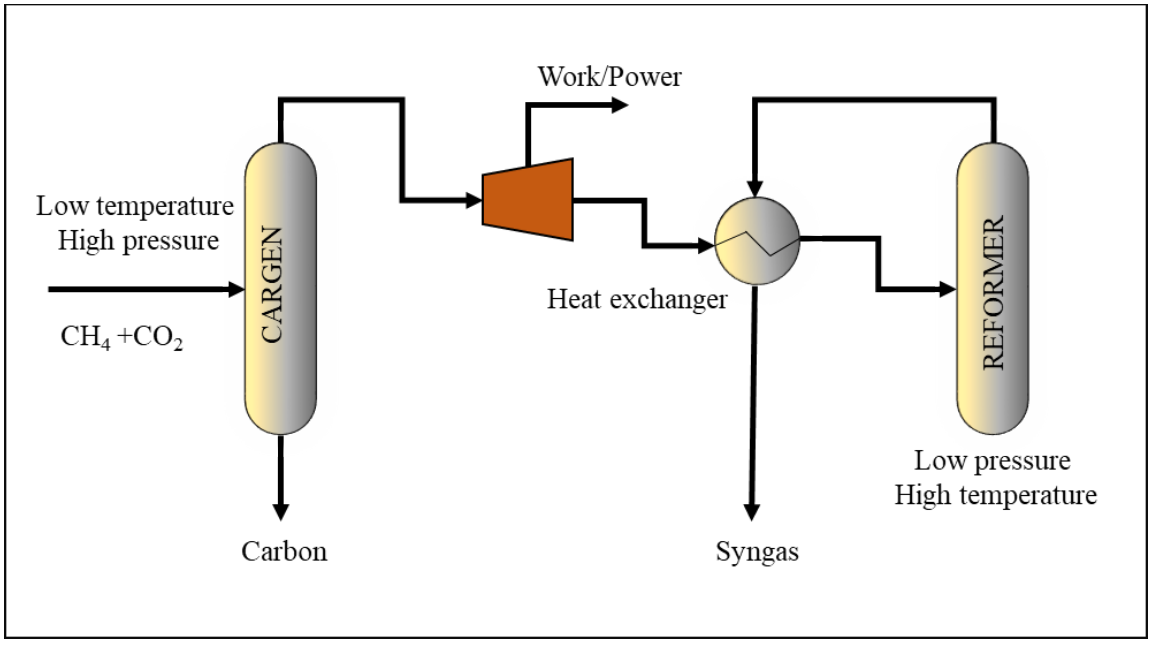

Figure 4.5 Illustration of the symbiotic relationship between the CARGEN™ and REFORMER reactors in terms of opportunities presented in terms of mass and heat exchange.

4.2.5 Variants of the Two-Reactor Setup

In this section, two variants of the two-reactor setup process are presented. These alternative designs are "sub-sets" or alternatives to the original process, and demonstrate a perspective into the flexibility of the proposed scheme to meet the different objective functions desirable by the end consumer or the downstream process plant. These case studies demonstrate the flexibility of the two processes in producing different products while utilizing the same energy requirements.

1. Case Study 1:

This case study demonstrates a situation in which the product gases from the first reactor are fed to the second reactor directly without any pre-treatment or mixing with external feed.

In this, a mixture of CH_4, CO_2, and O_2 is compressed and fed to the CARGEN™ reactor at 400 °C and 25 bar to produce solid carbon. The unreacted or partially reacted gases from the first reactor are fed to the second reactor wherein they are converted to syngas at a high temperature of 820 °C and 25 bar pressure. Figure 4.6 provides an illustration of this case study:

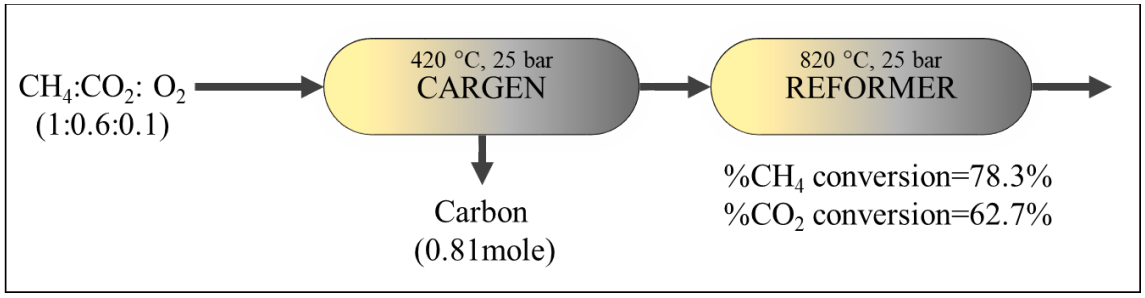

Figure 4.6 Case Study 1 block flow diagram of the two-reactor setup

As can be seen from Figure 4.6, the feed to the first reactor comprises of CH_4, CO_2, and O_2. The primary reason behind the utilization of a small quantity of oxygen is to promote an internal combustion reaction that could support the endothermic energy requirements of the DRM process. In-situ energy production in the reactor reduces the inefficiencies associated with the jacketed heat transfer, which is a general industrial practice. Energy assessment of the present case scenario indicates a total energy requirement of ~120kJ/mol, which is almost 50% that of DRM. In addition to this, the total CO_2 and CH_4 conversion from the overall process are seen to be about 62% and 78%, respectively. Energy reduction at this scale could reduce the CO_2 footprints associated with fuel combustion tremendously.

Additionally, the first reactor is also assessed to operate in Auto-thermal mode if the operating temperature is about 420 °C, indicating that the reactor is self-sustaining in terms of heat duty while at the same time produces a significant quantity of solid carbon. In this particular case scenario, about 0.81 moles of carbon are produced per 1.6 moles of carbon in the feed. This indicates almost 50% carbon capture in the first unit itself. The value-addition from the second reactor could be observed in the fact that it operates onto a "pretreated" and improved C/H ratio of the feed gas and therefore produces a higher quality syngas of ratio of 2.8, with an overall yield of 1.18 moles.

2. Case Study 2:

This case study is slightly different from the previous case as it utilizes an additional feed of methane to the second reactor to manipulate its syngas ratio and yield. Figure 4.7 below illustrates the block flow diagram of the two reactor set up under this scheme of operation.

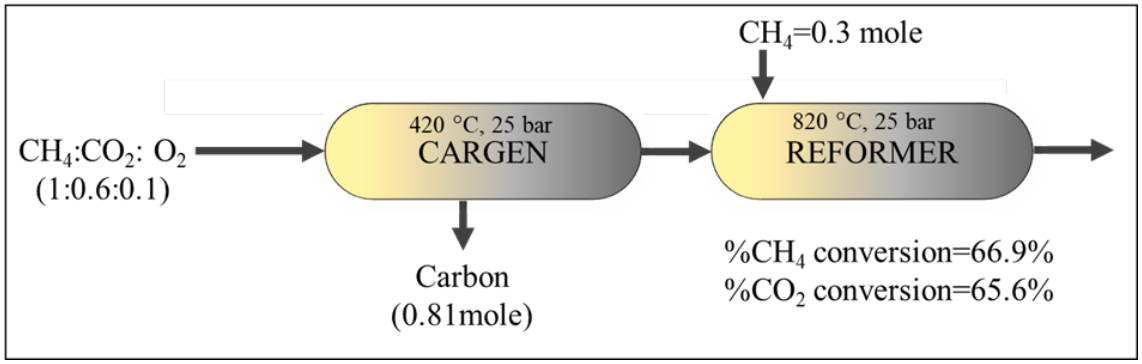

Figure 4.7 Case Study 2 block flow diagram of the two-reactor step

The operational pressure of both the reactors is set to 25 bar, while the two reactors operate at different temperature conditions. The temperature of the first reactor (Or CARGEN™ reactor) is at 420 ºC, while the second reactor is at 820 ºC. Similar to the previous case study, the carbon formed in the first reactor at 420 ºC and 25 bar is about 0.81, while the syngas produced from the second reactor is of a different quality due to additional methane co-feed. An energy assessment on the overall process suggests that this process would require about 118 kJ/mol of energy (47% of DRM) while producing a syngas ratio of 2.7 at a yield of 1.39 moles. The implication of the addition of methane is to demonstrate the flexibility of the process in producing different qualities of syngas by the addition of side reactants.

In terms of energy requirements, both case 1 and case 2 have almost equivalent performance as both the processes require ~120kJ/mol of energy. However, both the processes differ in terms of the quality of syngas produced. The key benefit of the two-reactor operation is, therefore, not just limited to its tendency to overcome carbon formation issues, but also in adjusting the syngas ratio depending upon downstream process requirements. In addition to this, lower energy requirements are also realized due to the breakdown of the DRM process into its two constituent reaction sets. Process optimization on different variables of the processes can further improve the performance of the CARGEN™ reactor system.

4.2.6 Carbon footprint and operating cost comparisons for proposed processes

Based on the approach described in a previous publication[128], the carbon footprint of the CARGEN™ process was calculated and is shown in Figure 4.8. The two CARGEN™ cases studied have a syngas ratio of about 2.75, and when compared to the ATR, which operates in this region, there is a marked reduction in the overall CO_2 emissions.

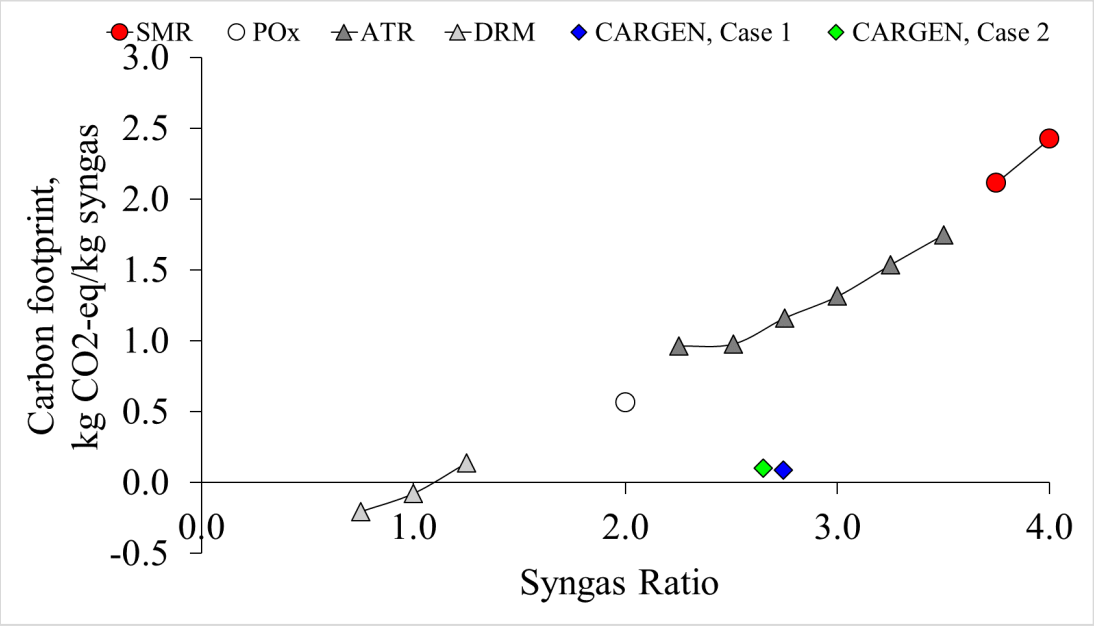

Figure 4.8 Carbon footprint comparison for proposed reforming processes with commercial processes

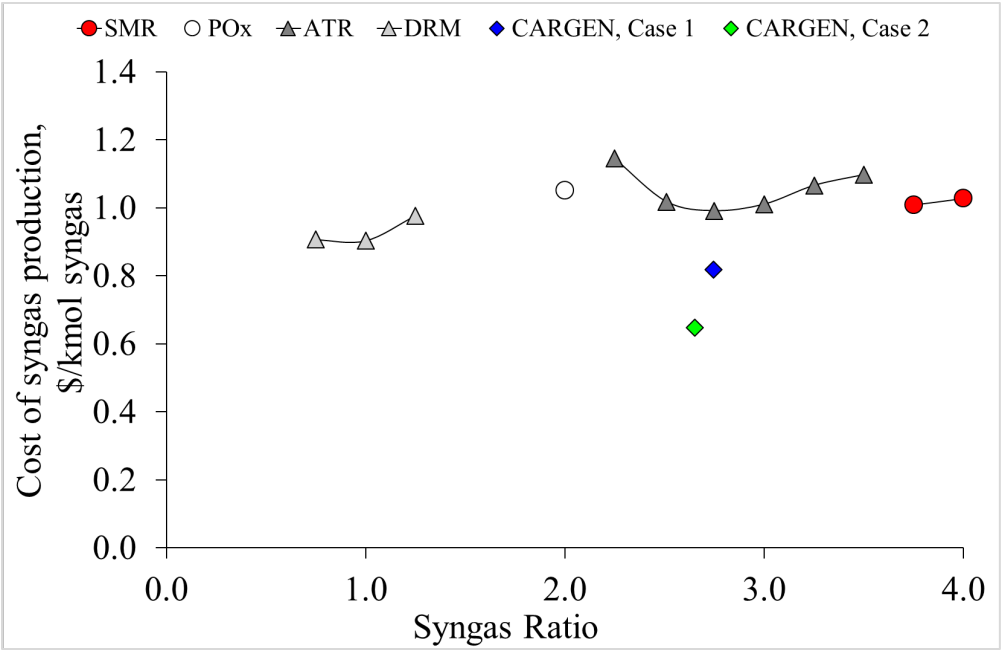

Figure 4.9 Operating cost comparison for proposed reforming processes

For a preliminary comparison of the operating costs of these processes, the costs of feedstock (natural gas), fuel for reformer (by natural gas firing), and oxidant production were considered. A selling price of $200/MT was considered for the coke. Spot market prices for coke are in the range of $300/MT, and refinery sources quote a price of $100/MT, and hence a median price of $200/MT was chosen for the analysis presented here. Removal of coke from the catalyst is still a technological challenge, and its cost has not been included in the analysis. The cost of syngas production via different competing processes across syngas ratios is shown in Figure 4.9. It can be seen that at least a 40% reduction in CO_2 footprint at 40% low operating cost could be easily achieved using the CARGEN™ process compared to industry benchmarks.

4.3 Experimental proof of CARGEN™ technology

4.3.1 Catalyst characterization and experimental approach

4.3.1.1 Catalyst Characterization

Inductive coupled plasma (ICP) analysis

The Nickel catalyst used for all the studies in this paper was purchased from a commercial vendor with the labeled chemical composition of 20% Ni/γ-Al_2O_3. In order to deduce the exact composition, we have conducted an inductively coupled plasma (ICP) test using the Plasma Quant PQ 9000 series ICP-OES device available in the applied catalysis lab at Texas A&M University at Qatar (TAMUQ). Following is the tabular representation of the components identified by this test:

Table 4.2 ICP-OES data from Plasma Quant PQ 9000instrument

sample name	expected Ni wt%	% Ni by ICP-OES
Riogen150-250	20	17.41667

Temperature programmed reduction (TPR) analysis

In order to find the most suitable reduction conditions for the 20% Ni/γ-Al_2O_3 catalyst, a temperature-programmed reduction (TPR) was conducted using an Autochem-II Micromeritics chemisorption equipment. The thermal conductivity detector (TCD) signal generation as a function of temperature is provided below in Figure 4.10.

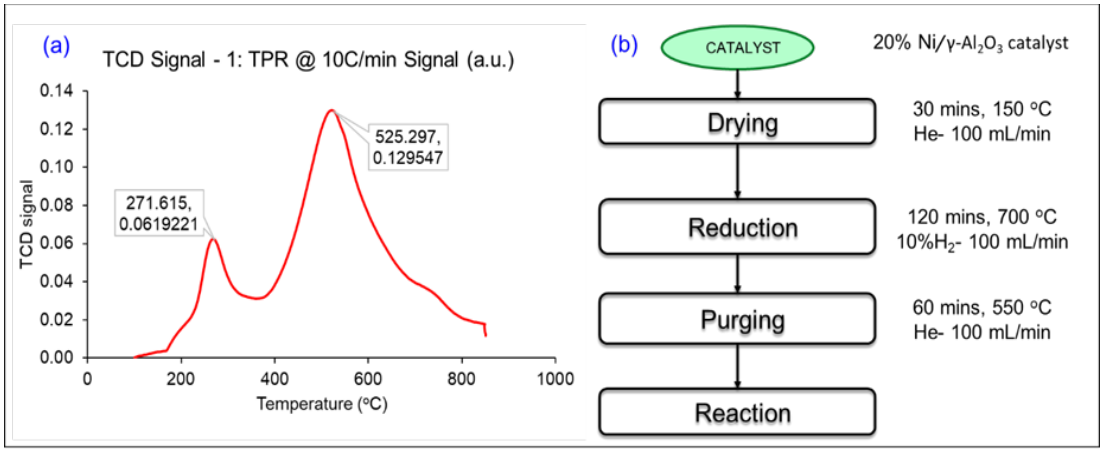

Figure 4.10 (a) TPR profile of the commercial 20% Ni/γ-Al_2O_3 catalyst, (b) Experimental protocol used for all the reactions.

There are two observable peaks in the TPR profile at 271 °C and 525 °C temperature respectively, and a further temperature increase does not result in a further reduction. Therefore, a temperature beyond 600 °C temperature will be sufficient for complete reduction. Nevertheless, in order to ensure complete catalyst activation, a temperature of 700 °C was chosen for reduction. The reduction protocol for all the tests conducted in this study is provided in Figure 4.10b.

Physisorption data

The physisorption data of the fresh catalyst sample was deduced using a standard Tri-star II Micromeritics instrument. Table 4.3 reports the key information from this study:

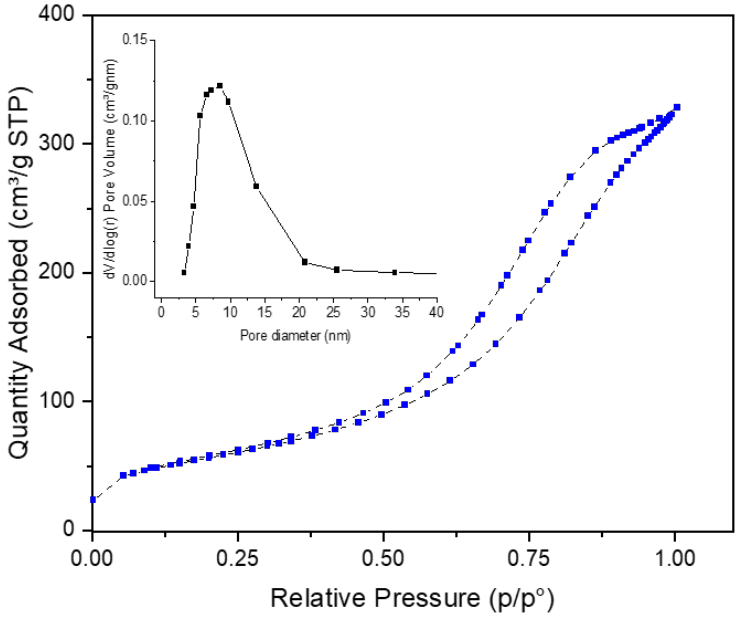

Figure 4.11 BET and BJH plots of the commercial 20% Ni/γ-Al_2O_3 catalyst

Table 4.3 Physisorption data of the fresh catalyst

S.No	Quantity	Value
1	Single point surface area at p/po=0.30117	198.8170 m^2/g
2	Brunauer-Emmett-Teller (BET) surface area	201.44 m^2/g
3	Barrett, Joyner, and Halenda (BJH) adsorption cumulative surface area of pores	255.020 m^2/g
4	BJH desorption cumulative surface area of pores	325.5852 m^2/g
5	BJH Adsorption cumulative volume of pores between 5.000Å and 1500.000Å radius	0.552825 cm^3/g
6	BJH Desorption cumulative volume of pores between 5.000Å and 1500.000Å radius	0.585498 cm^3/g
7	BJH Adsorption average pore radius (2V/A)	43.355 Å
8	BJH Desorption average pore radius (2V/A)	35.966 Å

4.3.1.2 Experimental analysis and quantification

Experiments conducted in this work were done using two reaction systems: (a) Thermo-gravimetric analysis (TGA) for weight gain measurement, and (b) Autochem II Micromeritics chemisorption equipment used as a flow-through reactor. The quantification of results was done using the material balance on the composition of the gases evolved during the reaction. The gaseous composition of various reaction species was detected using the standard residual gas analyzer (RGA) equipment (make HIDEN® HPR20) calibrated before each run using a calibration cylinder comprising of all the reaction gases (CH_4, CO_2, O_2, H_2, CO_2, He and Ar). The following two subsections provide more details on both the experimental procedure for each equipment as well as the quantification of results.

Experimental procedure

TGA analysis:

TGA analysis was conducted for weight gain testing and proof of concept studies of the CARGEN™ process. For this, the TGA/SDT Q600equipment by TA® at the applied catalysis laboratory of TAMUQ was used. All the experiments were done using approx. 20 mg of commercial 20% Ni/γ-Al_2O_3 catalyst at a constant gas composition of $CH_4/CO_2/O_2$=1/0.6/0.1 for CARGEN™ and CH_4/CO_2=1:1 for DRM. Figure 4.10b describes the standard experimental protocol followed for each test. Since the TGA equipment does not have a provision for extra mass flow controllers (MFCs), a specially designed bench with two calibrated mass flow controller(MFC) was used for mixing the two CARGEN™ cylinders (one flammable gas cylinder of methane and the other of oxidizer gases CO_2 and O_2) as shown in Figure 4.12. Both the MFCs were calibrated using

a wet flow meter, and calibration charts were developed for each reaction gas mixture for both the MFCs. In particular, both the MFCs were calibrated for 10% H_2/90% Ar, 10% O_2/90% He, 100% He, 100% Ar, 10% CH_4/10% CO_2/78% He/2% Ar, 100% N2, 30% CO_2/ 5% O_2/ 63% He/2% Ar and 80% CH_4/18%/He/2% Ar gases as they were required during different stages of the experiments. The mixed gas of the desired composition was fed to one of the two inlet ports of the TGA, while the second port was used for inert gas flow in between the reactions and for purging and drying operations. The TGA software enables the design of methods based on the desired protocol with the provision of switching of the gases at set time intervals while monitoring weight gain, while the exit of TGA is connected with HIDEN® HPR 20RGA for online monitoring of the reaction gas composition. The data obtained from TGA, as well as RGA therefore allows simultaneous analysis of both the weight gain as well as the gaseous composition of the reaction gases. The raw data provided by RGA are in partial pressure values, which are then later processed in an in house developed Microsoft® Excel® VBA Macros® code using a detailed material balance calculation to evaluate the overall CH_4 and CO_2 conversion.

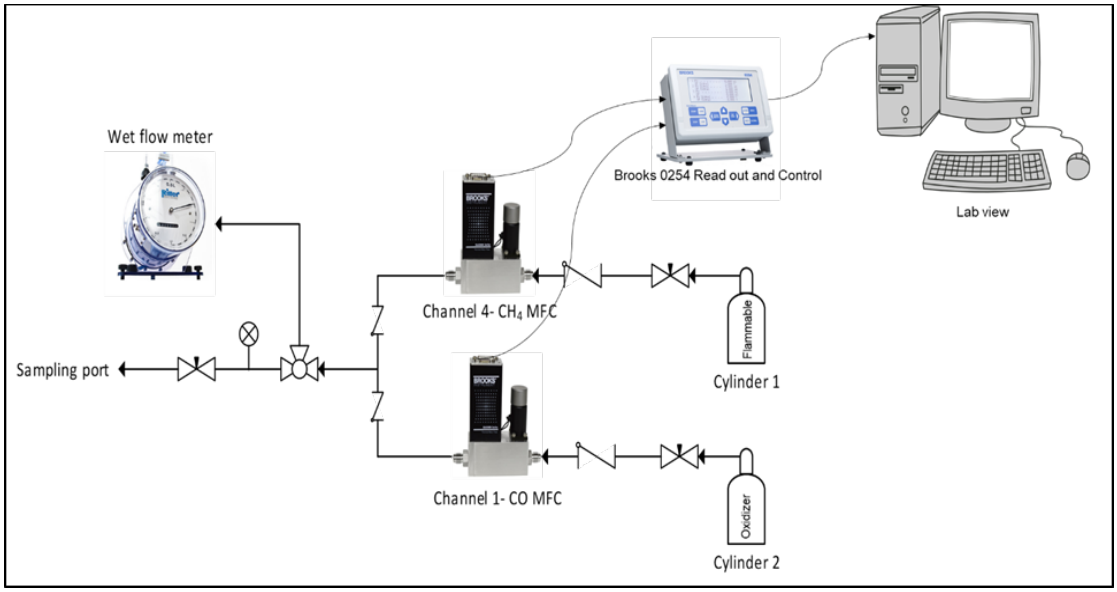

Figure 4.12 Process flow diagram of a specially designed MFC bench for CARGEN™ and DRM testing

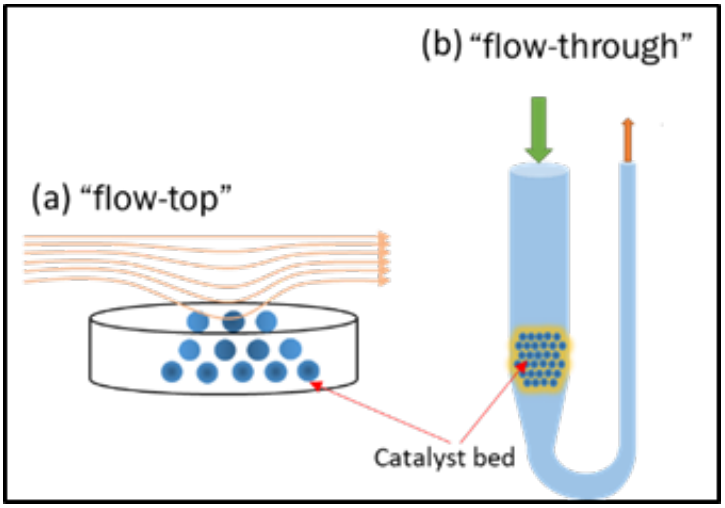

Figure 4.13 Comparison of flow profile between (a) flow-top and (b) flow-through reaction systems

Flow-through analysis

While the TGA instrument provides an estimate of the weight gain of carbon deposited during the CARGEN™ or DRM experiment, it does not allow sample analysis beyond the

20-40 mg scale. The second limitation of TGA is its inability to provide 100% contact of reaction gases with the catalyst due to its "flow-top" nature, as shown in Figure 4.13 a. Therefore, in order to test the behavior of the system in an actual industrial type "flow-through" or packed bed kind of reaction system, the standard chemisorption equipment by Micromeritics® Autochem II equipment was used. This instrument has a provision for connecting a "U" shaped reaction tube made up of quartz. The equipment also has several MFCs in its "carrier," "prep," and "loop" modes that allow the flow of the different reaction gases. In addition, the manual provided with the equipment provides an easy method for calculating the calibration factors of the various gas mixtures based on their thermal conductivity. Also, the equipment can be connected with standard RGA equipment, which in our case, was HIDEN® RGA. The same bench of calibrated MFCs was used as in the case of TGA to minimize the number of parameter variations and also to follow the same protocol as described in Figure 4.10b. The main advantage of this instrument is that larger sample quantity can be analyzed. In our case, we have used about 200 mg of commercial 20% Ni/γ-Al_2O_3 catalyst for all testing using this instrument, which about ten times more compared to the quantity used in the TGA, which also provides quick testing of the behavior of the system under ten times catalyst-scale up conditions.

Quantification

All the material balance conducted for both the TGA as well as the flow-through analysis, was done using HIDEN® RGA as described in the previous sections. The material balance was done by comparing the quantities of reactant gases in the inlet and the outlet of the reaction system using argon as an internal standard. A baseline reading of the inlet gas

composition was taken before the experiment in bypass mode to identify the reactant gas composition. The exit gas composition was recorded at approx. every one-minute interval in HIDEN® RGA. A material balance code was developed in Microsoft® Excel® VBA Macros® in order to quickly evaluate the conversion profiles. A case example of one data point calculation is provided below for further understanding.

Material Balance calculations:

Feed flow at STP condition shown by MFC:

Let C1 represent STP volume flow from a cylinder containing CH_4/He/Ar gas mix.

Let C2 represent STP volume flow from a cylinder containing CO_2/O_2/He/Ar gas mix.

C1= 30 mL/min

C2= 48 ml/min

Total Flow of feed gas = V1= C1+C2= 78 ml/min.

Table 4.4 Feed gas composition shown by RGA (vol%) at 120°C :

H_2	0
He	43.83
CH_4	30.11
H_2O	0.35
CO	0
CO_2	22.32
O_2	2.24
Argon	1.67

As these readings were taken without reaction and there was no phase change in the system (water was not present), % volume distribution at STP and at RGA conditions ($at\ 120°C$) are the same.

Volume of Argon ($V_{Ar,STP}$):

$V_{Ar,STP} = 1.67\ \%\ of\ 78 \frac{mL}{min}$

$V_{Ar,STP} = 1.3026 \frac{mL}{min}$

$\rho_{Ar,STP} = 1.76128192599771e-003 \frac{g}{mL}$ (Ref: ASPEN® HYSYS V8.8, using PR fluid package)

Mass of Argon entering the system (M_{Ar}):

$M_{Ar} = V_{Ar,STP} \times \rho_{Ar,STP}$

$M_{Ar} = 0.002294 \frac{g}{min}$

As the Mass of Argon will not change after the reaction, we will use Argon as an internal standard.

Similarly,

Mass of methane, Carbon dioxide and Oxygen entering the system ($M_{CH_4}, M_{CO_2}, M_{O_2}$) can be calculated as follows:

$M_{CH_4,FEED} = V_{CH4,STP} \times \rho_{CH4,STP}$

$\rho_{CH4,STP} = 7.08473178693596e-004 \frac{g}{mL}$ (Ref: ASPEN® HYSYS V8.8, using PR fluid package)

$M_{CH_4,FEED} = 0.016639 \frac{g}{min}$

$M_{CO2,FEED} = V_{CO_2,STP} \times \rho_{CO_2,STP}$

$\rho_{CO_2,STP} = 1.95178789837081e-003 \frac{g}{mL}$ (Ref: ASPEN® HYSYS V8.8, using PR fluid package)

$M_{CO2,FEED} = 0.03398 \frac{g}{min}$

$M_{O2,FEED} = V_{O_2,STP} \times \rho_{O_2,STP}$

$\rho_{O_2,STP} = 1.41087461527664e-003 \frac{g}{mL}$ (Ref: ASPEN® HYSYS V8.8, using PR fluid package)

$M_{O2,FEED} = 0.002465 \frac{g}{min}$

Table 4.5 Product gas composition shown by RGA (vol%) at $\boldsymbol{120°C}$:

	Product (Vol %)
H_2	2.74
He	40.73
CH_4	26.09
H_2O	6.39
CO	0.59
CO_2	21.7
O_2	0
Ar	1.7

Since Argon was taken as an internal standard and as it does not take part in the reaction mixture, its mass will not change after the reaction.

Therefore, the volume of product gas mixture at RGA conditions $(120°C)$ is as follows:

$V_{Ar,RGA} = \frac{M_{Ar}}{\rho_{Ar,RGA}}$

$\rho_{Ar,RGA} = 1.22236802820798e-003 \frac{g}{mL}$ (Ref: ASPEN® HYSYS V8.8, using PR fluid package)

$V_{Ar,RGA} = \frac{0.002294}{1.22236802820798e-003} \frac{mL}{min}$

$V_{Ar,RGA} = 1.876886 \frac{mL}{min}$

The volume of Product gases at RGA condition:

$V_{products,RGA} = \frac{V_{Ar,RGA}}{Vol\%_{RGA}}$

$V_{products,RGA} = \frac{1.876886 \times 100}{1.7} \frac{mL}{min}$

$V_{products,RGA} = 110.4050588 \frac{mL}{min}$

Therefore,

$V_{CH4,RGA} = Vol\%_{CH4,RGA} \times V_{products,RGA}$

$V_{CH4,RGA} = 0.2609 \times 110.4050588 \frac{mL}{min}$

$V_{CH4,RGA} = 28.80467984 \frac{mL}{min}$

Similarly, Volumes of CO_2, CO can be calculated as follows:

$V_{CO2,RGA} = 0.217 \times 110.4050588 \frac{mL}{min}$

$V_{CO2,RGA} = 23.95789776 \frac{mL}{min}$

$V_{CO,RGA} = 0.0059 \times 110.4050588 \frac{mL}{min}$

$V_{CO,RGA} = 0.65139 \frac{mL}{min}$

Mass of CH_4, CO_2 & O_2 can be calculated by using densities of these gases at RGA conditions.

$M_{CH4,products} = \rho_{CH4,RGA} \times V_{CH4,RGA}$

$M_{CH4,products} = 4.91174251876323e-004 \times 28.80467984 \frac{g}{min}$

$M_{CH4,products} = 0.014148 \frac{g}{min}$

Similarly,

$M_{CO2,products} = \rho_{CO2,RGA} \times V_{CO2,RGA}$

$M_{CO2,products} = 1.34932344363214e-003 \times 23.95789776 \frac{g}{min}$

$M_{CO2,products} = 0.032327 \frac{g}{min}$

$M_{CO,products} = 8.56784406887865e-004 \times 0.65139 \frac{g}{min}$

$M_{CO,products} = 0.000558 \frac{g}{min}$

$M_{H2O} = 5.55235167794238e-004 \times 0.0639 \times 110.4050588 \frac{g}{min}$

$M_{H2O} = 0.003917 \frac{g}{min}$

$M_{H2} = 6.16542972041666e-005 \times 0.0274 \times 110.4050588 \frac{g}{min}$

$M_{H2} = 0.000187 \frac{g}{min}$

Therefore,

$$CH_4\%\ conversion = \frac{M_{CH4,FEED} - M_{CH4,products}}{M_{CH4,FEED}} \times 100$$

$$CH_4\%\ conversion = \frac{0.016639 - 0.014148}{0.016639} \times 100$$

$CH_4\%\ conversion = 14.9709\ \%$

Similarly,

$CO_2\%\ conversion = 4.8646\ \%$

Atom balance for validation of results:

Feed:

Moles of CH_4 entering the system $= \frac{M_{CH4,FEED}}{MW_{CH4}} = \frac{0.016639\frac{g}{min}}{16\frac{g}{gmol}} = 0.0010399375\,\frac{gmol}{min}$

Moles of CO_2 entering the system $= \frac{M_{CO2,FEED}}{MW_{CO2}} = \frac{0.03398\frac{g}{min}}{44\frac{g}{gmol}} = 0.0007722727273\,\frac{gmol}{min}$

Moles of O_2 entering the system $= \frac{M_{O2,FEED}}{MW_{O2}} = \frac{0.002465\frac{g}{min}}{32\frac{g}{gmol}} = 0.00007703125\,\frac{gmol}{min}$

Total $C\ moles$ entering the system=$Moles\ of\ C\ in\ CH_4 + Moles\ of\ C\ in\ CO_2$

$= 0.0010399375 + 0.0007722727273$

$= 0.001812210227\ moles$

Total $O\ moles$ entering the system=$Moles\ of\ O\ in\ O2 + Moles\ of\ O\ in\ CO_2$

$= 2 \times 0.0007722727273 + 2 \times 0.00007703125$

$= 0.001698607955\ moles$

Total $H\ moles$ entering the system=$Moles\ of\ H\ in\ CH_4$

$= 4 \times 0.0010399375\ moles$

$= 0.00415975\ moles$

Product:

Moles of CH_4 leaving the system= $\frac{M_{CH4,products}}{MW_{CH4}} = \frac{0.014148\frac{g}{min}}{16\frac{g}{gmol}} = 0.00088425\,\frac{gmol}{min}$

Moles of CO_2 leaving the system= $\frac{M_{CO_2,products}}{MW_{CO_2}} = \frac{0.032327\frac{g}{min}}{44\frac{g}{gmol}} = 0.0007347045455\,\frac{gmol}{min}$

Moles of O_2 leaving the system= $\frac{M_{O_2,products}}{MW_{O_2}} = \frac{0\frac{g}{min}}{32\frac{g}{gmol}} = 0\frac{gmol}{min}$

Moles of H_2O leaving the system= $\frac{M_{H_2O,products}}{MW_{H_2O}} = \frac{0.003917\frac{g}{min}}{18\frac{g}{gmol}} = 0.000217611112\frac{gmol}{min}$

Moles of H_2 leaving the system= $\frac{M_{H_2,products}}{MW_{H_2}} = \frac{0.000187\frac{g}{min}}{2\frac{g}{gmol}} = 0.0000935\frac{gmol}{min}$

Moles of CO leaving the system= $\frac{M_{CO,products}}{MW_{CO}} = \frac{0.000558\frac{g}{min}}{28\frac{g}{gmol}} =$

$0.000019928577143\frac{gmol}{min}$

Total $C\ moles$ leaving the system= $Moles\ of\ C\ in\ CH4 + Moles\ of\ C\ in\ CO2 + Moles\ of\ C\ in\ CO$

$= 0.00088425 + 0.0007347045455 + 0.000019928577143$

$= 0.001638883123\frac{gmol}{min}$

Total $C\ moles$ accumulated in the reactor as solid carbon $= 0.001812210227 - 0.001638883123 = 0.0001733271044\frac{gmoles}{min}$

Total $O\ moles$ leaving the system= $Moles\ of\ O\ in\ CO_2 + Moles\ of\ O\ in\ CO + Moles\ of\ O\ in\ H_2O$

$= 0.0007347045455 \times 2 + 0.000019928577143 + 0.000019928577143 + 0.000217611112$

$= 0.001727\frac{gmol}{min}$

Total $H\ moles$ leaving the system= $Moles\ of\ H\ in\ CH4 + Moles\ of\ H\ in\ H2O + Moles\ of\ H\ in\ H_2$

$= 0.00088425 \times 4 + 0.000217611112 \times 2 + 0.0000935 \times 2$

$= 0.004159222224 \frac{gmol}{min}$

Validation of results:

In order for Mass balance to be correct, total $O\ moles$ entering the system should be equal to total $O\ moles$ leaving the system. Also, total $H\ moles$ entering the system should be equal to total $H\ moles$ leaving the system. $C\ moles$ will quantify carbon formation in the reactor as carbon is accumulated in the system.

Validation for $O\ moles$:

Total $O\ moles$ entering $= 0.001698607955 \frac{gmol}{min}$

Total $O\ moles$ leaving = $0.001727 \frac{gmol}{min}$

Error $= \frac{0.001698607955 - 0.001727}{0.001698607955} \times 100$= -1.67 %

Validation for $H\ moles$:

Total $H\ moles$ entering $= 0.00415975 \frac{gmol}{min}$

Total $H\ moles$ leaving = $0.004159222224 \frac{gmol}{min}$

Error $= \frac{0.00415975 - 0.004159222224}{0.00415975} \times 100$= 0.012688 %

Therefore, the overall error in mass balance calculated by the difference in the number of moles of hydrogen and oxygen entering and leaving the system is below 2%.

4.3.2 Results and Discussion

The thermodynamic equilibrium assessment of the CARGEN™ reactor, as discussed in section 4.2, showed that solid carbon is a favorable product in a temperature range of 420 to 600 ºC, as shown in Figure 4.14. The experimental proof, therefore, was conducted at a temperature of 550 ºC, which is within the operational range of the CARGEN™ process. In addition, to support the claim that the CARGEN™ process could be used for any feed gas that comprises of CH_4, CO_2, and O_2, a feed gas composition of $CH_4/CO_2/O_2$=1/0.6/0.1 was taken, that closely resembled flue/landfill/biogas composition[129]. However, this feed ratio may be changed depending upon available feed gas at the site, and optimization can also be done to achieve a desired quantity of carbon or achieve a specific syngas ratio. Figure 4.14 b shows the experimental conversion profile of the CARGEN™ reactor at a temperature of 550 ºC. It can be seen that experimental results closely match thermodynamic results within a margin of 10-15%. A closer examination of the actual spent catalyst from this experimental run using SEM and TEM (Figure 4.14 c) reveals the formation of MWCNTs.

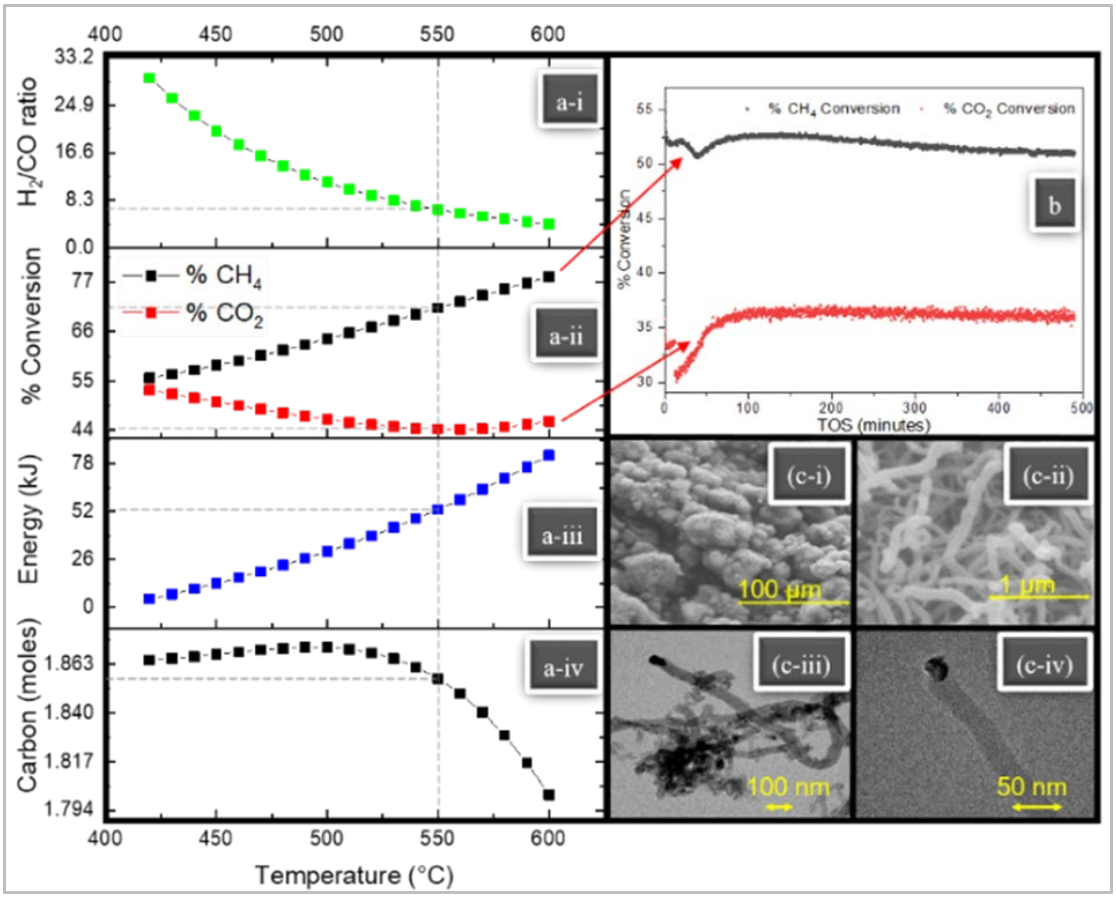

Figure 4.14 Thermodynamic profiles of the novel CARGEN™ reactor from 400°C to 600°C temperature, (b) % Experimental conversions vs. time on stream (TOS) in a flow-through the reactor for a TOS of 500 minutes at 550 ºC using 20 wt% Ni/Al_2O_3 catalyst (c-i, c-ii): SEM images at 100μm and 1 μm respectively, (c-iii, c-iv): TEM images at 100nm and 50nm, respectively.

A Raman analysis conducted by the project collaborators in Northwestern University of a 30-min CH_4 pyrolysis experiment on 20 wt% Ni/Al_2O_3 at 700, 600, 500, and 400°C showed that the MWCNT formation regime is gradually diminished with a decrease in temperature, and only nano-carbon remains at 400°C. These results demonstrate that MWCNT begins forming between 400 and 500°C. Figure 4.15 illustrates the corresponding ex-situ micro-Raman spectra, which indicates that the quality of the

MWCNT gets better (D/G ratio decreases while G'/G ratio increases) with an increase in temperature. It should be noted that the operational window of CARGEN™ is in the temperature range of 400-600 ºC, which is the most suitable condition for MWCNT formation per Raman results. High-value products coming from GHGs have attracted significant media attention[130–132] as well as interest from global energy corporations due to its encouraging preliminary economic data[133]. The commercial value of high-quality MWCNTs can be in the range of 1,000-10,000USD/kg[134].

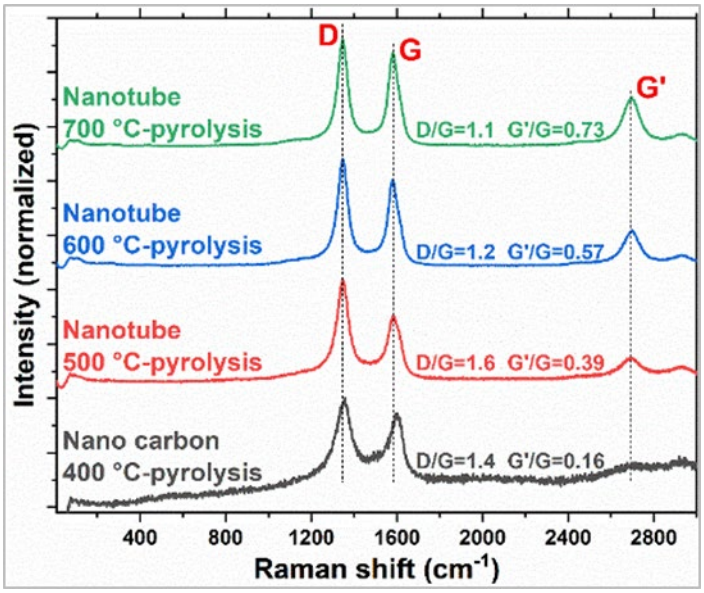

Figure 4.15 Raman spectra of surface carbon formed from 30-min CH_4 pyrolysis at 400, 500, 600 and 700°C respectively on 200 mg 20 wt% Ni/Al_2O_3 at a flow rate of 30 mL/min. The ratio of the intensity of D/G peaks is a measure of the defects present on carbon nanomaterials.

A thermo-gravimetric analysis (TGA) experiment coupled with a material balance on residual gas analyzer (RGA) data enabled a direct assessment of the CNT formation rate and feed conversions as a function of TOS. These results are provided in Figure 4.16.

Around 20 mg MWCNTs formation was observed in 138 min TOS at 550°C on 20 mg of commercial 20 wt% Ni/γ-Al_2O_3 catalyst entailing a remarkable CNT formation rate of 0.00722 $mg_{MWCNT}/mg_{Cat.}$/min. It should be reiterated that the target for the CARGEN™ reactor (the first reactor in CARGEN™ technology) is only to produce solid carbon (MWCNTs). The second reactor, on the other hand, which is a combined reformer, offers great flexibility in producing a desirable syngas ratio, as discussed in detail in the previous publications[135,136].

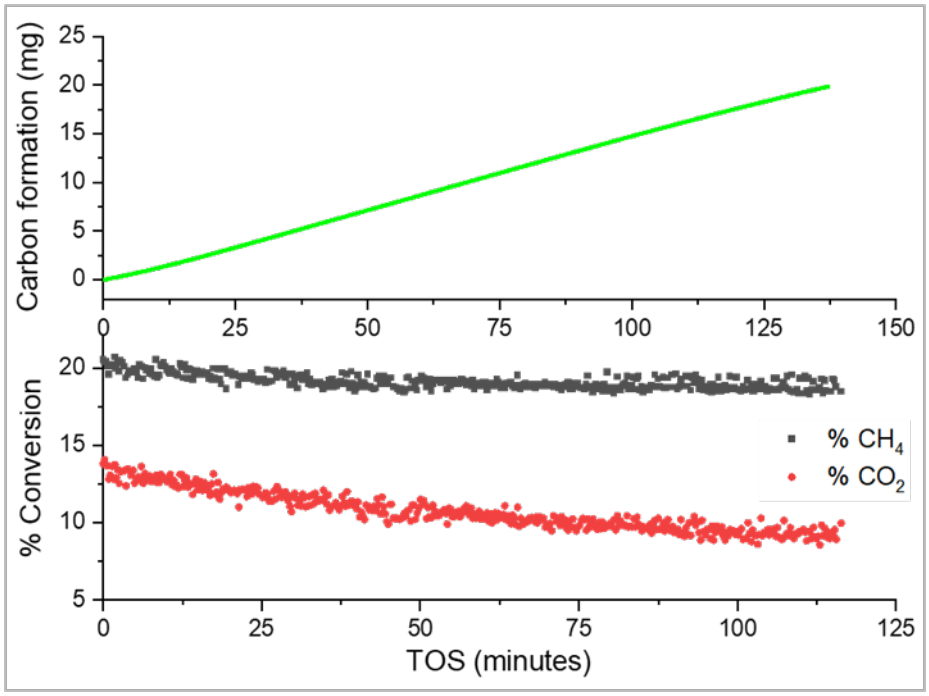

Figure 4.16 carbon growth vs. TOS on 20 mg of commercial 20% Ni/γ-Al_2O_3 catalyst and its corresponding conversion profiles of CH_4 and CO_2.

One of the primary challenges in any industrial process that involves carbon formation like DRM or catalytic cracker units is catalyst deactivation. Due to this, the entire plant has to be taken into maintenance, and the bulk of carbon has to be removed by either

scraping or by using other carbon removal techniques like etching, sonication, etc. However, even after the removal of bulk carbon, the catalyst nano sites are still covered with surface carbon[137], which needs to be removed to reactivate the catalyst.

4.4 A tailor-made catalyst for CARGEN™ technology

As indicated in the previous sections, the formation of solid carbon leads to the deactivation of the catalyst by reducing the accessibility to the active catalyst site, and therefore, does not allow a sustained reaction for a longer time[138]. Catalyst deactivation is particularly an issue in DRM, which has significantly offset its implementation on an industrial scale. As discussed in section 4.2.3, the reason behind such a peculiar carbon forming behavior is the unavailability of sufficient oxygen and hydrogen in the reaction gas. The O:C:H ratio in DRM is 1:1:2, while for other conventional reforming processes like for POX, it is 1:1:4, and for steam methane reforming (SRM) it is 1:1:6. Due to the scarcity of enough hydrogen and oxygen in the reaction gases, the surface carbon is unable to react and stays permanently at the surface. During this time, it continues binding with other surface carbon molecules and form strong C-C bonds that either result in the formation of amorphous or graphitic or carbon nanotube type of carbon[138]. The type and morphology of the surface carbon depend upon the type of the catalyst material, the surface energy, and the surface sites. CNT growth, in particular, is believed to happen via two different mechanisms[138,139]: (a) Tip growth mechanism- wherein CNT growth happens below the catalyst crystal site, and CNT is present between the active site and the support. In this case, the metal support interaction is not very strong, which allows for the

movement of the active material easily across the bed.[140] (b) Base growth mechanism-wherein CNT growth happens above the catalyst crystal site, and the active catalyst site is bound strongly at the support surface. It is believed that the tip growth mechanism is the most active pathway of carbon formation (and worst choice) for the DRM process since it enables significantly high carbon formation and accumulation due to weak metal-support interaction[140]. Also, the formation of CNTs will lead to a continuous change in the surface distribution of the active sites on the bed when the metal-support interaction is weak.

Since the objective of the CARGEN™ process is to form CNTs, it is required to synthesize a catalyst that provides specific characteristics that promote CNT formation growth. This approach of intensifying CNT growth formation on the surface is not a desirable feature of any methane reforming catalyst; however, it is a highly necessary feature for the CARGEN™ catalyst. The idea is to adjust the catalyst selectivity towards CNT and not towards syngas. Therefore, a catalyst material that provides essential features for CNT growth like the metal-support interaction, the acidity/basicity of the catalyst site, will be of use for the CARGEN™ process[140].

Based on an extensive literature review and experimental investigations, it was observed that the most critical parameter that influences the CNT growth is the metal-support interaction[141–146]. The weaker the interaction or the loosely bound the active metal is, the more will be its ability to grow CNT. Besides, the crystallite size also has a tremendous impact on the size (diameter) of the CNT, which was a direct result from microscopy assessment of the various spent CARGEN™ catalyst samples that were studied to develop the said CARGEN™ catalyst. Additionally, this assessment is also in

line with some of the previous works[141–148]. The tailor-made CARGEN™ catalyst presented in this work is synthesized in such a way that it benefits from the weak metal-support interaction to allow for the rapid growth of CNTs while facilitating active metal mobility. However, before getting into the details of the actual catalyst that was prepared for CARGEN™, a brief overview of the various catalyst synthesis techniques generally used for reforming catalyst synthesis is presented below.

Incipient Wet Impregnation (IWI) method: In this technique, the active target metal is dissolved in an organic or aqueous solution depending upon the type and nature of the active metal. This solution is poured on to support, which has the same pore volume as the volume of the metal solution. Due to capillary action, all of the metal solutions are drawn into the support pores. If the solution volume is more than the pore volume, then the diffusion process takes over, which results in much slower transport of the active metal to the pore. The catalyst slurry is then dried and calcined to eliminate all the volatile components within the solution while depositing the active metal on the catalyst support. The limitation is that the loading of the active metal is restricted to the solubility of the active metal solution. Therefore, the choice of solution is very critical in this process. The downside of this process, on the other hand, is that this process produces harmful and toxic volatile compounds upon calcination and also requires a large quantity of solvent for making the solution, sometimes even ten times in weight compared to the catalyst weight produced. Therefore, this type of catalyst is far from being environmentally sustainable.

Precipitation method: In this technique, precipitates are formed from a homogeneous liquid as a result of transformation in temperature or by chemical reaction.

The chemical reaction may happen due to the addition of acids or bases to a basic or acidic solution, respectively. It could also occur due to the addition of complex coagulating agents. In almost all the processes, either nucleation happens first, or simultaneously with agglomeration. Nucleation refers to the process in which small particles of solids start forming as a result of the transformation. In contrast, agglomeration refers to the growth of the particles due to the formation of new particles or association of existing particles. Again, due to the involvement of large quantities of chemical reagents and the production of wastes, this process is not environmentally sustainable.

Co-Precipitation method: This technique is a method for the synthesis of a multi-component system. In this method, macroscopic homogeneity is not easy to obtain, as the composition of the precipitate depends upon the differences in solubility between the components and the chemistry occurring during precipitation. One of the critical applications of this process is to synthesize molecular sieves.

Similar to the Precipitation and IWI method, this method also involves the use of numerous solvents and reagents that may lead to the generation of vast quantities of wastes that are not sustainable environmentally.

Other catalyst preparation methods include Sol-gel, hydrothermal, gelation, crystallization, etc., that require significant amounts of chemical reagents in quantities tens of times more in weight compared to the final weight of the synthesized catalyst[148]. Although these methods may have proven very useful for catalyst synthesis, there is significant trepidation in their implementation due to environmental concerns. Therefore, there is a need to identify better catalyst synthesis processes that are more sustainable and

scalable at the same time. More importantly, if the goal of the entire process (e.g., DRM or CARGEN™) is for improving sustainability and reduce carbon emissions, the role of green catalyst and sustainable approaches become very critical. With this as the final objective, the CARGEN™ catalyst was prepared using a unique catalyst synthesis technique that involves the use of traditional ball mills. Since the ball milling process is a unit operation that could be conducted using electricity, the generation of wastes from such a process is minimal.

Below is a detailed description of the traditional ball milling process used for catalyst synthesis:

Ball Milling Process for catalyst synthesis: The traditional ball milling process is a grinding method in which solids are ground together into very fine powders[145,146]. During this process, extremely high localized pressure is created at the point of collision of the rigid balls. These colliding balls are made from ceramics, flint pebbles, and stainless steel. Milling time, rpm of the rotational containers, size of the balls, and the ratio of sample weight to the number of balls are some of the critical control parameters. In addition to the benefit of ultra-fine grounding, the secondary advantage of the ball milling method is the homogenization of the solid mixture, which is significantly difficult to achieve.

The following Tailor-made catalyst for CARGEN™ technology g case example provides a step by step procedure followed in the laboratory to synthesize CARGEN™ catalyst:

4.4.1 Protocol to produce CARGEN™ catalyst using a ball milling method

Below is a step by step procedure that needs to be followed to prepare the CARGEN™ catalyst:

- To produce nickel oxide particles of size in the range of 50 to 500μm using conventional techniques that may include calcination of nickel nitrate etc.
- To mix alumina support available from any standard catalyst supplier (SASOL Purolox, Alpha Aesar, Sigma Aldrich, etc.) with the nickel oxide particles in such a ratio to produce 20% Ni/Al_2O_3.
    - For e.g., If 1 g of catalyst needs to be prepared, 0.253 g of NiO is mixed with 0.8 g of Al_2O_3. The extra 0.053 g of NiO is to account for the presence of oxygen in NiO as our ultimate target is to produce Ni and not NiO.
- Load the catalyst mixture and the balls in the ball milling container. For this experiment, Retsch(R) CRYOMILL apparatus was used. The parameters set for this experiment are the following:
    - Rotation rate: 50Hz at 250rpm,
    - sample weight (g): number of balls ratio= 1:10,
    - ball mass= 0.5 g,
    - milling time: 1 hour.
- After a milling time of 1 hour, unload the catalyst mixture and calcine at 400 ºC temperature for 4 hours to remove moisture and any other volatile compound that may be present in the catalyst mixture. For calcination, the muffle furnace was set

at a ramping rate of 5 ºC/min to reach a target of 400 ºC and then allowed to dwell for 240 minutes and then slowly ramped down to room temperature.

- After calcination, the sample was sieved at a 300µm size range. It was observed that all the particles passed through the sieve, indicating that the average particle size was below 300µm size.

4.4.2 Thermo-Gravimetric Analysis (TGA) Experiment:

A TGA analysis was conducted for weight gain testing and proof of concept studies of the CARGEN™ process. For this, the TGA/SDT 600equipment by TA® was used. Following is the step by step procedure that was adopted for this experiment:

- A 20 mg batch of fresh calcined catalyst is taken and placed in a sample Alumina crucible of the TGA equipment. An empty reference alumina crucible of the same weight is kept on the second weighing pan of the crucible to eliminate any weight fluctuation by temperature gain during the experiment.
- Next, the weighing pans are tared to record a zero weight value. Reduction protocol is initiated, which comprises the following steps:
    - Drying at 150 ºC temperature for 2 hours at 100 mL/min of argon gas.
    - Ramping up the temperature at the rate of 5 ºC/min to a target temperature of 800 ºC temperature and then hold for 2 hours. After reduction is complete, TGA temperature is reduced down to 550 ºC, which is the desirable CARGEN™ reactor temperature.

- CARGEN™ reaction gases comprising of O_2, CO_2, and CH_4 in the ratio of 0.1/0.6/1, respectively, are fed to the TGA reactor to initiate the reaction. The weight gain profile from this experiment is shown in Figure 4.17.

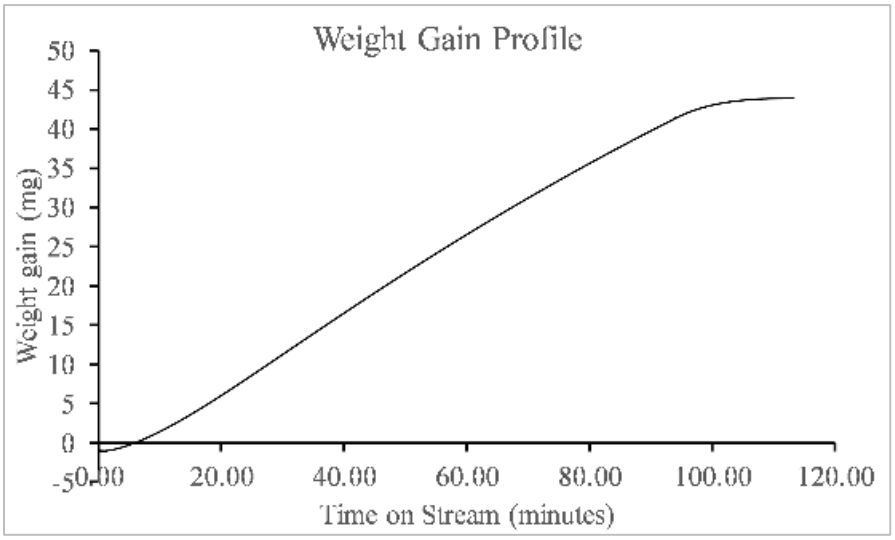

Figure 4.17 Weight gain profile in the TGA experiment of the CARGEN™ catalyst

4.4.3 Characterization results

4.4.3.1 Fresh catalyst physisorption

The physisorption data of the fresh catalyst sample was obtained from a standard Tri-star II Micromeritics instrument. Table 4.6 reports data on the Brunauer–Emmett–Teller (BET) surface area and the Barrett-Joyner-Halenda (BJH) pore volume, while the Adsorption/desorption isotherms linear plot is provided in Figure 4.18. The fresh catalyst exhibits type-IV type of isotherm with the presence of a type H1 hysteresis loop. BET results suggest that the catalysts particles are of mesoporous and are spherical in nature with uniform size and shape.

Table 4.6 Physisorption data of the fresh novel CARGEN™ catalyst

Quantity	Value
Single point surface area at p/po=0.30117	101.6899 m2/g
Brunauer-Emmett-Teller (BET) surface area	103.9172 m2/g
Barrett, Joyner, and Halenda (BJH) adsorption cumulative surface area of pores	108.369 m2/g
BJH desorption cumulative surface area of pores	128.757 m2/g
BJH Adsorption cumulative volume of pores between 5.000Å and 1500.000Å radius	0.513009 cm3/g
BJH Desorption cumulative volume of pores between 5.000Å and 1500.000Å radius	0.544415 cm3/g
BJH Adsorption average pore radius (2V/A)	94.931 Å
BJH Desorption average pore radius (2V/A)	84.565 Å

4.4.3.2 Fresh catalyst chemisorption

To find the most suitable reduction temperature conditions for the fresh as prepared catalyst, a TPR experiment was conducted in the standard Autochem-II Micromeritics chemisorption equipment. The TPR plot in terms of thermal conductivity change signal, is presented in Figure 4.19. It can be observed that a strong TCD peak at a temperature of 498 ^{o}C is formed, indicating that the material is reducible beyond the temperature of 498 ^{o}C. The reducibility of the catalyst was calculated using the hydrogen consumption in the

H_2-TPR experiment. The actual H_2 uptake was found to be 2287 μmoles/g of the catalyst at STP. As per the theoretical calculations, the H_2 uptake of the catalyst was found to be 3412 μmoles/g of the catalyst at STP. Therefore, the degree of reduction of the catalyst is 67%. It is also worth noting that Ni supported on a γ-Al_2O_3 exhibits two distinct reduction temperatures between 350-900°C as reported in many works of literature. This is due to the fact that the strong metal-support interaction increases the reduction temperature of bulk $_2O_3$ and also the formation of a difficultly reducible NiO due to strong interaction with support. In the present catalyst, only one reduction peak of the Ni around 498 °C is observed, which indicates the formation of weak support-metal-interaction (SMI), which is intended for the CNT tip growth mechanism. The TPR results further indicate that the catalyst thus forms an egg-shell type of structure.

4.4.3.3 X-Ray Diffractometer (XRD) study

The XRD analysis of the fresh and the reduced sample was done using the Rigaku Ultima IV diffractometer with Cu (Kα) radiation (40kV/40 mA). Both the samples were loaded separately, and recording was done in the 2θ range of 20–110°, in steps of 0.02° or 2 s intervals. Figure 4.20presents stacked XRD plots of both fresh and the reduced samples. It can be seen clearly that the all the peaks in the fresh sample are for NiO and Al_2O_3 catalyst, while for the reduced sample, most of them have been converted to Ni as noted by the peak shifts. The crystallite size of the fresh and reduced catalyst samples at Ni (012) and Ni (111) plane was calculated using the Scherrer equation. Mild (1.5X) sintering of the Ni0particles upon reduction with H_2 was observed as the crystallite size of the reduced

sampled increased to 35 nm from 21.4 nm of the fresh sample. The sintering due to coalescence is an established phenomenon by which NiO crystallite migrates at the support surface due to higher temperatures reduction and forms larger size crystallite. Coalescence of Ni0is an exothermic reaction which also contributes to the sintering of the crystallites.

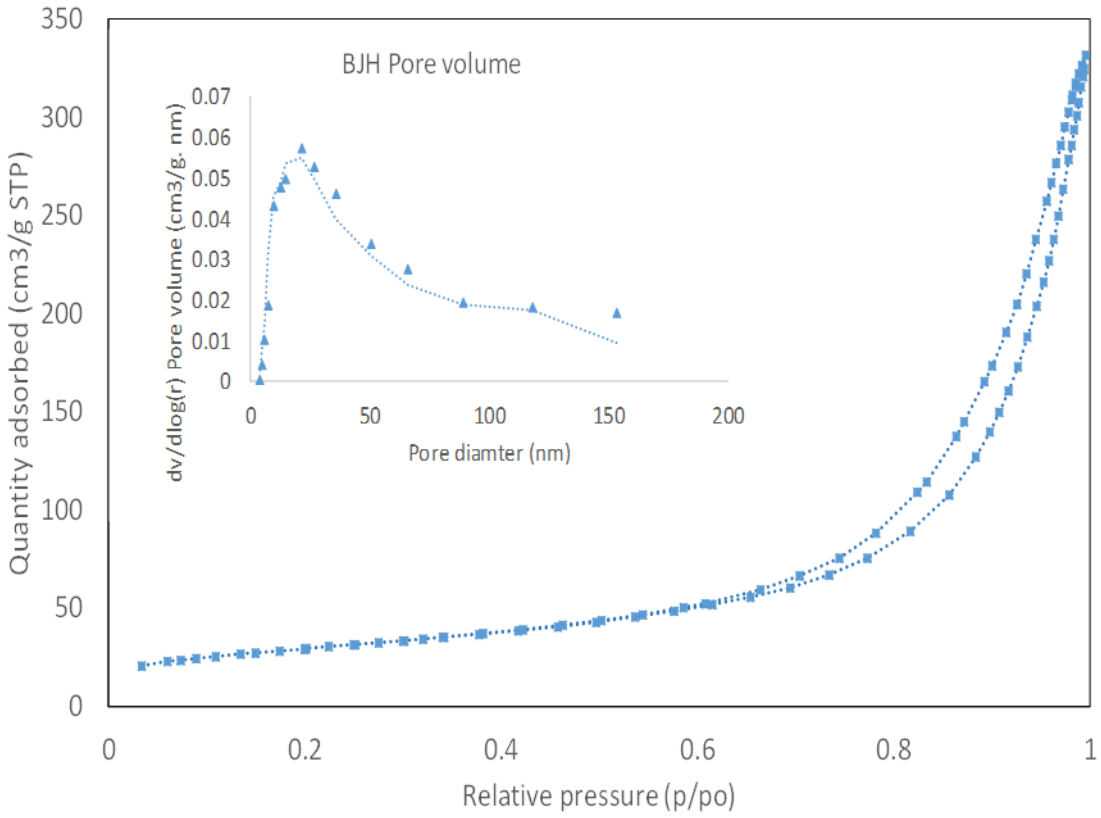

Figure 4.18 Isotherm linear plot

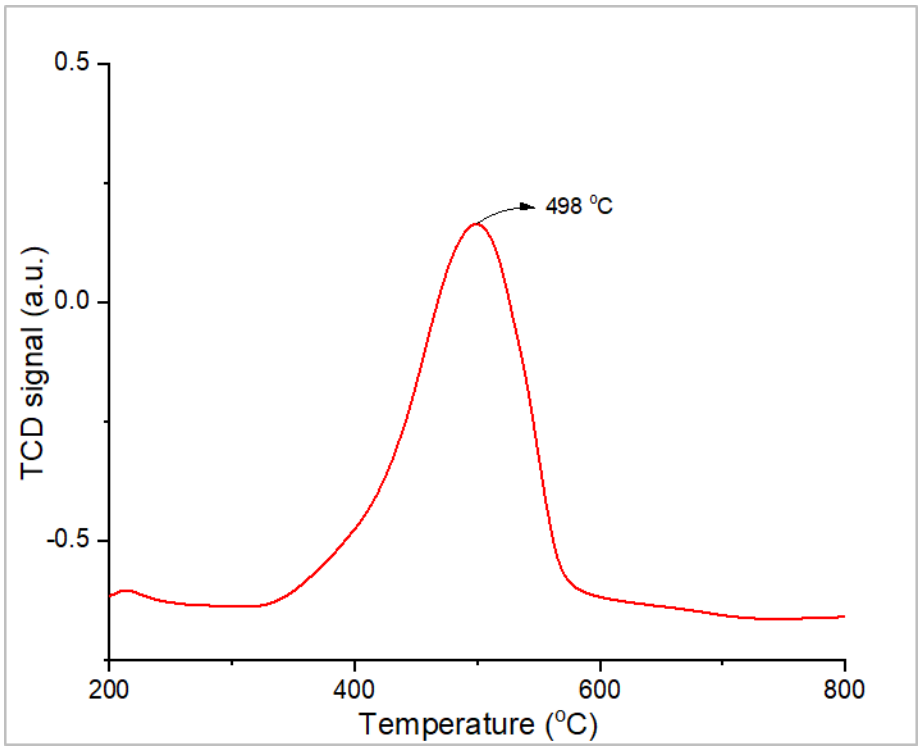

Figure 4.19 TPR profile of the CARGEN™ catalyst

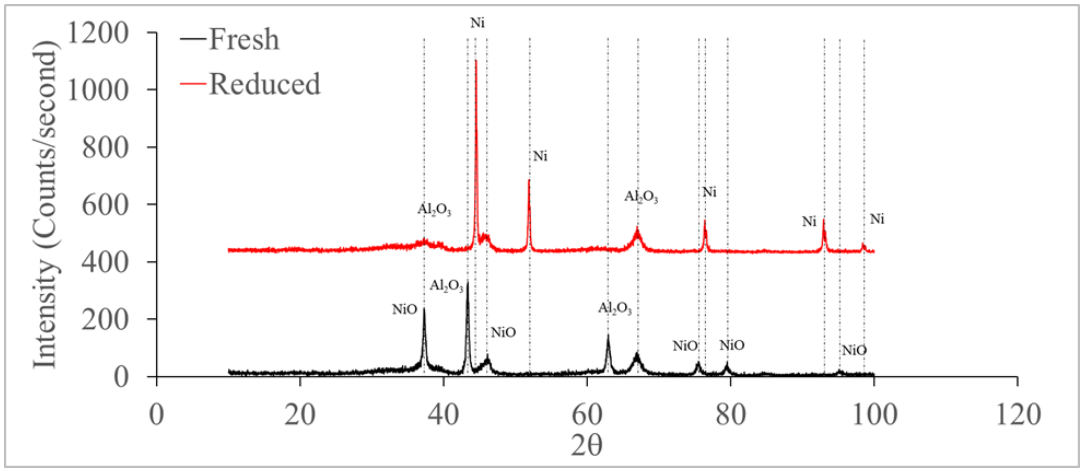

Figure 4.20 XRD profile of the fresh and the reduced catalyst sample

4.4.4 Microscopy assessments

In order to validate the formation of carbon, and in particular MWCNT, the spent catalyst from TGA analysis was analyzed under SEM and TEM. Figure 4.21 and Figure 4.22 presents some of the selected images from SEM and TEM microscopy study, respectively. Both SEM and TEM microscopy results demonstrate the formation of MWCNTs with diameters in the range of up to 100nm and length in the micrometer scale.

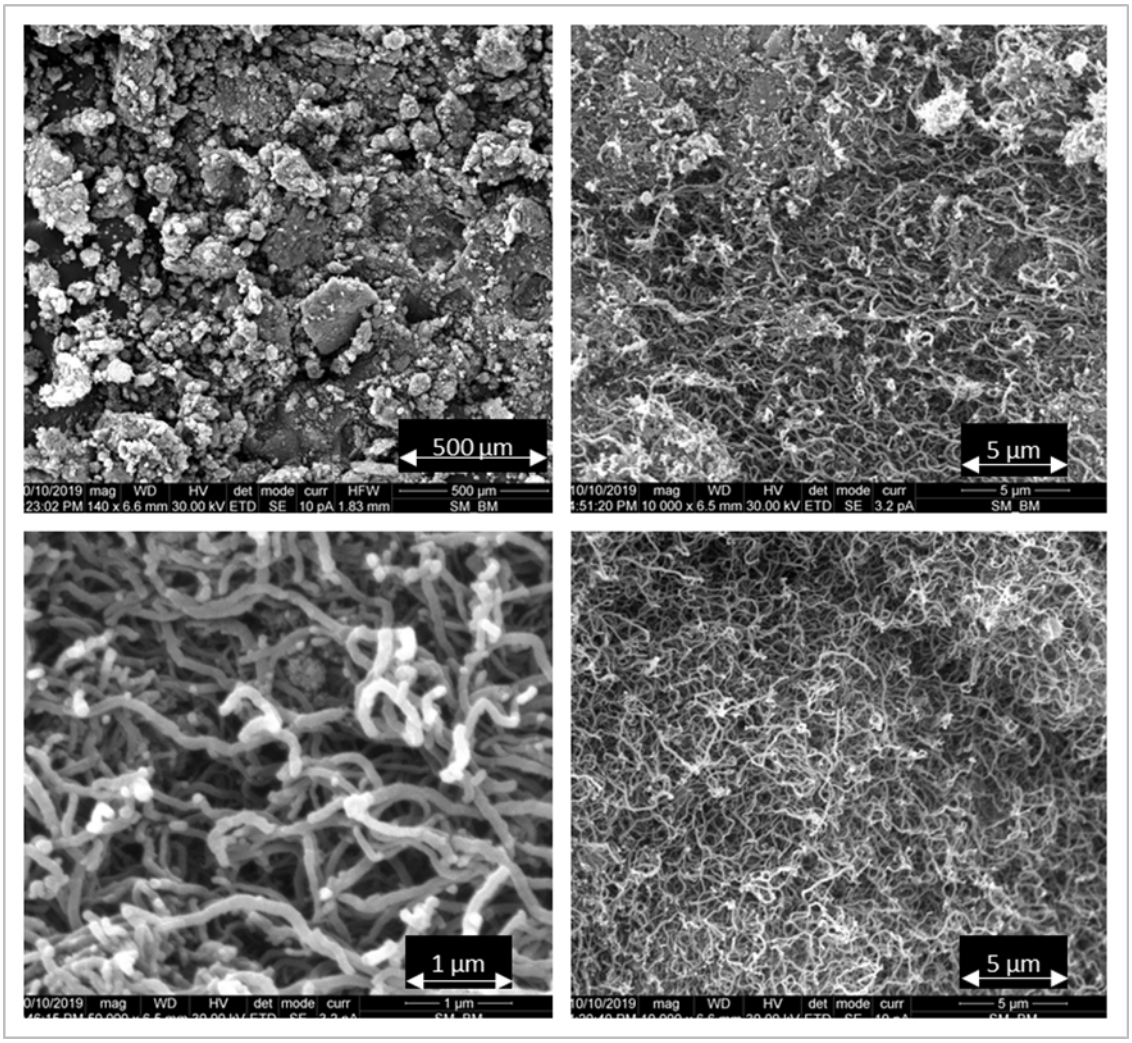

Figure 4.21 SEM images of the spent CARGEN™ catalyst

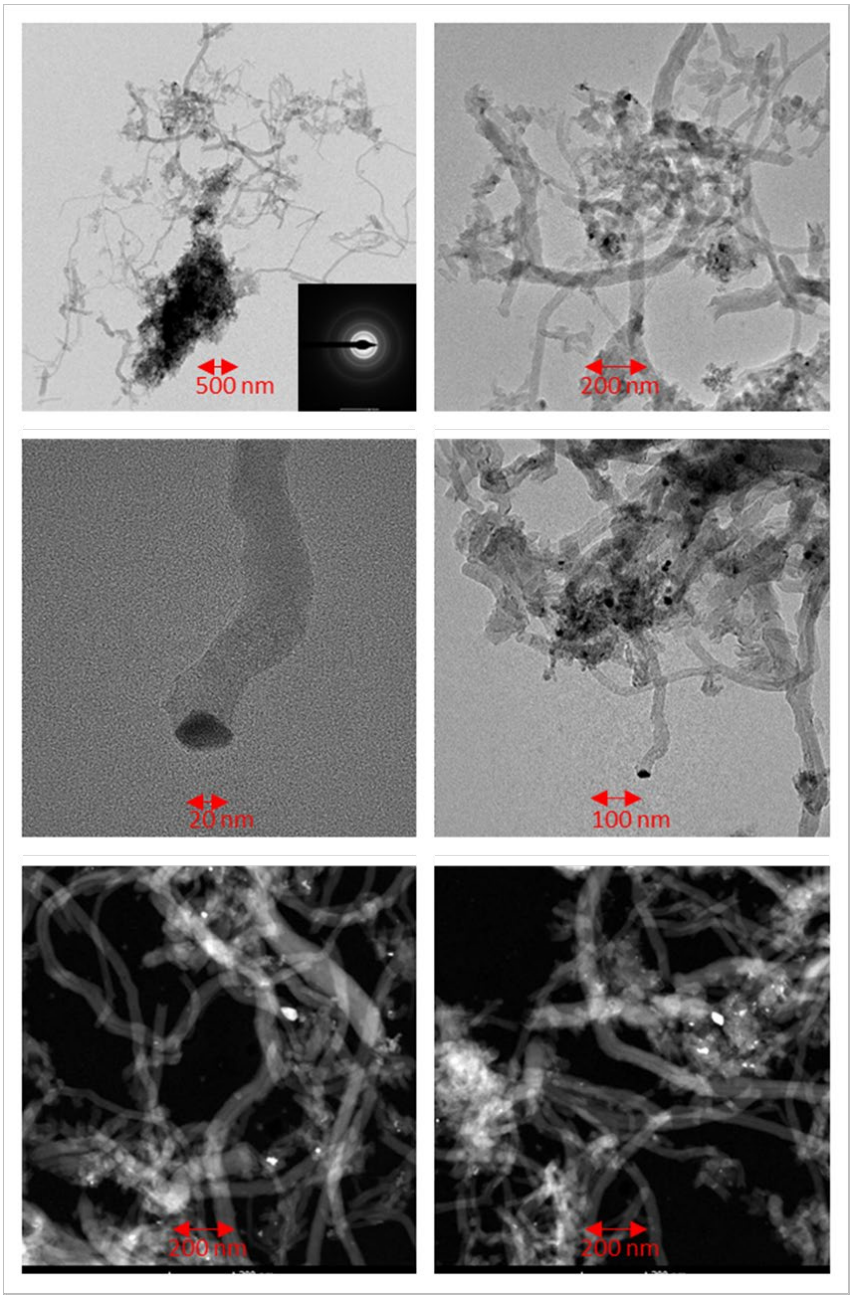

Figure 4.22 TEM and STEM images of the CARGEN™ catalyst

4.5 CARGEN™ scale-up testing

The results reported in this sub-section pertain to scale-up testing of the *CARGEN™ process* using three different and independent reaction systems. In particular, a flow-

through reactor was used to produce micrograms of carbon, a flow-top reactor for milligrams of carbon, and chemical vapor deposition (CVD) apparatus for grams of carbon production. For all the three experiments, a commercial nickel-based catalyst (20% Ni/ γ-Al_2O_3) was used. After each experiment, the spent samples were analyzed using a SEM and TEM instruments to (i) identify the form of carbon produced at each scale of operation, (ii) the consistency of the quality of carbon at various weight scales, and (iii) if CNTs are produced, then whether "tip-growth" mechanism is followed or "base-growth." The sections below, therefore, pertain to three independent reactions conducted to produce micrograms, milligrams, and grams of carbon with a single point objective of identifying the characteristics of the carbon produced via microscopy equipment.

4.5.1 Micrograms of carbon production:

This test was conducted in a compact Micro activity Effi unit (Micromeritics, USA). 5.5 mg of a commercial 20% Ni/ γ-Al_2O_3 (Riogen Inc., USA), dispersed in 100 mg of Quartz silica (Sigma, USA), loaded into a 9.2 mm internal diameter vertical quartz reactor. The sample is pre-treated by drying under helium for 2 hours at 150 ^oC. After reduction by ramping to 650 ^oC at 10°C/min in 10% H_2/He (50 mL/min flow), the system is purged with He for 1 hour and ramped down to 550 ^oC before introducing the CARGEN™ gas mixture. After 10hours of time-on-stream (TOS), the reaction is terminated, and the sample was saved for further characterization. Reaction data is acquired via an online Cirrus II mass spectrometer (MKS Instruments, UK). Individual m/z pressure signals from the mass spectrometer are converted into exit gas composition data using a standard RS

(Relative sensitivity) factor-based calibration approach. A detailed description of the calibration method is available in our recent publication in Afzal et al. .[149]

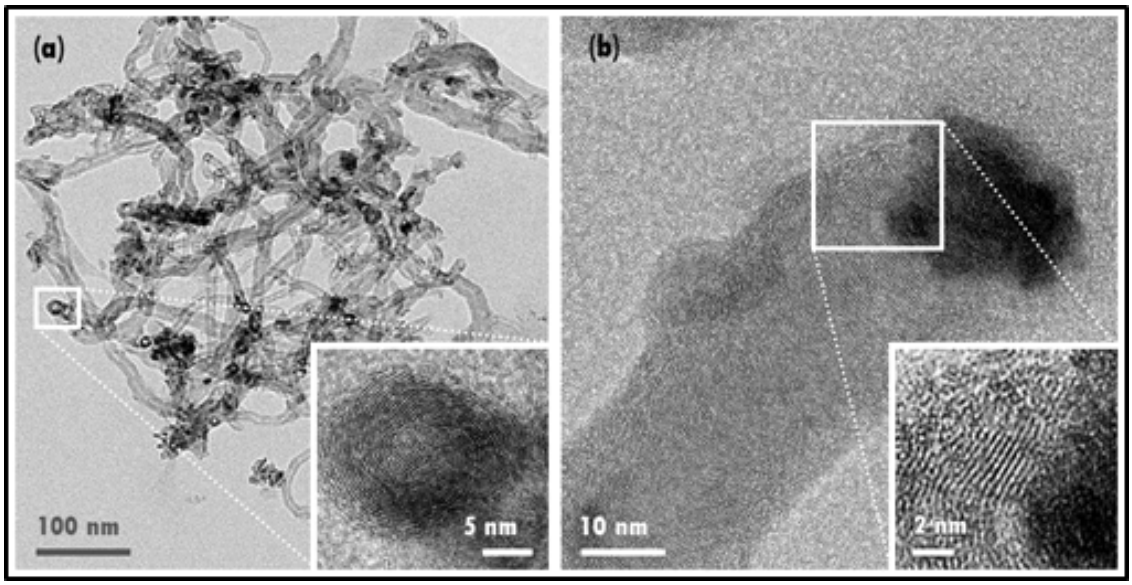

Figure 4.23 TEM images of the micrograms of carbon produced using MA Effi reactor at TAMUQ

Figure 4.23 presents the TEM images of the spent catalyst sample showcasing the morphology of the carbon deposited on the nickel cluster sites. From these images, three observations can be made: (i) Most of the carbon is present in cylindrical tubular form, (ii) All the tubes are hollow, (iii) There are multiple layers of carbon that confirms the presence of multiwalled carbon nanotubes (MWCNTs).

4.5.2 Milligrams of carbon production

In this experiment, 20 mg of commercial 20% Ni/ γ-Al_2O_3 catalyst was loaded in a thermogravimetric analyzer (TGA) equipment. The reaction protocol was exactly similar to that of the microgram assessment. It should be strictly noted that this test is not a scale-

up test, and should be regarded only as an independent experiment since the flow behavior of the gases and its contact pattern is different from the previous test.

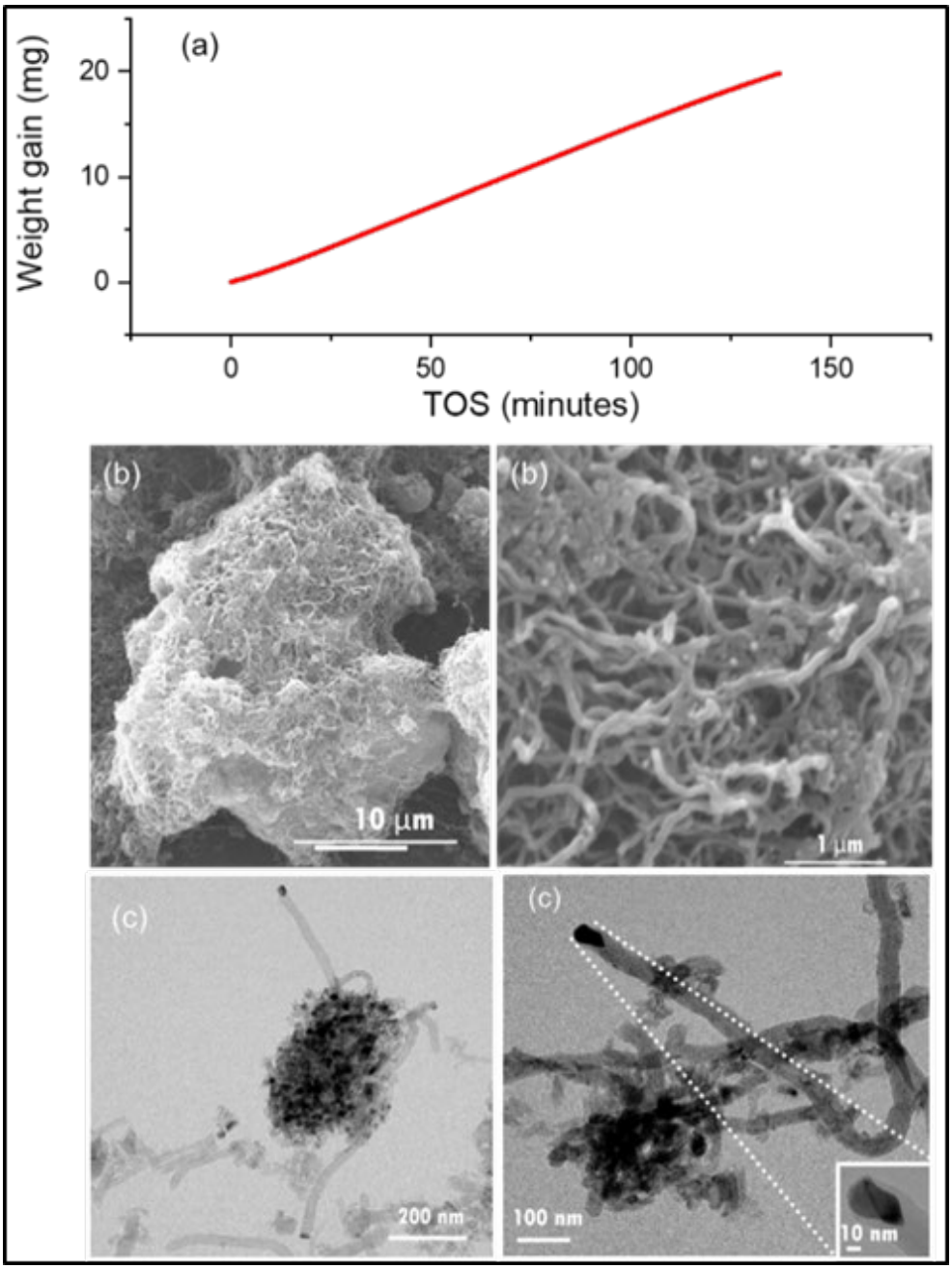

Figure 4.24 (a) Weight gain plot of CARGEN™ reaction in milligram scale assessment (b) SEM images (c) TEM images

A noticeable weight gain of 20 mg, as shown in Figure 4.24 a was observed during a TOS of 150 minutes, proving the formation of carbon during the course of the reaction. The SEM images in Figure 4.24 b taken at 10μm and 1μm magnification clearly show the presence of a dense quantity of carbon nanotubes. On the other hand, TEM images in Figure 4.24 c show the presence of a nickel cluster seemingly engrained at the tip of the tubes, pointing towards the possibility of a "tip-growth" kind of mechanism.

Comparison of the tubes in milligram assessment to that of microgram assessment shows the good similarity of the CNTs in terms of their hollow nature, as well as to their multi-walled type of structure.

4.5.3 Grams of carbon production

To produce multi-grams of carbon, an in-house bench-scale CVD unit was built. The experiment was conducted following a similar protocol to the microgram and milligram assessment studies. About 1 gram of the commercial 20% Ni/ γ-Al_2O_3 catalyst was loaded on a "ceramic boat" used as a holder for the catalyst and carbon that is produced during the reaction for 80hours TOS. An external video camera was also installed to record the growth of carbon live during the reaction, as shown in video Figure 4.25 a. Since the video was taken from a side view window, a complete 3D growth could not be captured, but the 2D side view evidently showed good carbon growth. After 80hours of TOS, the final weight of the overall sample (catalyst+carbon deposited) was found to be about 30 grams. This indicates a total growth of 29 grams over 1 gram of catalyst in 80hours at a rate of 6.04 mg $_{carbon}$/min/g_{cat}. Figures 4.25 b and 4.25 c shows SEM and TEM images of the

sample produced from the gram scale assessment. It could be seen that the type of carbon formed is very similar to both micro-gram as well as milligram of carbon experiments indicating that the form of carbon did not get affected by the change in the reactor type. Therefore CARGEN™ reaction is mostly a function of the reaction conditions and the reaction mixture composition and not the geometry of the reactor. However, to maximize contact time as well as enable the continuous mode of operation, a fluidized bed scheme of reaction will be more appropriate. Also, it will enable easy removal and reloading of the catalyst and carbon during multiple cycles of operation. Our current experimental studies are dedicated to building a fluidized bed reactor to conduct a similar scale assessment to demonstrate improvement in the productivity of the CARGEN™ process.

One of the MWCNT sample produced from this experiment was at ~ 80 wt% carbon purity (and remaining catalyst weight). In order to deduce the quality of the as-produced samples, a TGA air oxidation experiment was then conducted. The protocol for this test involved air combustion of carbon at 50 mL/min in the TGA on ca. 10 mg of the sample under a temperature ramp of 10 ºC/min from room temperature to 400 ºC, and at 5 ºC/min from 400 ºC to 800 ºC. Figure 4.26 (a-b) shows that only <1% of the sample was oxidized between 200 ºC to 500 ºC, which is the literature reported range of amorphous carbon[150–152]. As the combustion occurred in the range of 480 ºC to 700 ºC temperature indicates that crystalline form of carbon was primarily present, of which MWCNTs are predominant category[150–152]. Consolidating the TGA information to the SEM and TEM micrographs infers that most of the carbon belongs to MWCNT category with diameters in the range

of 50 to 100 nm and length in the range of 10 to 30 μm as shown in Figure 4.26. Moreover, the HR-TEM images at 10 nm scale bar shows that a tip-growth mechanism of CNT production would have taken place during the CARGEN™ process.

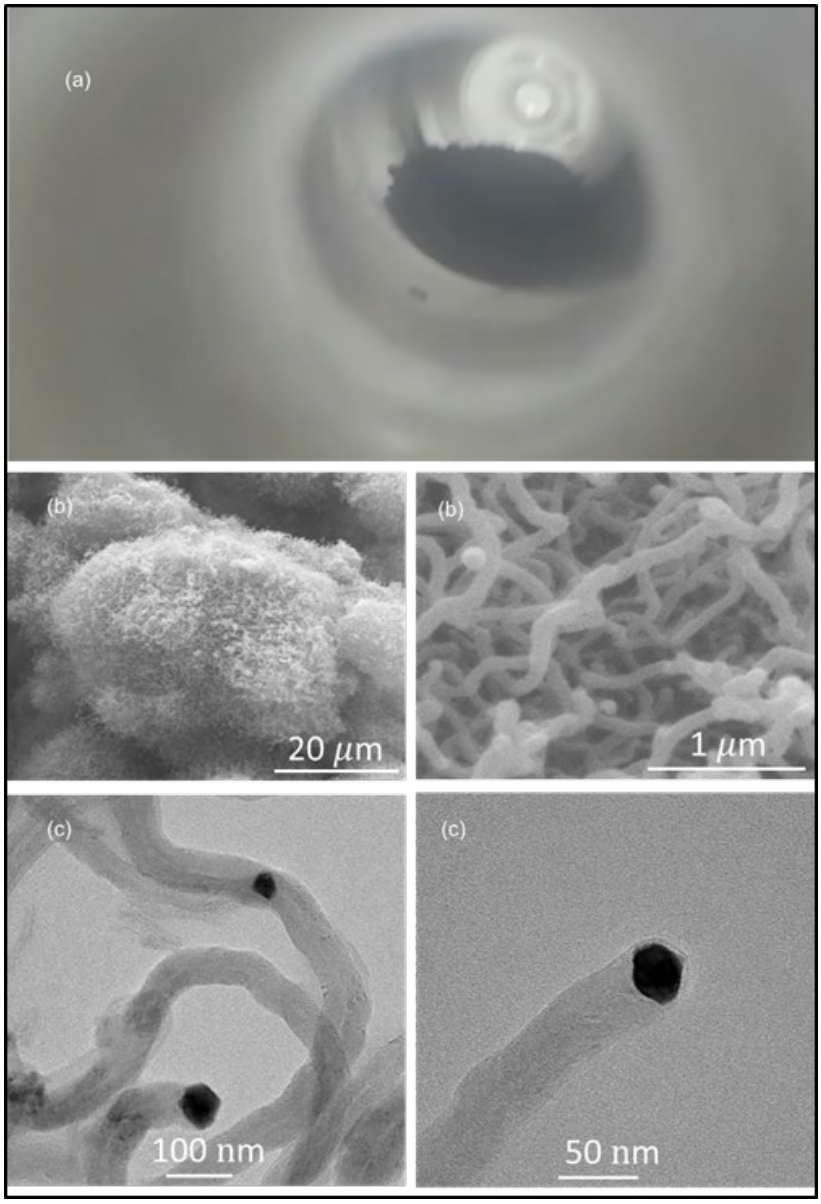

Figure 4.25 (a) 2D video of the CARGEN™ reaction in gram scale experiment (b) SEM images and (c) TEM images

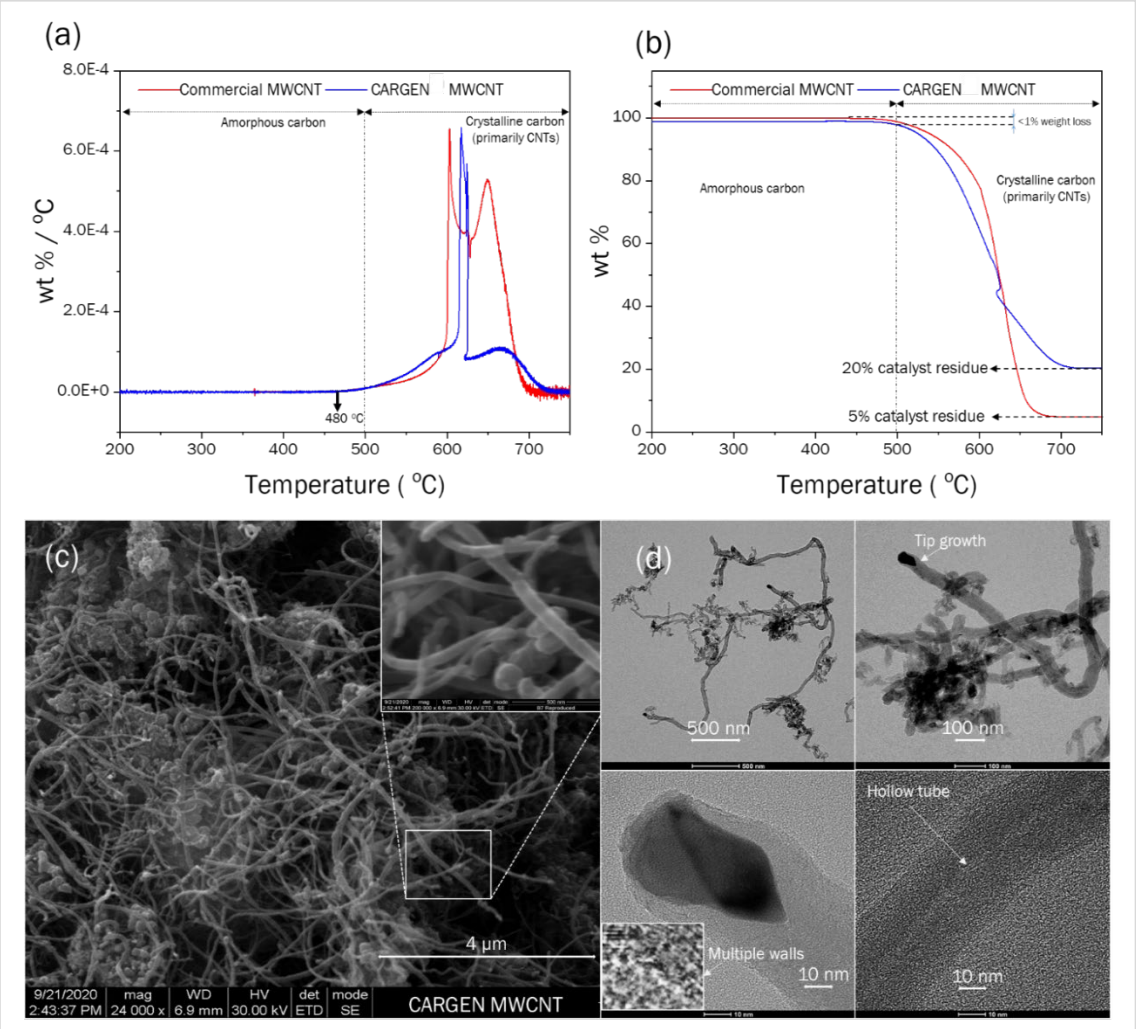

Figure 4.26 (a) Differential Thermogravimetric profiles of the MWCNTs produced from CARGEN™ and from commercial source (b) Weight loss profiles of the commercial MWCNTs and the CARGEN™ produced MWCNTs (c) Annotated SEM micrograph showing the length and diameter of the MWCNTs produced from CARGEN™ (d) TEM images of the MWCNTs showing tip-growth mechanism and the multi-walled hollow characteristic of the as-produced MWCNTs from CARGEN™

The MWCNTs produced in the CARGEN™ process have demonstrated great potential and comparability to the commercial quality MWCNTs. Figure 4.27 below elucidates the SEM images of the MWCNTs from the CARGEN™ process as well as the commercially

available MWCNTs. As shown in figure 4.27, the MWCNTs from CARGEN™ produces longer nanotubes compared to the commercially available. Moreover, the diameter of the CNTs is in the same range as that of the commercial sample. It is worth noting that the commercial material of this quality is available at a price range of 1,000-10,000 USD/kg[134]. In the current lab-scale process, CARGEN™ has been able to produce similar quality MWCNTs at much lower price (discussed further in section 4.6.1). However, when the CO_2 and natural gas is directly made available from an existing midstream process facility, the production price of these CNTs could be exponentially reduced (discussed further in section 4.6.2 and 4.6.3). Moreover, in which case syngas co-produced from the CARGEN™ process will also be used to produce liquid products in exiting GTL facility that would bring more economic benefits.

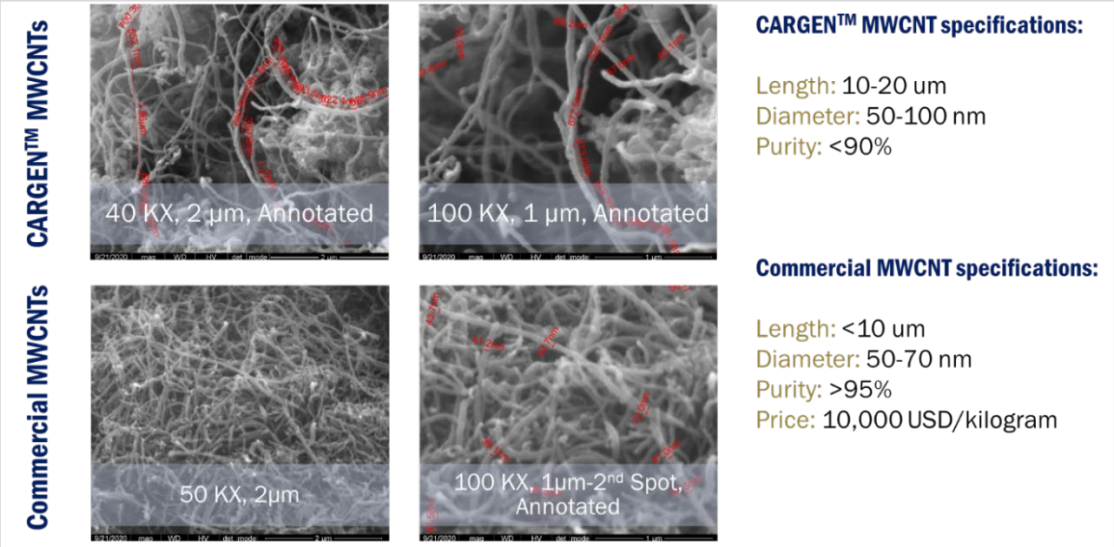

Figure 4.27 Comparison of the MWCNTs from the CARGEN™ process and the commercial source

4.6 Economics Assessment

The previous sections discuss about the conceptual development of the CARGEN™ technology, its proof of concept, catalyst development, and the scale-up. However, the economics evaluation and feasibility assessment is not discussed. This subsection covers the economics evaluation of the CARGEN™ within the context of GTL industry. As the scalability testing has been done at multi-gram scale, the first part in this section accounts for the operational costs required to produce 20 grams of the CNTs from CARGEN™. The second part presents an economic outlook for an industrial scale GTL facility that employs a CARGEN™ unit for reforming. In the latter case, the calculation is done assuming that 7000 Tons/day of CO_2 is available from the midstream process facility.

4.6.1 Costing estimation of multi-gram MWCNT production in a lab-scale unit

A typical batch of MWCNT produced from the CARGEN™ requires about 80 hours of time on stream inclusive of drying reduction and reaction. The first step in the protocol requires drying in Argon gas for 8 hours at 100 mL/min flow rate at 300 ^oC. The second step requires reduction in 10% H_2 at 100 mL/min 750 ^oC for 24 hours. The last step is for the reaction at 550 ^oC in 188 mL/min flowrate of CARGEN™ mix gas comprising of $CH_4/CO_2/O_2/He/Ar=64:32.4:5.4:82.44:3.76=1:0.506:0.08:1.289:0.0587$.

Calculation steps for 1 batch of carbon (20 grams) production

Cost of reaction gases for lab-scale production

Table 4.7 Cost of various reaction gases for lab-scale production

Required gas	Price/Cylinder (USD) 200bar, 50L	Mass flow rate (mL/min)	TOS (hours)
Argon, 4.5 grade	15.15	100	4
Hydrogen, 4.5 grade	41.32	100	24
Methane (CH_4:He:Ar=0.8/0.18/0.02)	674	80	52
Carbon dioxide (CO_2/O_2/He/Ar= 0.3/0.05/0.63/0.02)	24.79	108	52

Since all the cylinders are available at an initial pressure of 200bar, 50L, at ambient temperature condition, the total number of moles of gas in these cylinders become:

$$n = \frac{PV}{RT} = \frac{200\times10^5\times50\times10^{-3}}{298.15\times8.314}\left[\frac{Pa\times m^3}{K\times\frac{Pa\times m^3}{mol\times K}}\right] = 403.4\,\frac{moles}{cylinder}$$

At STP conditions (273.15 K, 1 atm pressure), $V = 22412\,\frac{mL}{mol\ of\ gas}$ by ideal gas law.

Therefore, as per the reported price of each of the cylinders in the table, the molar price of each of these gases become:

$$Argon = \frac{15.15}{403.15} = 0.0375\,\frac{USD}{mol} = \frac{0.0375}{22412}\,\frac{USD}{mL} = 1.6732\times10^{-6}\,\frac{USD}{mL}$$

$$Hydrogen = \frac{41.32}{403.15} = 0.1024\,\frac{USD}{mol} = \frac{0.0375}{22412}\,\frac{USD}{mL} = 4.5689\times10^{-6}\,\frac{USD}{mL}$$

$$Methane = \frac{674}{403.15} = 1.67\,\frac{USD}{mol} = 7.45136\times10^{-6}\,\frac{USD}{mL}$$

$CO_2 = \frac{24.79}{403.15} = 0.0614 \frac{USD}{mol} = 2.7396 \times 10^{-6} \frac{USD}{mL}$

Thus,

Effective price per batch by raw material prices becomes:

$=[(100 \times 1.6732 \times 10^{-6} \times 60 \times 4) + (100 \times 4.5689 \times 10^{-6} \times 60 \times 24) + (80 \times 7.45136 \times 10^{-5} \times 60 \times 52) + (108 \times 2.7396 \times 10^{-6} \times 60 \times 52)]$

=20.2198 USD/batch

Cost of catalyst for lab-scale production

Sine 4 grams of catalyst is required per batch of MWCNT production, and 500 grams of the catalyst costs 900USD, the effective price per 4 grams batch becomes 7.2 USD/batch

Cost of electricity

The maximum power rating of the furnace used for multigram MWCNT production= 1.040KW. As the total time for the entire batch is about 80hours, the maximum power consumption = $1.04 \times 80 = 83.2\ kWh$. The reported kWh of electricity in the US for commercial use= $13.31\ USD/kWh$, therefore, the electricity cost for $83.2\ kWh$ becomes $83.2\ kWh \times \frac{13.31}{100} = 11$ USD/batch.

Effective cost for 1 batch production

For the laboratory scale production, the cost of reaction gases, catalyst, and the electricity for 1 bath production of 20 grams MWCNT will provide an approximate operational cost. Therefore, the effective cost becomes: $20.22 + 7.20 + 11.07 = 38.49 \frac{USD}{batch}$

The effective price per gram of MWCNT therefore becomes: $38.49/20 \approx 2\ USD/batch$

It should be noted that this cost is inline and within the ball mark of the costs of similar quality MWCNT sold commercially.[134]

4.6.2 Economics evaluation of MWCNT production from existing industrial plants

It is known that Qatargas midstream processing plants comprise of 14 trains, and each process train emits at least 500 tons per day of CO_2. Therefore, the emission from 14 trains would become 700 tons/day.

A simulation study conducted on this capacity of CO_2 using CARGEN™ in ASPEN® plus process simulator is shown in figure 4.28 below:

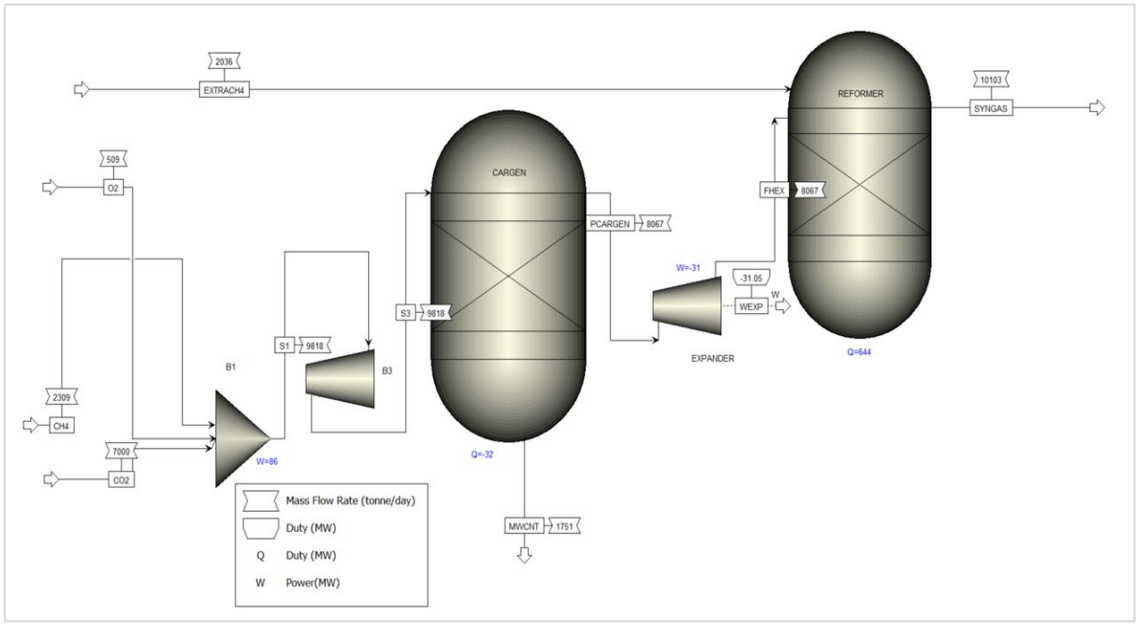

Figure 4.28 ASPEN® Plus simulation of 7000 tons/day CO2 conversion CARGEN™ two-reactor process

This simulation has been done using equilibrium model provided by RGibbs reactor in ASPEN® Plus. Also, the accountability of solid carbon has been done by configuring the RGibbs reactor to produce carbon in a solid phase while other species in gaseous phase. The operational conditions of the CARGEN™ and the tri-reforming reactor are provided below:

CARGEN™:

Temperature= 550 ºC

Pressure= 25 bar

Reformer:

Temperature= 800 ºC

Pressure= 1 bar

Feed composition:

CH_4= 2309+2036 Tonnes/day

CO_2= 7000 tonnes/day

O_2= 509 Tonnes/day

Products:

Carbon production from CARGEN™ =1751 tonne/day

Syngas production from reformer= 10,103 tonne/day

Overall conversions:

CO_2=83%

$CH_4 = 97\%$

Out of the said amount of syngas products, the actual syngas (H_2+CO) content in the mixture= (H_2+CO)= 977+6838 (TPD)

Out of this, 50% of the syngas is converted to hydrocarbon products.

Therefore, only 6838/2 of CO_2 and 977/2 of H_2 is converted to hydrocarbons.

Assuming that all of these are converted to gasoline products. Which contains C6 to C12 HCs these average at C9. Therefore, the overall stoichiometric equation becomes:

$$9CO + 18H_2 \rightarrow C_9H_{18} + 9H_2O$$

Therefore, total C_9H_{18} produced = $\frac{\left(\frac{6838}{2}\right)}{28} \times \frac{1}{9} \times 126$ = 3419 TPD

Therefore, volume of gasoline produced = $3419 \times 1000 \times \frac{1}{800} = 4273.75 \frac{m^3}{day}$

$= 4273.75 \times 6.289 = 26{,}877 \frac{bbl}{day}$

$\because 1\ bbl = 159\ litres$

$\therefore 4273.75 \frac{m^3}{day} = 4273.75 \times \frac{10^3}{159} \frac{bbl}{day} \approx 26{,}800 \frac{bbl}{day}$

$\because$ current market value per liter of gasoline in middle east $\approx 0.3 \frac{USD}{litre}$

$\therefore$ additional revenue generation possibility $\approx 4273.75 \times 1000 \times 0.3 \frac{USD}{day} \sim 1.2 \times 10^6 \frac{USD}{day}$

Or, the GTL products will itself generate about 1.2 M USD/day.

4.6.3 Costing estimation of the MWCNT produced from 7000 tonnes/day CARGEN™ process

For a 7000 tonnes/day capacity CARGEN™ reactor, it is shown in the previous section that there is a possibility to produce 1751 tonnes/day of solid carbon, which has been

proven in section 4.5 to be a MWCNT quality carbon. The calculations presented in this section pertain to the estimation of the cost of the MWCNT produced from such a plant capacity using greenhouse gas feed comprising of CH_4 and CO_2.

It has been reported in the literature that, for a 74,000bbl/day capacity plant, 360 mW energy is required. Therefore, if a linear scale-down is assumed, then for 26,000bbl/day GTL plant, the total electricity required= $\frac{26000}{74000} \times 360 = 126.49$ MW.

It is known that reformer units consume 60% of the overall energy duty of the GTL plant. Therefore, the energy requirement of such a reformer unit becomes $0.6 \times 126.49 = 75.394\ MW$.

As the cost of electricity is about 50USD/MWh for an industrial scale plant. The total electricity cost = $50 \times 75.394 \times 24 = 90{,}472\ \frac{USD}{day}$

As per the experimental protocol, for every 5 grams of carbon produced, 1 gram of catalyst is required. The reported cost of industrial catalyst $20\%\ Ni/\gamma - Al_2O_3$ is around 20,000USD/ton. Since 1751 tons/day of MWCNT batch is produced, therefore the catalyst quantity required for such a production capacity becomes $\approx 350\ t$PD. Therefore, the total cost for the catalyst becomes: $350 \times 20{,}000\ \frac{USD}{day} = 7\ M\ USD/day$.

Assuming a maintenance and miscellaneous cost of 100,000USD/day to cover for wear and tear and other unexpected work during the day and if about 50labours are required at a rate of 200 USD/day, the total cost for labor and maintenance becomes $(100{,}000 + 10{,}000) = 110{,}000\ \frac{USD}{day}$.

The total operating cost (OPEX) including that of energy, catalyst, labor and maintenance therefore becomes: $90{,}472 + 7{,}000{,}000 + 100{,}000 + 10{,}000 = 7{,}200{,}472\,\frac{USD}{day}$

CAPEX calculations:

It is reported in the literature[153] and on the Pearl GTL website[154] that the total CAPEX of the plant= 19 billion USD for 140,000 bbl/day GTL plant. Therefore, for a 26,000 bbl/day plant and after assuming a linear scale-up, the cost becomes $\frac{26{,}000}{74{,}000} \times 19{,}000{,}000{,}000 = 3{,}520{,}000{,}000\ USD$. If The reforming unit cost 50% of this cost, the overall plant cost becomes, $0.5 \times 3{,}520{,}000{,}000 = 1{,}760{,}000{,}000\ USD$.

Assuming a pay back of 10 years and a total of 340 working days, a daily CAPEX becomes, $\frac{1{,}760{,}000{,}000}{340\times10} = 518{,}000\,\frac{USD}{day}$.

The total daily CAPEX+OPEX therefore becomes $(7{,}200{,}472 + 518{,}000)\,\frac{USD}{day} = 7{,}718{,}000\,\frac{USD}{day}$.

As the total production per day= 1751 tons, the effective cost per kg of MWCNT becomes:

$\frac{7718000}{1751\times1000} = 4.41\,\frac{USD}{kg}$

For a case of 30% tax and 30% Return on investment demand, the effective price becomes:

$4.41 \times 1.3 \times 1.3 = 7.45\,\frac{USD}{kg}$

It should be noted that the current market price of MWCNT of similar quality is about 500-1000USD/kg. Therefore, in a worst-case scenario consideration, there is a possibility to drastically reduce the cost of MWCNTs by about 60 times. This price of MWCNT not

only beats the market competition, but also presents a sustainable pathway for converting and sequestering CO_2 into a solid stable product.

4.7 Conclusion

This study presents an important advancement in the field of Methane reforming process that enables the conversion of GHGs into solid carbon and syngas. In particular, the developed CARGEN™ technology conceived on a theoretical scale and proven practically had demonstrated cutting edge improvement in the sustainability aspect of the process plagued DRM process. The energy intensification attribute of CARGEN™ enables at least a 50% reduction in energy requirement compared to the DRM process on a standalone basis. Thermodynamic investigation proved that at least 65% CO_2 conversion is possible via the CARGEN™ process at 50% lower energy compared to the DRM process on an equal capacity basis. In addition, a preliminary LCA study showed a potential for reduction of at least 40% operational cost as well as CO_2 emission using CARGEN™ technology compared to the benchmark reforming processes. A dedicated experimental campaign using multiple reaction systems consistently proved the concept of the CARGEN™ technology that was conceived using thermodynamic studies. Furthermore, the scalability of the CARGEN™ process was also proved via a series of experiments using state-of-the-art reaction systems. In particular, it was proved via Raman, TEM, and SEM, that at TRL-3, the CARGEN™ process is capable of producing micro-gram, milli-gram, and gram-scale of MWCNTs, which is highly unique at its entirety. Finally, a tailor-made catalyst for the CARGEN™ process enabled un-hindered, highly sustained, and

high yield of MWCNTs. The efforts on the CARGEN™ process yielded two patents; first, on the concept of CARGEN™, and the second on the catalyst material for CARGEN™. The achievement of TRL-3 of the CARGEN™ process enabled the development of a *high-profile and dedicated million dollars proposal with leading energy company,* targeted towards scale-up of the CARGEN™ process from TRL-3 to TRL-6. Current efforts are underway to further this technology for its commercial implementation.

5. REGENERATION & ACTIVATION OF DRY REFORMING OF METHANE CATALYSTS USING CO_2[1,2,3,4]

5.1 Introduction

DRM is an attractive route for CO_2 conversion to reduce greenhouse gas emissions; however, as stated in section 1, this process faces major challenges towards its commercialization. Carbon formation, among other challenges, is the worst challenge as it rapidly clogs the active sites and deactivates the catalyst. During the DRM reaction, specifically at low-temperature conditions (450 ^oC-600 ^oC), carbon formation on the active site of the catalyst is highly favorable. In essence, methane decomposition and Boudouard reactions (disintegration of carbon monoxide to carbon dioxide and carbon) at the typical DRM conditions compete with the desired formation of syngas to form solid carbon. Given this, the DRM reaction is not industrially attractive unless a more sustainable and smart solution is implemented that could either offer a longer catalyst life or provide an efficient catalyst regeneration/reactivation process. In this work, proposed is a novel protocol, which systematically handles the deposited carbon to regenerate/ reactivate the spent DRM catalyst ultimately. The uniqueness of this novel protocol is that it utilizes CO_2 as a reactant and as a regeneration/activation media for the DRM catalyst. In contrast to a conventional catalyst regeneration process, which involves two steps (oxidation using pure O_2 followed by reduction with pure H_2), this protocol requires a single oxidation step by CO_2, as it selectively oxidizes the carbon without effecting the active metal site

A portion of this section has been published/submitted in:

[1]Advances in Carbon Management Technologies: Carbon Removal, Renewable and Nuclear Energy, Volume (2020): 253 Copyright 2020Taylor & Francis [114],

[2]Challiwala, M. S., et al. “Production of high-quality carbon nanotubes from natural gas and carbon dioxide using a novel CARGEN™ process”, Chemical Engineering Progress, AIChE, Wiley, (Submitted & Under review)

[3]Challiwala, M. S., et al. "A method for regeneration and reactivation of Dry reforming catalyst " – Provisional patent. Priority date: July 2018

reduction state to produce high purity CO from both CO_2 and carbon deposited on the catalyst surface. More importantly, this novel method saves a significant amount of energy compared to existing regeneration methods since it does neither require pure O_2 produced from the expensive air separation unit nor H_2 for reduction.

5.2 Background and Prior Art

Regeneration of the DRM catalyst is one of the few domains in the literature which has not gained much attention from the scientific community. In contrast to the very limited literature published in this field, the present work provides a unique approach to regenerate a spent DRM catalyst utilizing CO_2. Compared to the work reported in the literature on the subject, for instance, by John et al. [155]., in which the authors provided a method for reactivating a catalyst by steps involving oxidation with 2% O_2 followed by reduction with H_2 gas. This work instead proposes a single step process involving the utilization of CO_2 to oxidize solid carbon. A study by Robert et al.[156] proposed the utilization of halogen-free oxygen-containing gas at a temperature less than 416 °C for the regeneration of a reforming catalyst composed of Pt on an L-Zeolite molecular sieve. Similarly, a study by Paul et al.[157] proposed a regeneration process for carbon-contaminated catalyst particles by confining the carbon particles in a combustion section of a regeneration zone to a tapered bed configuration. The authors claim that the utilization of O_2 is more, and surface area loss of catalyst could be significantly reduced. A previous work by Shun et al.[158] proposed a method that involves contacting a mixture of inert gas, oxygen, and water at elevated temperatures (400-600°C) followed by treatment with a chemical containing

source of chlorine (HCl, or Cl_2, etc.). In this, the authors claim enhancement in the dispersion of a re-activated catalyst comprising of the L-Zeolite compound. Yet another work by Aggadin et al. .[159] proposed a process for the DRM catalyst regeneration utilizing a gas mixture composed of CO_2, hydrogen, and water to increase the CO content of the gas mixture. The objective of the authors was to utilize the benefit of RGWSR to convert CO_2 to CO by using excess hydrogen in the system. On a different note, a study by Shilpa et al. [160] provided a review of different techniques to oxidize carbon deposits formed on a catalyst surface during hydrocarbon treatments. The authors in this study discuss the mechanism and different conditions that help in reactivating such catalysts. In a study by Luciana et al. [161], the authors provided a mechanistic insight of a coked Fluid Catalytic Cracking (FCC) catalyst regeneration under different environments of O_2 in He and CO_2 in He over a range of temperature (starting from room temperature all the way to 1000°C). Similarly, a study by Abdelsadek et al. 2016[162] utilized hydrogen gas for the regeneration of a coked DRM catalyst. The reaction of adsorbed carbon with hydrogen produced methane gas. Their results after each recycle also showed significant improvement in both CH_4 and CO_2 conversions. As carbon formation is an inherent process challenge for gas oil hydrocracking in a typical refinery, and for large size FCC units, a short study by Sergio et al.[161] suggested an interesting technique of utilizing a combination of CO_2 and O_2 gases to “burn” off the carbon produced on the catalyst surface. They suggested that CO_2 could be activated in a site composed of V-O (group I or II) in carbon proximity, and found that the activation energy for a reverse-Boudard reaction is in the range of 242-253 kJ/mol that lies within the typical operating condition of FCC units. Another work by Sergio et al.

2016[163] discussed the prospects of the utilization of CO_2 in the O_2 atmosphere for an auto-thermal operation of an FCC unit. On the same lines, Thiago et al. 2014[164] conducted a very comprehensive experiment to unambiguously demonstrate that catalyst regeneration can be auto-thermally conducted by energy integration within an FCC unit to produce CO from coked catalyst. In a second study by the same group (Thiago et al. 2015[164]), the authors utilized a set of different catalyst materials (alumina modified by vanadium and potassium with active metal comprising of lithium, sodium, potassium, magnesium, and calcium) to prove the same concept. In the same context of FCC unit, another study by Alenazey et al. 2008[165] conducted a series of tests by using different oxidizer gases for regeneration of a spent Co-Ni catalyst. Their study concluded that carbon removal process is independent of the gasifying agent, and decreases in order of O_2> Air> CO_2> H_2> N2. They also conducted a mechanistic study to support their analysis.

An important goal of this work is to enhance the overall CO_2 consumption in the process apart from being only utilized in stoichiometric quantity in the DRM reaction. In addition, the process could also be regarded as an alternative route to produce CO, which is a valuable chemical commodity. Successful implementation of this protocol could aid in further enhancing the efficiency of the DRM process, as CO_2 is not only used as a reactant but also during the catalyst regeneration cycle.

5.3 The Concept

In this section, a novel approach of a single-step catalyst regeneration procedure, applicable for any process that suffers from catalyst deactivation via carbon formation, is

presented. The said process utilizes CO_2 as a soft oxidant[160] for the removal of surface carbon that deactivated the catalyst. This presents a great improvement over the conventional procedure, as the conventional procedure requires two steps- first, oxidation with O_2 for carbon removal as CO_2, followed by the reduction of nickel oxide with H_2 to produce active nickel. The new procedure is precisely similar to temperature-programmed oxidation (TPO) using O_2 but utilizes CO_2 in its place. The reaction is proposed to happen via the reverse-boudouard route as follows:

$$CO_2 + C \rightarrow 2CO \tag{5.1}$$

This reaction was first tested using a thermodynamic equilibrium assessment followed by a laboratory proof of concept study in a flow-through reactor. Provided below are more details on both the tests.

5.3.1 Thermodynamic Equilibrium Assessment

For a theoretical proof of this invention, we first tested the feasibility of the proposed regeneration procedure using thermodynamic equilibrium calculations. The thermodynamic calculations accounted for the Gibbs Free Energy of the system at the identified operating conditions of our system. The Gibbs Free Energy is essentially the energy available in the system to conduct an external work and is a measure of thermodynamic equilibrium (as the free energy available in the system is minimum at equilibrium). Therefore, this calculation requires to "minimize" or search for local minima of the system at a given set of operating conditions (e.g., temperature, pressure, and mole composition of the feed to the system). Comprehensive detail on the model development

is presented in section 3. The reaction species considered for this study include CO_2, CO, and solid carbon modeled as graphitic carbon.

For a thermodynamic proof of concept of the proposed invention, 1.5 moles of CO_2 was fed to a Gibbs reactor containing 1 mole of solid carbon. The temperature was varied from 500 °C to 750 °C with an increment of 50 °C at 1 bar pressure. It can be observed in Figure 5.1 that the only product produced from this reaction was carbon monoxide. Also, the decrease in molar concentration of CO_2 and carbon indicates that they are being consumed as per the following stoichiometric equation:

$$CO_2 + Carbon \rightarrow 2CO \qquad \text{(Eq.5.2)}$$

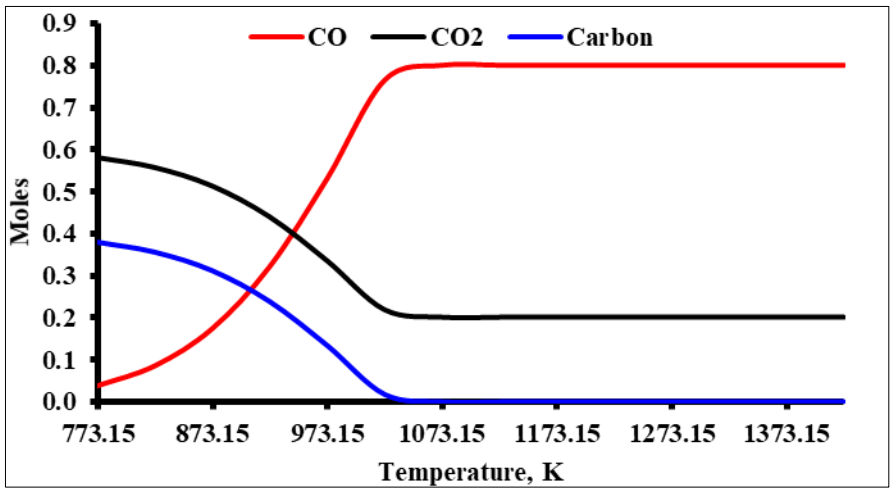

Figure 5.1 Thermodynamic equilibrium composition for the reaction of CO_2 with carbon

As can be noted from the above plot (Figure 5.1), the reaction is feasible above 500 °C, and complete conversion of carbon is possible at a temperature above 700 °C. This was then confirmed by an experimental proof of concept, in which the reaction of solid carbon deposited on the spent DRM catalyst with pure CO_2 was tested, and the results showed

the production of CO. Further details of these results with a description of the setup used are presented below.

5.3.2 Experimental Proof of concept.

After performing a thermodynamic feasibility test, a small demonstration experiment was conducted in our lab to prove this concept on an experimental scale. For all the experimental tests, we utilized a flow through the Quartz U-tube reactor of Micromeritics 2920 setup (As shown in Figure 5.2). A sheath type thermocouple touching the top of the catalyst bed was installed to monitor the temperature of the catalytic bed. The reactor loaded with the catalyst is encapsulated inside a clamshell-type furnace, which could be heated up to the desired reaction temperature. All gas flow was controlled by inbuilt Mass Flow Controllers (MFC). The Micromeritics 2920 setup has an inbuilt Thermal Conductivity Detector (TCD) to analyze the adsorbed gas quantity on the catalyst, which is sufficient for conducting catalyst in situ testing study. However, in the present study, we are using the Micromeritics 2920 as a microreactor, and therefore only a TCD detector cannot be used to analyze the composition of the produced gases from the reaction. Therefore, the outlet of the reactor is connected to RGA; (Hiden, model HPR-20) to analyze the evolved gases qualitatively as well as quantitatively. In order to quantify the gas concertation of the evolved gases, static Response Sensitivity (RS) factors were used for different gases, while Argon was used as an internal standard (2 vol %) to ensure the accuracy of the quantification of the gases composition. In addition, the RGA has also

been recalibrated prior to each experimental run to avoid drifting of the detected partial pressures of the gases.

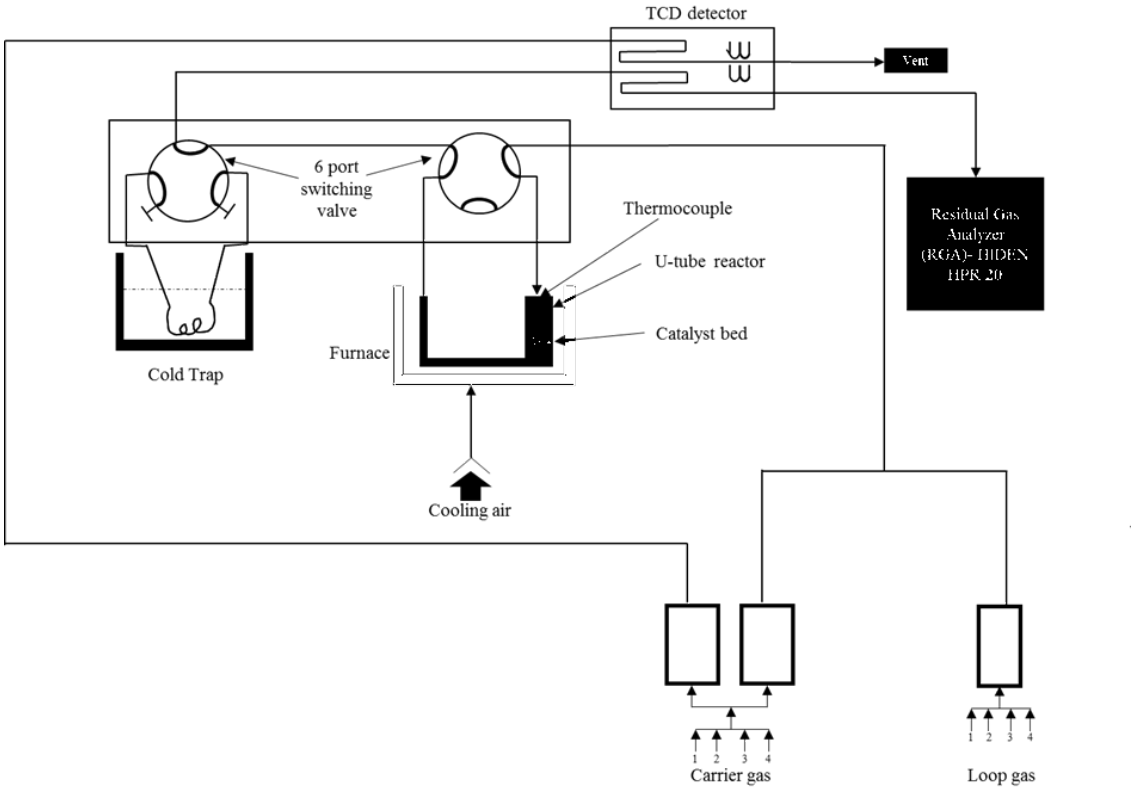

Figure 5.2 Schematic of the Micromeritics Autochem 2920 system connected to RGA

In this test, first, a spent DRM catalyst containing a significant quantity of carbon was loaded and purged with inert gas to get rid of the physisorbed DRM gas. Next, the reactor temperature was ramped up to 650°C under a steady flow of inert gas. When only the inert gas was detected in RGA, confirming that complete purging was achieved. Pure CO_2 gas was then introduced at a flow rate of 48 ml/min to the isothermal reactor. The temperature of the reactor was then ramped up to 950 ºC at a rate of 50 ºC/min and subsequently held at this condition for 10 minutes. It can be clearly observed from Figure 5.3 that CO

formation began immediately after CO_2 introduction. Initially, CO concentration started increasing rapidly with an increase in temperature, hinting rapid oxidation of carbon by CO_2. After reaching a maximum composition of about 70% in the emerging gas mix, the CO concentration dropped steadily to a zero level, confirming complete removal of carbon. At the same time, the opposite trend was noticed in the CO_2 composition. Two inverted Gaussian peaks can be observed in Figure 5.3 in which a normal Gaussian peak corresponds to total CO formation, and an inverted Gaussian peak corresponds to CO_2 consumption during the regeneration step. This indicates CO being formed at the expense of CO_2 in the reaction with carbon. Since the catalyst surface is now cleaned and free from carbon, the catalyst could be used for the next operation cycle and will be demonstrated in the subsequent sections.

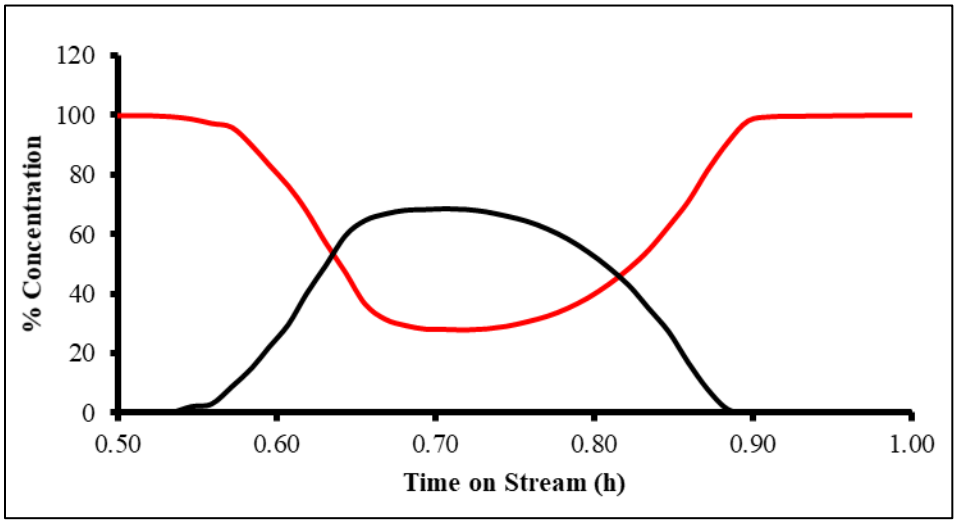

Figure 5.3 RGA provided concentration plot of the CO_2 and CO gases during a single regeneration cycle

5.4 Applicability to DRM and CARGEN™ processes

In the previous sub-section, the novel concept of the CO_2 regeneration technique was presented, and experimental proof of concept was also demonstrated. In this sub-section, firstly, a comprehensive experimental study is presented to better understand the importance of the new technique. Next, a dedicated sub-section presents experimental results on the novel CO_2 regeneration technique. Finally, characterization details using advanced material science equipment; XRD, XPS, and RAMAN provide strong evidence that reinforce the concept of the novel CO_2 regeneration process

5.4.1 Conventional Regeneration Technique

In a DRM process, the spent catalyst is generally regenerated using O_2-TPO. In this regeneration procedure, carbon deposited on a spent catalyst is "burnt off" as CO_2 by the reaction of pure O_2 gas with carbon at high-temperature conditions (700-800°C). After a typical DRM process, the activity of the spent catalyst is revived by doing an O_2-TPO followed by H_2 Temperature Programmed Reduction (TPR). The catalyst was again exposed to the reaction gases to compare its activity with the previous cycle. In this work, we performed two sets of experiments on the same catalyst to compare the activity of the spent catalyst when it was regenerated using conventional O_2-TPO and when it was compared with the proposed novel CO_2-TPO technique.

In a typical DRM and CARGEN™ experimental run, approx. 260 mg of sample was loaded in the U-tube quartz reactor and connected to the Micromeritics 2920 setup. In situ reduction of the catalyst was performed under 50 mL/min flow of 10% H_2 in Ar mixture

for 3 h at 700°C with a ramp rate of 2 °C/min. After the reduction of the catalyst, the reactor was purged with He for 2 hours, and cooled to a reaction temperature of 550°C. Feed gas comprising of CH_4, CO_2, Argon (Ar), Helium (He), and O_2 (as required in typical DRM/CARGEN™ reaction) was introduced at a specific flow rate in the range of 30 to 250 mL/min to the quartz tube reactor from the carrier port of the Micromeritics 2920 system. A blank run without any catalyst was recorded in the RGA by keeping Micromeritics 2920 system in reactor bypass mode to determine the inlet gas composition. Next, the reactant gases were introduced to the reactor tube at 550°C containing a quartz silica bed to confirm if there was no contribution from the homogeneous reaction. After this control experiment run, the mixed gas was introduced to a hot quartz reactor tube loaded with in-situ reduced 20% Ni/-γAl_2O_3 catalyst. DRM reaction was conducted for predefined Time on Stream (TOS), and then the reactor was purged with an inert gas.

The conventional O_2-TPO was performed with 10% O_2 in He gas at 800°C. A visual inspection of the spent catalyst after each TPO indicated that the Ni0oxidized (metallic gray) to inactive NiO (green color). Additionally, the formation of carbon was confirmed by the broad TPO peak of the evolved CO_2 detected in TCD signal, as shown in Figure 5.4. To recycle the catalyst, in situ TPR was performed again, and the DRM/CARGEN™ reaction was conducted with the mixed gas to achieve a comparable CO_2 and CH_4 conversion compared to the fresh catalyst cycle. This will be discussed in detail in the subsequent section.

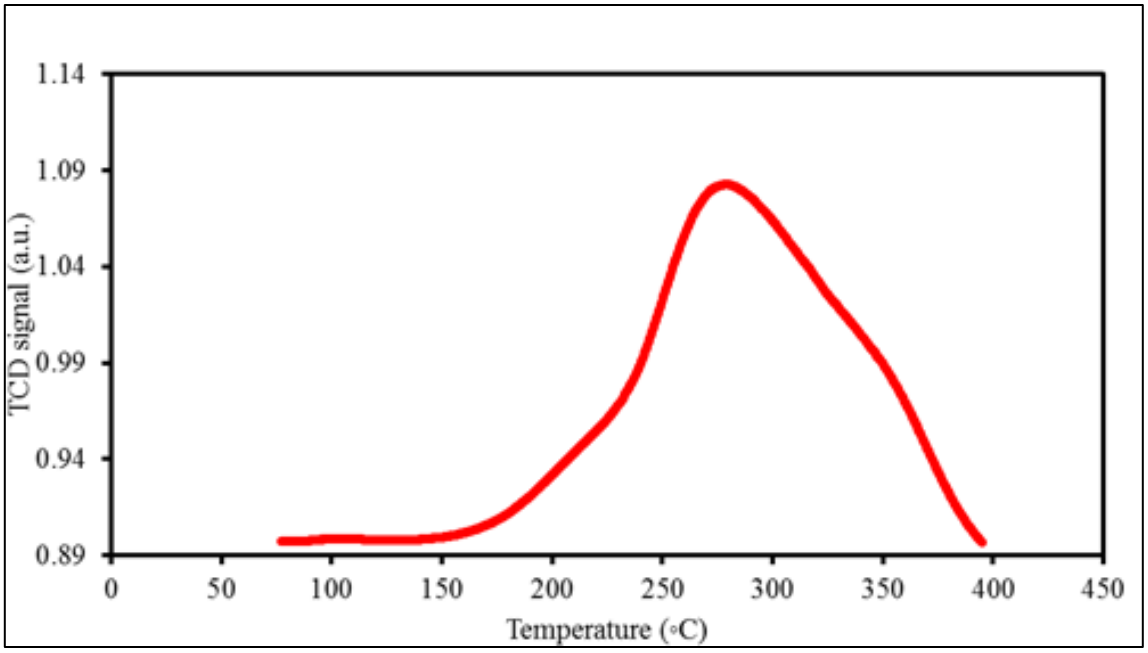

Figure 5.4 TCD signal of O_2-TPO of the 20% Ni/-γAl_2O_3 catalyst

5.4.2 The novel CO_2 regeneration Technique

In order to establish the general applicability of the novel CO_2 regeneration technique, experiments were conducted after both DRM as well as the CARGEN™ process. The results are discussed in detail in the sub-sections below:

5.4.2.1 DRM catalyst regeneration

In the proposed novel regeneration run, approx. 260 mg of commercial 20% Ni/-γAl_2O_3 catalyst was mixed with 500 mg of quartz silica and loaded in the U-tube quartz reactor, and connected to a Micromeritics 2920 setup. In situ reduction of the catalyst was performed as mentioned in the previous section. After complete reduction of the catalyst, the reactor was purged with Helium for 2 hours and cooled to a reaction temperature of 550°C. Feed gas comprising of 15% CH_4, 10% CO_2, 83% He, 2% Ar was introduced at a

rate of 248 ml/min to the quartz tube reactor from the carrier port of the Micromeritics system. DRM reaction was conducted for the next 10 h of TOS and then purged with Helium for 30 minutes. The TPO was performed with pure CO_2 gas at 650°C for 1 hour and the proposed regeneration reaction (Eq. 4) was confirmed by the evolution of CO peak followed by the return of the baseline peak in the RGA. Immediately after the CO_2-TPO, the reactor was cooled to 550°C while purging with Helium. After this, the second operation cycle was started by introducing the gas mixture, and the DRM reaction was performed for the next 5 hours TOS. It can be noted in Figure 5.5 that the activity trend of CO_2% conversion in the second cycle of operation is in the same range (~50%) as that of the first cycle after a regeneration cycle using pure CO_2. This indicates that the catalyst activity does not get affected after the regeneration cycle, and also provides a proof of concept for the proposed invention concerning the DRM reaction.

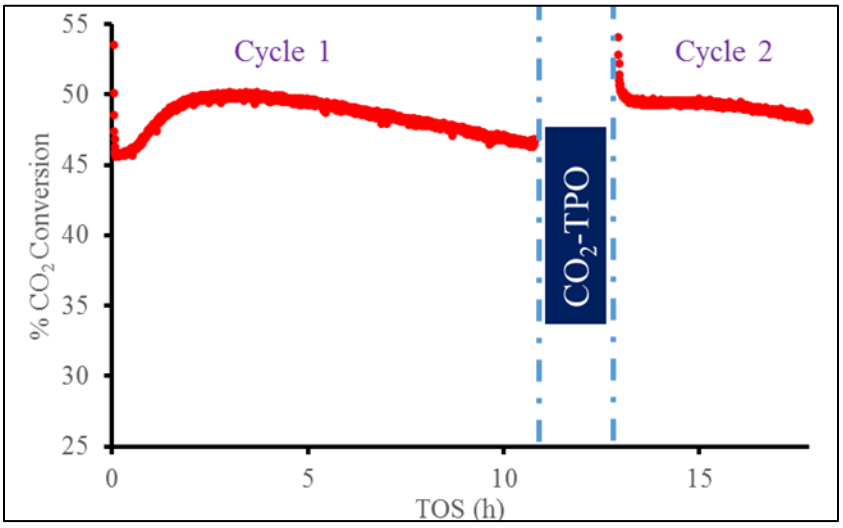

Figure 5.5 CO_2 activity during two cycles of DRM reaction with intermediate CO2-TPO regeneration.

5.4.2.2 CARGEN™ Catalyst Regeneration- Comparing the CO_2 regeneration and the conventional regeneration technique

In the previous experiment, two cycles of operation were conducted to prove that the activity of the DRM process catalyst is restored after a regeneration cycle with the proposed CO_2 TPO protocol. In this experiment, the objective is to demonstrate the equivalency between the proposed CO_2 TPO protocol and the conventional regeneration technique during the CARGEN™ process, comprising of a two-step procedure of first oxidation with O_2 followed by reduction with H_2. In this experiment, the activity of the catalyst is monitored in terms of CH_4% conversion and CO_2% conversion during each cycle of operation. Figure 5.8(a-b) shows the comparison between the activities of the CARGEN™ reaction when both regeneration techniques were performed. Similar to the procedure adopted in the previous example; first, we reduced 0.260 g of commercial 20% $Ni/\gamma - Al_2O_3$ catalyst with 10% H_2 in 90% Ar at 700°C for 2 hour. Subsequently, the temperature was ramped down to 550°C of reaction condition under He flow. CARGEN™ reaction was initiated by the introduction of mixed gas comprising of 30% CH_4, 18% CO_2, 3% O_2, 47% He, 2% Ar at a flow of 78 ml/min. RGA was used to monitor the composition of the evolved gases, and conversions of CH_4 and CO_2 shown in Figure 5.6 (a, b) were evaluated using mass balance. It can be observed that the CH_4 conversion of approx. 52% was achieved, while conversion of ~36% was achieved in CO_2. The reaction was continued for a TOS of approx. 9 h, and then TPO was performed by using 10% O_2 in 90% He for 2 h at 800°C. After complete oxidation with O_2 for 2 h, the oxidized catalyst was reduced with 10% H_2 in 90% Ar for the next 2 h. The second cycle of

CARGEN™ reaction was initiated and was continued for the next 8 h. It was observed that the activity of CH_4 and CO_2 (approx. 55% and 39%, respectively) was retained back to the value obtained in the previous cycle. Next, the reaction was stopped, and the reactor temperature was ramped up to 650°C while purging with Helium gas followed by the proposed CO_2-TPO regeneration for 10 minutes. A clear CO peak was observed in the RGA unit during the CO_2-TPO regeneration cycle, indicating the removal of carbon deposited during the operation cycle as per Eq. 4. Next, the temperature was ramped down to 550°C under He flow, and then CARGEN™ reaction was initiated again at 78 ml/min of the mix gas composition. It could be observed that the activity of the catalyst was retained back to the original conversion level of approx. 55% in CH_4 and 39% in CO_2. This shows that the proposed regeneration procedure was able to remove solid carbon as CO and was also able to retain the activity of the catalyst back to the original state. Also, it is noteworthy to mention that compared to the conventional regeneration procedure comprising of oxidation with O_2 and reduction with H_2, the proposed regeneration procedure utilized a greenhouse gas (CO_2) for regeneration. Also, compared to the regeneration time of 4 h (2 h of oxidation and 2 h of reduction) that is required in a conventional procedure, the proposed novel regeneration technique requires only 10 minutes, which results in a significant reduction in the downtime of the reactor. It should also be noted that a similar regeneration protocol could be applied using H_2 gas to convert carbon deposited during the DRM reaction and CARGEN™ to CH_4. However, it is recommended to utilize CO_2 for regeneration as a) it is a greenhouse gas b) does not require a special production facility like that of H_2 c) time required for regeneration is

significantly lower compared to H_2 regeneration, and d) CO produced has significantly high commercial value compared to CH_4. Upon combining the DRM process with the CO_2 TPO process, one can realize that a switching like process could be developed, as shown in Figure 5.7. The ultimate benefit of such a process would be uninterrupted CO_2 utilization, both during the operation and regeneration cycle.

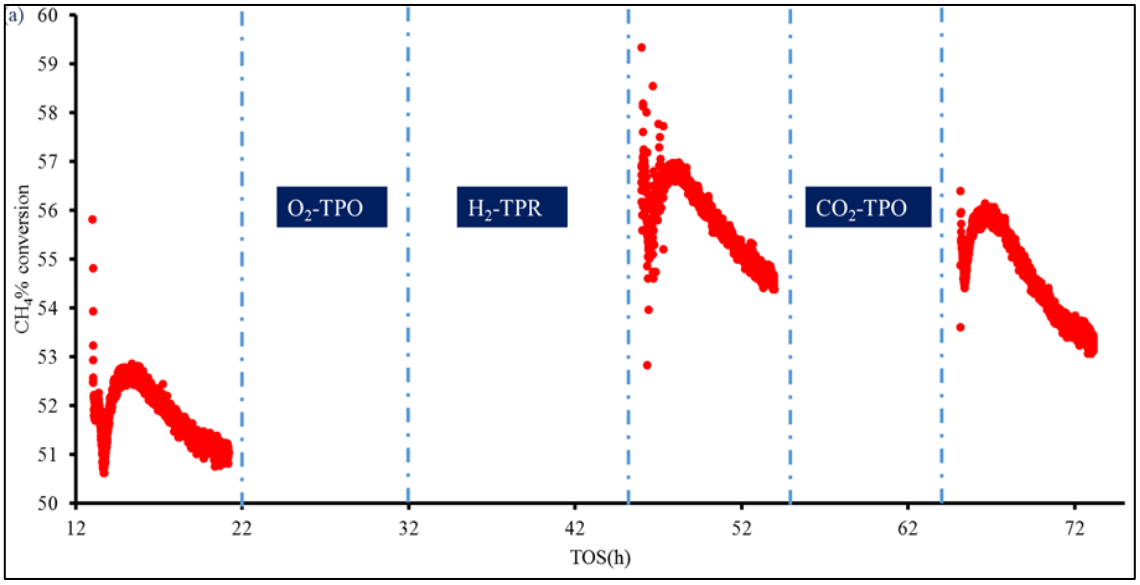

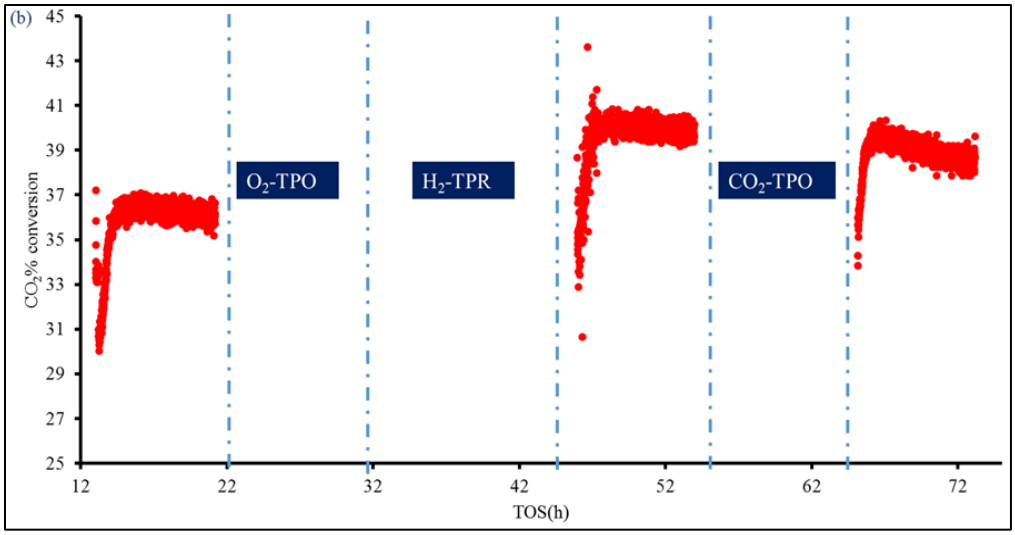

Figure 5.6 (a) CH_4% Conversion and (b) CO_2% Conversion comparison between the conventional regeneration procedure (O_2 TPO + H_2 TPR) Vs proposed novel regeneration technique (CO_2-TPO)

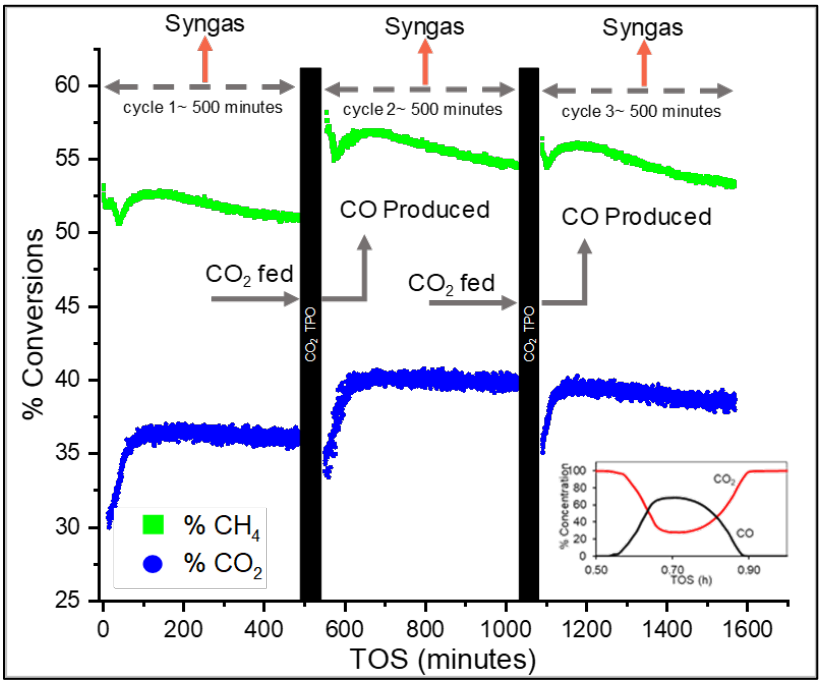

Figure 5.7 A combined DRM+CO_2 TPO process was showing uninterrupted utilization of CO_2 during both operation and regeneration cycles. Inset Figure: Concentration plot from RGA showing the release of CO during CO_2 TPO. Conditions: 200 mg 20% Ni/γ-Al_2O_3, flow: 94 mL/min, T: 550°C.

5.4.3 Advanced studies from a Material Science viewpoint

5.4.3.1 X-ray Photoelectron Microscopy (XPS) and X-Ray Diffraction (XRD) analysis

To understand the difference between the conventional regeneration and the new regeneration technique, an experiment was conducted in which two similar batches of fresh catalysts were taken and subjected to DRM reaction with identical activation protocol. After a TOS of 4 hours, the first batch of the spent catalyst was subjected to the new regeneration procedure with 99% CO_2 gas, while the second batch was subjected to a conventional regeneration procedure involving oxidation with 10% oxygen. The two catalysts were then subjected to the second cycle of operation, wherein the first batch in which O_2 was used showed activity, while the second batch in which O_2 was used did not. After this, both the spent samples were characterized by using ex-situ XRD and XPS analysis to identify their distinguishing features.

The XPS analysis was conducted using the Axis Ultra DLD instrument by Kratos, a Shimadzu company located in the United Kingdom, in which a magnesium ($K\alpha$) radiation of 1253.6 eV was operated at an emission current of 10 mA and 15 kV. First, a low-resolution survey was conducted at a step size of 0.1 eV and a pass energy of 80eV. Finally, all the peaks relative to C 1s, Ni 2p, O 1s, and Al 2p were separately identified at high resolution with a pass energy of 5 eV and a step size of 1 eV. This analysis was conducted individually for the spent DRM coked catalyst sample (Figure 5.8 a), post-CO_2 TPO of DRM coked catalyst sample (Figure 5.8 b), and post O_2 TPO sample (Figure 5.8 c). Table 5.1 provides surface elemental composition of C 1s, Ni 2p, O 1s and Al 2p of all three samples.

Table 5.1 Tabular representation of the XPS analysis surface composition of (a) spent carbon DRM catalyst, (b) O_2 TPO sample (c) CO_2 TPO sample

Name	Spent carbon DRM catalyst		O_2 TPO sample		CO_2 TPO sample	
	peak BE	atomic%	peak BE	atomic%	peak BE	atomic%
C 1s	284.83	75.84	284.73	4.56	284.88	5.37
Ni 2p	855.15	0.62	855.27	3.02	855.94	2.01
Al 2p	74.42	8.21	73.29	31.41	73.47	30.81
O 1s	531.2	15.34	530.21	61.01	530.66	61.82

The comparison of surface carbon in samples a, b, and c, as shown in Table 5.1 above, clearly demonstrates that both O_2 TPO, as well as CO_2 TPO, were able to reduce surface carbon from approx. 75% to approx. 5%. Further, the composition of other surface species, Ni, O, and Al, were almost the same, revealing complete equivalency of both the O_2 TPO process as well as CO_2 TPO.

Since XPS is a surface analysis of the sample, XRD was done, which is a bulk analysis to further understand the extent of oxidation of the nickel catalyst using both the regeneration techniques. The XRD image analysis of this experiment is provided in Figure 5.9. As can be seen, XRD of the CO_2 TPO treated catalyst is identical to that of a reduced catalyst indicating that the sample did not undergo any oxidation. While, the XRD pattern of the O_2 TPO treated sample showed the formation of NiO, which is inactive for the DRM reaction explaining why the catalyst wasn't active for the second cycle of operation. Further analysis of the XRD results using the Rietveld refinement method reveals that the

O_2 TPO sample had a significant quantity of NiO (16.2 %) as opposed to 2.1% in the CO_2 TPO sample. Moreover, this quantity of NiO in the O_2 TPO sample is similar to that of the reduced sample (1.3%).

Combined results of both XRD, as well as XPS conclusively establishes the soft oxidant characteristic of CO_2 in selectively oxidizing the surface carbon while leaving the metallic state of pure nickel intact. On the other hand, since O_2 is a strong oxidizing agent, it oxidizes not only the surface carbon but also the active metallic nickel sites to an oxidized state, which is inactive for reforming processes.

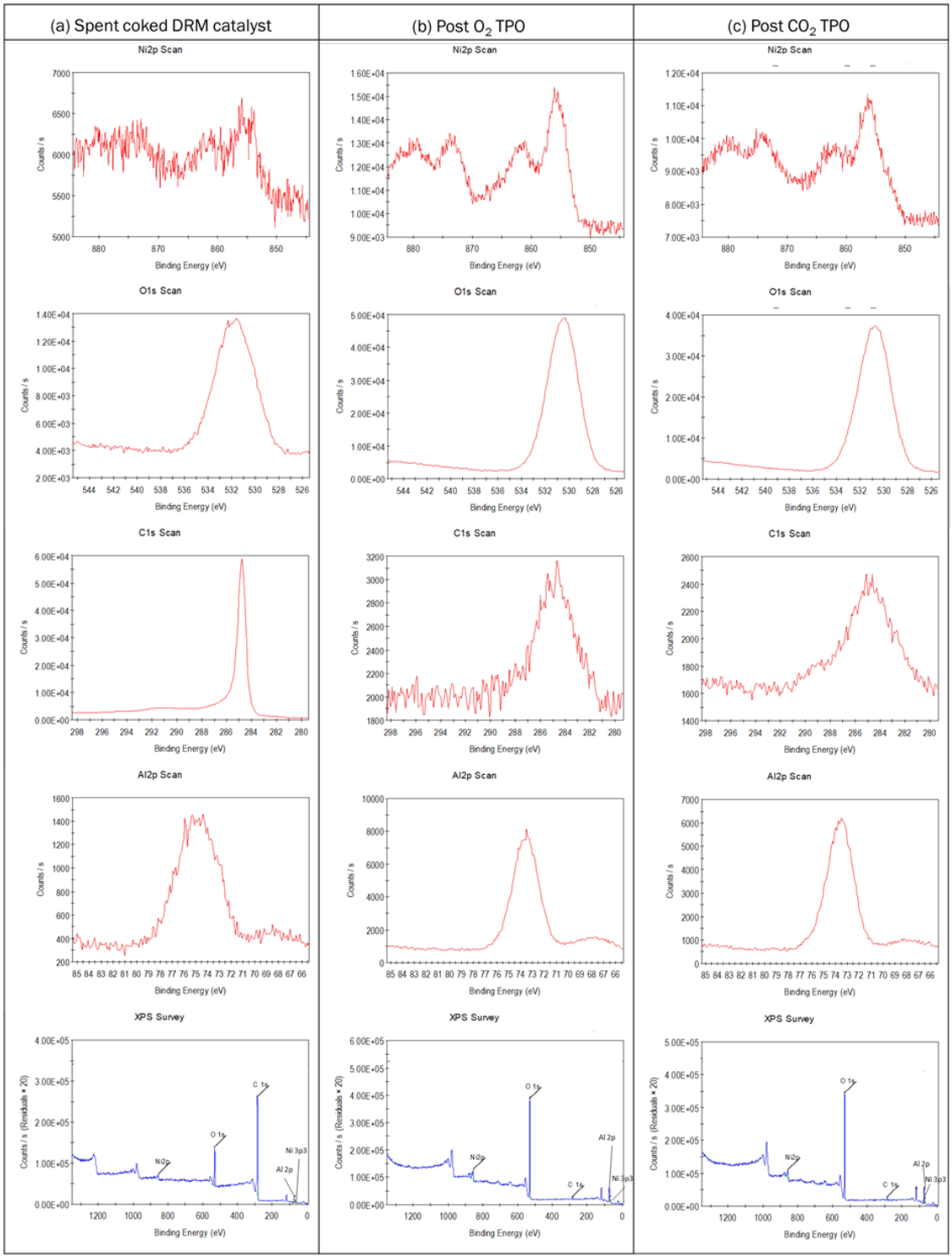

Figure 5.8 XPS plots of (a) Spent carbon DRM catalyst (b) Post O_2 TPO sample (c) Post CO_2 TPO sample

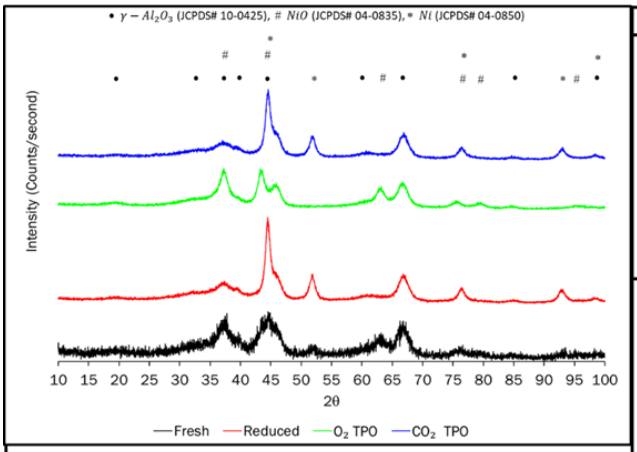

Compound	JCPDS#	2θ	h	k	l
γ-Al_2O_3	10-0425	19.466	1	1	1
		31.962	2	2	0
		37.635	3	1	1
		45.901	4	0	0
		60.951	5	1	1
		67.093	4	4	0
		85.099	4	4	4
		97.290	7	3	1
NiO	04-0835	37.278	1	1	1
		43.295	2	0	0
		62.913	2	2	0
		75.439	3	1	1
		79.387	2	2	2
		95.075	4	0	0
Ni	04-0850	44.505	1	1	1
		51.844	2	0	0
		76.366	2	2	0
		92.939	3	1	1
		98.440	2	2	2

Element	Rietveld refinement (%)			
	Fresh	Reduced	CO_2-TPO	O_2-TPO
Ni	NA	21.3	18	1
NiO	7.3	1.3	2.1	16.2
g-Al_2O_3	92.2	70.4	69.9	73.3
$NiAl_2O_4$	NA	7	10	9.5
Total	99.5	100	100	100

Figure 5.9 XRD plot of fresh 20% Ni/γ-Al2O3, reduced, post O_2 TPO and post CO_2 TPO samples with the JCPDS identification of the crystallographic phases and the Rietveld refinement composition comparison of each case.

5.4.3.2 Raman Analysis

To evaluate the CO_2 oxidation capability, a pre-reduced 20 wt% Ni/Al_2O_3 catalyst was heated continuously from room temperature to 700°C in CH_4, then the CH_4 supply was cut off, and one CO_2 pulse was injected for 5s and the 40 s, respectively in two independent experiments. Figure 5.10 shows the SEM and Raman results of this study. It was observed that the quality of the CO_2-treated MWCNTs becomes worse (D/G ratio increases while G'/G ratio decreases). It seems that the more defective carbon structures are preferentially removed from the Ni surface while the robust ones remain on the surface with more defects

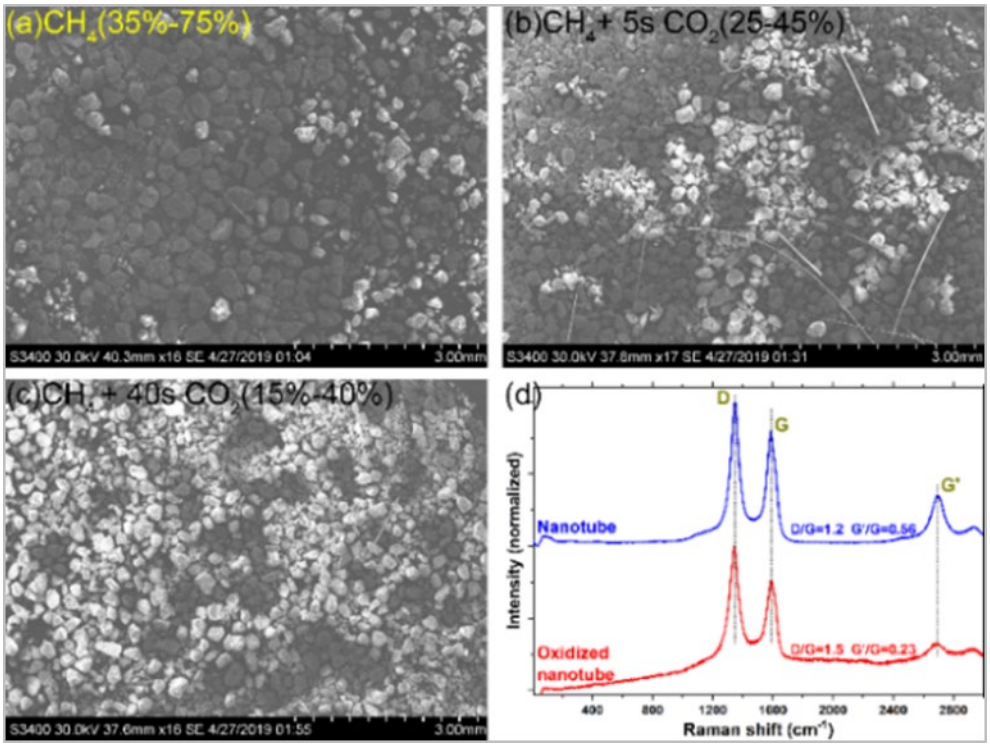

Figure 5.10 SEM images of (a) surface carbon deposited continuously from room temperature to 700°C during CH_4 pyrolysis, which undergoes oxidation by (b) a 5s-CO_2 pulse or (c) a 40 s CO_2 pulse. (d) Raman spectra of MWCNT without and with the 40 s-CO_2 treatment.

5.5 CO_2 footprint calculations

In order to compare the CO_2 footprints of the new regeneration procedure and the conventional regeneration procedure, both direct and indirect CO_2 emission and consumption information were accounted for. For energy calculations, energy balance was conducted using the equilibrium moles calculated from Gibbs free energy calculations. More details on the equilibrium assessment using Gibbs free energy calculation are provided in section 3. It should be noted that 1 kg of surface carbon removal was considered as a basis for both cases. The following step-by-step calculation provides details on this assessment:

Basis: 1 kg of surface carbon removal using CO_2 TPO or O_2 TPO process

Case 1: Novel CO_2 regeneration technique

Stoichiometric equation:

$$CO_2 + C \rightarrow 2\,CO \qquad \Delta H_{rxn,700°C} = 118.13 \frac{kJ}{mol} \tag{5.3}$$

∵ 1 kg carbon ≅ 83 moles (5.4)

∴ 83 moles of CO_2 will be utilized to convert 1 kg of carbon to 166 moles of CO (5.5)

∵ CO_2 TPO is conducted at $700°C$ temperature, by energy balance and using Gibbs free energy minimization, energy requirement at $700°C$ for the stoichiometric reaction in Eq. 5.3 = $9804.7 \frac{kJ}{83\ mol\ CO_2 + 83\ mol\ C}$ (5.6)

If the energy requirement for step 3 (Eq. 5.6) is fulfilled by methane combustion (Eq. 5.7 below) at $700°C$, the total number of moles of CO_2 emitted by it will be 13.6 moles.

$$CH_4 + 2O_2 \rightarrow CO_2 + 2H_2O \qquad \Delta H_{rxn,700°C} = -721.36 \frac{kJ}{mol} \tag{5.7}$$

Net CO_2 emission = $13.6 - 83 = -69.4\ moles \cong -3.05 \frac{kg\ CO_2\ produced}{kg\ of\ surface\ carbon\ removed}$

Therefore, the total CO_2 fixation achieved= $3.05\ \frac{kg\ CO_2\ produced}{kg\ of\ surface\ carbon\ removed}$

Case 2: Conventional regeneration technique

Stoichiometric equation:

$$C + O_2 \rightarrow CO_2 \qquad \Delta H_{rxn,700°C} = -361.7489 \frac{kJ}{mol} \tag{5.8}$$

∵ 1 kg carbon ≅ 83 moles (5.9)

∴ 83 moles of CO_2 will be produced per kg of surface carbon removed (5.10)

Carbon credits achieved from utilizing $-361.7489\frac{kj}{mol} \cong -30083\frac{kJ}{83\ moles\ CO_2\ emitted}=$

$\frac{30083}{721.3586} = 41\ moles$ (5.11)

This means, if this energy was to be completely utilized while replacing methane as the main source of heat, then the CO_2 emission was saved by burning 1 kg of carbon = 41 moles.

Total CO_2 emission= step 4 (Eq. 5.10– Eq. 5.11)

$$=83 - 41 = 42\frac{moles}{kg\ of\ surface\ carbon\ removed} = 0.49\frac{kg\ CO_2\ emitted}{kg\ surface\ carbon\ removed}$$

Therefore, the total CO_2 emission= $0.49\ \frac{kg\ CO_2\ produced}{kg\ of\ surface\ carbon\ removed}$

In summary, a simple comparison of the footprints associated with the CO_2 TPO and O_2 TPO, as demonstrated in cases 1 and 2 above, reveals that CO_2 TPO is a net CO_2 conversion process. At the same time, O_2 TPO is a net CO_2 emitting process. Also, the calculation above does not account for the footprint associated with the production of pure hydrogen, which is required for activating the post- O_2 TPO catalyst as the active phase in the reforming process is metallic compound and not its oxidized state. It should be appreciated that the CO_2 TPO does not oxidize the metallic sites, as it is not a potent oxidizing gas like O_2, which along with carbon, also oxidizes the metallic catalyst. Further, the second benefit of this process is that the carbon monoxide produced from CO_2 TPO could be used as a precursor for synthesizing a variety of chemicals and materials, which will bring additional economic benefit. Thirdly, the new procedure allows for reducing the

downtime of the reactors, as it is a single step process compared to a dual step conventional regeneration procedure.

5.6 Conclusion:

A novel CO_2-Temperature Programmed Oxidation (CO_2-TPO) protocol is designed to "burn off" carbon produced during a coke formation reaction. Several supporting theoretical and experimental results are provided to strongly advocate the efficacy of the new regeneration process and to establish a clear comparison with the conventional regeneration technique. In terms of benefits, it is realized that the "soft oxidant" tendency of CO_2 to selectively oxidize carbon without affecting catalyst morphology and oxidation state allows it to be effectively utilized over several cycles of regeneration. The second benefit is that the new regeneration process enables the production of pure CO gas that may be required for several downstream processes. The third benefit of this process is that it reduces the costs associated with the production of pure oxygen and hydrogen that were required during the erstwhile regeneration technique. From a process point of view, significantly less process downtime could be achieved in an extremely cost-effective manner at a reasonably low CO_2 emission, as observed from the preliminary sustainability assessment study.

6. CONCLUSIONS AND FUTURE PROSPECTS

6.1 Conclusion

The rise in global CO_2 emissions has led to a significant increase in the research and development efforts by the global scientific community to look for alternative and sustainable solutions. Natural gas utilization has gained significant traction due to its relatively cleaner nature compared to other fossil fuels like crude oil and coal. One of the important natural gas monetization pathways is to be converted to liquid fuels via various GTL processes. A critical intermediate and highly energy-intensive building block of GTL is the reforming of methane, which essentially is the conversion of natural gas to synthesis gas. Industrial reforming processes are extremely energy-intensive and contribute 30-50% of the overall GTL plant CO_2 emissions. DRM is a well-known process that presents an attractive option of converting two greenhouse gases CO_2 and CH_4, however, its commercial implementation is plagued by several process challenges that need to be addressed by smart solutions.

The first outcome of this work presented in section 3 is a thermodynamic assessment study that investigates the possibility of combining the benchmark industrial reforming process with DRM to address its process challenges. Firstly, a high-fidelity thermodynamic model was developed based on the Gibbs Free Energy minimization principle in MATLAB® to study the performance of various reforming processes under variable operational conditions. A detailed energy assessment is then conducted, and a comparison is established with DRM under similar operational conditions of temperature and pressure. Finally, presented is an optimal solution that combines the existing reforming processes

with DRM in one single reactor unit called as TRM (short for Tri-reforming of methane). It was observed that the combination of SRM, POX, and DRM by using a unique feed ratio enables the elimination of carbon at 750 ºC and 1 bar pressure, which pertains to about 47% reduction in energy requirement compared to the DRM process.

The second and the major outcome of this work presented in section 4 is the development of a novel technological solution called as the CARGEN™ process that addresses DRM challenges. The patented CARGEN™ technology comprises of two reactors which are tasked to produce solid carbon (MWCNTs) and syngas separately in two independent reactors in series. The approach and the operational conditions of both the reactors are optimized via a detailed thermodynamic study that enables up to 50% reduction in energy required by the standalone DRM process, in addition to about 65% CO_2 conversion per pass. A preliminary LCA study showed about a 40% reduction in overall CO_2 emissions compared to the benchmark ATR process. Also, an OPEX reduction of 40% is realized upon comparison with the ATR. Due to the high market cost of MWCNTs ranging from 500-1000 USD/kg, CARGEN™ presents a strong and economically attractive process that not only convert GHGs to syngas that meets downstream processes but also produces extremely valuable MWCNTs. Section 3 and section 4 of this thesis presents the thermodynamic assessment, as well as experimental studies that aided in conceptualization, optimization, and experimental validation of the CARGEN™ technology. In addition, section 4 presents various supporting characterization studies using state-of-the-art equipment SEM, HR-TEM, RAMAN, XRD, and XPS that unanimously demonstrate the production of MWCNTs under CARGEN™ specified

operational conditions. A scale-up study conducted using three independent reaction systems showed the scalability of the CARGEN™ process from micro-gram to milli-gram to multi-gram scale. A SEM and TEM study conducted for all the three scales of production shows consistency in the quality of MWCNTs, thus further confirming the scalability of the CARGEN™ process.

The third major outcome of this work presented in section 5 is the development of unique catalyst regeneration and reactivation protocol that utilizes CO_2 to remove coke formed on the catalyst surface during DRM reaction. The developed protocol is a single step reaction of carbon and CO_2 at 650 to 800 ^oC temperature to form carbon monoxide. The gasification of carbon in the form of CO unclogs the catalyst surface. In contrast to the conventional procedure of direct oxidation of carbon using air or oxygen, which produces CO_2, this process, on the other hand, utilizes CO_2 to produce valuable CO. Additionally, since the active catalyst for a reforming reaction is the metallic phase and not the oxidized phase, the need for post oxidation hydrogen reduction required during conventional regeneration is no longer necessary due to the soft oxidant nature of CO_2, which selectively oxidizes surface carbon only. In terms of sustainability benefits, it was observed that the new CO_2 regeneration process is capable of converting at least 3kg of CO_2 per kg of surface carbon removed, while O_2 TPO leads to about 0.5 kg of CO_2 emission per kg of surface carbon. It should be emphasized that the use of the CO_2 regeneration technique also saves the active catalyst (Ni) from undergoing cycles of oxidation (forming inactive NiO) and reduction (forming Ni) as in the case of conventional regeneration technique.

6.2 Future Prospects

In summary, this work lays the foundation of the novel CARGEN™ technology, starting from its conceptualization to TRL-3 achievement. To ready the CARGEN™ technology for future commercial implementation, various studies, and development stages are needed. Some of the important future milestones are stated below:

1. CARGEN™ catalyst and fluidization:

   Since the CARGEN™ process is a carbon forming process, a packed bed type of reactor will lead to significant pressure drop issues during operation. Therefore, it is necessary to operate the CARGEN™ process under a fluidized bed type of contact pattern. The CARGEN™ catalyst developed in this work, therefore, needs to be optimized to be operated under a fluidized bed mode of operation. Moreover, dedicated kinetics studies will be necessary to predict reactor performance under different flow regimes. Also, a computational fluid dynamics (CFD) study of the flow pattern and the fluidized bed reactor geometry would be required to find the most optimal contacting pattern that provides maximum MWCNT yield during the reaction.

Figure 6.1 Targeting a scaled-up fluidized bed CARGEN™ process

2. MWCNT and catalyst separation:

Since MWCNTs are produced over the nickel crystal sites during the CARGEN™ process via a tip-growth mechanism, it will be necessary to develop a separation process that would separate nickel and the MWCNT to produce pure MWCNT. The current purity levels from gram-scale production are above 90%; therefore, in order to achieve 99% purity, it will be essential to separate the catalyst material from the MWCNTs. Also, in the current process, the catalyst is considered as sacrificial material, which may not be very attractive when tons of quantity will be required during industrial implementation. Therefore, it will be critical to separate and recycle back the catalyst material for subsequent cycles of operation.

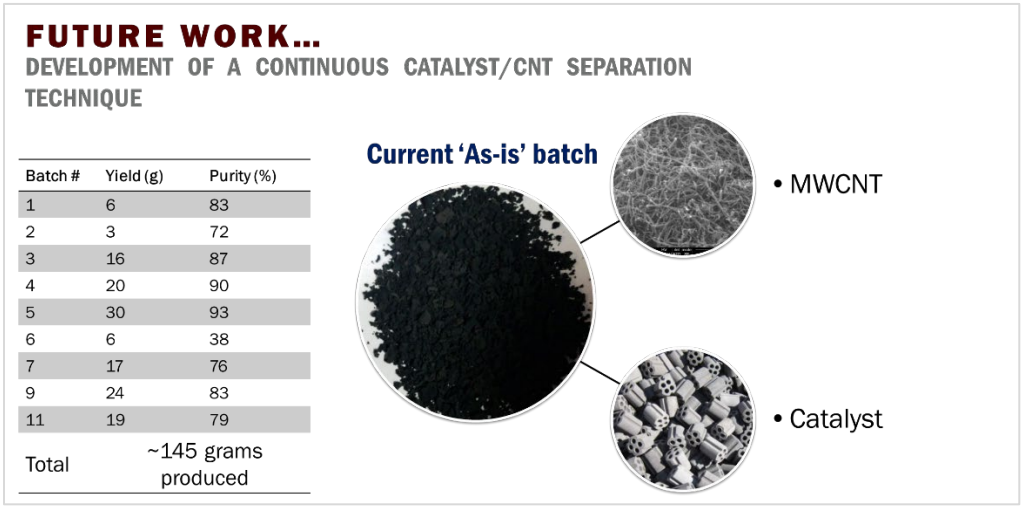

Figure 6.2 Targeting a continuous MWCNT/catalyst separation and recycle system for catalyst reuse while improving MWCNT purity

3. CARGEN™ scale-up beyond TRL-3:

For any technology to reach the maturation level for commercial implementation, significant R & D efforts are necessary for TRL escalation, validation, and testing. As

CARGEN™ technology is currently at TRL-3, since it is experimentally validated and capable of producing MWCNTs at gram-scale quantities, the next step is further scale-up to kg scale. This entails proper reactor designing and testing. As discussed in point 1, fluidization presents a plausible option for CARGEN™ implementation; however, it needs to be done after proper CFD modeling, reactor geometry optimization, and fabrication. Also, experimental validation at each stage of development and comparison with the base case will be critical to ensure proper scale-up. Therefore, the immediate target for scale-up is to design, fabricate, and test the CARGEN™ process at TRL- 4 and 5 in a bench-scale reactor. Once a reasonable and consistent operational performance is reached, further scale-up to TRL-6 and 7 should be undertaken with industry and professional support. A techno-economic assessment is also critical to establish and prove the technical and economic sustainability. Our research group's efforts are currently underway to develop a proposal that will involve several experts from industry and academic backgrounds. The proposal will be aimed towards a systematic scale-up of the CARGEN™ process beyond TRL-3 for future commercial implementation.

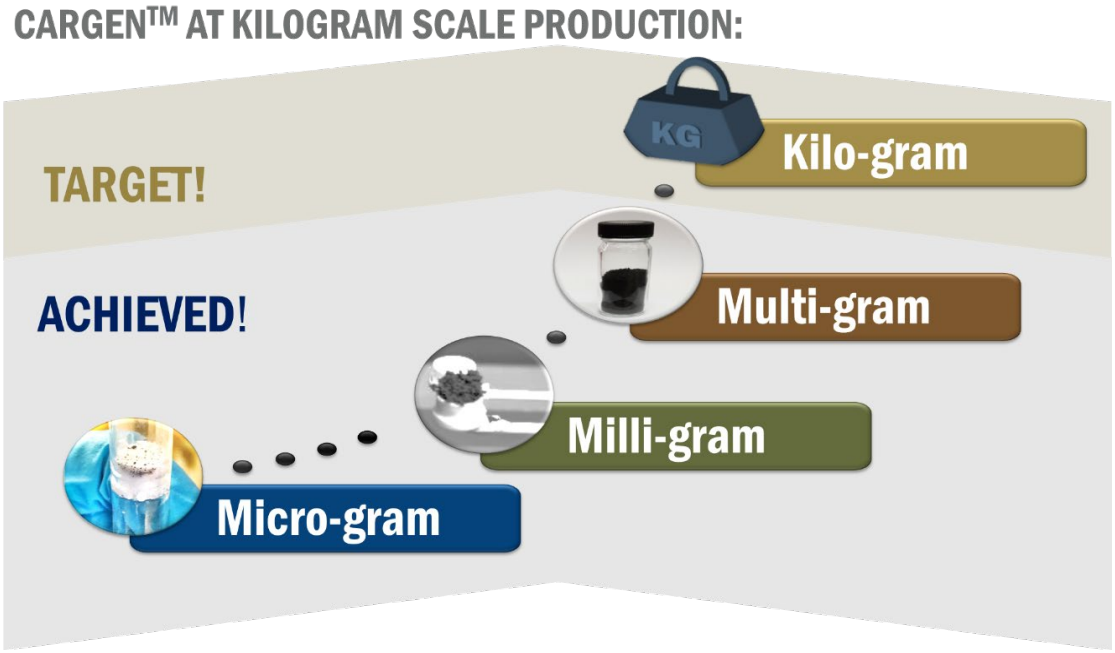

Figure 6.3 Targeting CARGEN™ scale-up beyond TRL-3

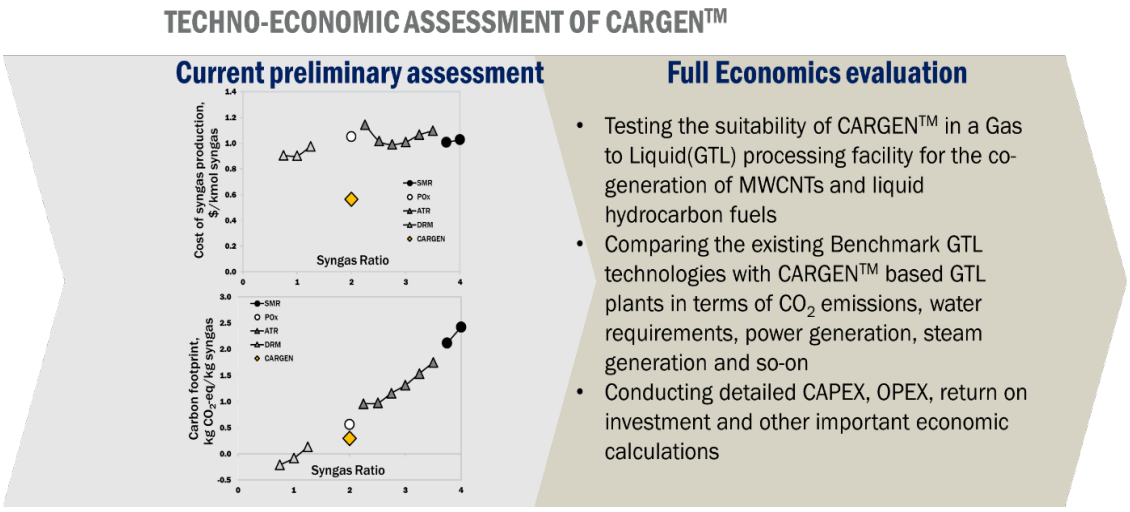

Figure 6.4 A comprehensive Techno-economics assessment and comparison should be conducted to compare various reforming technologies with CARGEN™

4. CARGEN™ based GTL process simulation:

Since the CARGEN™ process falls under the category of methane reforming process, it will be necessary to have a one to one comparison of the CARGEN™ process with the benchmark reforming processes of POX, ATR, and SRM. An ASPEN® flowsheet development will be a critical activity that will involve CARGEN™ as the reforming process. However, it should be noted that MWCNTs are additional products of CARGEN™, and therefore, the ASPEN flowsheet will involve handling all three states of matter-solid, liquid, and gas, which is typically difficult for a process simulation software. A one on one comparison with the existing flowsheet would only be possible if all the flowsheets will either be compared at the same production capacity or feed capacity of the natural gas. Previous work by El-Halwagi group [166,167] demonstrated a key performance index (KPI) comparison of SRM, POX, and ATR processes in terms of CO_2 emission, power generation, water requirement. A similar assessment for the CARGEN™ process will be crucial to establish its techno-economic viability.

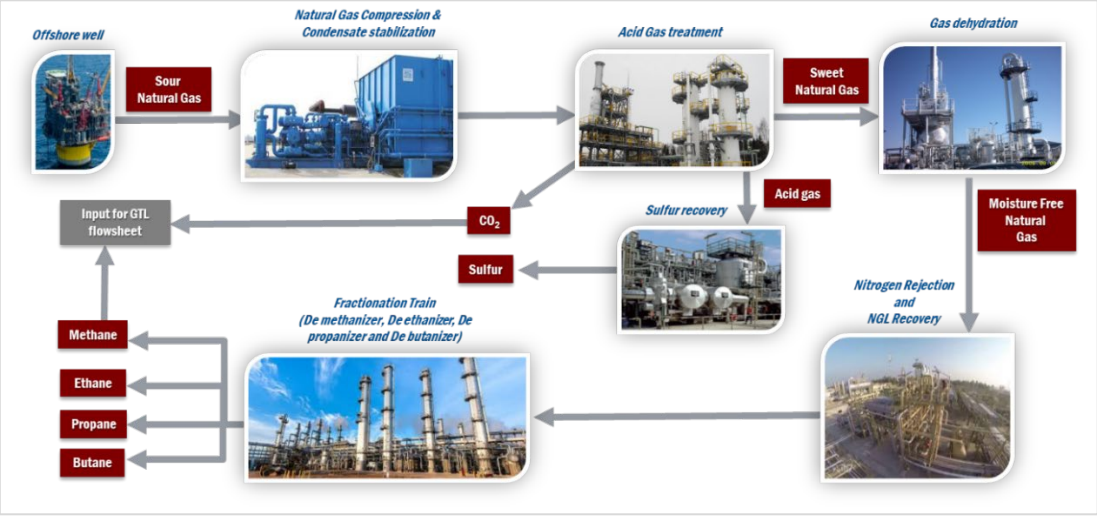

Figure 6.5 An illustration of various process plants in a typical midstream process train.

5. Midstream Process Simulation:

For a country like the state of Qatar, whose entire wealth is dependent on natural gas exploration, production, and export, CARGEN™ presents an attractive solution, since natural gas processing leads to the production of both pure CO_2 and CH_4. A single train of natural gas processing of Qatargas company produces approximately 500 tons/day of CO_2, and with the current 14 trains online, a daily CO_2 production of 7000 tons/day is inevitable. The source of CO_2 from the natural process train is typically from acid-gas treatment, which is part of midstream processing. Therefore, simulation of a mid-stream process train will be crucial to identify the exact sources, composition, and capacity of CARGEN™ suitable CO_2. PROMAX® is a promising process simulation software that has proved significant accuracy for midstream flowsheet development. Therefore the use of PROMAX® for this application would be essential. The ultimate goal of this work will therefore be to simulate a single midstream process train in PROMAX® to deduce the capacity and purity of CO_2 available from midstream. This will help in determining the capacity of CARGEN™ based GTL process plant and the final production quantity of MWCNTs that could be produced. Such an attempt will obviously open several doors for monetization, as the market of MWCNTs is untapped in the state of Qatar.

REFERENCES

1. A Snapshot of Exxon Mobil's 2018 World Energy Outlook - IER. https://www.instituteforenergyresearch.org/uncategorized/snapshot-exxon-mobils-2018-world-energy-outlook/. Accessed September 2, 2020.
2. Saha D, Grappe HA, Chakraborty A, Orkoulas G. Postextraction separation, on-board storage, and catalytic conversion of methane in natural gas: a review. *Chem Rev*. 2016;116(19):11436-11499.
3. Enerdata. World Natural gas production. Yearbook. https://yearbook.enerdata.net/natural-gas/world-natural-gas-production-statistics.html. Published 2020.
4. Times G. Qatar set to be world's largest LNG producer, says al-Attiyah. https://www.gulf-times.com/story/650563/Qatar-set-to-be-world-s-largest-LNG-producer-says-. Published 2019.
5. Bai Y, Meng J, Meng F, Fang G. Stochastic analysis of a shale gas investment strategy for coping with production uncertainties. *Energy Policy*. 2020;144(May). doi:10.1016/j.enpol.2020.111639
6. Talmadge M, Dutta A, Bain R. Techno-economic and Market Analysis of Pathways from Syngas to Fuels and Chemicals. *Chicago, Illinois*. 2013.
7. Statista.com. The Carbon Age: 150 Years of CO2 Emissions. https://www.statista.com/chart/13584/worldwide-carbon-emissions-from-fossil-fuel-consumption-and-cement-production/. Published 2018.

8. Schmal M, Toniolo FS, Kozonoe CE. Perspective of catalysts for (Tri) reforming of natural gas and flue gas rich in CO2. *Appl Catal A Gen*. 2018;568(September):23-42. doi:10.1016/j.apcata.2018.09.017

9. Ghoneim SA, El-Salamony RA, El-Temtamy SA. Review on innovative catalytic reforming of natural gas to syngas. *World J Eng Technol*. 2016;4(1):116.

10. Qatargas. *Qatargas Sustainability Report 2018*. Doha; 2019. http://www.qatargas.com/english/sustainability/Sustainability Reports/Sustainability Report 2018 English.pdf.

11. International Energy Agency. *Putting CO2 to Use*. Paris; 2019. https://www.iea.org/topics/carbon-capture-and-storage/policiesandinvestment/.

12. Abusrafa AE, Challiwala MS, Choudhury HA, Wilhite BA, Elbashir NO. Experimental Verification of 2-Dimensional Computational Fluid Dynamics Modeling of Supercritical Fluids Fischer Tropsch Reactor Bed. *Catal Today*. 2019. doi:https://doi.org/10.1016/j.cattod.2019.05.027

13. Alsuhaibani AS, Afzal S, Challiwala M, Elbashir NO, El-Halwagi MM. The impact of the development of catalyst and reaction system of the methanol synthesis stage on the overall profitability of the entire plant: A techno-economic study. *Catal Today*. 2019. doi:https://doi.org/10.1016/j.cattod.2019.03.070

14. Challiwala MS, Wilhite BA, Ghouri MM, Elbashir NO. Multi-Dimensional Modeling of a Microfibrous Entrapped Cobalt Catalyst Fischer-Tropsch Reactor Bed. *AIChE J*. 2017;[under rev(5):1723-1731. doi:10.1002/aic.16053

15. Elbashir N, Challiwala MS, Ghouri MM, Linke P, El-Halwagi M. Modeling

Development of a Combined Methane Fixed Bed Reactor Reformer. In: *Qatar Foundation Annual Research Conference Proceedings*. Vol 2016. HBKU Press Qatar; 2016:EESP2384.

16. Choudhury HA, Cheng X, Afzal S, Prakash A V., Tatarchuk BJ, Elbashir NO. Understanding the deactivation process of a microfibrous entrapped cobalt catalyst in supercritical fluid Fischer-Tropsch Synthesis. *Catal Today*. 2019;(September 2018):0-1. doi:10.1016/j.cattod.2019.01.031
17. Van Hook JP. Methane-steam reforming. *Catal Rev Eng*. 1980;21(1):1-51.
18. Rostrup-Nielsen J. Steam reforming of hydrocarbons. A historical perspective. In: *Studies in Surface Science and Catalysis*. Vol 147. Elsevier; 2004:121-126.
19. Dybkjaer I. Ammonia production processes. In: *Ammonia*. Springer; 1995:199-327.
20. Appl M, Gössling H. Production of synthesis gas after the steam reforming process. *Chem Zeitung*. 1972;96(3).
21. Rostrup-Nielsen JR. CATALYTIC STEAM REFORMING. *Catal Sci Technol*. 1984;5:1-117. https://www.scopus.com/inward/record.uri?eid=2-s2.0-0021158095&partnerID=40&md5=f91480d485d3760a1ba6198ccfe28060.
22. Töpfer HJ. No Title. *Gas Erdgas Gas Wasserfach Wasser Abwasser*. 1976;117:412.
23. Rostrup-Nielsen JR, Rostrup-Nielsen T. Large-scale hydrogen production. *CATTECH*. 2002;6(4):150-159. doi:10.1023/A:1020163012266
24. Rostrup-Nielsen JR. Sulfur-passivated nickel catalysts for carbon-free steam

reforming of methane. *J Catal*. 1984;85(1):31-43. doi:10.1016/0021-9517(84)90107-6

25. Trimm DL. Coke formation and minimisation during steam reforming reactions. *Catal Today*. 1997;37(3):233-238. doi:10.1016/S0920-5861(97)00014-X
26. Rostrup-Nielsen JR, Christiansen LJ, Bak Hansen JH. Activity of steam reforming catalysts: Role and assessment. *Appl Catal*. 1988;43(2):287-303. doi:10.1016/S0166-9834(00)82733-5
27. Rostrup-Nielsen JR. Syngas in perspective. *Catal today*. 2002;71(3-4):243-247.
28. Prettre M, Eichner C, Perrin M. The catalytic oxidation of methane to carbon monoxide and hydrogen. *Trans Faraday Soc*. 1946;42:335b - 339.
29. Wood DA, Nwaoha C, Towler BF. Gas-to-liquids (GTL): A review of an industry offering several routes for monetizing natural gas. *J Nat Gas Sci Eng*. 2012;9:196-208. doi:10.1016/j.jngse.2012.07.001
30. Özkara-Aydınoğlu Ş. Thermodynamic equilibrium analysis of combined carbon dioxide reforming with steam reforming of methane to synthesis gas. *Int J Hydrogen Energy*. 2010;35(23):12821-12828.
31. Nematollahi B, Rezaei M, Lay EN, Khajenoori M. Thermodynamic analysis of combined reforming process using Gibbs energy minimization method: In view of solid carbon formation. *J Nat Gas Chem*. 2012;21(6):694-702.
32. Noureldin MMBB, Elbashir NO, El-Halwagi MM. Optimization and selection of reforming approaches for syngas generation from natural/shale gas. *Ind Eng Chem Res*. 2014;53(5):1841-1855. doi:10.1021/ie402382w

33. Noureldin MMB, Elbashir NO, Gabriel KJ, El-Halwagi MM. A process integration approach to the assessment of CO2 fixation through dry reforming. *ACS Sustain Chem Eng*. 2015;3(4):625-636. doi:10.1021/sc5007736

34. Baltrusaitis J, Luyben WL. Methane Conversion to Syngas for Gas-to-Liquids (GTL): Is Sustainable CO<inf>2</inf> Reuse via Dry Methane Reforming (DMR) Cost Competitive with SMR and ATR Processes? *ACS Sustain Chem Eng*. 2015;3(9):2100-2111. doi:10.1021/acssuschemeng.5b00368

35. Zhang Y, Zhang S, Gossage JL, Lou HH, Benson TJ. Thermodynamic analyses of tri-reforming reactions to produce syngas. *Energy and Fuels*. 2014;28(4):2717-2726. doi:10.1021/ef500084m

36. Chein RY, Chen YC, Yu CT, Chung JN. Thermodynamic analysis of dry reforming of CH<inf>4</inf> with CO<inf>2</inf> at high pressures. *J Nat Gas Sci Eng*. 2015;26:617-629. doi:10.1016/j.jngse.2015.07.001

37. Amin NAS, Yaw TC. Thermodynamic equilibrium analysis of combined carbon dioxide reforming with partial oxidation of methane to syngas. *Int J Hydrogen Energy*. 2007;32(12):1789-1798. doi:http://dx.doi.org/10.1016/j.ijhydene.2006.12.004

38. Nikoo MK, Amin NAS. Thermodynamic analysis of carbon dioxide reforming of methane in view of solid carbon formation. *Fuel Process Technol*. 2011;92(3):678-691. doi:10.1016/j.fuproc.2010.11.027

39. Liu S, Zhang K, Fang L, Li Y. Thermodynamic analysis of hydrogen production from oxidative steam reforming of ethanol. *Energy & Fuels*. 2008;22(2):1365-

1370.

40. Wang X, Li S, Wang H, Liu B, Ma X. Thermodynamic analysis of glycerin steam reforming. *Energy & Fuels*. 2008;22(6):4285-4291.

41. Faungnawakij K, Kikuchi R, Eguchi K. Thermodynamic analysis of carbon formation boundary and reforming performance for steam reforming of dimethyl ether. *J Power Sources*. 2007;164(1):73-79.

42. Semelsberger TA, Borup RL. Thermodynamic equilibrium calculations of dimethyl ether steam reforming and dimethyl ether hydrolysis. *J Power Sources*. 2005;152:87-96.

43. Song C, Pan W, Srimat ST, et al. Tri-reforming of methane over Ni catalysts for CO 2 conversion to Syngas with desired H 2 CO ratios using flue gas of power plants without CO 2 separation. *Stud Surf Sci Catal*. 2004;153:315-322.

44. Choudhary VR, Mondal KC, Mamman AS, Joshi UA. Carbon-free dry reforming of methane to syngas over NdCoO 3 perovskite-type mixed metal oxide catalyst. *Catal Letters*. 2005;100(3-4):271.

45. Lee SH, Cho W, Ju WS, Cho BH, Lee YC, Baek YS. Tri-reforming of CH4 using CO2 for production of synthesis gas to dimethyl ether. *Catal Today*. 2003;87(1-4):133-137. doi:10.1016/j.cattod.2003.10.005

46. Freitas ACD, Guirardello R. Thermodynamic analysis of methane reforming with CO2, CO2+ H2O, CO2+ O2 and CO2+ air for hydrogen and synthesis gas production. *J CO2 Util*. 2014;7:30-38.

47. Zhang Z, Verykios XE, MacDonald SM, Affrossman S. Comparative study of

carbon dioxide reforming of methane to synthesis gas over Ni/La2O3 and conventional nickel-based catalysts. *J Phys Chem*. 1996;100(2):744-754.

48. Sutthiumporn K, Kawi S. Promotional effect of alkaline earth over Ni–La2O3 catalyst for CO2 reforming of CH4: role of surface oxygen species on H2 production and carbon suppression. *Int J Hydrogen Energy*. 2011;36(22):14435-14446.

49. Ferreira-Aparicio P, Marquez-Alvarez C, Rodrıguez-Ramos I, Schuurman Y, Guerrero-Ruiz A, Mirodatos C. A transient kinetic study of the carbon dioxide reforming of methane over supported Ru catalysts. *J Catal*. 1999;184(1):202-212.

50. Carrara C, Munera J, Lombardo EA, Cornaglia LM. Kinetic and stability studies of Ru/La 2 O 3 used in the dry reforming of methane. *Top Catal*. 2008;51(1-4):98-106.

51. Kehres J, Jakobsen JG, Andreasen JW, et al. Dynamical properties of a Ru/MgAl2O4 catalyst during reduction and dry methane reforming. *J Phys Chem C*. 2012;116(40):21407-21415.

52. Steinhauer B, Kasireddy MR, Radnik J, Martin A. Development of Ni-Pd bimetallic catalysts for the utilization of carbon dioxide and methane by dry reforming. *Appl Catal A Gen*. 2009;366(2):333-341.

53. Pawelec B, Damyanova S, Arishtirova K, Fierro JLG, Petrov L. Structural and surface features of PtNi catalysts for reforming of methane with CO2. *Appl Catal A Gen*. 2007;323:188-201.

54. Garcia-Dieguez M, Pieta IS, Herrera MC, Larrubia MA, Alemany LJ. RhNi

nanocatalysts for the CO2 and CO2+ H2O reforming of methane. *Catal Today*. 2011;172(1):136-142.

55. Hou Z, Yashima T. Small amounts of Rh-promoted Ni catalysts for methane reforming with CO 2. *Catal Letters*. 2003;89(3-4):193-197.

56. Menegazzo F, Signoretto M, Pinna F, Canton P, Pernicone N. Optimization of bimetallic dry reforming catalysts by temperature programmed reaction. *Appl Catal A Gen*. 2012;439:80-87.

57. Hu YH, Ruckenstein E. Transient response analysis via a broadened pulse combined with a step change or an isotopic pulse. Application to CO2 reforming of methane over NiO/SiO2. *J Phys Chem B*. 1997;101(38):7563-7565.

58. Gallego GS, Mondragón F, Barrault J, Tatibouët J-M, Batiot-Dupeyrat C. CO2 reforming of CH4 over La–Ni based perovskite precursors. *Appl Catal A Gen*. 2006;311:164-171.

59. Stagg SM, Romeo E, Padro C, Resasco DE. Effect of Promotion with Sn on Supported Pt catalysts for CO2Reforming of CH4. *J Catal*. 1998;178(1):137-145.

60. Panu M, Topolski K, Abrash S, El-Halwagi MM. CO2 footprint reduction via the optimal design of Carbon-Hydrogen-Oxygen SYmbiosis Networks (CHOSYNs). *Chem Eng Sci*. 2019;203:1-11. doi:https://doi.org/10.1016/j.ces.2019.03.066

61. Zhang Y, Zhang S, Lou HH, Gossage JL, Benson TJ. Steam and Dry reforming processes coupled with partial oxidation of methane for CO2 emission reduction. *Chem Eng Technol*. 2014;37(9):1493-1499.

62. Noureldin MMB, Elbashir NO, Gabriel KJ, El-Halwagi MM. A process

integration approach to the assessment of CO2 fixation through dry reforming. *ACS Sustain Chem Eng*. 2015;3(4):625-636.

63. Najera M, Solunke R, Gardner T, Veser G. Carbon capture and utilization via chemical looping dry reforming. *Chem Eng Res Des*. 2011;89(9):1533-1543.

64. Challiwala MS, Ghouri MM, Sengupta D, El-Halwagi MM, Elbashir NO. *A Process Integration Approach to the Optimization of CO2 Utilization via Tri-Reforming of Methane*. Vol 40.; 2017. doi:10.1016/B978-0-444-63965-3.50334-2

65. Challiwala MS, Ghouri MM, Linke P, El-Halwagi MM, Elbashir NO. A combined thermo-kinetic analysis of various methane reforming technologies: Comparison with dry reforming. *J CO2 Util*. 2017;17:99-111. doi:10.1016/j.jcou.2016.11.008

66. Abatzoglou N, Gitzhofer F, Blanchard J, De Oliveira Vigier K, Gravelle D. Carbon sequestration and dry reforming process and catalysts to produce same. 2010. https://www.google.com/patents/US7794690.

67. Benjamin A. Process for removal of carbonaceous deposits. 1958. https://www.google.com/patents/US2843509.

68. Olah GA, Goeppert A, Czaun M, Prakash GKS. Bi-reforming of methane from any source with steam and carbon dioxide exclusively to metgas (CO-2H2) for methanol and hydrocarbon synthesis. *J Am Chem Soc*. 2013;135(2):648-650. doi:10.1021/ja311796n

69. Afzal S, Sengupta D, Sarkar A, El-Halwagi M, Elbashir N. Optimization Approach to the Reduction of CO2 Emissions for Syngas Production Involving

Dry Reforming. *ACS Sustain Chem Eng*. 2018;6(6):7532-7544. doi:10.1021/acssuschemeng.8b00235

70. Shi L-Y, Li Y-X, Xue D-M, et al. Fabrication of highly dispersed nickel in nanoconfined spaces of as-made SBA-15 for dry reforming of methane with carbon dioxide. *Chem Eng J*. 2020;390:124491. doi:https://doi.org/10.1016/j.cej.2020.124491

71. Gavrilova NN, Sapunov VN, Skudin V V. Intensification of dry reforming of methane on membrane catalyst. *Chem Eng J*. 2019;374:983-991. doi:https://doi.org/10.1016/j.cej.2019.05.168

72. Durán P, Sanz-Martínez A, Soler J, Menéndez M, Herguido J. Pure hydrogen from biogas: Intensified methane dry reforming in a two-zone fluidized bed reactor using permselective membranes. *Chem Eng J*. 2019;370:772-781. doi:https://doi.org/10.1016/j.cej.2019.03.199

73. Benguerba Y, Virginie M, Dumas C, Ernst B. Computational fluid dynamics study of the dry reforming of methane over Ni/Al 2 O 3 catalyst in a membrane reactor. Coke deposition. *Kinet Catal*. 2017;58(3):328-338.

74. Song Y, Ozdemir E, Ramesh S, et al. Dry reforming of methane by stable Ni–Mo nanocatalysts on single-crystalline MgO. *Science (80-)*. 2020;367(6479):777-781. doi:10.1126/science.aav2412

75. Kim SM, Abdala PM, Margossian T, et al. Cooperativity and dynamics increase the performance of NiFe dry reforming catalysts. *J Am Chem Soc*. 2017;139(5):1937-1949. doi:10.1021/jacs.6b11487

76. Wang Y, Yao L, Wang Y, et al. Low-Temperature Catalytic CO2 Dry Reforming of Methane on Ni-Si/ZrO2 Catalyst. *ACS Catal*. 2018;8(7):6495-6506. doi:10.1021/acscatal.8b00584

77. Akri M, Zhao S, Li X, et al. Atomically dispersed nickel as coke-resistant active sites for methane dry reforming. *Nat Commun*. 2019;10(1):1-10.

78. Foppa L, Margossian T, Kim SM, et al. Contrasting the Role of Ni/Al2O3 Interfaces in Water-Gas Shift and Dry Reforming of Methane. *J Am Chem Soc*. 2017;139(47):17128-17139. doi:10.1021/jacs.7b08984

79. Steinfeld A. Solar thermochemical production of hydrogen - A review. *Sol Energy*. 2005;78(5):603-615. doi:10.1016/j.solener.2003.12.012

80. Agrafiotis C, Von Storch H, Roeb M, Sattler C. Solar thermal reforming of methane feedstocks for hydrogen and syngas production - A review. *Renew Sustain Energy Rev*. 2014;29:656-682. doi:10.1016/j.rser.2013.08.050

81. Usman M, Wan Daud WMA, Abbas HF. Dry reforming of methane: Influence of process parameters - A review. *Renew Sustain Energy Rev*. 2015;45:710-744. doi:10.1016/j.rser.2015.02.026

82. Kodama T. *High-Temperature Solar Chemistry for Converting Solar Heat to Chemical Fuels*. Vol 29.; 2003. doi:10.1016/S0360-1285(03)00059-5

83. Jarvis SM, Samsatli S. Technologies and infrastructures underpinning future CO2 value chains: A comprehensive review and comparative analysis. *Renew Sustain Energy Rev*. 2018;85:46-68. doi:https://doi.org/10.1016/j.rser.2018.01.007

84. Nematollahi B, Rezaei M, Lay EN, Khajenoori M. Thermodynamic analysis of

combined reforming process using Gibbs energy minimization method: In view of solid carbon formation. *J Nat Gas Chem*. 2012;21(6):694-702. doi:http://dx.doi.org/10.1016/S1003-9953(11)60421-0

85. KHALESI A, ARANDIYAN HR, PARVARI M. Effects of Lanthanum Substitution by Strontium and Calcium in La-Ni-Al Perovskite Oxides in Dry Reforming of Methane. *Chinese J Catal*. 2008;29(10):960-968. doi:10.1016/S1872-2067(08)60079-0

86. Liu D, Lau R, Borgna A, Yang Y. Carbon dioxide reforming of methane to synthesis gas over Ni-MCM-41 catalysts. *Appl Catal A Gen*. 2009;358(2):110-118.

87. Cui Y, Zhang H, Xu H, Li W. Kinetic study of the catalytic reforming of CH4 with CO2 to syngas over Ni/α-Al2O3 catalyst: The effect of temperature on the reforming mechanism. *Appl Catal A Gen*. 2007;318:79-88. doi:10.1016/j.apcata.2006.10.044

88. Smith JM. Van ness, HC; Abbott, MW Introduction to Chemical Engineering Thermodynamics. *McGraw-Hill, Bost*. 2001;329:354.

89. Froment GF, Bischoff KB, De Wilde J. *Chemical Reactor Analysis and Design*. 3rd editio. Wiley; 2010.

90. Soave G. Equilibrium constants from a modified Redlich-Kwong equation of state. *Chem Eng Sci*. 1972;27(6):1197-1203.

91. Özkara-Aydnolu Ş. Thermodynamic equilibrium analysis of combined carbon dioxide reforming with steam reforming of methane to synthesis gas. *Int J*

Hydrogen Energy. 2010;35(23):12821-12828. doi:10.1016/j.ijhydene.2010.08.134

92. Peng D-Y, B. Robinson D. A New Two-Constant Equation of State. *Ind Eng Chem Fundam*. 1972;15(1):59-64.

93. Bartholomew CH, Farrauto RJ. *Fundamentals of Industrial Catalytic Processes*. John Wiley & Sons; 2011.

94. Xu J, Froment GF. Methane steam reforming, methanation and water-gas shift: I. Intrinsic kinetics. *AIChE J*. 1989;35(1):88-96.

95. Zhang ZL, Verykios XE. Carbon dioxide reforming of methane to synthesis gas over supported Ni catalysts. *Catal Today*. 1994;21(2-3):589-595.

96. Shahkarami P, Fatemi S. Mathematical modeling and optimization of combined steam and dry reforming of methane process in catalytic fluidized bed membrane reactor. *Chem Eng Commun*. 2015;202(6):774-786. doi:10.1080/00986445.2013.867257

97. Levenspiel O. Chemical reaction engineering. *Ind Eng Chem Res*. 1999;38(11):4140-4143.

98. Fogler HS. *Essentials of Chemical Reaction Engineering: Essenti Chemica Reactio Engi*. Pearson Education; 2010.

99. Baktash E, Littlewood P, Schomäcker R, Thomas A, Stair PC. Alumina coated nickel nanoparticles as a highly active catalyst for dry reforming of methane. *Appl Catal B Environ*. 2015;179:122-127. doi:https://doi.org/10.1016/j.apcatb.2015.05.018

100. Dey G, Ren J, El-Ghazawi T, Licht S. How does an amalgamated Ni cathode

affect carbon nanotube growth? A density functional theory study. *RSC Adv*. 2016;6(32):27191-27196. doi:10.1039/c6ra03460h

101. Liu X, Ren J, Licht G, Wang X, Licht S. Carbon Nano-Onions Made Directly from CO2 by Molten Electrolysis for Greenhouse Gas Mitigation. *Adv Sustain Syst*. 2019;3(10):1-10. doi:10.1002/adsu.201900056

102. Licht S, Douglas A, Ren J, Carter R, Lefler M, Pint CL. Carbon nanotubes produced from ambient carbon dioxide for environmentally sustainable lithium-ion and sodium-ion battery anodes. *ACS Cent Sci*. 2016;2(3):162-168. doi:10.1021/acscentsci.5b00400

103. Ren J, Li FF, Lau J, González-Urbina L, Licht S. One-Pot Synthesis of Carbon Nanofibers from CO2. *Nano Lett*. 2015;15(9):6142-6148. doi:10.1021/acs.nanolett.5b02427

104. Ren J, Lau J, Lefler M, Licht S. The Minimum Electrolytic Energy Needed to Convert Carbon Dioxide to Carbon by Electrolysis in Carbonate Melts. *J Phys Chem C*. 2015;119(41):23342-23349. doi:10.1021/acs.jpcc.5b07026

105. Johnson M, Ren J, Lefler M, Licht G, Vicini J, Licht S. Data on SEM, TEM and Raman Spectra of doped, and wool carbon nanotubes made directly from CO2 by molten electrolysis. *Data Br*. 2017;14:592-606. doi:10.1016/j.dib.2017.08.013

106. Wang X, Liu X, Licht G, Wang B, Licht S. Exploration of alkali cation variation on the synthesis of carbon nanotubes by electrolysis of CO2 in molten carbonates. *J CO2 Util*. 2019;34(May):303-312. doi:10.1016/j.jcou.2019.07.007

107. Licht S. Co-production of cement and carbon nanotubes with a carbon negative

footprint. *J CO2 Util*. 2017;18:378-389. doi:10.1016/j.jcou.2017.02.011

108. Johnson M, Ren J, Lefler M, et al. Carbon nanotube wools made directly from CO2 by molten electrolysis: Value driven pathways to carbon dioxide greenhouse gas mitigation. *Mater Today Energy*. 2017;5:230-236. doi:10.1016/j.mtener.2017.07.003

109. Lau J, Dey G, Licht S. Thermodynamic assessment of CO2 to carbon nanofiber transformation for carbon sequestration in a combined cycle gas or a coal power plant. *Energy Convers Manag*. 2016;122:400-410. doi:10.1016/j.enconman.2016.06.007

110. Wu H, Li Z, Ji D, et al. One-pot synthesis of nanostructured carbon materials from carbon dioxide via electrolysis in molten carbonate salts. *Carbon N Y*. 2016;106:208-217. doi:10.1016/j.carbon.2016.05.031

111. Licht S, Liu X, Licht G, Wang X, Swesi A, Chan Y. Amplified CO2 reduction of greenhouse gas emissions with C2CNT carbon nanotube composites. *Mater Today Sustain*. 2019;6:100023. doi:10.1016/j.mtsust.2019.100023

112. Ren J, Licht S. Tracking airborne CO2 mitigation and low cost transformation into valuable carbon nanotubes. *Sci Rep*. 2016;6(June):1-11. doi:10.1038/srep27760

113. Douglas A, Carter R, Li M, Pint CL. Toward Small-Diameter Carbon Nanotubes Synthesized from Captured Carbon Dioxide: Critical Role of Catalyst Coarsening. *ACS Appl Mater Interfaces*. 2018;10(22):19010-19018. doi:10.1021/acsami.8b02834

114. SkyNano Technologies. https://www.skynanotechnologies.com/. Accessed August 30, 2020.

115. Mubarak NM, Abdullah EC, Jayakumar NS, Sahu JN. An overview on methods for the production of carbon nanotubes. *J Ind Eng Chem*. 2014;20(4):1186-1197.

116. Tennent HG. Carbon fibrils, method for producing same and compositions containing same. May 1987.

117. Resasco DE, Kitiyanan B, Alvarez WE, Balzano L. Process and apparatus for producing single-walled carbon nanotubes. July 2005.

118. Kitiyanan B, Alvarez WE, Harwell JH, Resasco DE. Controlled production of single-wall carbon nanotubes by catalytic decomposition of CO on bimetallic Co–Mo catalysts. *Chem Phys Lett*. 2000;317(3-5):497-503.

119. Nikolaev P. Gas-phase production of single-walled carbon nanotubes from carbon monoxide: a review of the HiPco process. *J Nanosci Nanotechnol*. 2004;4(4):307-316.

120. Nikolaev P, Bronikowski MJ, Bradley RK, et al. Gas-phase catalytic growth of single-walled carbon nanotubes from carbon monoxide. *Chem Phys Lett*. 1999;313(1-2):91-97.

121. Smalley RE, Colbert DT, Guo T, Rinzler AG, Nikolaev P, Thess A. Method of making ropes of single-wall carbon nanotubes. 2001.

122. Wang Y, Wei F, Luo G, Yu H, Gu G. The large-scale production of carbon nanotubes in a nano-agglomerate fluidized-bed reactor. *Chem Phys Lett*. 2002;364(5-6):568-572.

123. Wei F, Wang Y, Luo G, et al. Continuous mass production of carbon nanotubes in a nano-agglomerate fluidized-bed and the reactor. July 2009.

124. Philippe R, Morançais A, Corrias M, et al. Catalytic production of carbon nanotubes by fluidized-bed CVD. *Chem Vap Depos*. 2007;13(9):447-457.

125. MacKenzie KJ, Dunens OM, Harris AT. An updated review of synthesis parameters and growth mechanisms for carbon nanotubes in fluidized beds. *Ind Eng Chem Res*. 2010;49(11):5323-5338.

126. Danafar F, Fakhru A, Amran M, Salleh M, Radiah D, Biak A. Fluidized bed catalytic chemical vapor deposition synthesis of carbon nanotubes — A review. 2009;155:37-48. doi:10.1016/j.cej.2009.07.052

127. See CH, Harris AT. A Review of Carbon Nanotube Synthesis via Fluidized-Bed Chemical Vapor Deposition. *Ind Eng Chem Res*. 2007;46:997-1012. doi:10.1021/ie060955b

128. Afzal S, Sengupta D, Sarkar A, El-Halwagi M, and, Elbashir N. Optimization Approach to the Reduction of CO2 Emissions for Syngas Production Involving Dry Reforming. *ACS Sustain Chem Eng*. 2018;6(6):7532-7544. doi:10.1021/acssuschemeng.8b00235

129. Usman M, Wan Daud WMA, Abbas HF. Dry reforming of methane: Influence of process parameters - A review. *Renew Sustain Energy Rev*. 2015;45:710-744. doi:10.1016/j.rser.2015.02.026

130. Qatar Researchers Develop Natural Gas Processing Technology That Could Reduce Qatar's Carbon Footprint - Texas A&M Today.

https://today.tamu.edu/2019/10/24/qatar-researchers-develop-natural-gas-processing-technology-that-could-reduce-qatars-carbon-footprint/. Accessed February 16, 2020.

131. Qatar Researchers Develop Natural Gas Processing Technology That Could Reduce Qatar's Carbon Footprint. https://www.pollutiononline.com/doc/qatar-researchers-develop-natural-gas-processing-carbon-footprint-0001. Accessed February 16, 2020.

132. Researchers Develop Technology to Reduce Qatar's Carbon Footprint | Qatar-America Institute. https://qataramerica.org/researchers-develop-technology-to-reduce-qatars-carbon-footprint/. Accessed February 16, 2020.

133. Challiwala M, Afzal S, Choudhury HA, Sengupta D, El-halwagi M, Elbashir NO. Alternative pathways for CO2 utilization for enhanced methane dry reforming technology. In: *Advances in Carbon Management Technologies*. ; 2019.

134. Cheaptubes.com. Multi Walled Carbon Nanotubes. https://www.cheaptubes.com/product-category/multi-walled-carbon-nanotubes/.

135. Noureldin MMB, Elbashir NO, Gabriel KJ, El-Halwagi MM. A process integration approach to the assessment of CO2 fixation through dry reforming. *ACS Sustain Chem Eng*. 2015. doi:10.1021/sc5007736

136. Elbashir NO, Challiwala MS, Sengupta D, El-Halwagi MM. System and method for carbon and syngas production. Property WI, Organization, eds. 2018.

137. Gili A, Schlicker L, Bekheet MF, et al. Surface Carbon as a Reactive Intermediate in Dry Reforming of Methane to Syngas on a 5% Ni/MnO Catalyst. *ACS Catal*.

2018;8(9):8739-8750. doi:10.1021/acscatal.8b01820

138. Gili A, Schlicker L, Bekheet MF, et al. Surface carbon as a reactive intermediate in dry reforming of methane to syngas on a 5% Ni/MnO catalyst. *ACS Catal*. 2018;8(9):8739-8750.

139. Amelinckx S, Zhang XB, Bernaerts D, Zhang XF, Ivanov V, Nagy JB. A formation mechanism for catalytically grown helix-shaped graphite nanotubes. *Science (80-)*. 1994;265(5172):635-639.

140. Dupuis A-C. The catalyst in the CCVD of carbon nanotubes—a review. *Prog Mater Sci*. 2005;50(8):929-961.

141. Yeoh W-M, Lee K-Y, Chai S-P, Lee K-T, Mohamed AR. Effective synthesis of carbon nanotubes via catalytic decomposition of methane: Influence of calcination temperature on metal–support interaction of Co–Mo/MgO catalyst. *J Phys Chem Solids*. 2013;74(11):1553-1559.

142. Cheung CL, Kurtz A, Park H, Lieber CM. Diameter-controlled synthesis of carbon nanotubes. *J Phys Chem B*. 2002;106(10):2429-2433.

143. Kumar M, Ando Y. Controlling the diameter distribution of carbon nanotubes grown from camphor on a zeolite support. *Carbon N Y*. 2005;43(3):533-540.

144. Huh Y, Green MLH, Kim YH, Lee JY, Lee CJ. Control of carbon nanotube growth using cobalt nanoparticles as catalyst. *Appl Surf Sci*. 2005;249(1-4):145-150.

145. Bahruji H, Esquius JR, Bowker M, Hutchings G, Armstrong RD, Jones W. Solvent Free Synthesis of PdZn/TiO 2 Catalysts for the Hydrogenation of CO 2 to

Methanol. *Top Catal*. 2018;61(3-4):144-153.

146. Lu M, Fatah N, Khodakov AY. Solvent-free synthesis of alumina supported cobalt catalysts for Fischer–Tropsch synthesis. *J energy Chem*. 2016;25(6):1001-1007.

147. Ahmed W, El-Din MRN, Aboul-Enein AA, Awadallah AE. Effect of textural properties of alumina support on the catalytic performance of Ni/Al2O3 catalysts for hydrogen production via methane decomposition. *J Nat Gas Sci Eng*. 2015;25:359-366.

148. Bayat N, Rezaei M, Meshkani F. Methane decomposition over Ni–Fe/Al2O3 catalysts for production of COx-free hydrogen and carbon nanofiber. *Int J Hydrogen Energy*. 2016;41(3):1574-1584.

149. Afzal S, Prakash A, Littlewood P, et al. Controlling the rate of change of Ni dispersion in commercial catalyst by ALD overcoat during dry reforming of methane. *Int J Hydrogen Energy*. 2020.

150. Mansfield E, Kar A, Hooker SA. Applications of TGA in quality control of SWCNTs. *Anal Bioanal Chem*. 2010;396(3):1071-1077. doi:10.1007/s00216-009-3319-2

151. Trigueiro JPC, Silva GG, Lavall RL, et al. Purity evaluation of carbon nanotube materials by thermogravimetric, TEM, and SEM methods. *J Nanosci Nanotechnol*. 2007;7(10):3477-3486. doi:10.1166/jnn.2007.831

152. Murakami Y, Miyauchi Y, Chiashi S, Maruyama S. Characterization of single-walled carbon nanotubes catalytically synthesized from alcohol. *Chem Phys Lett*.

2003;374(1-2):53-58. doi:10.1016/S0009-2614(03)00687-0

153. Wood DA, Nwaoha C, Towler BF. Gas-to-liquids (GTL): A review of an industry offering several routes for monetizing natural gas. *J Nat Gas Sci Eng*. 2012;9:196-208. doi:https://doi.org/10.1016/j.jngse.2012.07.001

154. Shell. Pearl GTL- overview. https://www.shell.com/about-us/major-projects/pearl-gtl/pearl-gtl-an-overview.html.

155. Condrasky JA, Kline RE, Kwolek SJ. Process for reactivating a reforming catalyst. 1971.

156. Innes RA, Holtermann DL, Mulaskey BF. Low temperature regeneration of coke deactivated reforming catalysts. 1992.

157. Sechrist PA, Koves WiJ. Regeneration method with reduced catalyst heat exposure. 1989.

158. Fung SC, Huang Y-JR, Walsh JF, McVicker GB, Clem KR. Regeneration of severely deactivated reforming catalysts. 1998.

159. Mamedov AK, Bashir M. Process for increasing the carbon monoxide content of a syngas mixture. 2016.

160. Mahamulkar S, Yin K, Agrawal PK, et al. Formation and oxidation/gasification of carbonaceous deposits: a review. *Ind Eng Chem Res*. 2016;55(37):9760-9818.

161. Santos LT dos, Santos FM, Silva RS, et al. Mechanistic insights of CO2-coke reaction during the regeneration step of the fluid cracking catalyst. *Appl Catal A Gen*. 2008;336(1):40-47. doi:https://doi.org/10.1016/j.apcata.2007.10.005

162. Abdelsadek Z, Sehailia M, Halliche D, et al. In-situ

hydrogasification/regeneration of NiAl-hydrotalcite derived catalyst in the reaction of CO2 reforming of methane: A versatile approach to catalyst recycling. *J CO2 Util*. 2016;14:98-105.

163. Pereira SC, Ribeiro MF, Batalha N, Pereira MM. Catalyst regeneration using CO2 as reactant through reverse-Boudouard reaction with coke. *Greenh Gases Sci Technol*. 2017;7(5):843-851.

164. da Silva TC, Pinto JF, Santos FM, et al. Vanadium and alumina modified with groups I and II elements for CO2 and coke reaction under fluid catalytic cracking process. *Appl Catal B Environ*. 2015;164:225-233.

165. Alenazey F, Cooper CG, Dave CB, Elnashaie S, Susu AA, Adesina AA. Coke removal from deactivated Co–Ni steam reforming catalyst using different gasifying agents: An analysis of the gas–solid reaction kinetics. *Catal Commun*. 2009;10(4):406-411.

166. Martínez DY, Jiménez-Gutiérrez A, Linke P, Gabriel KJ, Noureldin MMB, El-Halwagi MM. Water and energy issues in gas-to-liquid processes: assessment and integration of different gas-reforming alternatives. *ACS Sustain Chem Eng*. 2013;2(2):216-225.

167. Gabriel KJ, El-Halwagi MM, Linke P. Optimization across the Water-Energy Nexus for Integrating Heat, Power, and Water for Industrial Processes, Coupled with Hybrid Thermal-Membrane Desalination. *Ind Eng Chem Res*. 2016;55(12):3442-3466. doi:10.1021/acs.iecr.5b03333

APPENDIX A

LIST OF PATENTS AND PUBLICATIONS

List of Patents

1. Challiwala, M. S., et al. "Method and Apparatus for producing Carbon black and Syngas from Carbon dioxide" – Provisional patent. US Patent $WO_2018187213A1$, October 2018.
2. Challiwala, M. S., et al. "A method for regeneration and reactivation of Dry reforming catalyst " – WO2020185107A1, Provisional patent. Priority date : July 2018
3. Challiwala, Mohamed Sufiyan; Choudhury, H. Ahmed; Elbashir, Nimir, " CATALYSTS FOR CARGEN™, METHODS OF PREPARING, AND USES OF SAME", Provisional Application Number (62/949,133), Disclosure submitted on: 6 November 2019
4. Choudhury, H. Ahmed; Challiwala, Mohamed Sufiyan; Elbashir, Nimir O, " METHODS OF PRODUCING DIMETHYL CARBONATE", Provisional Application Number (62/949,139), Disclosure submitted on: 23 August 2019
5. Challiwala, Mohamed Sufiyan; Choudhury, H. Ahmed; Elbashir, Nimir, " Novel Carbon-Catalyst separation technique for CARGEN™ Process ", (Under Disclosure)
6. Challiwala, Mohamed Sufiyan; Choudhury, H. Ahmed; Elbashir, Nimir, " A Novel Multi-Walled Carbon Nanotube (MWCNT) production protocol via CARGEN™ technology ", (Under Disclosure)

List of Journal Publications

1. Challiwala, M. S., et al. "A combined thermo-kinetic analysis of various methane reforming technologies: Comparison with dry reforming." Journal of CO_2 Utilization 17 (2017): 99-111.
2. Challiwala, M. S., et al. " Multidimensional Modeling of a microfibrous entrapped cobalt catalyst Fischer-Tropsch reactor bed. " AIChE Journal (2017). doi:10.1002/aic.16053.
3. Aya E.Abusrafa, Mohamed S.Challiwala, Hanif A.Choudhury, Benjamin A.Wilhite, Nimir O.Elbashir, " Experimental verification of 2-dimensional computational fluid dynamics modeling of supercritical fluids Fischer Tropsch reactor bed", https://doi.org/10.1016/j.cattod.2019.05.027, 16 May 2019.
4. Abdulrahman S. Alsuhaibani, Shaik Afzal, Mohamedsufiyan Challiwala, Nimir O.Elbashir, Mahmoud M.El-Halwagi; "The impact of the development of catalyst and reaction system of the methanol synthesis stage on the overall profitability of the entire plant: A techno-economic study"https://doi.org/10.1016/j.cattod.2019.03.070, 20 april 2019
5. Aya E.Abusrafa, Mohamed S.Challiwala, Benjamin A.Wilhite, Nimir O.Elbashir, " Thermal assessment of a Micro fibrous Fischer Tropsch Fixed bed reactor using Computational Fluid Dynamics", MDPI processes 8 (1213), 2020, equal first authorship
6. Mohamed S Challiwala; Hanif A Choudhury; Anuj V. Prakash; Debalina Sengupta; Mahmoud M El-Halwagi; Nimir O Elbashir, “Production of high-quality carbon

nanotubes from natural gas and carbon dioxide using a novel CARGEN™ process", Chemical Engineering Progress, AIChE, Wiley, October 2020

7. Mohamed S Challiwala; Hanif A Choudhury; Dingdi Wang; Mahmoud M El-Halwagi; Eric Weitz; Nimir O Elbashir, "A novel CO_2 utilization technology for the synergistic co-production of multi-walled carbon nanotubes and syngas", Scientific Reports, Nature, (Just accepted)

List of Book chapters

1. Mohamed S Challiwala; Shaik Afzal; Hanif A Choudhury; Debalina Sengupta; Mahmoud M El-Halwagi; Nimir O Elbashir,"Alternative Pathways for CO_2 Utilization via Dry Reforming of Methane", Book: "Advances in Carbon Management Technologies: Carbon Removal, Renewable and Nuclear Energy", Volume 1, ISBN: 9780367198428, CAT# K418172, CRC Press, Taylor and Francis Group
2. Challiwala, M. S., et al. " A Process Integration Approach to the Optimization of CO_2 Utilization via Tri-Reforming of Methane." Computer Aided Chemical Engineering (2017): 40, 1993-1998.
3. Abdulrahman S. Alsuhaibani, Shaik Afzal, Mohamedsufiyan Challiwala, Nimir O.Elbashir, Mahmoud M.El-Halwagi; Process Systems Engineering and Catalysis: A Collaborative Approach for the Development of Chemical Processes, https://doi.org/10.1016/B978-0-12-818597-1.50065-5, Computer Aided Chemical Engineering, Volume 47, 2019, Pages 409-414

APPENDIX B

LIST OF PRESENTATIONS

1. Challiwala, Mohamed Sufiyan; Choudhury, H. Ahmed; Sengupta, Debalina, El-Halwagi, Mahmoud M; Elbashir, Nimir, "Process Systems approach in modeling an Advanced Dry Reforming Process- Pathway towards a novel technology of CARGEN™ reaction", International Computational Science and Engineering Conference (ICSEC19), Doha, Qatar, October 21-22, 2019

2. Challiwala, Mohamed Sufiyan; Choudhury, Hanif Ahmed; El-Halwagi, Mahmoud M; Elbashir, Nimir,"Carbon- An Alternative Product from Dry Reforming of Methane", 4th International Conference on Functional Materials and Chemical Engineering, Thailand, December 2019

3. Prakash, Anuj; Challiwala, Mohamed Sufiyan; Shaik, Afzal; Choudhury, Hanif Ahmed; Ghouri, Mohammed Minhaj; Chatla, Anjaneyulu; Elbashir, Nimir;"Advanced Reactor Technology For CO_2 Utilization in Methane Reforming",12th Natural Gas Conversion Symposium (NGCS), 2-6 June 2019, San Antonio, Texas, United States

4. Abdulrahman S. Alsuhaibani, Shaik Afzal, Mohamedsufiyan Challiwala, Nimir O.Elbashir, Mahmoud M.El-Halwagi ; "Developing a Systematic Approach for the Collaboration between Process Systems Engineering and Catalysis to Accelerate the Improvements of Chemical Processes", 422a, 2019 AIChE Annual meeting, Nov 12, 2019

5. Mohamed Sufiyan Challiwala, Hanif Choudhury, Anjaneyulu Chatla, Debalina Sengupta, Mahmoud M El-Halwagi, Nimir Elbashir; "Dry Reforming of Methane: An

Alternative Option for Carbon Capture", 175a, 2019 Spring Meeting and 15th Global Congress on Process Safety, 2019 AIChE Annual meeting, April 3, 2019,

6. M.S. Challiwala, D. Sengupta, M. M. Ghouri, M. M. El-Halwagi, N. O. Elbashir, " A Process Integration approach for a Sustainable GTL process using Tri Reforming of Methane", Bukur Reaction Engineering and Catalysis Symposium, December 2017, Doha, Qatar.

7. M.S. Challiwala, B. A. Wilhite, M. M Ghouri, N. O. Elbashir, " 2D Modeling of Fischer Tropsch reactor in COMSOL® Multiphysics", Bukur Reaction Engineering and Catalysis Symposium, December 2017, Doha, Qatar.

8. M.S. Challiwala, D. Sengupta, M. M. Ghouri, M. M. El-Halwagi, N. O. Elbashir, " A Process Integration approach for a Sustainable GTL process using Tri Reforming of Methane", AIChE Annual Meeting, November 2017, Minneapolis, MN, USA.

9. M.S. Challiwala, B. A. Wilhite, M. M Ghouri, N. O. Elbashir, " 2D Modeling of Fischer Tropsch reactor in COMSOL® Multiphysics", AIChE Annual Meeting, November 2017, Minneapolis, MN, USA.

10. M.S. Challiwala, B. A. Wilhite, M. M Ghouri, N. O. Elbashir, " 2D Modeling of Fischer Tropsch reactor in COMSOL® Multiphysics", 2nd International Supercomputing conference, October 2017, Doha, Qatar.

11. M.S. Challiwala, B. A. Wilhite, D. Sengupta, M. M Ghouri, M. M. El-Halwagi, N. O. Elbashir, " A Process Integration approach for a Sustainable GTL process using Tri Reforming of Methane", 10 th World Congress of Chemical Engineering – 27th European Symposium on Computer-Aided Process Engineering, October 2017, Barcelona, Spain.

12. M.S. Challiwala, B. A. Wilhite, M. M Ghouri, N. O. Elbashir, " Multiscale Modeling of supercritical Fischer-Tropsch Synthesis Fixed-Bed Reactor", The 5th International Gas Processing Symposium, Qatar University, November 2016, Doha, Qatar

13. D. Sengupta, S. Afzal, M. S. Challiwala, N. O. Elbashir, M M. El-Halwagi, "Modeling for the Life Cycle Assessment of Dry Reforming Technology – Challenges and Lesson Learnt", November 2016, AIChE Annual meeting, San Francisco, USA.

14. M.S. Challiwala, M. M. El-Halwagi, N. O. Elbashir, "Kinetic and Thermodynamic Analysis of Combined Dry, Steam and Partial Oxidation Reforming of Methane", Process Science and Technology Center, October 2016, Austin, TX, USA

15. M. S. Challiwala, M.M Ghouri, P. Linke, M. El-Halwagi, N. O. Elbashir, "Modeling Development of a Combined Methane Fixed Bed Reactor Reformer " in Natural Gas Conversion Symposium (NGCS-11), June 2016 at Tromso, Norway.

16. M. S. Challiwala, M.M Ghouri, N. O. Elbashir, "Modeling Development of a Combined Methane Fixed Bed Reactor Reformer " in Annual Research-Industry Partnership Showcase 2016 hosted by Texas A&M University at Qatar, Doha, Qatar.

17. M. S. Challiwala, M.M Ghouri, N. O. Elbashir, "Modeling Development of a Combined Methane Fixed Bed Reactor Reformer " in Annual Research Conference (ARC) , March 22, 2015, Doha, Qatar.

18. Ghouri, Mohammed Minhaj; Hussain, Rehan; Challiwala, Mohamed Sufiyan; Elbashir, Nimir, "Systematic Multi-scale Modeling for Supercritical Fischer-Tropsch Fixed Bed Reactor" in International Symposium on Supercritical Fluids (ISSF) 2015, Korea.

19. Noureldin, Mohamed, Ghouri, Mohammed Minhaj, Challiwala, Mohamed Sufiyan, Bao, Buping, El-Halwagi, Mahmoud, Elbashir, Nimir, “An Energy Integrated Solvent Recovery Setup for Supercritical Fluids” in International Symposium on Supercritical Fluids (ISSF) 2015, Korea.

20. M. S. Challiwala, M.M Ghouri, P. Linke, M. El-Halwagi, N. O. Elbashir, “Kinetic and Thermodynamic Modeling of Methane Reforming Technologies: Comparison of Conventional Technologies with Dry Reforming” in American Institute of Chemical Engineers (AIChE) Annual meeting 2015, November 08-13, 2015, Salt Lake City, Utah, USA.

21. M. S. Challiwala, M.M Ghouri, P. Linke, N. O. Elbashir, “Modeling of Reformer Technologies and Fischer Tropsch In Gas to Liquid Processes” in Annual Research-Industry Partnership Showcase 2015 hosted by Texas A&M University at Qatar, Doha, Qatar.

APPENDIX C

MATLAB CODE DEVELOPED FOR EQUILIBRIUM ASSESSMENT

FOR THERMODYNAMIC STUDY:

```
clc;
clear;
warning('off','all');
imole=0;
Systemcomp=[1,27,28,29,30,32,47];
ch1=Systemcomp;
dummy=size(ch1);
n=dummy(2);
imole=[3561,14076,0,0,18768,0,0];
R=8.314;
T=298.15;
t11=[1173,50,1173];
p0=1;
P=28.43;
compoundnames={'Methane';'Ethane';'propane';'n-Butane';'n-pentane';'n-hexane';'n-heptane';'n-
octane';'ethylene';'propylene';'1-Butene';'1-Pentene';'1-Hexene';'1-Heptene';'Acetaldehyde
';'Acetylene';'Benzene(g)';'3-
Butadiene';'Cyclohexane(g)';'Ethanol';'Ethylbenzene';'EthyleneOxide';'Formaldehyde';'Methanol(g)';'Styre
ne';'Toluene(g)';'water';'oxygen';'carbon
monoxide';'carbondioxide';'carbondisulphide';'hydrogen';'nitrogen';'chlorine';'hydrogen sulphide';'sulphur
di oxide';'sulphur tri oxide';'nitric oxide';'hydrogen chloride';'hydrogen
cyanide';'ammonia';'Glycerol';'Crude Glycerol';'Acetol';'Acetaldehyde';'Formaldehyde';'Carbon'};
eos=3;              %   This to set PR EOS
ch=eos;
[ta,atoms,X,data,G,x1]=options11(ch1,n,imole);
totatoms=imole*atoms';          % This is to set the no. of atoms of each element in the feed
[ta,atoms,X,data,G,x1]=options11(ch1,n,imole);
for i=1:n
   data(1,i)=ch1(i);
end
for i=(n+1):(n+4)
   data(1,i)=0;
end
l=1;
for loop=t11(1):t11(2):t11(3)
   T1=loop;
   moles=0;
   for i=1:n
      for j=1:9
         x2(j)=x1(i,j);
      end
      [G(i),phi(i)]=specie(n,T,T1,P,p0,x2,ch);

   end
```

```
    for i=1:n
        for j=1:n
            if i==j
                moles(i,j)=1;
            end
        end

    end

    atom1=atoms';

    [z,v]=newsolvingnew(n,X,ta,moles,R,T1,phi,G,atom1,atoms,totatoms,P,p0,ch1);
    X=z;
    SUM=sum(z);
    for i=1:n
        z(i)=z(i)/SUM;
    end
    for j=1:n
        data(l,j)=z(j);
    end



    temperatureforplot(l)=loop;
    l=l+1;

end
newdata=0;
for m=1:n
    for o=1:(l-1)
        newdata(o,m)=data(o,m);
    end
end
[m5]=molematrix(atom1,newdata,totatoms);
[energypertemp1]=energycalculator(x1,t11,n,m5,T,imole,ch1);
    for i=1:n

        legendedcompounds(i)=compoundnames(ch1(i));
    end
%     t=temperatureforplot';
%     en=energypertemp1;
%     write_gnuplot_file(t11,P,imole,m5,t,en);
A=[temperatureforplot',m5,energypertemp1'];

 function [ta,atoms,X,data,G,x1]=options11(ch1,n,imole)


    %dummy=size(totatoms);

    %ta=dummy(2);
```

```
ta=3;                % I am fixing the total types of ataoms to Carbon, Oxygen and Hydrogen
   atoms=0;
   M=0;
   for i=1:n
      [M,atomdummy]=compound(ch1(i));
      for j=1:9
         x1(i,j)=M(j);
      end
      for j=1:ta
         atoms(i,j)=atomdummy(j);
      end
   end

   atoms=atoms';

   X=0;

   for i=1:n
      X(i)=0.5;
   end


%    for i=(n+1):(n+ta+1)
%       X(i)=1;
%    end

   data=0;
   l=1;
   G=0;
end


function [M,atoms]=compound(e1)
   cpm=[-6.567,7.466,-2.164,0.701,190.6,45.99,-74520,-50460,0.012;-12.158,16.417,-
5.561,1.455,305.3,48.72,-83820,-31855,0.1;-17.096,24.784,-8.824,2.229,369.8,42.48,-104680,-
24290,0.152;-21.394,31.721,-11.402,3.003,425.1,37.96,-125790,-16570,0.2;-25.885,38.964,-
14.111,3.777,469.7,33.7,-146760,-8650,0.252;-30.344,46.142,-16.791,4.551,507.6,30.25,-
166920,150,0.301;-34.819,53.354,-19.486,5.3250,540.2,27.4,-187780,8260,0.25;-39.301,60.601,-
22.208,6.099,568.7,24.9,-208750,16260,0.4;-8.616,12.008,-4.392,1.548,282.3,50.4,52510,68460,0.087;-
13.423,19.127,-6.915,2.322,268.6,46.65,19710,62205,0.14;-18.113,26.858,-9.873,3.096,420,40.43,-
540,70340,0.191;-22.429,33.788,-12.447,3.87,0,0,-21280,78410,0;-26.9,41.031,-15.157,4.644,0,0,-
41950,86830,0;-31.372,48.237,-17.847,5.418,0,0,-62760,0,0;-15.1865,14.146,-6.158,2.4355,466,55.5,-
166190,-128860,0.291;-0.659,-0.012,0,0.342,0,0,227480,209970,0;-20.579,33.172,-
13.301,4.923,0,0,82930,129665,0;-14.095,22.436,-8.882,3.189,425.2,42.77,109250,149795,0.19;-
33.996,56.091,-20.928,4.644,560.4,43.5,-123140,31920,0.212;-11.5905,16.94,-6.002,1.5685,513.9,61.48,-
235100,-168490,0.645;-24.269,48.295,-18.476,5.697,617.2,36.06,29920,130890,0.303;-13.869,20.613,-
9.296,1.615,0,0,-52630,-13010,0;-4.5755,5.576,-1.877,0.8875,408,65.9,-108570,-102530,0.282;-
7.8775,10.348,-3.45,0.7945,512.6,80.97,-200660,-161960,0.564;2.05,50.192,-
16.662,0,636,38.4,147360,213900,0.297;0.29,47.052,-15.716,0,591.8,41.06,50170,122050,0.262;-
1.5985,0.775,0,0.1415,647.1,220.55,-241818,-228572,0.345;0,0,0,0,154.6,50.43,0,0,0.022;-0.2145,-
0.467,0,0.9495,132.9,34.99,-110525,-137169,0.048;0.047,-0.232,0,-0.063,304.2,73.83,-393509,-
```

```
394359,0.224;-3.688,3.49,0,1.527,552,79,0,0,0.111;0,0,0,0,33.19,13.13,0,0,-
0.216;0,0,0,0,126.2,34,0,0,0.038;0,0,0,0,417.2,77.1,0,0,0.069;-3.432,2.796,0,0.458,373.5,89.63,-20630,-
33560,0.094;-2.054,2.203,0,-0.005,430.8,78.84,-296830,-300194,0.245;-1.5125,2.025,0,-
0.9045,490.9,82.1,-441040,0,0.424;-5.3515,-0.723,0,0.3145,180.2,64.8,90250,86550,0.583;-
2.9105,0.223,0,0.4485,324.7,83.1,-92307,-95299,0.132;4.736,1.359,0,-
0.725,456.7,53.9,135100,1247100,0.41;-4.5755,1.794,0,-0.3655,405.7,112.8,-46110,-16450,0.253;-
24.8195,-4.701973,-0.038973,2.5695,723,40,-528.8,-448.49,1.32;-22.21541,-2.54020705,-
0.51612705,2.29672,692.785,47.5413,-30960.06,25341.3365,1.20441;-30.23849296,-8.06724E-05,-
0.000121009,0,595.15,57.4,0,0,0.77358;7.71971845,-6.71685E-05,-
0.000100753,0,461,55.7,0,0,0.303;23.4987753,1.99156E-05,2.98734E-
05,0,407,65.9,0,0,0.25299;0,0,0,0,6810,2230,0,0,0.326841];
   %delta values


atomdatabase=[1,0,4,0,0,0;2,0,6,0,0,0;3,0,8,0,0,0;4,0,10,0,0,0;5,0,12,0,0,0;6,0,14,0,0,0;7,0,16,0,0,0;8,0,18,
0,0,0;2,0,4,0,0,0;3,0,6,0,0,0;4,0,8,0,0,0;5,0,10,0,0,0;6,0,12,0,0,0;7,0,14,0,0,0;3,1,6,0,0,0;2,0,2,0,0,0;6,0,6,0
,0,0;4,0,6,0,0,0;6,0,12,0,0,0;2,1,6,0,0,0;7,0,8,0,0,0;2,1,4,0,0,0;1,1,2,0,0,0;1,1,4,0,0,0;0,0,0,0,0,0;6,0,7,1,0,0
;0,1,2,0,0,0;0,2,0,0,0,0;1,1,0,0,0,0;1,2,0,0,0,0;1,0,0,0,2,0;0,0,2,0,0,0;0,0,0,2,0,0;0,0,0,0,0,0;0,0,2,0,1,0;0,2,
0,0,1,0;0,3,0,0,1,0;0,3,1,1,0,0;0,0,1,0,0,1;0,0,0,0,0,0;0,0,3,1,0,0;3,3,8,0,0,0;2.69,2.7,7.38,0,0,0;3,2,6,0,0,0;
2,1,4,0,0,0;1,1,2,0,0,0;1,0,0,0,0,0];

   M=0;
   for j=1:9
      M(j)=cpm(e1,j);
   end
   atoms=0;
   for j=1:6
      atoms(j)=atomdatabase(e1,j);
   end
end


function [G,fugacity]=specie(n,T,T1,P,p0,x1,choice)

   a=x1(1);
   b=x1(2);
   c=x1(3);
   d=x1(4);
   Pc=x1(6);
   Tc=x1(5);
   H0=x1(7);
   G0=x1(8);
   ch=choice;
   R=8.314;
   syms TN
   H=int(a+b*TN*10^(-3)+c*10^(-6)*TN^2+d*TN^(-2)*10^5,T,T1);
   S=int(a/TN+b*10^(-3)+c*10^(-6)*TN+d*TN^(-3)*10^5,T,T1);
   G=H0-T1/T*(H0-G0)+R*H-R*T1*S;

   if ch==0                % Ideal Gas
      fugacity=0;
   end
```

```
   if (ch==1)              % RK
      [z,I,q,B]=genericcubiceos(ch,T1,P,Tc,Pc,x1(9));
      fugacity=z-1-log(z-B)-q*I;
   end
   if (ch==2)              % SRK
      [z,I,q,B]=genericcubiceos(ch,T1,P,Tc,Pc,x1(9));
      fugacity=z-1-log(z-B)-q*I;
   end
   if (ch==3)              % PR
      [z,I,q,B]=genericcubiceos(ch,T1,P,Tc,Pc,x1(9));
      fugacity=z-1-log(z-B)-q*I;
   end

   fugacity=exp(fugacity);                % the fugacity here refers to ln(fi)=GResidual/RT and I is G
residual
end


function [zv,Iv,q,B]=genericcubiceos(ch,T,P,Tc,Pc,w)
   R=8.314;
   mur=0;
   [alpha,sigma,epsi,omega,shi]=getvalueofeos(ch,T,Tc,w,mur);
   A=shi*alpha*R^(2)*Tc^(2)/Pc;
   b=omega*R*Tc/Pc;
   q=shi*alpha/omega*Tc/T;
   B=omega*P/Pc*(Tc/T);
   mat4=q*B^2+epsi*sigma*B^2*(1+B);
   mat3=(sigma*B*(1+B)+epsi*B*(1+B)-epsi*sigma*B^2-q*B);
   mat2=(1+B-sigma*B-epsi*B);
   mat1=-1;
   var=[mat1 mat2 mat3 mat4];
   z=roots(var);
   z=real(z);
   zv=max(z);
   Iv=1/(sigma-epsi)*log((zv+sigma*B)/(zv+epsi*B));
end


function [alpha,sigma,epsi,omega,shi]=getvalueofeos(ch,T,Tc,w,mur)
   mat=ones(3,5);                  % ch=1 for RK, ch=2 for SRK, ch=3 for PR
   mat(1,1)=(T/Tc)^(-0.5);
   mat(1,2)=1;
   mat(1,3)=0;
   mat(1,4)=0.08664;
   mat(1,5)=0.42748;
   mat(2,1)=(1+(0.480+1.574*w-0.176*w^2)*(1-(T/Tc)^(0.5)))^2;
   mat(2,2)=1;
   mat(2,3)=0;
   mat(2,4)=0.08664;
   mat(2,5)=0.42748;
   mat(3,1)=(1+(0.37464+1.574226*w-0.26692*w^2)*(1-(T/Tc)^(0.5)))^2;
```

```
   mat(3,2)=1+2^(0.5);
   mat(3,3)=1-2^(0.5);
   mat(3,4)=0.07779;
   mat(3,5)=0.45724;
   if ch<4
      mur=0;
   end
   mat(4,1)=(1+(0.406691+1.524095*w-0.158751*w^2-0.0003*mur)*(1-(T/Tc)^(0.5)))^2;
   mat(4,2)=1+2^(0.5);
   mat(4,3)=1-2^(0.5);
   mat(4,4)=0.07779;
   mat(4,5)=0.45724;

   alpha=mat(ch,1);
   sigma=mat(ch,2);
   epsi=mat(ch,3);
   omega=mat(ch,4);
   shi=mat(ch,5);
end



function [z,v]=newsolving(n,X,ta,moles,R,T1,phi,G,atom1,atoms,totatoms,P,p0,ch1)

   function G1 = func(X)
      Enj=0;
      for i=1:(n-1)
      Enj = Enj+X(i);
      end

      for i=1:(n-1)
         m(i)=(G(i)/R/T1 + log(phi(i)*X(i)/Enj*P/p0));
      end
%        m(n)=G(n)/R/T1;
       m(n) = G(n);
      G1 = sum(X.*m);

   end


Aeq=atoms;
beq=totatoms';


for i=1:n
   LB(i)=0;
end
options = optimset('Algorithm','sqp');
%z = fmincon(@func,X,[],[],Aeq,beq,LB,[],[],options);
z = fmincon(@func,X,[],[],Aeq,beq,LB,[],[],options);
```

```
v=0;

end

function [m5]=molematrix(atom1,newdata,totatoms)

[s1,s2]=size(atom1);
[s3,s4]=size(newdata);

m1=atom1;
m11=zeros(s1,s2);
m12=zeros(s1,s2);
m13=zeros(s1,s2);
m2=newdata;
m3=totatoms;
m4=m2';
% m5=zeros(s3,s4);
m21=zeros(s4,s3,s2);

for i=1:s4
   for j=1:s3

      for k=1:s2

         m21(i,j,k)=m4(i,j)*m1(i,k);

      end
   end

end
m24=zeros(1,s3,s2);
m24=sum(m21,1);

m23=zeros(s3,s2);
for i=1:s3
   for j=1:s2
   m23(i,j)=m24(1,i,j);
   end
end



for i=1:s4
   for j=1:s3

      for k=1:s2
         if m1(i,k)==0
            m11(i,k)=1;  %this will give atom3
            m12(i,k)=1;    % this will give atom4
         end
```

```
        if m1(i,k)~=0
           m11(i,k)=m1(i,k);      %atom3
           m12(i,k)=0;            %atom4
        end

        m4(i,j,k)=m21(i,j,k)/m23(j,k)/m11(i,k)*m3(k);




     end
  end
end

m41=zeros(s4,s3);

for i=1:s4
   for j=1:s3
      sum1=0;
      sum2=0;
      for k=1:s2
         sum1=sum1+m4(i,j,k);
         if m1(i,k)~=0
            sum2=sum2+1;
         end



      end
      if sum2==0
         sum2=1;
      end
      m41(i,j)=sum1/sum2;
   end
end
m5=m41';
end

function   [Ein]=energycalculator(x1,t11,n,m5,T,imole,ch1)

load('ENTHALPYDATAYAWS.mat');
l=1;
for loop=t11(1):t11(2):t11(3)
   sumforH0=0;                    % Calculates sum of Enthalpy of entering Streams
   sumforH1=0;                    % Calculates sum of Enthalpy of exiting Streams
   for i=1:n

      a= Enthalpydatabase(i,1);
      b= Enthalpydatabase(i,2);
      c= Enthalpydatabase(i,3);
      d= Enthalpydatabase(i,4);
```

```
        H0= Enthalpydatabase(i,5);
        T1=loop;
        syms TN
        R=8.314/1000;
        H1=c+b*T1+a*T1^2;

        %H1=int(a+b*TN*10^(-3)+c*10^(-6)*TN^2+d*TN^(-2)*10^5,T,T1);
%       H0=int(a+b*TN*10^(-3)+c*10^(-6)*TN^2+d*TN^(-2)*10^5,T,T);

        sumforH1=H1*m5(l,i)+H0*m5(l,i)+sumforH1;
        sumforH0=H0*imole(i)+sumforH0;
    end

    Ein(l)=sumforH1-sumforH0;
    l=l+1;
end
end

function write_gnuplot_file(t11,P,imole,m5,t,energy)
%UNTITLED5 Summary of this function goes here
%   Detailed explanation goes here
%% To write a file to use with Gnuplot
filename = sprintf('Plotfile_Temperature
Range_%1.1f_to_%1.1f_Pressure_%1.1f_FeedMole_ratios_CH4_H2O_O2_CO2_%3.3f_%3.3f_%3.3f_%
3.3f.txt', t11(1), t11(3), P, imole(1),imole(2),imole(3),imole(5));
A = [t';m5(:,1)';m5(:,2)';m5(:,3)';m5(:,4)';m5(:,5)';m5(:,6)';m5(:,7)';energy];
fileID = fopen(filename,'w');
fprintf(fileID,['### The Temperature Range is [%1.1f, %1.1f] K.\n' ...
'### The Pressure is %d bar.\n' ...
'### The Feed Ratio of CH4:H2O:O2:CO2 is [%1.1f :%1.1f :%1.1f :%1.1f] .\n' ...
'### %12s %15s %15s %15s %15s %15s %15s %15s %15s
\n'],t11(1),t11(3),P,imole(1),imole(2),imole(3),imole(5),
'Temperature','Methane','Water','Oxygen','Carbonmonoxide','Carbondioxide','Hydrogen','Carbon','Energy');
fprintf(fileID,'%15.4f %15.4f %15.4f %15.4f %15.4f %15.4f %15.4f %15.4f %15.4f \n',A);
fclose(fileID);
%%-------------------------------------------------------------------------


end


function write_gnuplot_file_HC_ratio(t11,P,imole,m5,HC)
%UNTITLED5 Summary of this function goes here
%   Detailed explanation goes here
%% To write a file to use with Gnuplot
filename = sprintf('Plotfile_Temperature
Range_%1.1f_to_%1.1f_Pressure_%1.1f_FeedMole_ratios_CH4_H2O_O2_CO2_%3.3f_%3.3f_%3.3f_%
3.3f.txt', t11(1), t11(3), P, imole(1),imole(2),imole(3),imole(5));
A = [];
fileID = fopen(filename,'w');
fprintf(fileID,['### The Temperature Range is [%1.1f, %1.1f] K.\n' ...
```

```
'### The Pressure is %d bar.\n' ...
'### The Feed Ratio of CH4:H2O:O2:CO2 is [%1.1f :%1.1f :%1.1f :%1.1f] .\n' ...
'### %12s %15s %15s %15s %15s %15s %15s %15s %15s
\n'],t11(1),t11(3),P,imole(1),imole(2),imole(3),imole(5),
'Temperature','Methane','Water','Oxygen','Carbonmonoxide','Carbondioxide','Hydrogen','Carbon','Energy');
fprintf(fileID,'%15.4f %15.4f %15.4f %15.4f %15.4f %15.4f %15.4f %15.4f %15.4f \n',A);
fclose(fileID);
%%-------------------------------------------------------------------------


end


function write_gnuplot_file_fugacitycoeff(t11,P,imole,m5,t,energy)
%UNTITLED5 Summary of this function goes here
%   Detailed explanation goes here
%% To write a file to use with Gnuplot
filename = sprintf('Plotfile_fugacity_Temperature
Range_%1.1f_to_%1.1f_Pressure_%1.1f_FeedMole_ratios_CH4_H2O_O2_CO2_%3.3f_%3.3f_%3.3f_%
3.3f.txt', t11(1), t11(3), P, imole(1),imole(2),imole(3),imole(5));
A = [t';m5(:,1)';m5(:,2)';m5(:,3)';m5(:,4)';m5(:,5)';m5(:,6)';m5(:,7)'];
fileID = fopen(filename,'w');
fprintf(fileID,['### The Temperature Range is [%1.1f, %1.1f] K.\n' ...
'### The Pressure is %d bar.\n' ...
'### The Feed Ratio of CH4:H2O:O2:CO2 is [%1.1f :%1.1f :%1.1f :%1.1f] .\n' ...
'### %12s %15s %15s %15s %15s %15s %15s %15s
\n'],t11(1),t11(3),P,imole(1),imole(2),imole(3),imole(5),
'Temperature','Methane','Water','Oxygen','Carbonmonoxide','Carbondioxide','Hydrogen','Carbon');
fprintf(fileID,'%15.4f %15.4f %15.4f %15.4f %15.4f %15.4f %15.4f %15.4f \n',A);
fclose(fileID);
%%-------------------------------------------------------------------------


end


function write_gnuplot_file_for_twelve_column_data(A)
%UNTITLED5 Summary of this function goes here
%   Detailed explanation goes here
%% To write a file to use with Gnuplot
filename =
sprintf('Plotfile_twelve_column_data_200C_to_400C_Pressure_9_FeedMole_ratios_CH4_H2O_O2_CO2
_1_1.0_0.0_1.txt');

fileID = fopen(filename,'w');
fprintf(fileID,['### The Temperature Range is [200 , 400] C.\n' ...
'### The Pressure is 9 bar.\n' ...
'### The Feed Ratio of CH4:H2O:O2:CO2 is [1 : 0 : 0.50 : 1] .\n' ...
'### %12s %15s %15s %15s %15s %15s %15s %15s %15s %15s %15s %15s
\n'],'Temperature','Methane','Steam','Oxygen','Carbnmonoxi','Carbdioxi','Hydrogen','Carbon','H2/CO','CH4
% Con','CO2% Conv','Energy(KJ)');
```

```
fprintf(fileID,'%15.4f %15.4f %15.4f %15.4f %15.4f %15.4f %15.4f %15.4f %15.4f %15.4f %15.4f
%15.4f \n',A');
fclose(fileID);
%%-------------------------------------------------------------------------


end


function write_gnuplot_file_for_thirteen_column_data(A,T,P,imole);
%UNTITLED5 Summary of this function goes here
%   Detailed explanation goes here
%% To write a file to use with Gnuplot
filename =
sprintf('thirteen_column_data/Plotfile_thirteen_column_data_%1.1f_to_%1.1f_Pressure_%1.1f_FeedMole
_ratios_CH4_H2O_O2_CO2_%2.2f_%2.2f_%2.2f_%2.2f.txt',T(1),T(3),P,imole(1),imole(2),imole(3),imol
e(5));

fileID = fopen(filename,'w');
fprintf(fileID,['### The Temperature Range is [%1.1f , %1.1f] K.\n' ...
'### The Pressure is %1.1f bar.\n' ...
'### The Feed Ratio of CH4:H2O:O2:CO2 is [%1.1f : %1.1f : %1.1f : %1.1f] .\n' ...
'### %12s %15s %15s %15s %15s %15s %15s %15s %15s %15s %15s %15s %15s
\n'],T(1),T(3),P,imole(1),imole(2),imole(3),imole(5),'Temperature(C
)','Methane','Steam','Oxygen','Carbnmonoxi','Carbdioxi','Hydrogen','Carbon','H2/CO','CH4% Con','CO2%
Conv','H2O% Conv','Energy(KJ)');
fprintf(fileID,'%15.4f %15.4f %15.4f %15.4f %15.4f %15.4f %15.4f %15.4f %15.4f %15.4f %15.4f
%15.4f %15.4f\n',A');
fclose(fileID);
%%-------------------------------------------------------------------------


end


function write_gnuplot_file_for_pcentconvCO2(t11,P,imole,m5,t,energy)
%UNTITLED5 Summary of this function goes here
%   Detailed explanation goes here
%% To write a file to use with Gnuplot
filename =
sprintf('Plotfile_CO2_Percentage_Conversion_%1.1f_to_%1.1f_Pressure_%1.1f_FeedMole_ratios_CH4_
H2O_O2_CO2_%3.3f_%3.3f_%3.3f_%3.3f.txt', t11(1), t11(3), P, imole(1),imole(2),imole(3),imole(5));
A = [t,m5];

fileID = fopen(filename,'w');
fprintf(fileID,['### The Temperature Range is [%1.1f, %1.1f] K.\n' ...
'### The Pressure is %d bar.\n' ...
'### The Feed Ratio of CH4:H2O:O2:CO2 is [%1.1f :%1.1f :%1.1f :%1.1f] .\n' ...
'### %12s %15s \n'],t11(1),t11(3),P,imole(1),imole(2),imole(3),imole(5), 'Temperature','Carbondioxide %
Conv');
fprintf(fileID,'%15.4f %15.4f \n',A');
```

```
fclose(fileID);
%%-------------------------------------------------------------------------


end


function write_gnuplot_file_for_pcentconvCH4(t11,P,imole,m5,t,energy)
%UNTITLED5 Summary of this function goes here
%   Detailed explanation goes here
%% To write a file to use with Gnuplot
filename =
sprintf('Plotfile_CH4_Percentage_Conversion_%1.1f_to_%1.1f_Pressure_%1.1f_FeedMole_ratios_CH4_
H2O_O2_CO2_%3.3f_%3.3f_%3.3f_%3.3f.txt', t11(1), t11(3), P, imole(1),imole(2),imole(3),imole(5));
A = [t,m5];

fileID = fopen(filename,'w');
fprintf(fileID,['### The Temperature Range is [%1.1f, %1.1f] K.\n' ...
'### The Pressure is %d bar.\n' ...
'### The Feed Ratio of CH4:H2O:O2:CO2 is [%1.1f :%1.1f :%1.1f :%1.1f] .\n' ...
'### %12s %15s \n'],t11(1),t11(3),P,imole(1),imole(2),imole(3),imole(5), 'Temperature','Methane %
Conv');
fprintf(fileID,'%15.4f %15.4f \n',A');
fclose(fileID);
%%-------------------------------------------------------------------------


end


function write_gnuplot_file_for_pcentconvC(t11,P,imole,m5,t,energy)
%UNTITLED5 Summary of this function goes here
%   Detailed explanation goes here
%% To write a file to use with Gnuplot
filename =
sprintf('Plotfile_Carbon_Percentage_Conversion_%1.1f_to_%1.1f_Pressure_%1.1f_FeedMole_ratios_CH
4_H2O_O2_CO2_%3.3f_%3.3f_%3.3f_%3.3f.txt', t11(1), t11(3), P, imole(1),imole(2),imole(3),imole(5));
A = [t,m5];

fileID = fopen(filename,'w');
fprintf(fileID,['### The Temperature Range is [%1.1f, %1.1f] K.\n' ...
'### The Pressure is %d bar.\n' ...
'### The Feed Ratio of CH4:H2O:O2:CO2 is [%1.1f :%1.1f :%1.1f :%1.1f] .\n' ...
'### %12s %15s \n'],t11(1),t11(3),P,imole(1),imole(2),imole(3),imole(5), 'Temperature','Carbon % Conv');
fprintf(fileID,'%15.4f %15.4f \n',A');
fclose(fileID);
%%-------------------------------------------------------------------------


end
```

```
function write_gnuplot_file_for_pcentconvCO2(t11,P,imole,m5,t,energy)
%UNTITLED5 Summary of this function goes here
%   Detailed explanation goes here
%% To write a file to use with Gnuplot
filename = sprintf('Plotfile_CO2 Percentage
Conversion_%1.1f_to_%1.1f_Pressure_%1.1f_FeedMole_ratios_CH4_H2O_O2_CO2_%3.3f_%3.3f_%3.
3f_%3.3f.txt', t11(1), t11(3), P, imole(1),imole(2),imole(3),imole(5));
A = [t,m5];

fileID = fopen(filename,'w');
fprintf(fileID,['### The Temperature Range is [%1.1f, %1.1f] K.\n' ...
'### The Pressure is %d bar.\n' ...
'### The Feed Ratio of CH4:H2O:O2:CO2 is [%1.1f :%1.1f :%1.1f :%1.1f] .\n' ...
'### %12s %15s \n'],t11(1),t11(3),P,imole(1),imole(2),imole(3),imole(5), 'Temperature','Carbondioxide %
Conv');
fprintf(fileID,'%15.4f %15.4f \n',A');
fclose(fileID);
%%-------------------------------------------------------------------------


end


function write_gnuplot_file_for_fugacitycoeffmix_EOS(A)
%UNTITLED5 Summary of this function goes here
%   Detailed explanation goes here
%% To write a file to use with Gnuplot
filename =
sprintf('Plotfile_Mixture_fugacity_coefficient_200_C_to_1200_C_Pressure_20_bar_FeedMole_ratios_CH
4_H2O_O2_CO2_1_0.6_0.1_0.6_EOS.txt');
%A = [t,m5];

fileID = fopen(filename,'w');
fprintf(fileID,['### The Temperature Range is [200 , 1200] Celcius.\n' ...
'### The Pressure is 20 bar.\n' ...
'### The Feed Ratio of CH4:H2O:O2:CO2 is [1 :0.6 :0.1 :0.6] .\n' ...
'### %12s %15s %15s %15s %15s \n'], 'Temperature','Ideal', 'RK', 'SRK', 'PR');
fprintf(fileID,'%15.4f %15.4f %15.4f %15.4f %15.4f \n',A');
fclose(fileID);
%%-------------------------------------------------------------------------


end


function write_gnuplot_file_for_fugacitycoeffmix(t11,P,imole,m5,t,energy)
%UNTITLED5 Summary of this function goes here
%   Detailed explanation goes here
```

```
%% To write a file to use with Gnuplot
filename =
sprintf('Plotfile_Mixture_fugacity_coefficient_%1.1f_to_%1.1f_Pressure_%1.1f_FeedMole_ratios_CH4_
H2O_O2_CO2_%3.3f_%3.3f_%3.3f_%3.3f.txt', t11(1), t11(3), P, imole(1),imole(2),imole(3),imole(5));
A = [t,m5];

fileID = fopen(filename,'w');
fprintf(fileID,['### The Temperature Range is [%1.1f, %1.1f] K.\n' ...
'### The Pressure is %d bar.\n' ...
'### The Feed Ratio of CH4:H2O:O2:CO2 is [%1.1f :%1.1f :%1.1f :%1.1f] .\n' ...
'### %12s %15s \n'],t11(1),t11(3),P,imole(1),imole(2),imole(3),imole(5), 'Temperature',',Mixture
Fugacity');
fprintf(fileID,'%15.4f %15.4f \n',A');
fclose(fileID);
%%-------------------------------------------------------------------------


end
```

FOR KINETIC STUDY:

```
clear;
%% This code file is the main reformer bed script
% brief introduction explaining the reason for them.

%% This complete code will have the following use(s):
% 1) Simulation of Pseudo homogeneous fixed bed reformer
% 2) To be able to simulate the SRM/DRM both individually and
% in combined mode.

%% SIMULATION BEGINS:
% Call for properties from the database function:

[D, W_F0, T0, P0, dp, E_s, tau, rho_b, E_b]= reactor_database();

% Kinetics:
% This code uses the following kinetic models:
%   1) Steam reforming of methane LHHW model using : J. Xu et al., AIChE Journal, 1989, 35, 88.
%   2) Dry reforming of methane LHHW model using : X. E. Verykios et al., International journal of
Hydrogen Energy, 2003, 28, 1045.

% Chemical reactions involved :
%   1) CH4 + 2H2O <---> 3H2 + CO
%   2) CO + H2O <---> H2 + CO2
%   3) CH4 + 2H2O <---> 4H2 + CO2
%   4) CH4 + CO2 <---> 2H2 + 2CO
%% Using solver script :
```

```
% Model selection choices:
% 1) choice 1 : SRM
% 2) choice 2 : DRM
% 3) choice 3 : SRM+DRM
dt=0.0795;      %m
At=pi/4*dt^2;   % m^2
mod_sel=3;
rho_b = 946800;     %g/m^3

[o1, o2] = solver_script(mod_sel,D, W_F0, T0, dp, E_s, tau, rho_b, E_b);
o1=o1/(rho_b*At);
%Temperature Profile
figure;
subplot(2,1,1);
plot(o1, o2(:,7));
xlabel('bed length, m');
ylabel('Temperature K');
%

subplot(2,1,2);
plot(o1, o2(:,(1:6)));
xlabel('bed length, m');
ylabel('mole/hr');

legend('CO','H_2O','CO_2','H_2','He','CH_4');
%


function [o1 , o2]= solver_script(mod_sel,D, W_F0, T0, P0, dp, E_s, tau, rho_b, E_b)

lspan=[0:1:1000];
% a = CO
% b = H2O
% c = CO2
% d = H2
% e = He
% f = CH4
if mod_sel==1 % SRM is chosen as kinetic model
   initials=[0.00001,5,0.00001,0.00001,0.00001,5,1273];   %  following order :
[CO,H2O,CO2,H2,He,CH4,T] This is to fix the feed mole ratio entering the reactor
   [o1 , o2]=ode15s('SRM',lspan,initials);
end

if mod_sel==2 % DRM is chosen as kinetic model
   initials=[0.00001,0.00001,1,0.00001,0.00001,1];   %  following order : [CO,H2O,CO2,H2,He,CH4]
This is to fix the feed mole ratio entering the reactor
   [o1 , o2]=ode45('DRM',lspan,initials);
end

if mod_sel==3 % SRM+DRM is chosen as kinetic model
```

```
   initials=[0.00001,100,100,0.00001,0.00001,150,1173,28.37];   %  following order :
[CO,H2O,CO2,H2,He,CH4,T] This is to fix the feed mole ratio entering the reactor
   [o1 , o2]=ode15s('SRM_DRM_rev1',lspan,initials);
end

% if mod_sel==3 % SRM+DRM is chosen as kinetic model
%     initials=[0.00001,1000,1000,0.00001,0.00001,1273];   %  following order :
[CO,H2O,CO2,H2,He,CH4,T] This is to fix the feed mole ratio entering the reactor
%     [o1 , o2]=ode15s('SRM_DRM_rev2',lspan,initials);
% end

end


function dfdw=SRM_DRM_rev1(~,F)
Fco=F(1);
Fh2o=F(2);
Fco2=F(3);
Fh2=F(4);
Fhe=F(5);
Fch4=F(6);
P1 = F(8);     % partial pressures in bar
T= F(7);
R=8.314;        % Universal gas constant Pa.m3/mol/K
Ftot=F(1)+F(2)+F(3)+F(4)+F(5)+F(6);
P(1) = P1*F(1)/Ftot;
P(2) = P1*F(2)/Ftot;
P(3) = P1*F(3)/Ftot;
P(4) = P1*F(4)/Ftot;
P(5) = P1*F(5)/Ftot;
P(6) = P1*F(6)/Ftot;
% Steam reforming LHHW parameters using Xu and Froment (1989) expressions
K1=exp(30.420-27106/T);
K2=exp(-3.798+4160/T);
K3=exp(34.218-31266/T);
%
KCH4=6.65e-4*exp(38280/8.314/T);
KCO=8.23e-5*exp(70650/8.314/T);
KH2=6.12e-9*exp(82900/8.314/T);
KH2O=1.77e5*exp(-88680/8.314/T);
%
kin1=4.2248e15*exp(-240100/8.314/T);
kin2=1.955e6*exp(-67130/8.314/T);
kin3=1.0202e15*exp(-243900/8.314/T);
%
DEN=1+KCH4*P(6)+KCO*P(3)+KH2*P(4)+KH2O*P(2)/P(4);
% Dry reforming LHHW parameters using Verykios (2003) expressions
K1_k2 = 2.61*10^(-1)*exp(-4300/T)*3600;
K_3 = 5.17*10^(-3)*exp(8700/T);
k_4 = 5.35*10^(-1)*exp(-7500/T)*3600;
%
r1=kin1/P(4)^2.5/DEN^2*(P(6)*P(2)-P(4)^3*P(1)/K1);
```

```
r2=kin2/P(4)/DEN^2*(P(1)*P(2)-P(4)*P(3)/K2);
r3=kin3/P(4)^3.5/DEN^2*(P(6)*P(2)^2-P(4)^4*P(3)/K3);
r4 = (K1_k2*K_3*k_4*P(6)*P(3)/(K1_k2*K_3*P(6)*P(3)+K1_k2*P(6)+K_3*k_4*P(3)));

Dh1=535655+R*(4.4810*(T-298.15)-0.0102*((T-298.15)^2)/2+2.164e-06*((T-298.15)^3)/3+2400*(1/T-
1/298.15));
Dh2=2846+R*(1.86*(T-298.15)-0.00054*((T-298.15)^2)/2+0*((T-298.15)^3)/3+116400*(1/T-1/298.15));
Dh3=252671+R*(9.811*(T-298.15)-0.009248*((T-298.15)^2)/2+2.164e-06*((T-
298.15)^3)/3+106700*(1/T-1/298.15));
Dh4=246979+R*(6.091*(T-298.15)-0.008168*((T-298.15)^2)/2+2.164e-06*((T-
298.15)^3)/3+126100*(1/T-1/298.15));

cp1=R*(3.37600000000000*((T-298.15))+0.00055700000000000000*((T^2-298.15^2))/2+0*((T^3-
298.15^3))/3-3100*(1/T-1/298.15));
cp2=R*(3.47000000000000*((T-298.15))+0.00145000000000000*((T^2-298.15^2))/2+0*((T^3-
298.15^3))/3+12100*(1/T-1/298.15));
cp3=R*((T-298.15)+5.45700000000000*((T-298.15))+0.00104500000000000*((T^2-
298.15^2))/2+0*((T^3-298.15^3))/3-115700*(1/T-1/298.15));
cp4=R*(3.24900000000000*((T-298.15))+0.00042200000000000000*((T^2-298.15^2))/2+0*((T^3-
298.15^3))/3+8300*(1/T-1/298.15));
cp5=R*(3.63980000000000*((T-298.15))+0.00340000000000000*((T^2-
298.15^2))/2+2.00000000000000e-06*((T^3-298.15^3))/3+0*(1/T-1/298.15));
cp6=R*(1.70200000000000*((T-298.15))+0.00908100000000000*((T^2-298.15^2))/2-
2.16400000000000e-06*((T^3-298.15^3))/3+0*(1/T-1/298.15));

%U=HTP(T);    % j/m2.hr.K
U=350;          %http://www.engineersedge.com/thermodynamics/overall_heat_transfer-table.htm
Tr=1173;        %K
dt=0.0795;      %m
At=pi/4*dt^2;   % m^2
rho_g = P1*10^5/(Fco*28+Fh2o*18+Fco2*44+Fco2+Fh2*2+Fhe*4+Fch4*16)/Ftot/(R*T);
u_s = (Fco*28+Fh2o*18+Fco2*44+Fco2+Fh2*2+Fhe*4+Fch4*16)/Ftot*rho_g/At;
rho_b = 946800;     %g/m^3
Cp= (Fco*cp1+Fh2o*cp2+Fco2*cp3+Fco2+Fh2*cp4+Fhe*cp5+Fch4*cp6)/Ftot; % j/(mol.K)
dfdw(1,1)=(r1-r2+2*r4);
dfdw(2,1)=-(r1+r2+2*r3);
dfdw(3,1)=(r2+r3-r4);
dfdw(4,1)=(3*r1+r2+4*r3+2*r4);
dfdw(5,1)=0;
dfdw(6,1)=-(r1+r3+r4);
%dfdl(7,1)=(-1*(r1*Dh(1)+r2*Dh(2)+r3*Dh(3)+r4*Dh(4))*rho_b-4*U/dt*(T-
Tr))/(u_s*rho_g*(sum(F(1:6).*cp(1:6)')/sum(F(1:6).*M(1:6)')));
%dfdl(7,1)=(-1*(r1*Dh(1)+r2*Dh(2)+r3*Dh(3)+r4*Dh(4))*rho_b)/(u_s*rho_g*Cp);
dp=17.41/1000;
a=6/dp;
dfdw(7,1)= -(r1*Dh1+r2*Dh2+r3*Dh3+r4*Dh4)/(Cp*Ftot)*1000+U*a*(Tr-T)/rho_b;
%dfdw(7,1)= -(r1*Dh1+r2*Dh2+r3*Dh3+r4*Dh4)/(Cp*Ftot)*1000;
% G=rho_g*u_s;
% phi=0.5319;
% mu=viscosity(F);
% beta0=G*(1-phi)/(rho_g*dp*phi^3)*(150*(1-phi)*mu/dp+1.75*G);
% dfdw(8,1)=-beta0/(At*rho_b);
```

```
G=rho_g*u_s;
phi=0.5319;
mu=viscosity(F);    %Pa.S
beta0=G/(3600000)*(1-phi)/(rho_g*(1/1000)*dp*phi^3)*(150*(1-phi)*mu/dp+1.75*G/(3600000));
%pa/m
dfdw(8,1)=-beta0/(At*rho_b)/100000;            %bar/g


end

function dfdl=SRM(l,F)
% feed conditions
% a = CO
% b = H2O
% c = CO2
% d = H2
% e = He
% f = CH4

% Rearranging the order of species
% F_dummy(1)=F(3);
% F_dummy(2)=F(2);
% F_dummy(3)=F(4);
% F_dummy(4)=F(5);
% F_dummy(5)=F(6);
% F_dummy(6)=F(1);
%
% F = F_dummy;
R=8.314;
eta1=1;
eta2=1;
eta3=1;
eta4=1;
% partial pressures in bar
Ptot0 = 28.37;
% temperatures in K
% T = 1000;
%
Ftot=F(1)+F(2)+F(3)+F(4)+F(5)+F(6);
P(1) = Ptot0*F(1)/Ftot;
P(2) = Ptot0*F(2)/Ftot;
P(3) = Ptot0*F(3)/Ftot;
P(4) = Ptot0*F(4)/Ftot;
P(5) = Ptot0*F(5)/Ftot;
P(6) = Ptot0*F(6)/Ftot;

K1=exp(30.420-27106/F(7));
K2=exp(-3.798+4160/F(7));
K3=exp(34.218-31266/F(7));
%
```

```
KCH4=6.65e-4*exp(38280/8.314/F(7));
KCO=8.23e-5*exp(70650/8.314/F(7));
KH2=6.12e-9*exp(82900/8.314/F(7));
KH2O=1.77e5*exp(-88680/8.314/F(7));
%
kin1=4.2248e15*exp(-240100/8.314/F(7));
kin2=1.955e6*exp(-67130/8.314/F(7));
kin3=1.0202e15*exp(-243900/8.314/F(7));
%
DEN=1+KCH4*P(6)+KCO*P(3)+KH2*P(4)+KH2O*P(2)/P(4);
r1=kin1/P(4)^2.5/DEN^2*(P(6)*P(2)-P(4)^3*P(1)/K1);
r2=kin2/P(4)/DEN^2*(P(1)*P(2)-P(4)*P(3)/K2);
r3=kin3/P(4)^3.5/DEN^2*(P(6)*P(2)^2-P(4)^4*P(3)/K3);
%
load('specie_data');
for i=1:6
T1=F(7);
cp(i)=double(R*(specie_data(i,2)+specie_data(i,3)*T1+specie_data(i,4)*T1^2+specie_data(i,5)*T1^(-
2)));
end
%
%
load('rxn_data');
syms T
for i=1:4

  dh(i)=rxn_data(i,1)+R*double(int(rxn_data(i,2)+rxn_data(i,3)*T+rxn_data(i,4)*T^2+rxn_data(i,5)*T^(-
2),T,298.15,F(7)));

end
%
U=HTP(F(7));          %
Tr=900;         %K
dt=0.0978;      %m
At=pi/4*dt^2;   % m^2
G=0.003953;     %g.mol/hr
rhob=1.362;     %g/m^3
Cp=sum(cp(1:6).*F(1:6)')/sum(F(1:6));
dfdl(1,1)=(r1-r2)/(At*rhob);
dfdl(2,1)=(-(r1+r2+2*r3))/(At*rhob);
dfdl(3,1)=(r2+r3)/(At*rhob);
dfdl(4,1)=(3*r1+r2+4*r3)/(At*rhob);
dfdl(5,1)=0;
dfdl(6,1)=(-(r1+r3))/(At*rhob);
%dfdw(7,1)=(-1*(dh(1)*eta1*r1+dh(2)*eta2*r2+dh(3)*eta3*r3)-4*U*(F(7)-
Tr)/dt)/(F(1)*cp(1)+F(2)*cp(2)+F(3)*cp(3)+F(4)*cp(4)+F(5)*cp(5)+F(6)*cp(6));
dfdl(7,1)=1/(G*Cp)*(4*U*(Tr-F(7))/dt-(dh(1)*eta1*r1+dh(2)*eta2*r2+dh(3)*eta3*r3)*rhob);
end
```